Raman Microscopy of some Thin Films Produced by Atmospheric Pressure Chemical Vapour Deposition

Amanda Mary Ellen Hardy

University College London

Submitted for a Ph.D. in Chemistry

ProQuest Number: U643166

All rights reserved

INFORMATION TO ALL USERS
The quality of this reproduction is dependent upon the quality of the copy submitted.

In the unlikely event that the author did not send a complete manuscript
and there are missing pages, these will be noted. Also, if material had to be removed,
a note will indicate the deletion.

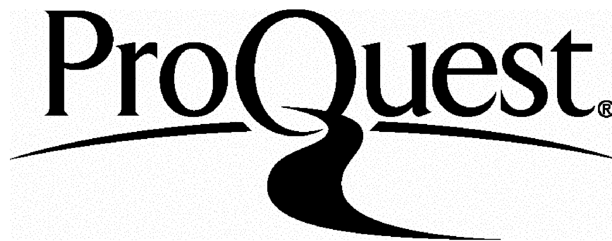

ProQuest U643166

Published by ProQuest LLC(2015). Copyright of the Dissertation is held by the Author.

All rights reserved.
This work is protected against unauthorized copying under Title 17, United States Code.
Microform Edition © ProQuest LLC.

ProQuest LLC
789 East Eisenhower Parkway
P.O. Box 1346
Ann Arbor, MI 48106-1346

Abstract

Thin films of a variety of oxides, sulfides and oxysulfides has been produced by atmospheric pressure chemical vapour deposition (APCVD). These were all characterised by Raman microscopy.

The APCVD reaction of oxovanadium(V) chloride and hydrogen sulfide was studied between 300 – 600 °C, with films deposited at 400 - 600 °C. EDX results indicate that V_2O_4S was produced at 400 - 450 °C, $V_2O_3S_2$ at 500 °C, $V_2O_2S_3$ at 550 °C and V_2O_4S at 600 °C. This reaction has not been reported previously. Various analytical techniques including Raman microscopy were used to identify the composition of the films deposited in this study. No Raman spectra have been reported for vanadium oxysulfides previously, therefore the Raman results constitute new information about this class of compounds.

Vanadium sulfide films were produced by the APCVD reaction of vanadium tetrachloride and hydrogen sulfide. Reactions were performed at temperatures between 300 - 600 °C. Films of the following compounds were produced; VS_2 at 300 and 350 °C, V_2S_3 at 400, 450 and 500 °C, V_3S_4 at 550 °C and VS at 600 °C. The films were characterised by EDX, electron microprobe, XPS, XRD, and Raman microscopy.

Films were grown from the APCVD reactions of titanium tetrachloride and hydrogen sulfide at 400, 500 and 600 °C. The film deposited at 400 °C was found to consist of TiS_2; films produced at higher temperatures all showed the presence of both TiS_2 and TiO_2 in the form of anatase. None of the coatings contained TiS_3. The coatings were analysed by EDX, XRD and Raman microscopy. No Raman spectra of TiS_2 films are known to have been reported previously.

In addition a selection of other films was characterised by Raman microscopy including; vanadium oxides, chromium oxide, titanium dioxide and tin/vanadium sulfides and oxysulfides. These results are all presented in this thesis.

Contents

1 **Abstract**

2 **Contents**

8 **List of illustrations**

22 **Acknowledgements**

23 **Glossary**

28 **Chapter 1** **Introduction**

28 1.1 The aim of this study

28 1.2 History of the Raman effect

28 1.3 Developments in Raman spectrometers

28 - 1.3.1 The excitation source

29 - 1.3.2 The spectrometer

30 - 1.3.3 The detector

31 1.4 Theory of the Raman effect

32 1.5 Theory – molecular vibrations

33 1.6 Previous Raman studies of thin films

33 - 1.6.1 Raman analysis of thin films for technological uses

35 - 1.6.2 Raman microscopy used for manuscript analysis

36 1.7 Chemical vapour deposition history and theory

36 - 1.7.1 Definition

36 - 1.7.2 History of chemical vapour deposition

37 - 1.7.3 Theory of CVD

39 - 1.7.4 Growth mechanisms

40 - 1.7.5 Growth rate of films

40 - 1.7.6 Thermal CVD

41 - 1.7.7 Aerosol Assisted CVD

41 - 1.7.8 Plasma Enhanced CVD

41 - 1.7.9 Photo CVD

42 1.8 Possible applications of the films produced in this study

42 - 1.8.1 Heat-mirrors

44 1.9 X-ray diffractometry

45 1.10 X-ray photoelectron spectroscopy

45 1.11 Scanning electron microscopy

47 1.12 Energy dispersive analysis by X-rays (EDX)
49 **Chapter 2** 2.1 Raman microscopy
49 - 2.1.1 Dilor XY
49 - 2.1.2 Dilor Infinity Raman microscope
49 - 2.1.3 Renishaw Raman system 1000, Ramascope
49 2.2 Energy dispersive analysis by X-rays
50 2.3 Electron microprobe
50 2.4 Scanning electron microscopy
50 2.5 X-ray diffractometry
50 2.6 X-ray photoelectron spectroscopy
50 2.7 UV/visible spectroscopy
50 2.8 Scotch tape test
51 2.9 Solubility
51 2.10 FTIR spectroscopy
51 2.11 Construction of the APCVD rig
52 2.12 Gas flow through the reactor
54 2.13 APCVD Experimental
55 2.14 Preparation of Tri-n-butyltin trifluoroacetate
56 2.15 Calibration of Raman spectra
56 - 2.15.1 Signal intensity corrections
56 - 2.15.2 Raman shift wavenumber correction
58 **Chapter 3** **Vanadium oxysulfide**
58 3.1 Introduction
58 3.2 Background
60 3.3 Experimental
61 3.4 Results
61 - 3.4.1 Film colour and uniformity
64 - 3.4.2 Film adhesion
64 - 3.4.3 Solubility
64 - 3.4.4 Four-probe resistance measurements
65 - 3.4.5 Raman microscopy and Infrared spectroscopy
73 - 3.4.6 Energy dispersive analysis by X-rays
75 - 3.4.7 Scanning electron microscopy
77 - 3.4.8 Electron microprobe
77 - 3.4.9 X-ray diffractometry

78 - 3.4.10 X-ray photoelectron spectroscopy
80 - 3.4.11 UV/visible spectroscopy
80 - 3.4.12 Transmittance/reflectance spectroscopy
82 3.5 Discussion
85 **Chapter 4** **Vanadium sulfide**
85 4.1 Introduction
85 4.2 Background
87 4.3 Experimental
88 4.4 Results
88 - 4.4.1 Film colour and uniformity
89 - 4.4.2 Film adhesion
89 - 4.4.3 Solubility
90 - 4.4.4 Raman microscopy
96 - 4.4.5 Energy dispersive analysis by X-rays
97 - 4.4.6 Electron microprobe
97 - 4.4.7 Scanning electron microscopy
100 - 4.4.8 X-ray diffractometry
101 - 4.4.9 X-ray photoelectron spectroscopy
103 - 4.4.10 UV/visible spectroscopy
103 - 4.4.11 Four-probe resistance measurements
104 - 4.4.12 Transmittance/reflectance spectroscopy
106 4.5 Discussion
109 **Chapter 5** **Titanium sulfides**
109 5.1 Introduction
109 5.2 Background
109 - 5.2.1 Titanium monosulfide
109 - 5.2.2 Titanium disulfide
111 - 5.2.3 CVD reactions used to deposit titanium disulfide
114 - 5.2.4 Titanium trisulfide
115 - 5.2.5 Non-stoichiometric titanium sulfides
115 5.3 Experimental
117 5.4 Results
117 - 5.4.1 Film colour and uniformity
118 - 5.4.2 Four-probe resistance measurements
118 - 5.4.3 Raman microscopy

122 - 5.4.4 Energy dispersive analysis by X-rays
123 - 5.4.5 Scanning electron microscopy
124 - 5.4.6 X-ray diffractometry
125 - 5.4.7 Transmittance/reflectance spectroscopy
128 - 5.4.8 Film adhesion
128 - 5.4.9 Solubility
129 5.5 Discussion
132 **Chapter 6** **Chromium oxysulfide**
132 6.1 Introduction
132 6.2 Chromium oxysulfide
132 6.3 Experimental
133 6.4 Results
133 - 6.4.1 Film colour and uniformity
134 - 6.4.2 Four-probe resistance measurements
134 - 6.4.3 Energy dispersive analysis by X-rays
135 - 6.4.4 Raman microscopy
138 - 6.4.5 Scanning electron microscopy
138 - 6.4.6 Transmittance/reflectance spectroscopy
140 - 6.4.7 Solubility
140 - 6.4.8 Film adhesion
141 6.5 Discussion
143 **Chapter 7** **Tin Sulfides**
143 7.1 Introduction
143 7.2 Tin Sulfides
147 7.3 Experimental, results and discussion
147 - 7.3.1 APCVD reactions of $SnCl_4$ and H_2S
147 - 7.3.2 Results
147 - 7.3.3 Raman spectroscopy
150 - 7.3.4 Scanning electron microscopy
151 7.4 APCVD reactions of $SnBr_4$ and H_2S
152 - 7.4.1 Results
152 - 7.4.2 Raman spectroscopy
155 7.5 APCVD reactions of n-$Bu_3SnO_2CCF_3$ and H_2S
155 - 7.5.1 Results
155 - 7.5.2 Raman spectroscopy

156 7.6 AACVD reactions of $(C_6H_{11}S)_4Sn$ and H_2S
156 - 7.6.1 Results
157 - 7.6.2 Raman spectroscopy
158 7.7 Discussion
160 7.8 Conclusion
161 **Chapter 8** **Mixed metal coatings**
161 8.1 Introduction
161 8.2 Background
162 8.3 Tin vanadium oxysulfide
162 - 8.3.1 Experimental
163 8.4 Results
163 - 8.4.1 Film colour and uniformity
164 - 8.4.2 Raman microscopy
169 8.5 Tin vanadium sulfide
169 8.5.1 Experimental
170 8.6 Results
170 - 8.6.1 Raman microscopy
175 8.7 Discussion

178 **Conclusions** **9.0 Conclusions**
179 **9.1 Future work**
180 **Appendix 1** **Appendix 1**
183 **Appendix 2** **Other films analysed by Raman microscopy**
183 **Vanadium dioxide**
183 - Experimental
183 - Results and discussion
184 **Vanadium pentoxide**
184 - Experimental
184 - Results and discussion
185 **Chromium oxide**
185 - Experimental
186 - Results and discussion
186 **Titanium dioxide**
186 - Experimental
188 - Results and discussion

189 **Appendix 3** **A list of abbreviations used in this thesis**

190 **References**

List of illustrations

32 **Figure 1.1** a.) a Stokes Raman transition, b.) a Rayleigh transition, c.) an anti-Stokes Raman transition. The incident radiation is depicted in red, the scattered radiation is depicted in blue and the energy difference between these, where applicable, is depicted in black. The black line represents a Raman transition of energy hv.

38 **Figure 1.2** A schematic representation of processes leading to 3-D nucleation and film growth.

39 **Figure 1.3** A schematic diagram of film growth mechanisms.

42 **Figure 1.4** Diagram of a perfect heat mirror showing how the coating depicted in grey on a transparent glass substrate behaves when illuminated by solar radiation.

42 **Figure 1.5** The visible region of the electromagnetic spectrum.

43 **Figure 1.6** Graph showing the reflectance and transmittance profiles for a perfect heat mirror.

43 **Figure 1.7** A graph showing the reflectance and transmittance profiles of a glass substrate supplied for use in these studies by Pilkington. The glass has a coating of tin oxide with a silicon dioxide top coating.

47 **Figure 1.8** Schematic representation of an electron gun.

47 **Figure 1.9** Schematic diagram of a scanning electron microscope.

52 **Figure 2.1** (a) shows the entrance flange from the side elevation. (b) shows the entrance flange from the top.

53 **Figure 2.2** A schematic diagram of the quartz tube reactor.

53 **Figure 2.3** A cross-sectional view of the bubbler used in this study, showing the passage of gas through a liquid precursor.

54 **Figure 2.4** A schematic diagram of the APCVD rig.

57 **Figure 2.5** A schematic diagram of a recent Raman microscope.

59 **Figure 3.1** A schematic representation of the first coordination shell of vanadium in $V_2O_3S.3H_2O$.

61 **Table 3.2** Reaction conditions used during the APCVD reaction of oxovanadium(V) chloride and hydrogen sulfide. a.) for reactions of 0.5 min duration b.) for reaction of 3 min duration.

62 **Table 3.3** Descriptions of the visual appearance of films produced by the APCVD reaction of oxovanadium(V) chloride and hydrogen sulfide. a.) from reactions of 0.5 min duration b.) from a reaction of 3 min duration.

63 **Figure 3.4** Sketches after two weeks of the appearances of films deposited by the APCVD reaction (30 s) of oxovanadium(V) chloride and hydrogen sulfide at a.) 400 °C, b.) 450 °C and c.) 600 °C.

63 **Figure 3.5** Photograph of a green area of a film deposited by the APCVD reaction (30 s) of oxovanadium(V) chloride and hydrogen sulfide at 450 °C. Shown at 180x magnification using an EDX (Jeol) instrument.

65 **Table 3.6** Resistance measurements of the films deposited from the APCVD reaction of oxovanadium(V) chloride and hydrogen sulfide. a.) for reactions of 0.5 min duration b.) for the reaction of 3 min duration.

66 **Figure 3.7a** Raman spectrum of the film deposited at 400 °C by the APCVD reaction (30 s) of oxovanadium(V) chloride and hydrogen sulfide.

66 **Figure 3.7b** Raman spectrum of the film deposited at 400 °C by the APCVD reaction (30 s) of oxovanadium(V) chloride and hydrogen sulfide. Spectrum shows the effect of prolonged laser irradiation on a film produced at 400 °C.

67 **Figure 3.7c** Raman spectrum of the film deposited at 450 °C by the APCVD reaction (30 s) of oxovanadium(V) chloride and hydrogen sulfide.

67 **Figure 3.7d** Raman spectrum of the film deposited at 450 °C by the APCVD reaction (180 s) of oxovanadium(V) chloride and hydrogen sulfide.

68 **Figure 3.7e** Raman spectrum of the film deposited at 500 °C by the APCVD reaction (30 s) of oxovanadium(V) chloride and hydrogen sulfide.

68 **Figure 3.7f** Raman spectrum of the film deposited at 550 °C by the APCVD reaction (30 s) of oxovanadium(V) chloride and hydrogen sulfide.

69 **Figure 3.7g** Raman spectrum of the film deposited at 600 °C by the APCVD reaction (30 s) of oxovanadium(V) chloride and hydrogen sulfide.

69 **Figure 3.7h** Raman spectrum of oxovanadium(V) sulfate. This spectrum was recorded using the same conditions as used in the analysis of the films deposited by the APCVD reaction (30 s) of oxovanadium(V) chloride and hydrogen sulfide.

70 **Figure 3.7i** A vanadium pentoxide standard Raman spectrum. A Raman spectrum recorded from a film deposited at 500 °C by the APCVD reaction of oxovanadium(V) chloride and water.

71 **Table 3.8** Showing the Raman and IR bands recorded from a sample of a film deposited at 450 °C by the 3 min APCVD reaction of oxovanadium(V) chloride and hydrogen sulfide.

73 **Table 3.9** Table comparing the atomic concentrations of vanadium and sulfur as determined by EDX. Recorded from samples of the black films produced by the APCVD reaction of oxovanadium(V) chloride and hydrogen sulfide with 0.5 dm^3 min^{-1} flow of H_2S.

74 **Table 3.10** Table comparing the atomic concentrations of vanadium and sulfur as determined by EDX. Recorded from samples of the films produced by the APCVD reaction of oxovanadium(V) chloride and hydrogen sulfide at 500 °C with either a 0.5 or 1.0 $dm^3 min^{-1}$ flow of H_2S.

74 **Figure 3.11** A representation of a 1 x 1.2 cm sample of the film deposited at 400 °C by the APCVD reaction (30 s) of oxovanadium(V) chloride and hydrogen sulfide. The

diagram depicts the sample which includes the boundary region between the green and black areas of the film.

74 **Table 3.12** EDX results from a line crossing the boundary between green and black regions of the film deposited at 400 °C by the APCVD reaction (30 s) of oxovanadium(V) chloride and hydrogen sulfide.

76 **Figure 3.13** Scanning electron micrographs of films deposited at: a.) 400 °C, b.) 450 °C, c.) 500 °C, e.) 550 °C and f.) 600 °C by the APCVD reaction (30 s) of oxovanadium(V) chloride and hydrogen sulfide; each with 0.5 dm^3 min^{-1} flow of hydrogen sulfide. d.) 500 °C with 1.0 dm^3 min^{-1} flow of hydrogen sulfide.

77 **Figure 3.14** A picture of a 2 mm^2 sample green (LHS in picture) and black film boundary using 180 x magnification. This film was deposited at 400 °C by the APCVD reaction (30 s) of oxovanadium(V) chloride and hydrogen sulfide.

78 **Figure 3.15** An X-ray diffraction pattern recorded from the film deposited at 600 °C by the APCVD reaction (30 s) of oxovanadium(V) chloride and hydrogen sulfide.

79 **Figure 3.16** XPS results from a film deposited at 600 °C by the APCVD reaction (30 s) of oxovanadium(V) chloride and hydrogen sulfide. a.) survey spectrum, b.) vanadium, c.) oxygen, d.) sulfur peaks and e.) shows the atomic concentrations of these elements at different levels in the film as revealed by argon etching.

80 **Figure 3.17** An UV/visible spectrum of a thin film of vanadium oxysulfide deposited at 500 °C by the APCVD reaction (30 s) of oxovanadium(V) chloride and hydrogen sulfide.

81 **Figure 3.18a** Transmittance and reflectance plots for the film deposited at 500 °C by the APCVD reaction (30 s) of oxovanadium(V) chloride and hydrogen sulfide.

81 **Figure 3.18b** Transmittance and reflectance plots for the film deposited at 600 °C by the APCVD reaction (30 s) of oxovanadium(V) chloride and hydrogen sulfide.

86 **Figure 4.1** A schematic representation of locations of vanadium atoms inside the unit cell of V_5S_8.

87 **Table 4.2** Deposition conditions for the APCVD reactions of vanadium tetrachloride and hydrogen sulfide.

88 **Table 4.3** Descriptions of the appearances of films deposited by the APCVD reactions of vanadium tetrachloride and hydrogen sulfide.

89 **Figure 4.4** A schematic representation of two films deposited by the APCVD reaction of vanadium tetrachloride and hydrogen sulfide. a.) at 300 °C, c.) 500 °C on the day of deposition and b.) the same film as in (a.) after 2 months storage in air.

90 **Figure 4.5a** Raman spectrum of vanadium(III) sulfide powder used as a standard. Prepared by a liquid mediated metathesis reaction of sodium sulfide and vanadium trichloride in toluene at reflux.

91 **Figure 4.5b** Raman spectrum of the film deposited at 300 °C by the APCVD reaction of vanadium tetrachloride and hydrogen sulfide.

91 **Figure 4.5c** Raman spectrum of the film deposited at 300 °C by the APCVD reaction of vanadium tetrachloride and hydrogen sulfide.

92 **Figure 4.5d** Raman spectrum of the film deposited at 350 °C by the APCVD reaction of vanadium tetrachloride and hydrogen sulfide.

92 **Figure 4.5e** Raman spectrum of the film deposited at 400 °C by the APCVD reaction of vanadium tetrachloride and hydrogen sulfide.

93 **Figure 4.5f** Raman spectrum of the film deposited at 450 °C by the APCVD reaction of vanadium tetrachloride and hydrogen sulfide.

Page	Item	Description
93	**Figure 4.5g**	Raman spectrum of the film deposited at 500 °C by the APCVD reaction of vanadium tetrachloride and hydrogen sulfide.
94	**Figure 4.5h**	Raman spectrum of the film deposited at 550 °C by the APCVD reaction of vanadium tetrachloride and hydrogen sulfide.
94	**Figure 4.5i**	Raman spectrum of the film deposited at 600 °C by the APCVD reaction of vanadium tetrachloride and hydrogen sulfide.
96	**Table 4.6**	Table of the atomic concentrations by percentage of vanadium and sulfur for films deposited by the APCVD reaction of vanadium tetrachloride and hydrogen sulfide.
97	**Figure 4.7**	A plot of vanadium and sulfur composition by atomic percentage along a 2 cm line. On the film deposited at 500 °C by the APCVD reaction of vanadium tetrachloride and hydrogen sulfide.
98	**Figure 4.8a**	Scanning electron micrographs of films deposited by the APCVD reaction of vanadium tetrachloride and hydrogen sulfide at: a.) 300 °C, b.) 350 °C, c.) 400 °C with 0.5 dm^3 min^{-1} flow of hydrogen sulfide, and d.) 400 °C with 1.0 dm^3 min^{-1} flow of hydrogen sulfide.
99	**Figure 4.8b**	Scanning electron micrographs of films deposited by the APCVD reaction of vanadium tetrachloride and hydrogen sulfide at: e.) 450 °C and f.) 500 °C, g.) 550 °C and h.) 600 °C with 0.5 dm^3 min^{-1} flow of hydrogen sulfide.
100	**Figure 4.9**	An X-ray diffraction pattern recorded from the film deposited at 500 °C by the APCVD reaction of vanadium tetrachloride and hydrogen sulfide.
101	**Figure 4.10**	An X-ray diffraction pattern recorded from the film deposited at 600 °C by the APCVD reaction of vanadium tetrachloride and hydrogen sulfide.

102 **Figure 4.11** XPS results from a film deposited at 500 °C by the APCVD reaction of vanadium tetrachloride and hydrogen sulfide showing peaks for a.) vanadium, b.) oxygen, and c.) sulfur with d.) a plot of the atomic concentrations during argon etching of the surface.

103 **Table 4.12** Resistance measurements of the films deposited by the APCVD reaction of vanadium tetrachloride and hydrogen sulfide.

104 **Figure 4.13** Reflectance and transmittance spectra from a green region of the film deposited at 300 °C by the APCVD reaction of vanadium tetrachloride and hydrogen sulfide.

105 **Figure 4.14** Reflectance and transmittance spectra of the film deposited at 350 °C by the APCVD reaction of vanadium tetrachloride and hydrogen sulfide.

105 **Figure 4.15** Reflectance and transmittance spectra of the film deposited at 600 °C by the APCVD reaction of vanadium tetrachloride and hydrogen sulfide.

110 **Figure 5.1** Structure of TiS_2. Titanium atoms are represented by dark blue circles and sulfur as yellow.

111 **Figure 5.2** A schematic diagram of a thin film lithium/titanium disulfide cell on a glass substrate.

115 **Figure 5.3** Crystal structure of the iso-structural ZrS_3 showing the projection along (010) in figure 4.3a.) and a representation of two chains along the *b*-axis; with broken lines indicating inter-chain bonds.

116 **Table 5.4** Deposition and bubbler temperatures used during the APCVD reaction of titanium tetrachloride and hydrogen sulfide.

117 **Table 5.5** Descriptions of the visual appearance of films produced by the APCVD reaction of titanium tetrachloride and hydrogen sulfide.

118 **Figure 5.6** Schematic representation of two of the films deposited by the APCVD reaction of titanium tetrachloride and

hydrogen sulfide. These were deposited at a.) 400 °C and b.) 500 °C.

118 **Table 5.7** Resistance measurements of the films deposited from the APCVD reaction of titanium tetrachloride and hydrogen sulfide.

119 **Figure 5.8a** Raman spectrum recorded from the film deposited at 500 °C, 0.5 dm^3 min^{-1} hydrogen sulfide by the APCVD reaction of titanium tetrachloride and hydrogen sulfide.

120 **Figure 5.8b** Raman spectrum recorded from the film deposited at 600 °C by the APCVD reaction of titanium tetrachloride and hydrogen sulfide.

120 **Figure 5.8c** Raman spectrum recorded from the film deposited at 600 °C by the APCVD reaction of titanium tetrachloride and hydrogen sulfide.

121 **Table 5.9** Table of Raman bands recorded from films deposited by the APCVD reaction of titanium tetrachloride and hydrogen sulfide.

122 **Table 5.10** A summary of elemental analysis by EDX of titanium sulfide films produced by the APCVD reaction of titanium tetrachloride and hydrogen sulfide.

124 **Figure 5.11** Scanning electron micrographs of films deposited at: a.) 400 °C, b.) 500 °C c.) 600 °C with 0.5 dm^3 min^{-1} flow of hydrogen sulfide. d.) 500 °C with 1.0 dm^3 min^{-1} flow of hydrogen sulfide. These photos were taken of the films deposited by the APCVD reaction of titanium tetrachloride and hydrogen sulfide.

125 **Figure 5.12** An XRD pattern recorded from the film deposited by the APCVD reaction of titanium tetrachloride and hydrogen sulfide at 600 °C.

126 **Figure 5.13a** Reflectance and transmittance spectra of the black film deposited at 400 °C by the APCVD reaction of titanium tetrachloride and hydrogen sulfide.

126 **Figure 5.13b** Reflectance and transmittance spectra of the black film deposited at 500 °C by the APCVD reaction of titanium tetrachloride and hydrogen sulfide.

127 **Figure 5.13c** Reflectance and transmittance spectra of the grey region of the film deposited at 600 °C by the APCVD reaction of titanium tetrachloride and hydrogen sulfide.

128 **Table 5.14** Table of film adhesion data for coatings produced by the APCVD reaction of titanium tetrachloride and hydrogen sulfide.

129 **Table 5.15** Table of solubility data for coatings produced by the APCVD reaction of titanium tetrachloride and hydrogen sulfide.

133 **Table 6.1** Deposition and bubbler temperatures used during the APCVD reaction of chromyl chloride and hydrogen sulfide.

134 **Figure 6.2** Schematic representations of films deposited at a.) 400 °C and b.) 500 °C by the APCVD reaction of chromyl chloride and hydrogen sulfide.

135 **Table 6.3** EDX results for the films deposited by the APCVD reaction of chromyl chloride and hydrogen sulfide.

136 **Figure 6.4** Raman spectrum recorded from the film deposited at 600 °C by the APCVD reaction of chromyl chloride and hydrogen sulfide.

136 **Figure 6.5** Raman spectrum recorded from the film deposited at 550 °C by the APCVD reaction of chromyl chloride and hydrogen sulfide.

137 **Figure 6.6** Raman spectrum recorded from the film deposited at 400 °C by the APCVD reaction of chromyl chloride and hydrogen sulfide.

138 **Figure 6.7** Scanning electron micrographs of the films produced by the APCVD reaction of chromyl chloride and

hydrogen sulfide. At a.) 550 °C and b.) 600 °C with 0.5 dm^3 min^{-1} hydrogen sulfide flow.

139 **Figure 6.8** Reflectance and transmittance spectra of the film deposited at 400 °C by the APCVD reaction of chromyl chloride and hydrogen sulfide.

139 **Figure 6.9** Reflectance and transmittance spectra of the film deposited at 450 °C by the APCVD reaction of chromyl chloride and hydrogen sulfide.

145 **Figure 7.1** A schematic representation of SnS_2 with sulfur shown in yellow and tin in red.

146 **Figure 7.2** A schematic representation of the ribbon structure of Sn_2S_3 with sulfur shown in yellow and tin in red. The structure has trigonal-pyramidal tin(II) located at the edges of the ribbon and octahedral tin(IV) at the centre.

146 **Figure 7.3** A schematic representation of the structure of a layer of SnS with sulfur shown in yellow and tin in red.

148 **Figure 7.4** Raman spectrum of a film deposited at 300 °C by the APCVD reaction of tin tetrachloride and hydrogen sulfide.

149 **Figure 7.5** Raman spectrum of a film deposited at 525 °C by the APCVD reaction of tin tetrachloride and hydrogen sulfide.

149 **Figure 7.6** Raman spectrum of a film deposited at 545 °C by the APCVD reaction of tin tetrachloride and hydrogen sulfide.

150 **Figure 7.7** Raman spectrum recorded from the edge of the film deposited at 545 °C by the APCVD reaction of tin tetrachloride and hydrogen sulfide.

151 **Figure 7.8** Scanning electron micrographs of films deposited from the APCVD reaction of tin tetrachloride and hydrogen sulfide at a.) 300°C, b.) 450 °C, c.) 525 °C and d.) 545 °C.

153 **Figure 7.9** Raman spectrum of a film deposited at 450 °C by the APCVD reaction of tin tetrabromide and hydrogen sulfide.

154 **Figure 7.10** Raman spectrum of a film deposited at 525 °C by the APCVD reaction of tin tetrabromide and hydrogen sulfide.

154 **Figure 7.11** Raman spectrum of a film deposited at 600 °C by the APCVD reaction of tin tetrabromide and hydrogen sulfide.

156 **Figure 7.12** Raman spectrum of a film deposited at 450 °C by the APCVD reaction of tri-n-butyltin trifluoroacetate and hydrogen sulfide.

157 **Figure 7.13** Raman spectrum of a film deposited at 450 °C by the AACVD reaction of tetra(phenylthiolato) stannane and hydrogen sulfide.

158 **Figure 7.14** Raman spectrum of a film deposited at 500 °C by the AACVD reaction of tetra(phenylthiolato) stannane and hydrogen sulfide.

161 **Figure 8.1** Vapour pressure plots of the precursors used in this chapter. The blue line represents tin tetrachloride, the green line vanadium oxychloride and the red one vanadium tetrachloride.

163 **Table 8.2** Table of conditions used for the APCVD reactions of oxovanadium(V) chloride, tin tetrachloride and hydrogen sulfide.

164 **Table 8.3** Colours of films deposited from the APCVD reaction of tin tetrachloride, oxovanadium(V) trichloride and hydrogen sulfide. (Lists of colours are in order from inlet end to the exhaust end of the glass plate.)

165 **Figure 8.4** Raman spectrum of a film deposited by the APCVD reaction of $SnCl_4$ + $VOCl_3$ + H_2S at 350 °C. The ratio of $SnCl_4$ to $VOCl_3$ was 5:3.

166 **Figure 8.5** Raman spectrum of a film deposited by the APCVD reaction of $SnCl_4 + VOCl_3 + H_2S$ at 480 °C. The ratio of $SnCl_4$ to $VOCl_3$ was 1:1.

166 **Figure 8.6** Raman spectrum of a film deposited by the APCVD reaction of $SnCl_4 + VOCl_3 + H_2S$ at 470 °C. The spectrum was smoothed by averaging five adjacent points around each data point plotted. The ratio of $SnCl_4$ to $VOCl_3$ was 1:2.

167 **Figure 8.7** Raman spectrum of a film deposited by the APCVD reaction of $SnCl_4 + VOCl_3 + H_2S$ at 470 °C. The ratio of $SnCl_4$ to $VOCl_3$ was 1:2.

167 **Figure 8.8** Raman spectrum of a film deposited by the APCVD reaction of $SnCl_4 + VOCl_3 + H_2S$ at 575 °C. The ratio of $SnCl_4$ to $VOCl_3$ was 5:3.

168 **Table 8.9** Raman band positions for compounds identified on films deposited by the APCVD reaction of $SnCl_4 + VOCl_3 + H_2S$.[3,4,5] The notation a, b or c after the temperature refer to different spot analyses on the same sample.

169 **Table 8.10** A table of conditions used for the APCVD reactions of vanadium tetrachloride, tin tetrachloride and hydrogen sulfide.

170 **Figure 8.11** Raman spectrum of a film deposited by the APCVD reaction of $SnCl_4 + VCl_4 + H_2S$ at 400 °C. The ratio of $SnCl_4$ to VCl_4 was 1:2.

170 **Figure 8.12** Raman spectrum of a film deposited by the APCVD reaction of $SnCl_4 + VCl_4 + H_2S$ at 500 °C. The ratio of $SnCl_4$ to VCl_4 was 1:1.

171 **Figure 8.13** Raman spectra recorded from a film deposited by the APCVD reaction of $SnCl_4 + VCl_4 + H_2S$ at 600 °C. The spectrum labelled 'a' was at the edge of the substrate nearest the entrance to the reactor, with 'e' near the centre of the substrate. Raman spectra were recorded at different points along a line on the film

from the entry end towards the exhaust end of the reactor. The ratio of $SnCl_4$ to VCl_4 was 2:1.

172 **Figure 8.14** Raman spectra recorded from a film deposited by the APCVD reaction of $SnCl_4 + VCl_4 + H_2S$ at 600 °C. Raman spectra were recorded at different points along a line on the film from the entry end towards the exhaust end of the reactor. The spectrum labelled 'a' was at the edge of the substrate nearest the entrance to the reactor, with 'e' near the centre of the substrate. The ratio of $SnCl_4$ to VCl_4 was 1:2.

173 **Figure 8.15** Raman spectra recorded from a film deposited by the APCVD reaction of $SnCl_4 + VCl_4 + H_2S$ at 600 °C. The ratio of $SnCl_4$ to VCl_4 was 1:1.

174 **Table 8.16** Raman band positions for compounds identified on films deposited by the APCVD reaction of $SnCl_4 + VCl_4 + H_2S$.

180 **Figure 9.1** Plot showing the vapour pressure of oxovanadium(V) chloride against temperature.

180 **Figure 9.2** Plot of vapour pressure of vanadium tetrachloride against temperature.

181 **Figure 9.3** Plot of vapour pressure of titanium tetrachloride against temperature.

181 **Figure 9.4** Plot of vapour pressure of chromyl chloride against temperature.

182 **Figure 9.5** A vapour pressure plot of tin tetrabromide against temperature.

183 **Figure 10.1** Raman spectrum recorded from the film deposited by the APCVD reaction of vanadium tetrachloride and water at a deposition temperature of 500 °C.

185 **Figure 10.2** A Raman spectrum recorded from a film deposited at 500 °C by the APCVD reaction of oxovanadium(V) chloride and water.

186 **Figure 10.3** A Raman spectrum recorded from a film deposited at 600 °C by the APCVD reaction of chromyl chloride and water.

187 **Figure 10.4** A Raman spectrum recorded from a film deposited at 600 °C by the 180 s APCVD reaction of titanium tetrachloride and methanol.

187 **Figure 10.5** A Raman spectrum recorded from a film deposited at 500 °C by the 30 s APCVD reaction of titanium tetrachloride and propan-2-ol.

Acknowledgements

I would like to thank my supervisors Professors Robin Clark and Ivan Parkin for their help and ideas for this thesis. In addition I would like to acknowledge the Horsell fund for financial support, which enabled me to continue my studies.

My thanks go to Dave Morfett and Dave Knapp for maintenance of the APCVD rig and to Louise Price for teaching me how to operate it. In addition I would like to thank all other members of the Parkin group for useful discussions.

Thanks also go to members of the Clark group for their support and encouragement during my studies.

Finally thanks go to my Mum, Dad and brother for all their support during my studies at University.

Glossary

Adsorption, the reversible process by which atoms or molecules are attached to a surface by Van de Waals forces.

Atmospheric Pressure Chemical Vapour Deposition, APCVD, is a process leading to deposition of a thin film or powder from gas phase reactants (see CVD, below). APCVD occurs in systems in which the total gas vapour pressure is between 10^{-2} atm to a value in excess of atmospheric pressure; this allows the flow of gas via mass transport through the reactor, with reaction byproducts flowing out of the system leaving behind the coating or powder.

Background (in spectroscopy), this refers to the signal detected in a spectrometer with no input from the sample being studied. It is caused by noise in the electronic components of the detector, and may also be due to fluorescence of the sample, or stray-light entering the spectrometer.

Bubbler, this is a device to add solid or liquid precursors to the gas stream flowing through a CVD reactor. It consists of a heated vessel with a long internal inlet pipe and a shorter internal outlet pipe, which enables an inert gas to be bubbled through the contents. The inert gas leaving the bubbler contains vapour from the precursor, and the concentration of the precursor in the gas stream can be set by adjusting the temperature of the bubbler to alter the precursor vapour pressure. A diagram is shown in the Chapter 2 of this thesis.

Charge Coupled Device, CCD, this is a device that contains a radiation-sensitive semi-conductor. In the spectrometers used for the studies reported here the CCD's were sensitive to visible light. CCD's contain an array of metal oxide semiconductor capacitors which transfer charge, the amount transferred depending on the spectral region being scanned. The CCD is part of an electronic circuit that produces the output signal or spectrum.

Calibration is a procedure that combines experimental data and mathematical processing to calculate absolute data from arbitrary data.

Chemical Vapour Deposition, CVD, is a process leading to deposition of a thin film or powder from gas phase reactants. The various forms of CVD are discussed in chapter 1 of this thesis.

Coherent, a term used to describe waves that are in phase both temporally and spatially.

Desorption, this is the reverse of the process of adsorption.

Diode Array Detector, this consists of an array of light-sensitive semiconductor devices, which have different electronic properties when illuminated by visible radiation and allow an output voltage to pass creating a signal that is turned into a spectrum.

Doping is a process of incorporating small known amounts of another material into an otherwise pure compound; it is done to modify the behaviour of the bulk material.

Excitation line, a term used to refer to a monochromatic emission from a laser, and which may be used as a light source to cause inelastic scattering in Raman spectroscopy.

Fourier transformation, FT, is a mathematical process which can be used to extract spectroscopic information from the interaction of electromagnetic radiation with matter. See Michelson interferometer below for further explanation.

Fluorescence, is a process in which electromagnetic radiation is absorbed by a molecule causing an electron to be promoted to a higher energy level; this produces an unstable excited state. The excited atom or molecule loses its excess energy as the electron drops back to its original state with the emission of electromagnetic radiation of longer wavelength than that of the incident radiation.

Four-way valve, this is a valve with two separate sets of inlet and outlet pipes at 90° to one another. The flow through each of these pipes is independent of that through the other. This is clarified in the diagram shown in Chapter 2.

Franck van-der-Merwe growth, is the name given to describe the process of layer-by-layer deposition. Layers are deposited when atoms or molecules deposited have stronger bonds to the substrate than their intralayer bonding. Epitaxial growth, leading to lattice matching with the substrate is possible where Franck van-der-Merwe growth occurs.

Grating, (diffraction grating) in spectroscopy. This is a device with a large number of equally spaced parallel lines ruled on its surface. A diffraction grating is used to produce spectra by diffraction and may be used to measure wavelength.

Horizontal bed cold-wall design, as used in this APCVD study. This term refers to the reactor in which the substrate was placed for coating. The reactor consists of a horizontal bed, which contains heater cartridges to heat the substrate, which is placed on top of it during the deposition process. The reactor itself however is contained in an unheated quartz tube, so has a 'cold' wall, heated only by radiation from the substrate heater block and convection via the gases flowing through the system.

Heat mirror is a term that describes a material which transmits visible radiation and reflects infrared radiation.

Inelastic scattering is caused by interaction between incident radiation and matter. This occurs in Raman spectroscopy and causes scattering of radiation of a different frequency from that entering the system. This is described in further detail in chapter 1.

Irradiance is a measure of the flux of electromagnetic radiation incident on a surface per unit area, and is measured in Joules per square metre.

Interference occurs when coherent waves, of approximately equal intensity interact with each other. This can be constructive, where the waves are in-phase and so reinforce each other, or destructive where the waves are out-of-phase. With visible light this effect causes bands of light and dark to be formed where constructive and destructive interference is caused respectively.

Interferogram, a signal produced by the interaction of two waves giving rise to an interference pattern with intensity oscillating with respect to time.

Illuminated manuscripts are handwritten documents that are decorated with coloured ink, paintings and sometimes gold.

in vacuo, in vacuum.

LPCVD, low pressure chemical vapour deposition. LPCVD describes a process of CVD that occurs in a sealed system at low pressure, *c.* 0.001 atm. Film deposition therefore occurs at a lower rate, *c.* 1 $\mu m\ h^{-1}$, *cf.* 1 $\mu m\ min^{-1}$ for APCVD.

Michelson interferometer, (in FT spectroscopy). Light transmitted or reflected by a sample is directed into a Michelson interferometer where it is split into two beams. Variation of the path length of one of these beams causes an interference pattern. The resulting interferogram, formed by the recombination of the beams may then be turned into a spectrum by Fourier transformation.

Monochromatic light is light consisting of a single wavelength.

Microelectronics are electronic devices consisting of extremely small components.

Miller indices are used in crystallography. Miller indices are the reciprocals of intersection distances between crystal planes and the unit cell of a crystal lattice.

Noise, in spectroscopy. Spurious unwanted energy detected by a spectrometer and giving a random and varying signal.

Notch-filter, a device used in Raman spectroscopy to reduce substantially the Rayleigh scattered radiation reaching the detector.

Optical path length, the distance light scattered from a sample travels through a spectrometer before reaching the detector.

Optoelectronics, electronic devices, which incorporate the use of light in addition to electron conduction.

Photo-multiplier tubes, may be used as detectors in spectrometers. Photomultipliers have a light sensitive surface, on which photons eject electrons; these electrons are then accelerated through a potential difference to another screen. The second screen repeats the process causing a cascade reaction with electrons going on to hit other screens. The current at a final screen may be used in an external circuit, which produces a spectrum by recording the intensity of the signals received at different wavelengths.

Plasma lines, the term used to describe laser lines in addition to the Rayleigh line appearing in a Raman spectrum.

Photo- degradation, chemical reactions initiated by light. These can lead to chemical changes in samples during Raman analysis.

Physical deposition, processes that deposit films or powders by physical rather than chemical means, e.g. sublimation, or evaporation followed by condensation.

Pigments, strongly coloured compounds, which may be used to decorate objects (when painted or glazed).

Pixel. The smallest element forming an image on a screen. When magnified it appears as a single dot.

Precursors, a term used to describe reactants in a CVD system.

Rayleigh line, radiation which has been elastically scattered by a sample and appears at 0 cm^{-1} on a Raman spectrum.

Resolution, a measure of the ability to distinguish two independent objects or features placed side by side.

Rig, a term used to describe the collection of components joined together, including pipework, bubblers, reactor, etc, used to deposit a thin film by CVD.

Reactor, the quartz tube containing the heater block on which the substrate is placed during deposition.

SiCO (a compound containing silicon, carbon and oxygen,) is a material deposited onto glass as a thin film by Pilkington. This is done to prevent diffusion of metal ions from the glass substrate into additional thin films deposited on to the substrate by chemical vapour deposition.

Stray light, a term referring to any light in a Raman spectrometer other than Rayleigh or Raman scattered light.

Spatial resolution, the ability to identify separately two objects placed side by side.

Spectral response, the component of the output of a spectrometer which is instrument rather than sample specific.

sp^3 hybridisation, the combination of one s- and three p-orbitals of similar energy to yield four equivalent hybrid orbitals. These hybrid orbitals are arranged in the shape of a tetrahedron.

Sputtering is a process of evaporation of molecules from a cathode caused during the discharge of electricity through a gas.

Sublimation is the transition of a substance from the solid state to the gaseous state, without melting to produce a liquid.

Substrate, in CVD. An object that is placed in a CVD reactor with the intention of depositing a film on its surface.

Stranski-Krastanov growth is a film growth mechanism which produces layers with islands.

Thermal degradation is a result of the thermal initiation of chemical reactions. This is an important consideration in Raman analysis as the sample in the laser beam may heat up.

Thin films are thin coatings deposited on a substrate to alter the surface properties of the material. They lie between a monolayer and tens of micrometres thick.

Tribological coatings are coatings added to a substrate to alter its coefficient of friction, or to protect its surface from wear due to abrasion.

Volmer-Weber pattern of growth. These lead to films consisting of discrete 3-D islands on the initial nucleation sites if the deposition is stopped before the islands coalesce.

1.0 Chapter – Introduction

1.1 The aim of this study

The aim of this study was to produce novel thin films of vanadium oxides, sulfides and oxysulfides and chromium oxysulfides by atmospheric pressure chemical vapour deposition (APCVD); and to show the suitability of Raman microscopy for the characterisation of coatings produced by APCVD.

1.2 History of the Raman effect

C.V. Raman and his co-worker K.S. Krishnan first observed the effect, which is now known as the Raman effect, and is the basis of Raman spectroscopy.[5] Two Russians, Landsberg and Mandelstam also independently reported the same phenomenon, however their report was published after Raman's paper.[6] Raman was therefore credited with the experimental discovery. Raman initially noticed the effect of inelastic light scattering using solar radiation focused onto a sample. He found that focused light on a pure sample held between complementary filters was not fully extinguished, as it would be if it remained unchanged on passing through the sample.[5]

1.3 Developments in Raman spectrometers

1.3.1 The excitation source

Raman initially noticed the effect of inelastic scattering using solar radiation focused onto a sample. The first artificial source of excitation energy used to produce a Raman spectrum of a compound was a mercury discharge lamp. The advantages of the use of a discharge lamp to produce spectra were its availability and high irradiance at certain narrow bands of wavelengths, rather than consisting of a broad continuum of emission. However, the main problem with using a mercury lamp was interference caused by a multitude of plasma lines (other atomic emission lines), some of which are strong enough to cause secondary Raman spectra (Raman spectra caused by another wavelength, superimposed onto the first spectrum). These had to be filtered out to achieve a usable excitation source. Another problem was the requirement of long accumulation times to record useful spectra of many compounds due to the low

intensity of light produced by the lamp. Spectra might take hours to record rather than minutes if a brighter light source such as a laser were used.

The invention of lasers has improved the quality of spectra that can be recorded in a given time. The irradiance of monochromatic laser light can be used to record a Raman signal. This enables spectra with higher signal-to-noise ratios to be measured. The use of more intense excitation provided by lasers allows better stray light rejection by use of longer optical paths incorporating triple grating optics. It is also easier using polarised laser light to conduct polarisation studies to identify symmetric vibrational modes of molecules. However, it is only recently that cheaper and often air-cooled lasers suitable for Raman spectroscopy have been available. Prior to the availability of smaller lasers, the lasers used in laboratories were large and had to be cooled by water circulating around the laser tubes. This meant that the use of laser Raman spectroscopy was limited to relatively few, generally academic, groups rather than being adopted as a routine analytical method used in industry. The use of infrared lasers enables Fourier Transform (FT-) Raman spectrometers to be used for analysis; other sources of infrared radiation such as heated wires or ceramics are not appropriate for Raman spectroscopy as they emit a continuum of radiation. The use of FT spectrometers means that fluorescence is avoided, or at least reduced, for most samples because infrared excitation has less energy per photon than visible light so is less likely to cause fluorescence; such spectrometers allow the analysis of compounds that have proved difficult to study using visible excitation.

1.3.2 The spectrometer

The spectrometers used for Raman spectroscopy have improved in quality since 1930. When prisms were used to separate out light of different wavelengths, the Rayleigh line could be separated out from the Raman scattered light. Modern spectrometers use notch filters to reduce the intensity of the Rayleigh line. This protects the detector from saturation, which could lead to permanent damage, but it also causes variations in the signal intensity near the Rayleigh line. Most spectrometers using notch filters to reject the laser line yield reduced band intensities below *c.*150 cm^{-1}. Even the best notch filters reduce band intensities between ± 30 cm^{-1} of the excitation line, whereas good triple grating spectrometers may allow spectra to be recorded to *c.* ± 3 cm^{-1} from the excitation line (for gaseous oxygen).

The advantage of using modern Raman spectrometers is that they are smaller due to their shorter optical paths, thereby allowing a greater signal throughput than with older instruments. The new spectrometers therefore allow spectra to be recorded of even some weakly Raman scattering compounds, with the speed of data collection being much faster than before.

FT spectrometers use infrared laser excitation, such as that produced by a Nd:YAG laser, with a Michelson interferometer. This allows the analysis at 1064 nm of organic compounds that fluoresce when visible excitation is used because quanta of 1064 nm light have a lower energy than quanta of visible light, so are less likely to excite fluorescence in the sample. This leads to Raman spectra with lower background counts due to lower fluorescence. In addition, as infrared photons have a lower energy than those of visible light, samples are less likely to undergo photodegradation but are more likely to be thermally degraded. The sample may heat up due to the increased laser power required to produce a spectrum. Therefore a cold cell may be required to protect the sample.

The addition of a microscope to the optics allows analysis with a spatial resolution of *c.* 1 μm. That means that, when using a microscope, Raman spectra may be resolved for different compounds in a mixture if the particle sizes are greater than 1 μm; if not the spectrum is a sum of the Raman spectra of all of the compounds together. A schematic diagram of a Raman microscope set up is shown in Chapter 2.

1.3.3 The detector

The first type of detector used to record Raman spectra was a photographic plate. This was cheap and readily available to many laboratories in the 1930s, but photographic plates require time and skill to develop. This was important as damage to a plate might mean that the many hours spent recording the spectra had been wasted. Later, photomultiplier tubes were used as detectors; these record the signal one spectral element at a time, and so the time taken to record an entire spectrum was dependent on the intensity of scattered radiation at the detector and the resolution required.

Diode array detectors record data in blocks of several hundred cm^{-1}, with resolution being determined by the optics of the spectrometer and the number of diodes for each block of the spectrum. The resolution of spectra recorded on the recent spectrometers

using charge coupled device (CCD) detectors is limited by the reduced optical path length, and the size of the pixels of the CCD itself.

As can be seen above the choice of components used for a spectrometer depends on many factors. Therefore the spectrometer chosen must be suitable for the tasks required in an experiment. The use of Raman spectroscopy is becoming more widespread today because of the production of Raman spectrometers/microscopes that are easy to use and provide results more quickly than was possible previously.

1.4 Theory of the Raman effect

It is possible to induce a dipole in a molecule by the application of an electric field gradient, which can be achieved with electromagnetic radiation. The dipole induced will have frequencies caused by changes in electrical, vibrational and rotational energies, however only the vibrational changes are of interest in this study. The induced dipole in a vibrating molecule will have frequencies, ν_0, $\nu_0 + \nu_{vib}$ and $\nu_0 - \nu_{vib}$, where ν_0 is the frequency of the exciting radiation and ν_{vib} is a frequency of vibration of the molecule. Scattered radiation with the frequency ν_0 is called Rayleigh scattering, radiation with the frequency $\nu_0 + \nu_{vib}$, is called anti-Stokes Raman scattering, and $\nu_0 - \nu_{vib}$ called Stokes Raman scattering. The Stokes Raman bands are always more intense than the anti-Stokes Raman bands, due to the population of vibrational states of molecules. Under normal circumstances, the lower energy states of molecules will have a higher population than higher energy ones. The relative population of an energy level is given by the Boltzmann distribution:

$$\frac{n'}{n} = \frac{g'}{g} \exp(-\Delta E / kT) \qquad \text{Equation 1.1}$$

where n is the population, g is the degeneracy, and ′ denotes the upper level. ΔE is the energy difference between two energy levels $\nu_0 + \nu_{vib}$ or $\nu_0 - \nu_{vib}$.[7]

Raman scattered intensity depends on the irradiance of the excitation source, the volume of the sample irradiated by the source and the degree of covalency for each bond, and

therefore also of the identity of each molecule. The intensities of Raman bands also depend on the concentration of the sample analysed, if the sample is in solution or in the gas phase, or on the amount/thickness of the sample in the solid state. Additionally the experimental intensities of Raman bands depend on the alignment of the laser beam and of the scattered radiation through the spectrometer.

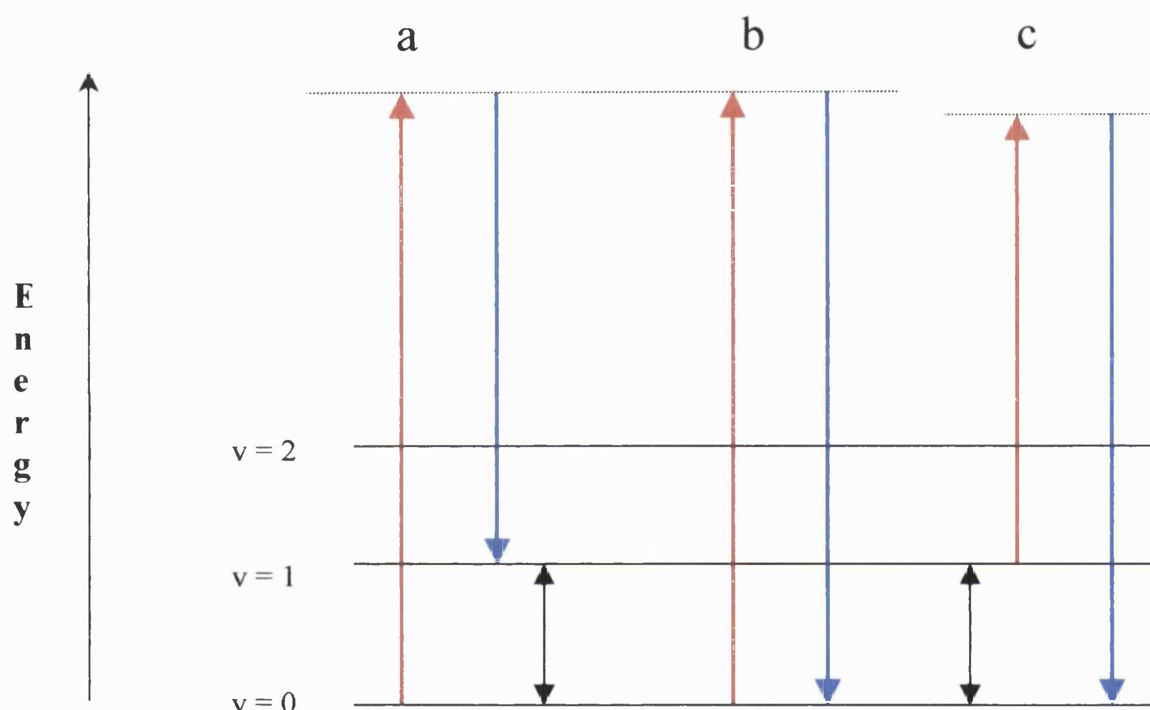

Figure 1.1 a.) a Stokes Raman transition, b.) a Rayleigh transition, c.) an anti-Stokes Raman transition. The incident radiation is depicted in red, the scattered radiation is depicted in blue and the energy difference between these, where applicable, is depicted in black. The black line represents a Raman transition of energy $h\nu$. The dashed line depicts the presence of a virtual state. The virtual state has the energy of the photon and the molecule as they interact during the process of Raman scattering. The incident radiation has an energy of $h\nu_0$, Stokes scattered radiation has an energy of $h(\nu_0 - \nu)$, and anti-Stokes scattered radiation has an energy of $h(\nu_0 + \nu)$.

1.5 Theory – molecular vibrations

The simplest view of molecular vibrations comes from considering a diatomic molecule, with a chemical bond being treated as two masses separated by a spring. This allows

the application of Hooke's law, which results in the so-called harmonic model of vibrational frequencies.

$$F = kx \qquad \text{Equation 1.2}$$

where F is the force, in N, that restores the masses to their equilibrium position on displacement, k is the force constant in N m^{-1}, and x is the displacement in m.

Using the above formula the vibrational frequency of a diatomic molecule is given by the formula:

$$\nu = \frac{1}{2\pi} \frac{\sqrt{k}}{\sqrt{\mu}} \qquad \text{Equation 1.3}$$

where μ is the reduced mass:

$$\mu = \frac{m_1 m_2}{m_1 + m_2} \qquad \text{Equation 1.4}$$

This harmonic model is only an approximation to real molecular behaviour as vibrations are in fact anharmonic. The vibrational energy levels of a molecule are quantised.[7] The calculations for real molecular vibrations are much more complicated than implied by the above formulae, however these formulae may be used to estimate vibrational frequencies for real molecules.

1.6 Previous Raman studies of thin films

1.6.1 Raman analysis of thin films for technological uses

Many compounds have been produced as thin films. Many have also been produced using chemical vapour deposition (CVD), rather than by the other physical deposition processes mentioned in this chapter. To reduce the number of examples given here only thin films produced by CVD and studied by Raman spectroscopy will be mentioned. A search of the Chemical Abstracts (CAS) database was performed using SciFinder covering the years 1969-2000. A search for abstracts that mentioned Raman, thin films

and CVD found 469 entries. The most frequently mentioned films are discussed first; these include diamond-like and silicon coatings.

Silicon films have been produced for several applications such as solar cells in which the films contain crystalline silicon granules with diameters >0.05 μm. Solar cells contain an n- or p-doped layer of the thin hydrogenated crystalline silicon film, and can be prepared by chemical vapour deposition at 100 - 500 °C. These solar cells have high energy conversion efficiency.[8]

Raman spectroscopy has been used to study the composition of the species formed in the gas phase, during laser enhanced chemical vapour deposition (LECVD) of silicon and silicon carbonitride thin films. The increase in the temperature of species found in the gas phase in the reaction zone may be deduced from total density measurements. If the gas phase composition is recorded at different heights in the reaction zone the flow profile of the reactants and the formation of reaction intermediates may be studied. The Raman spectra of the reactants indicate that, in this particular set-up, molecular species are detectable at the 100-1000 ppm level at room temperature. Raman spectroscopy may therefore be used to study reaction kinetics and pathways during the deposition of thin films.[9]

Diamond-like thin films have been produced and studied by Raman spectroscopy for a diverse range of applications including tribological coatings to reduce friction on a surface, heat sinks for use in semiconductors and protective optical coatings.[10] Raman spectroscopy is useful in determining the hybridisation of carbon because the exact Raman band positions vary between sp^2 hybridisation as it occurs in graphite and sp^3 hybridisation, which occurs in diamond. Stuart *et al.* have also shown that there is a variation in the Raman band shape for diamond-like films, which is due to crystallographic orientation. Stuart recorded spectra of isolated diamond crystals which had been deposited on wire tips by CVD. Raman spectra of the [100] and [111] surfaces were recorded by focusing the laser spot onto the adjacent [100] and [111] growth faces of the same crystal.[10] This shows that for certain materials Raman spectroscopy may be used to determine crystal orientation in deposited films. This may be done non-destructively and with good spatial resolution if Raman microscopy is used to analyse thin films.

Alers *et al.* have reported using a correlation between Raman scattering and thermal expansion to assess the quality of thin films of diamond produced by CVD for use in high temperature applications. Data were reported for both a natural single crystal of diamond and a thin diamond-like film. Alers reported using Raman measurements to determine the linear thermal expansion coefficient of diamond in the temperature range 20-600 °C. Producing comparable data is difficult because diamond-like films are polycrystalline; however Raman spectroscopy provides a useful indication of how good an approximation a film may be to natural diamond.[11]

Fan *et al.* reported that Raman spectra of diamond-like films deposited on titanium-coated copper substrates change with film thickness. With an increase in the film thickness the characteristic Raman band of diamond at $\geq$ 1337 cm^{-1} shifts to a lower wavenumber, approaching 1332 cm^{-1}. [12,13,14] This would suggest that the thickness of the film could be correlated with the Raman band wavenumber.

Raman spectroscopy has been used by several groups to identify the composition of vanadium oxide thin films. Okuhara *et al.* reported using vanadium oxide thin films deposited on silica substrates by CVD for the oxidative dehydrogenation of alcohols. Raman spectra of the films showed that they were single phase V_2O_5.[15] McGraw *et al.* reported on investigations of thin-film cathodes of vanadium oxide prepared by different synthetic techniques. Raman spectroscopy was used to identify the composition of all films. [16]

1.6.2 Raman microscopy used for manuscript analysis

Raman microscopy can also be used to analyse thin films of pigments, such as those found on illuminated manuscripts, decorated pottery and paintings. Many other techniques have been used for this analysis, for example scanning electron microscopy (SEM), X-ray fluorescence (XRF) and X-ray diffraction (XRD). These methods of analysis are usually intrusive, involving sampling which is not desirable even if the sample remains unchanged by the analysis. In addition, of these techniques only XRD is compound specific; it does, however, usually require the removal of *c.* 5 – 10 mg of material for analysis, which may not be possible for certain art objects.

A non-intrusive analytical technique which is compound specific is required for the analysis of pigments or degradation products on art objects. Raman microscopy is both non-intrusive, as measurements may be made *in-situ*, and compound specific. The principal difficulty with the technique lies in the possible laser-induced thermal, or photo-degradation of the sample. This can be avoided by the use of the lowest possible laser power or by choice of the most suitable excitation wavelength, i.e. either by use of infrared excitation or by matching the colour of the laser light used to the colour of the sample so as to minimise light absorption which would lead to localised heating at the laser spot. Fluorescence may be avoided by using a different wavelength or by recording an anti-Stokes Raman spectrum. The use of anti-Stokes Raman scattering is limited by the intensity of scattering, which is lower than that of Stokes Raman scattering, such that bands at >800 cm^{-1} are very weak and may be missed.

Raman microscopy is potentially a very important tool for conservators because an understanding of the underlying chemical problems of an art object can lead to methods of protecting it from further damage. It is also important to identify the original pigments used when restoring paintings, etc. This prevents future problems of pigment compatibility, i.e. making sure that the pigments used will not react with one another to form compounds that are a different colour.[17]

1.7 Chemical vapour deposition history and theory

1.7.1 Definition

Chemical Vapour Deposition (CVD) is a chemical process that leads to the production of a thin film by the reaction of gaseous reactants to produce a solid product.[18]

1.7.2 History of chemical vapour deposition

The earliest example of CVD (Blocher, 1966)[18] is probably that of condensed soot produced by burning wood. The soot was collected and used in some prehistoric art. It was a similar process that led to an early patent for a CVD process being granted to John Howarth *c.*1880[18] for a process of making the pigment carbon black. Early industrial processes employing CVD were: the production of carbon lamp filaments

(Sawyer and Mann 1880)[18], metal lamp filaments (Aylsworth 1896), the purification of nickel (Mond 1890, 1891)[18] and the production of silicon from the reaction between hydrogen and silicon tetrachloride (Pring and Fielding, 1909).[18] The production of thin films of silicon led to its use as a semiconductor in electronic devices. Many semiconducting materials are now produced by CVD, developments in which are generally led by the requirements of industry. The four main industrial uses of CVD to produce thin films are microelectronics, optoelectronics, protective or decorative coatings and optical coatings.[18]

1.7.3 Theory of CVD

Atmospheric Pressure (AP)CVD is performed in a rig with gas flow through the system between atmospheric pressure and 10^{-2} torr to allow gas transport. A schematic diagram of an APCVD rig is shown in figure 2.4 in Chapter 2. This is different from low pressure CVD which takes place in a closed system with an internal pressure below 10^{-2} torr. Liquid and solid precursors are admitted to the system via a bubbler as described in Chapter 2.

As APCVD was used for the studies in this thesis it will be described in detail below. The physical and chemical steps involved in APCVD are as follows:

1. Flow of precursors through the rig to enable preheating to occur before reaching the reactor. Gas phase reactants, for example H_2S, which are stored in pressurised cylinders, may be admitted directly into the gas stream. Liquid or solid phase reactants, however, must be vaporised, which can be achieved by using a bubbler (described below), before entering the gas stream.
2. Mass flow from the reactor inlet to the deposition zone.
3. Gas phase reactions leading to the production of the material to be laid down as a film or precursors of the film and reaction byproducts which will not be incorporated into the film.
4. Mass flow of precursors onto the substrate.
5. Adsorption of film precursors onto the substrate.
6. Diffusion across the substrate surface to film nucleation and growth sites.
7. Incorporation of product molecules into the growing film.

8. Desorption of reaction by-products from the substrate.
9. Mass transport of by-products and unreacted precursors from the reactor to the exhaust.

These steps are summarised in figure 1.2 below.

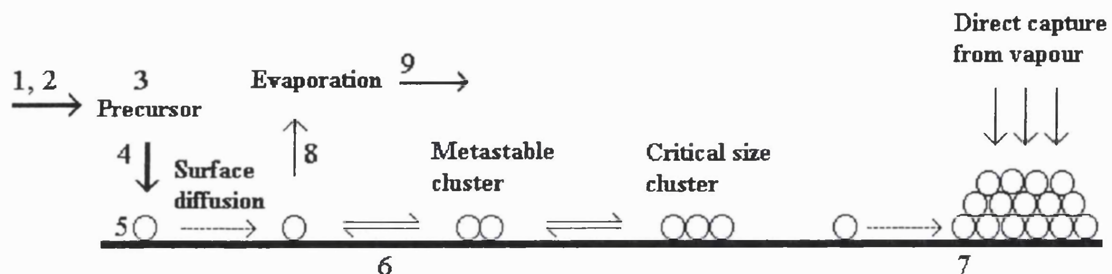

Figure 1.2 A schematic representation of processes leading to 3-D nucleation and film growth.[19]

If the contents of the bubbler are at thermodynamic equilibrium, the flow rate of the precursor (F) is given by the following equation

$$F = \frac{F_{carrier\ gas}\ P}{(P_{total} - P)} \qquad \text{Equation 1.5}$$

where P is the partial pressure of the precursor. It is likely that thermodynamic equilibrium will be reached with liquid precursors, but solid sources are more difficult to control. Pipes carrying reactants that are not a gas at normal temperature and pressure must be heated to prevent these reactants from condensing. It is also important that materials used in the construction of the rig do not corrode too rapidly. Pipes are made from stainless steel with high temperature plastic (Vespel) inserts, which are made from a polymer which is inert, and will not melt at the temperatures used for CVD.

It is important that precursors do not mix too far ahead of entry to the reactor, as this could lead to prereaction, and a blockage in the pipe going into the reactor. It is also important that the precursors are able to mix in the reactor. When using a high flow rate of carrier gas, precursors admitted to the rig might not have a long enough residence time in the reactor to adsorb on the surface to give an even coating. Unreacted precursors could then go on to react in the exhaust pipework, which again could lead to a blockage; to minimise the chances of this occurring the exhaust is heated during a reaction.[18]

1.7.4 Growth mechanisms

The patterns of growth of thin films deposited by CVD can be explained by three growth mechanisms, figure 1.3 (a) represents the Volmer-Weber pattern of growth, which can lead to films consisting of discrete 3-D islands on the initial nucleation sites if the deposition is stopped before the islands coalesce. Volmer-Weber growth occurs if atoms in the film form stronger bonds to each other than they do to the substrate, e.g. Si growth on insulators like SiO_2. Volmer-Weber is also a common growth mechanism for metal films on insulating substrates.

Figure 1.3 (b) represents an intermediate mechanism called Stranski-Krastanov growth which produces layers with islands. Initially one or two monolayers are deposited before growth switches to form islands as this mechanism becomes more favourable.
Figure 1.3 (c) represents a film formed by a layer deposition mechanism called Franck van-der-Merwe growth, in which layers are deposited when the atoms or molecules deposited have stronger bonds to the substrate than is their intralayer bonding. Epitaxial growth, leading to lattice matching with the substrate is possible where Franck van-der-Merwe growth occurs. The three growth patterns are represented below.

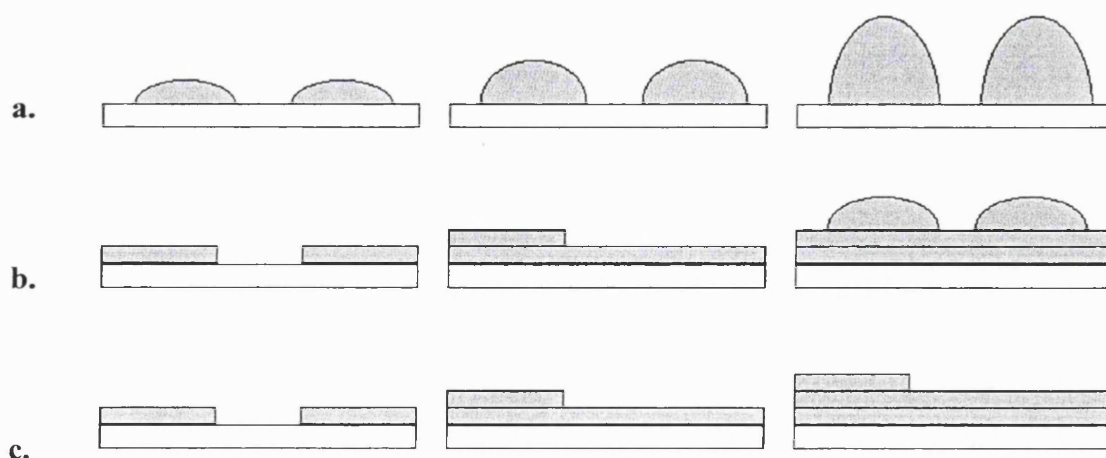

Figure 1.3 A schematic diagram of film growth mechanisms.

Substrate temperature, composition of the gas phase, and total gas pressure over the substrate affect the growth rate and type of film deposited. Control of these factors also gives control over surface diffusion and nucleation processes on the substrate which in turn allow the final stoichiometry of the product to be controlled. Films deposited at

low temperatures and at high growth rates may be amorphous, where the rate of surface diffusion is low with respect to the supply of precursors to the surface. The converse of this leads to crystalline film growth.

1.7.5 Growth rate of films

The growth rate of films produced at temperatures below 600 °C is controlled by the kinetics of the reaction and increases exponentially with temperature as described by the Arrhenius equation:

$$k = A\,e^{-E_a/RT} \qquad \text{Equation 1.6}$$

E_A is the apparent activation energy, R is the gas constant and T is the temperature of the substrate. The growth rate at temperatures above 800 °C may decrease due to increased rate of desorption and the development of competing reaction pathways. The increased rate of gas phase reactions at higher temperatures can lead to the formation of powders. The growth rate of a film produced by low pressure CVD depends on the Arrhenius equation. The growth rate of a film produced by APCVD also depends on the rate of mass transfer.

The reactions employed in producing coatings by CVD usually require energy activation at the substrate to produce a thin film. The activation energy may be supplied thermally, by electromagnetic radiation or by a plasma. Some of the methods of producing thin films are described below.

1.7.6 Thermal CVD

The substrate is heated to provide activation energy at the surface to be coated. Thermal activation may be achieved by direct resistive heating if the substrate is an electrically conducting material. This leads to a reactor with 'cold' walls because, although the walls do get warm, they are not heated intentionally. Radio-frequency induction heating can be used if the substrate is conducting or placed on a conducting block or 'susceptor'. Electromagnetic radiation from a bright lamp or a laser may also be used to heat the substrate. The use of light to heat the substrate requires that the reactants are transparent to the wavelength used in order to prevent powder formation caused by reaction above, rather than on, the surface of the substrate. The use of a laser to heat the

substrate can lead to patterns being deposited by moving the beam, leading to deposition only on areas that have been heated. The use of a laser to heat small regions of the substrate also leads to the possibility of using a sealed system rather than a flow cell arrangement. The use of cold walled reactors leads to the production of films that are controlled by transport of reactants to the substrate. This can lead to uneven coatings, which may not cover all of the substrate. The use of a hot–walled reactor, in which the reactor is placed inside a furnace, leads to a more even substrate temperature. Kinetic product control is possible in a hot–walled reactor; however, as the entire reactor is at thermal equilibrium, all surfaces inside the reactor, including those of the reactor, are coated.

1.7.7 Aerosol Assisted CVD

Aerosol assisted (AA)CVD uses a piezoelectric device to create an aerosol from a solution of the precursor, the aerosol being then transported to the reactor where it produces a film on a heated substrate. The aerosol is produced at room temperature and the rig pipework does not require heating, as this would cause the solvent to evaporate rather than form an aerosol including the precursor. AACVD may be used to produce films from heat sensitive precursors as the only hot area of the rig is the reactor.

1.7.8 Plasma Enhanced CVD

Plasma enhanced CVD (PECVD) uses a plasma to initiate a reaction on the substrate. The plasmas may be produced using radio frequency or microwave radiation. PECVD uses lower deposition temperatures than standard thermally activated CVD, but there are more variables to control film deposition, including reactor dimensions and plasma properties.

1.7.9 Photo CVD

Photo- or photo-assisted CVD employs a source of electromagnetic radiation to apply activation energy directly to reactants rather than the substrate. As with thermal CVD, use of a laser can enable patterns to be produced by scanning the beam over the substrate.

1.8 Possible applications of the films produced in this study

The principal applications for films produced on glass substrates are as coatings on window glass, or for use in semiconducting devices. Window glass may be coated with a transparent thin film that acts as a solar control coating, letting visible light in but reflecting ultra-violet light. Semiconducting thin films may also be deposited onto glass substrates for applications such as batteries with high energy density, see diagram in Chapter 5 figure 5.2.

1.8.1 Heat-mirrors

Heat mirrors allow the transmission of visible light, but block ultra-violet radiation, i.e. for use as window glass. They keep heat in a room by reflecting infrared radiation back into the room. This is shown in figure 1.4. Figure 1.5 below shows the region of the electromagnetic spectrum of interest.

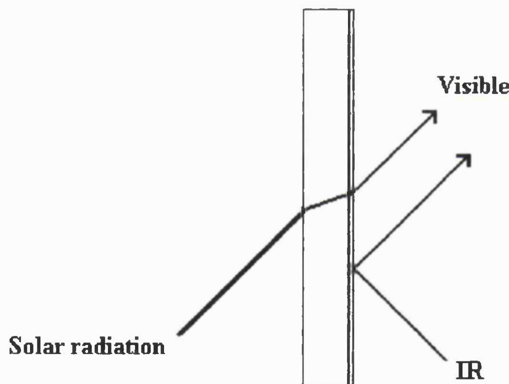

Figure 1.4 Diagram of a perfect heat mirror showing how the coating depicted in grey on a transparent glass substrate behaves when illuminated by solar radiation.

Figure 1.5 The visible region of the electromagnetic spectrum.[20]

The idealised spectrum below in figure 1.6 shows the required reflectance and transmittance spectra for a heat mirror. Figure 1.7 below shows that prior to receiving a coating the glass substrate does not act as a heat mirror.

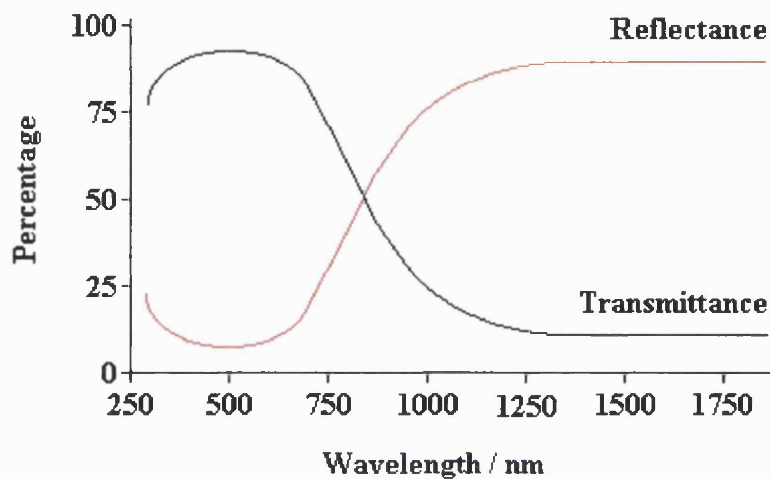

Figure 1.6 Graph showing the reflectance and transmittance profiles for a perfect heat mirror.

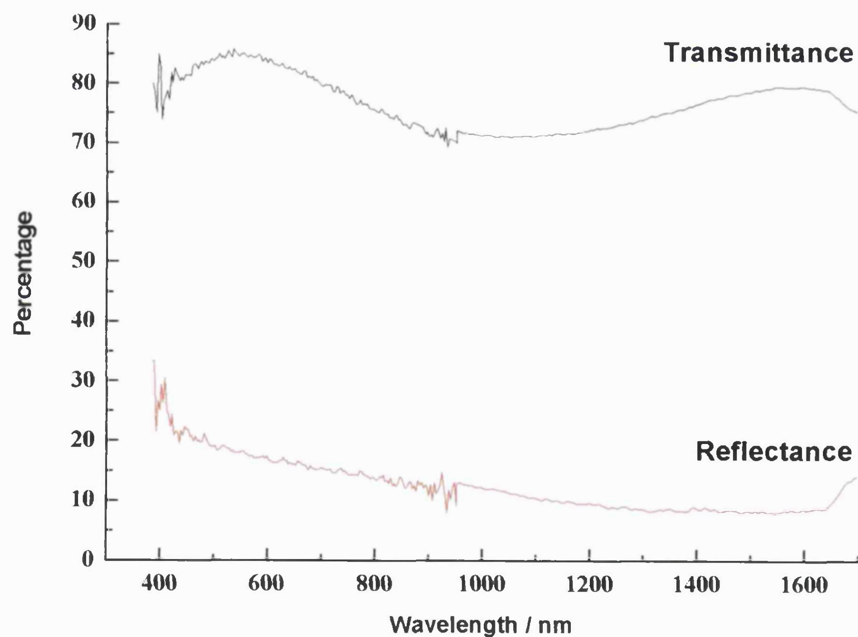

Figure 1.7 A graph showing the reflectance and transmittance profiles of a glass substrate supplied for use in these studies by Pilkington.

1.9 X-ray diffractometry

X-ray powder diffractometry allows the identification of substances in the solid-state by comparison of the positions and intensities of diffraction lines with those stored in a database. The powder diffraction file is maintained by the Joint Committee on Powder Diffraction Standards, JCPDS, whose database has over 30,000 entries. Powder diffraction data may be used to establish the identity of an unknown compound or to determine the phase diagram of a compound, although the latter was not done in the studies described here. It is in principle possible to quantify the amounts of each phase present in a mixture. It is this analytical method which is used to identify the constituent compounds in thin films; this is because the films consist of many crystallites, so single crystal X-ray diffraction is inappropriate.

The Debye-Scherrer method uses monochromatic radiation to analyse a powdered sample. In a powder, crystallites are assumed to have random orientation, therefore some of the crystallites will obey the Bragg law, $\lambda = 2d \sin\theta$ for each value of d. Each crystal plane should be represented in the diffraction pattern as there should be a number of crystals orientated correctly for each diffraction angle. The diffracted radiation travels away from the sample in a cone shape. If a strip of film or a solid state detector is used to record these cones in the same plane as that of the incident radiation, a series of lines with varying intensities will be produced. The powder patterns produced this way may be used as a 'fingerprint' to identify compounds.

It is possible to determine the unit cell dimensions from an X-ray powder diffraction pattern. Each reflection corresponds to a different value of θ, and each value of θ corresponds to a different spacing in accordance with Bragg's law.[20] If the Miller indices are also known for each reflection, it is possible to calculate the dimensions of the unit cell, this process being called indexing, as Miller indices are assigned to each reflection. This may be done quickly by use of computer programs such as 'Unit Cell'. This process is used to confirm the identity of a compound studied by XRD by comparison with literature data for the compound.

1.10 X-ray photoelectron spectroscopy

X-ray photoelectron spectroscopy (XPS) allows the identification of individual atoms in a material by the ionisation energies of electrons in different orbitals. This allows the orbital energies to be measured and these are characteristic of each element. Electromagnetic radiation is used to ionise electrons from atoms in the top few atomic layers for solids, so that their analysis may be used to identify surface species on a solid. Radiation that penetrates deeper than this is absorbed by the solid and causes the emission of electrons, but these electrons are not generally emitted as they cannot escape from the bulk of the material. Only electrons from the top few nanometres may escape from a solid for analysis.

The law of conservation of energy dictates that the incident photon energy, $h\nu$ is the sum of the ionisation energy, I, of the element ejecting the electron, plus the kinetic energy of the ejected electron, $0.5m_ev^2$. Thus $h\nu = 0.5m_ev^2 + I$. h is Planck's constant, ν is the frequency of the ejected photon, m_e is the mass of an electron, v is the speed of the electron. Photoelectrons may be ejected from a number of different orbitals, resulting in a spectrum of electron kinetic energies present due to each orbital having a different ionisation energy. With electrons being ejected from as many orbitals as is allowed by the above formula, XPS leads to a 'fingerprint', or 'signature' of kinetic energies representing the difference between the incident photon energy and the energies of emitted electrons. The signature of each element may be recognised from the resulting spectra leading to the identification of surface layers on a solid.

The use of X-rays in photoelectron spectroscopy enables the identification to be made of individual atoms rather than molecules as described above. X-ray photons have a high enough incident energy to ionise core electrons which are largely unaffected by interatomic forces. This leads to lines in the spectra which are characteristic of the elements present.[20]

1.11 Scanning electron microscopy

Scanning electron microscopy (SEM) uses electrons to image a sample, rather than photons of visible light as used in a conventional light microscope. Samples for SEM must be conducting, or have conducting layers of carbon or gold deposited on them to

prevent the build up of charge as they are bombarded by electrons during imaging. The samples also have to be small enough to fit into the sample chamber because the analysis must be performed *in vacuo*. This is because molecules in air would be ionised by the electron beam rather than imaging the surface. The main advantage which SEM has over light microscopy is the ability to image objects that may be as small as tens of nanometres across. This is not possible using optical microscopy as resolution is dependent on the wavelength of the incident radiation; thus it is not possible to achieve a resolution of better than about 200 nm.

Electrons are emitted from a tungsten filament in an 'electron gun' and are fired towards the sample by attraction to an anode, which has an aperture above the sample, allowing some electrons to be accelerated down to the sample. A schematic diagram of an electron gun is shown below in figure 1.8. The electrons are then focused by a magnetic field acting as a lens which allows only the electrons travelling straight down to reach the sample. The electrons hitting the sample may either be reflected or cause secondary electrons to be ejected. These are then detected and converted to a voltage, which is amplified and the output is displayed on a cathode ray tube (screen) on the instrument, which displays an image that corresponds to the topography of the sample. Secondary electrons are produced by inelastic collisions of beam electrons with atoms on the surface of the sample. The electrons emitted from the sample have kinetic energy of *c.* 50 eV and come from the conduction or valence bands of atoms. Secondary electrons may be used to provide topographical information as described. Back-scattered electrons are elastically scattered electrons having lost less than 1 eV; these electrons are Rutherford back-scattered, i.e. scattered by the nuclei of atoms, and convey information on the atomic number and topography. Both secondary and back-scattered electrons may be used to form an SEM image. The magnification achieved by the microscope is dependant on the ratio of currents I_S:I_C, as seen in fig. 1.9. It is possible to achieve *c.* 2 nm resolution under optimal conditions. A schematic representation of a SEM instrument is shown below in figure 1.9.

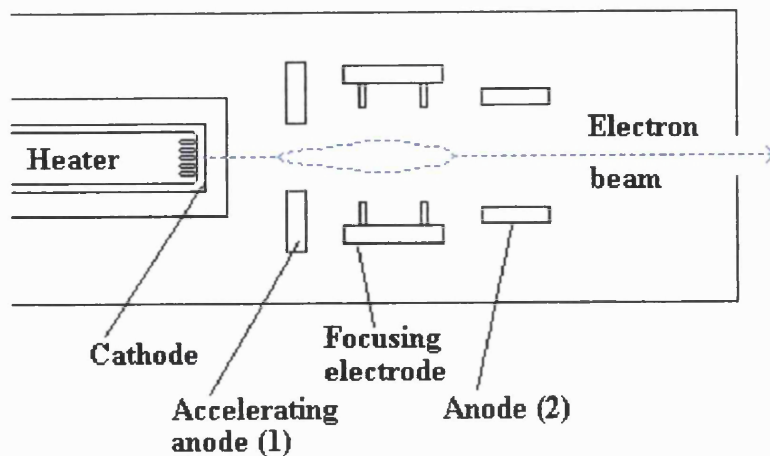

Figure 1.8 Schematic representation of an electron gun.

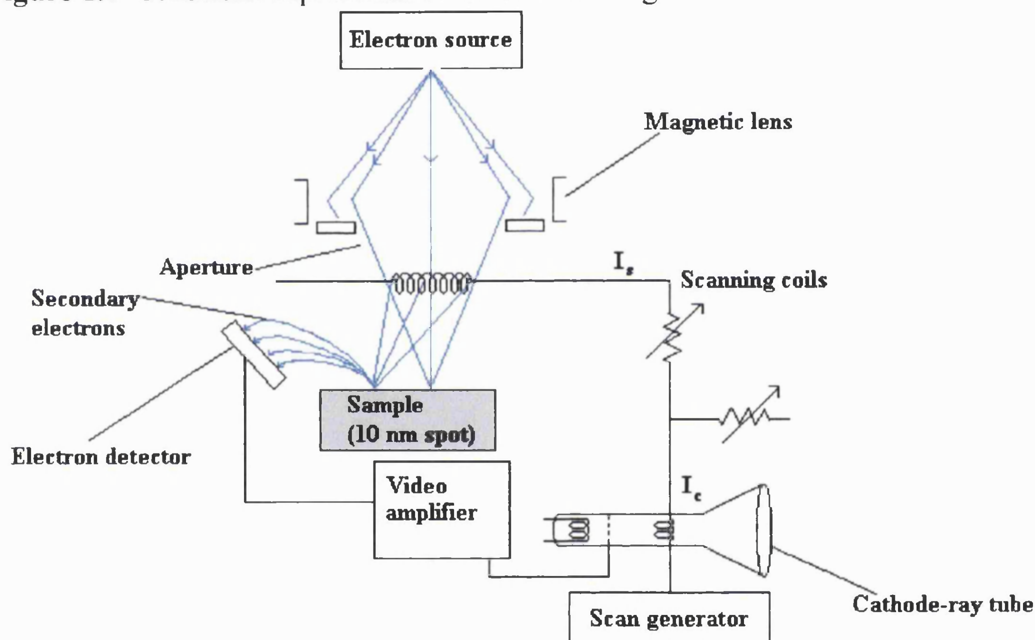

Figure 1.9 Schematic diagram of a scanning electron microscope.

1.12 Energy dispersive analysis by X-rays (EDX)

In energy dispersive analysis by X-rays (EDX), electrons are 'fired' from an electron gun and will hit the sample if they have sufficient energy. The beam electrons interact with the electrons of the sample during the collision to produce X-rays. This occurs because the electrons fired at the sample result in some atoms ejecting electrons from inner shells, which results in high-energy or excited-state ions being produced. These ions lose their excess energy when outer electrons fall into the core vacancies produced, this process causes the emission of an X-ray photon of equivalent energy. These X-rays

are characteristic of the elements from which they were produced because their energy (or wavelength, depending on which is the more convenient to measure) is dependent upon the difference in orbital energies involved in the electronic transition.[21]

2.0 Experimental

Details of instrumentation used for the analysis of thin films produced by chemical vapour deposition are listed below.

2.1 Raman microscopy

Three Raman systems were used in the (room temperature) analysis of thin films and bulk materials produced in this study these were as follows. All Raman spectra presented were recorded using red excitation at 632.8 nm with the exception of figures 7.4, 7.5 and 7.9-11 which used 647.1 nm and figure 10.3 for which 532 nm was used.

2.1.1 Dilor XY – This used an Olympus BH-2 microscope coupled to a Dilor XY triple grating spectrometer. The excitation wavelength used was 647.1 nm from a Coherent Innova 300 Kr^+ laser. Analysis was performed *in-situ* with a 10x eyepiece and a 50x or 100x objective lens. 10 - 30 s signal integration times were used with up to 200 accumulations in signal/dark mode.

2.1.2 Dilor Infinity Raman microscope – This used a holographic notch-filter to reduce radiation in the spectrum at the excitation wavelength and had an air-cooled CCD detector. The excitation line used was 632.8 nm from a HeNe air-cooled laser or 532.0 nm from a frequency doubled YAG laser. This system used an Olympus microscope with a 100x objective lens. Analysis was performed *in-situ* with a static grating recording 50 – 1000 cm^{-1}, with integration times of between 1 - 30 s with between 10 - 30 accumulations.

2.1.3 Renishaw Raman system 1000, Ramascope - This used a BH-2 confocal microscope. The excitation wavelength used was 632.8 nm from a 10 mW HeNe laser or 514.5 nm from a 10 mW Ar^+ laser. This instrument uses a notch filter to reduce radiation in the spectrum at the excitation wavelength. Analysis was performed *in-situ* with a static grating centred at 400 cm^{-1} with integration times of between 1 - 30 s with between 10 - 30 accumulations. The objective used for analysis provided magnification of x50 or x100.

2.2 Energy dispersive analysis by X-rays

EDX measurements were made using two instruments. All samples were analysed using a Hitachi S570 Filament Scanning Electron Microscope, with a 20 keV electron

beam excitation source. In addition some samples were analysed using a Jeol SEM set up to record EDX measurements using either 20 or 10 keV excitation to produce spectra. EDX measurements were standardised relative to a polished cobalt surface.

2.3 Electron microprobe

The standards used to calibrate the detector were as follows; the mineral wollastonite, $CaSiO_3$ for silicon and oxygen, iron pyrite FeS_2 for sulfur and vanadium metal for vanadium. These standards were all freshly polished prior to calibration.

2.4 Scanning electron microscopy

SEM photos were taken using a Hitachi S570 Filament Scanning Electron Microscope. This used 20 keV excitation to produce images.

2.5 X-ray diffractometry

XRD measurements were performed using a Philips Xpert diffractometer. Cu-Kα radiation was used in the reflection mode with PC-APD version 4.0b software.

2.6 X-ray photoelectron spectroscopy

X-ray photoelectron spectra were recorded with a VG ESCALAB 220i XL instrument using focussed (300 μm spot) monochromatic Al-K_α radiation at a pass energy of 20 eV. Scans were acquired with steps of 50 meV. A flood gun was used to control charging. Depth profile measurements were obtained by using argon beam sputtering.

2.7 UV/visible spectroscopy

UV/visible spectra were recorded using a Shimadzu double beam spectrometer, with band gaps being calculated using the direct method.

2.8 Scotch tape test

The Scotch tape test was performed by taking two small strips of Scotch tape pressing it in a cross shape onto a film, removing the tape, then, examining both the tape and the coating. A failure in this test would be indicated by clean glass under the tape leaving

the film adhering to the adhesive tape. A film is said to pass if the coating is undamaged after removal of the tape.

2.9 Solubility

Film solubility was assessed by leaving a 1 cm^2 piece of glass in 1 cm depth or so of solvent for 24 h. The solubility was defined as being either soluble, or insoluble depending upon the apparent change in colour and opacity of the film in comparison to a dry control piece of coated glass.

2.10 FTIR spectroscopy

The sample was incorporated into a translucent potassium bromide disk, which was analysed by infrared spectroscopy using a Nicolet Fourier transformation spectrometer employing 32 scans with the gain set to 1 and a resolution of 2 cm^{-1}.

2.11 Construction of the APCVD rig

Two nitrogen gas cylinders supply carrier gas into the rig via four gas lines. The gas is heated as it flows through three metres of coiled pipework in a tube furnace. This allows delivery of preheated gas to the reactor, which prevents reactants from condensing in the pipes. All of the pipes used in the reactor are made of stainless steel, mostly having a quarter-inch diameter. The exhaust and a pipe running from the four-way valve to the reactor have a half-inch diameter. The bubbler (fig. 2.3) is a four-inch long cylindrical vessel with a one-and-a-half inch diameter and one-sixteenth inch thick walls. This is surrounded by a brass sleeve to conduct heat from the heater plate below it to the bubbler contents. The entry and exit pipes of the bubbler are a quarter-inch in diameter. The four-way valve has Vespel SP (Du Pont) insert joining the pipes together to provide a good seal at 150 °C. Other pipes are joined with quarter-inch Swagelok fittings. Later in the study, for the titanium and chromium systems, a three-way valve with Swagelok fittings was used, as the Vespel inserts needed replacement due to wear and tear. With this modification the nitrogen line was blocked because it had become redundant with the fitting of the three-way valve.

The entry and exit flange to the reactor, the graphite block and the quartz tube of the reactor were supplied by Pilkington, PLC. Other parts of the rig were manufactured or assembled at UCL. All thermocouples are K-type, with the reactor thermocouples being mineral insulated.

2.12 Gas flow through the reactor

There are two reactant gas streams flowing through the rig prior to the reactor, one from the hydrogen sulfide cylinder and the other from the bubbler. These two gas streams meet in the concentric pipes that connect on to the reactor entrance flange. This allows the reactants to mix prior to entering the reactor, so that they can react and coat the glass substrate evenly to give a uniform coating. It also minimises the chance of products condensing in the gas lines. The entrance flange is designed to allow the gases to mix and emerge as an even wave of gas, which can flow over the substrate surface as shown in figure 2.1.[22]

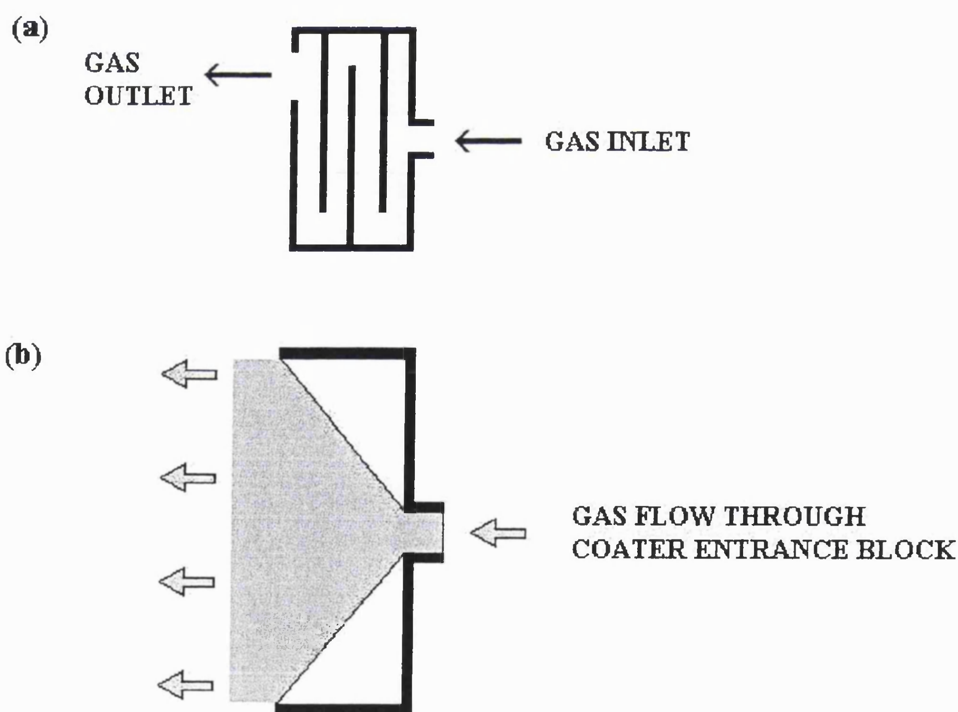

Figure 2.1 (a) shows the entrance flange from the side elevation. (b) shows the entrance flange from the top.

The reactor is a horizontal-bed cold-wall design, containing a graphite block with Whatman heater cartridges to heat the substrate. The difference between this and a hot

walled reactor is that the latter is heated in a furnace, which means the walls are also heated. The reactor and rig schematics are shown below in figures 2.2 and 2.4.

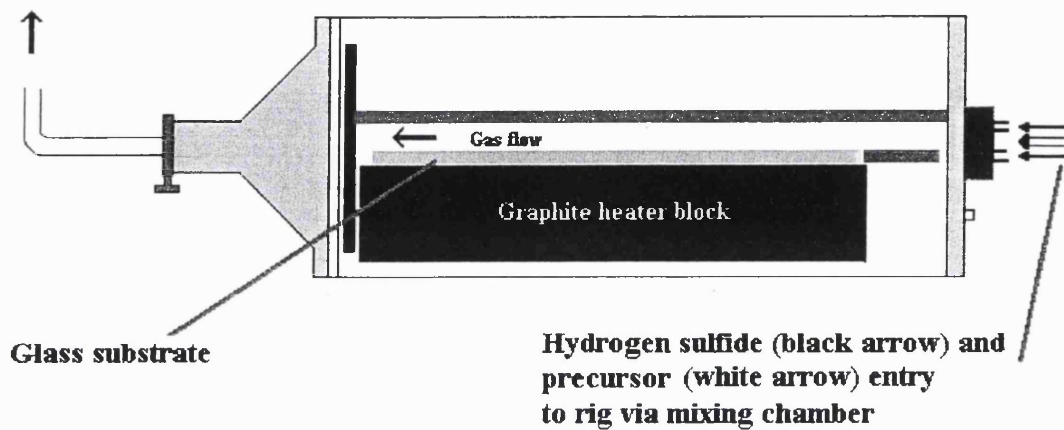

Figure 2.2 A schematic diagram of the quartz tube reactor.

The bubbler, the design of which is shown below in figure 2.3, allows the introduction into the gas stream of materials, which are either liquid or solid at room temperature and pressure.

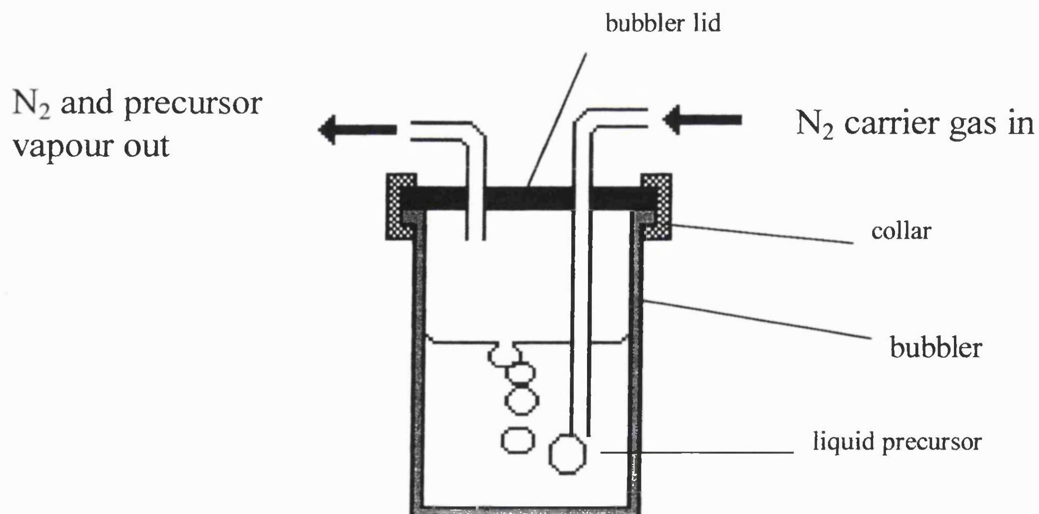

Figure 2.3. A cross-sectional view of the bubbler used in this study, showing the passage of gas through a liquid precursor.

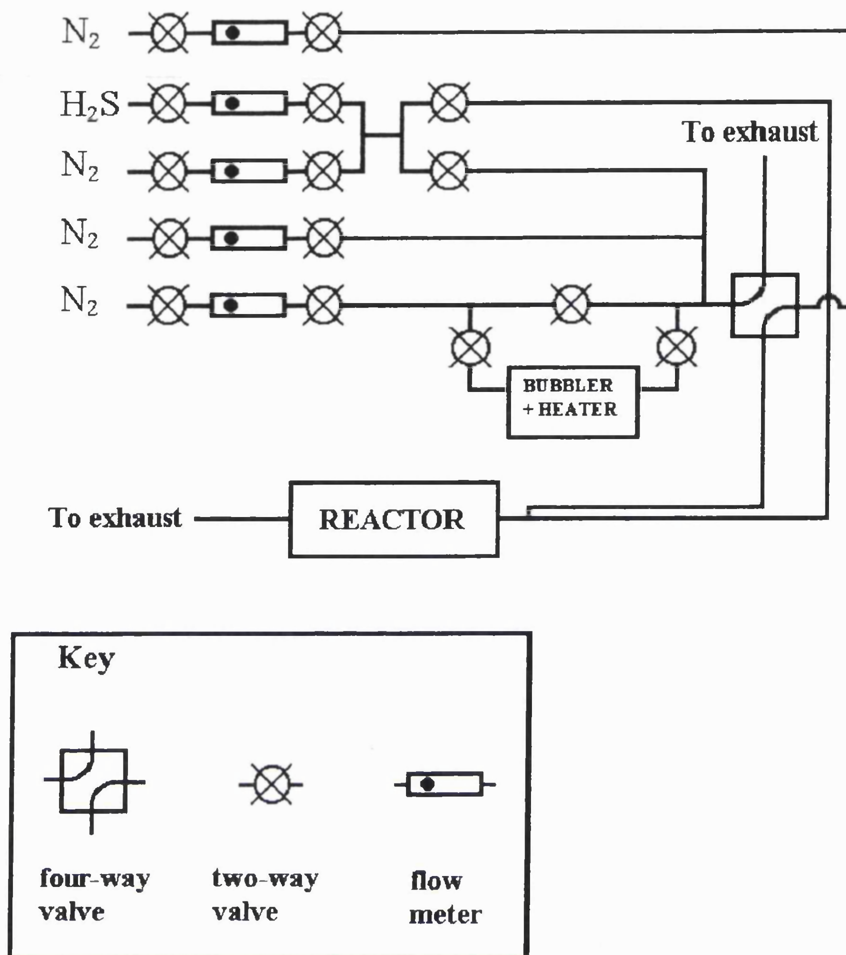

Figure 2.4 A schematic diagram of the APCVD rig.

2.13 APCVD Experimental

The glass substrates (225 x 90 x 4 mm) used in this investigation were supplied (Pilkington Glass plc) with a pre-coating of SiCO (a silicon, carbon and oxygen containing compound used by Pilkington) or SiO_2 to act as a diffusion barrier. The substrates were cleaned prior to coating with petroleum spirit (40 - 60 °C) followed by propan-2-ol. The substrates were then air-dried prior to being placed in the atmospheric pressure chemical vapour deposition (APCVD) reactor.

Nitrogen (99.99%) was used as supplied by the British Oxygen Company as the inert carrier gas for the precursors. The precursors used were hydrogen sulfide gas (99.7%,

BOC) and vanadium, chromium or titanium precursor liquids used as supplied (Chapters 3 - 8) and volatilised using a bubbler before entry to the reactor.

The bubbler was heated to 68 - 103 °C for all deposition experiments in isolation from the carrier gas flow through the rig. The temperature for each experiment was chosen to provide *c.* 150 mmHg vapour pressure of the precursor. The pipes carrying reactive and nitrogen gases to the reactor were heated to 150 °C, the reactor bed and substrate being heated to temperatures of 300 – 600 °C at 50 °C intervals. After the reactor and bubbler had reached the required temperature they were left for 5 min to stabilise at that temperature. Then nitrogen gas was passed through the bubbler to carry the metal precursor into the reactor. Hydrogen sulfide was admitted to the rig. The precursors passed out through the exhaust before and after the reaction. The four-way valve was turned at the start and end of each reaction. The gas flow rates used were as follows: nitrogen carrier gas 10 dm^3 min^{-1}, nitrogen through the bubbler 0.5 dm^3 min^{-1} and hydrogen sulfide either 0.5 or 1 dm^3 min^{-1}. After the 30 – 180 s reaction the hydrogen sulfide cylinder was closed and the bubbler isolated from the gas stream through the reactor. The substrate was then allowed to cool to 60 °C under a 1 dm^3 min^{-1} flow of nitrogen before removal from the reactor; this was done to minimise further reaction of the deposited film. The coated pieces of glass were stored in air after having been cut into 1 cm squares for scanning electron microscopy (SEM) and energy dispersive X-ray analysis (EDX), and into 5 cm squares for Raman microscopy.

2.14 Preparation of Tri-n-butyltin trifluoroacetate

Tri-n-butyltin trifluoroacetate was prepared by refluxing 3.83 g (28 mmol) sodium trifluoroacetate with 9.14 g (28 mmol) tri-n-butyltin chloride in 0.12 dm^3 ethanol for 2 h. The ethanol was removed *in vacuo* and the resultant white solid recrystallised from diethyl ether. The result was colourless crystals (mp. 49 – 50 °C) of the desired compound in 68 % yield.[23]

2.15 Calibration of Raman spectra

2.15.1 Signal intensity corrections

The spectral response of an individual Raman spectrometer (a schematic representation of which is shown below in figure 2.5) is dependent on the optics used in the spectrometer. Therefore any corrections made have to be instrument specific. Assuming that the laser and scattered light are aligned correctly, there are two features of spectral response, which require calibration, specifically the data values on the x and the y-axes of a Raman spectrum. The intensity values are dependent on the amount of stray light reaching the spectrometer and the detector response, the baselines of spectra generally sloping upwards towards the Rayleigh line. These factors may be corrected for by dividing the y-axis values of the Raman spectrum with those of a light source which has a calibrated but featureless emission spectrum, such as that from a temperature-calibrated tungsten lamp. This procedure allows the response of the detector to be allowed for, and results in a spectrum with a flat background (assuming there there is no fluorescence) and corrected intensity.

2.15.2 Raman shift wavenumber correction

Raman band wavenumbers may be corrected by comparison with those of emission lines from a noble gas or mercury vapour discharge lamp. As atomic emission lines are narrow, it is possible to measure their wavenumbers precisely. If an atomic emission spectrum is superimposed onto a Raman spectrum, the difference between the known and measured line wavenumbers can be plotted as a calibration curve. The formula describing this curve is used to adjust the Raman spectrum of the compound under study. Therefore, the corrected Raman spectrum may be used to measure the exact Raman band wavenumbers of the compound analysed.

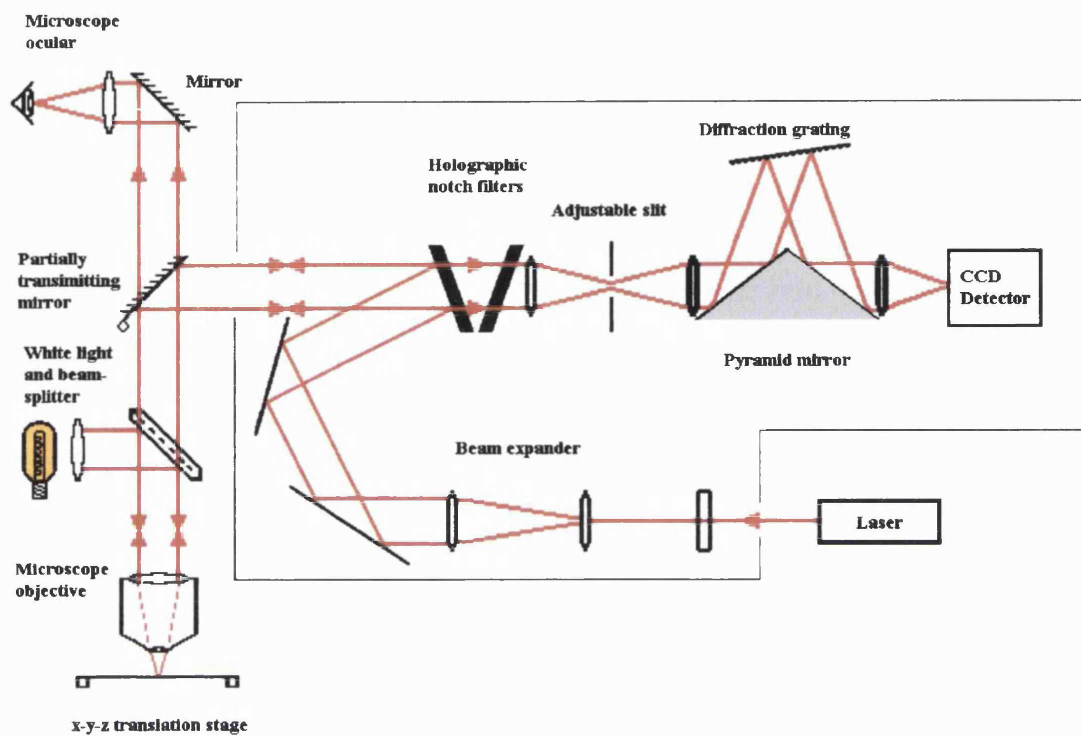

Figure 2.5 A schematic diagram of a recent Raman microscope.[24]

3.0 Vanadium oxysulfide

3.1 Introduction

The APCVD reaction of oxovanadium(V) chloride and hydrogen sulfide was studied at deposition temperatures between 300 – 600 °C. This reaction has not been reported previously. The only reference to vanadium oxysulfide in the literature describes the production of the hydrated precipitates $V_2O_4S.2H_2O$ and $V_2O_3S.3H_2O$, produced from the reaction of $Na_2S.9H_2O$ with either $VOCl_2.2H_2O$ or $VOSO_4.5H_2O$.[25,26,27] Various analytical techniques including Raman microscopy were used to identify the composition of the films deposited in this study.

3.2 Background

There are only three reports of vanadium oxysulfides in the literature[25,26,27], these oxysulfides having the compositions $V_2O_4S.2H_2O$ and $V_2O_3S.3H_2O$. They were prepared as bulk materials from the aqueous reaction of $Na_2S.9H_2O$ with either $VOCl_2.2H_2O$ or $VOSO_4.5H_2O$ at room temperature. The vanadium oxysulfides isolated in these reactions are grey amorphous solids. The vanadium has a distorted octahedral geometry with the oxo group *trans* to the sulfur atom. A schematic representation of the first coordination shell of vanadium in $V_2O_3S.3H_2O$ is shown below in figure 3.1.[26]

$V_2O_3S.3H_2O$ produced from the bulk preparation outlined above did not contain a sulfate group according to infrared spectroscopy. IR spectroscopy was used to confirm the presence of the vanadyl group.[25,27] The vanadyl group has Raman and IR bands in the range 900 - 1025 cm^{-1} attributed to the stretching vibration of the V=O bond.[28] Electron paramagnetic resonance spectroscopy was used to assign the vanadium oxidation state. The gyromagnetic ratio, g was measured at 1.97 indicating the presence of vanadium in the +4 oxidation state. The vanadium – vanadium bond length was deduced from EXAFS to be 3.14 Å, which is similar to that found in V_2O_5.[27] The material probably has a chain-like structure with edge-sharing O-O groups, the vanadium atoms being alternately above and below the chains. TGA experiments showed that some water was included in the structure, and could not be removed without loss of sulfur from the material.[27]

Vanadium oxysulfide has been investigated as a cathode material for lithium batteries.[25,27] Oxysulfide materials should have intermediate properties between those of oxides and sulfides; and transition metal oxide / sulfides are currently considered promising candidates for lithium batteries.[27] Batteries built with sulfides as the positive terminal show good reversibility, so are suitable for use as rechargeable batteries; however they have a low voltage.[25] Batteries using metal oxides have a higher voltage, but are not as suited to use in rechargeable batteries because they have a lower reversibility.[25]

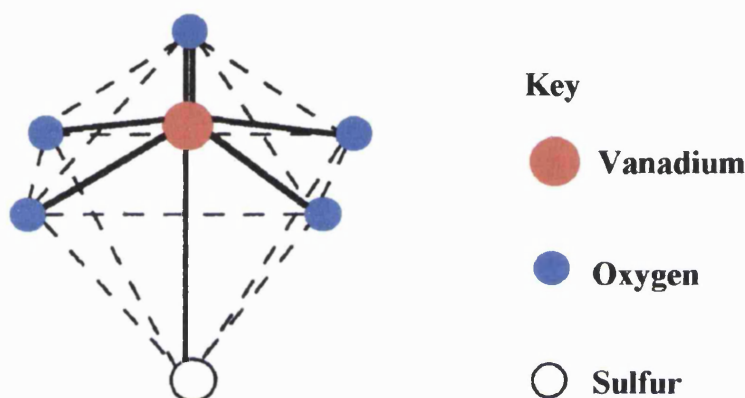

Figure 3.1 A schematic representation of the first coordination shell of vanadium in $V_2O_3S.3H_2O$.[26]

Other transition metal oxysulfides include; HfOS, which has been reported to have a cubic structure, with the $P2_13$ space group, and a = 5.6824(6) Å. HfOS is reported to be isostructural with ZrOS.[29] Molybdenum and titanium oxysulfides have also been reported and tested for use as positive terminals in lithium batteries.[27]

Vanadium oxide and vanadium sulfides are related compounds as both are vanadium chalcogenides, and can potentially be deposited by APCVD. Vanadium pentoxide films have been deposited from the APCVD reaction of oxovanadium(V) chloride and water at substrate temperatures of between 350 – 600 °C. They have also been deposited from the APCVD reaction of vanadium tetrachloride and water. This reaction only produced films at a substrate temperature of 450 °C or above.[30]

Vanadium sulfide films deposited by CVD have not been reported prior to this work.

3.3 Experimental

Vanadium oxysulfide thin films were grown from the APCVD reaction of oxovanadium(V) chloride and hydrogen sulfide. The oxovanadium(V) chloride was admitted to the reactor from a bubbler, which was heated to 90 – 96 °C. A nitrogen gas flow of 0.5 $dm^3 min^{-1}$ was passed through the bubbler to carry the oxovanadium(V) chloride towards the reactor. The hydrogen sulfide was allowed to flow into the gas stream at a rate of 0.5 or 1.0 $dm^3 min^{-1}$ with 1 $dm^3 min^{-1}$ nitrogen as a diluent gas. The precursors were separately transported to the reactor via mass flow with the addition of 10 $dm^3 min^{-1}$ of nitrogen carrier gas. The precursor gas flows joined at the inlet of the reactor and were premixed in the brass block prior to passing over the glass substrate. See Chapter 2 for diagrams and full experimental details.

Eleven deposition experiments were carried out for this system at temperatures between 300 – 600 °C inclusive, at 50 °C intervals. Deposition times of 0.5 or 3 min were employed. This was timed between the opening and closing of the four-way valve. Eleven substrates were used in this investigation, although not every reaction produced a coating on the substrate in the reactor. The conditions used for each run are shown below in table 3.2.

The variables investigated were substrate temperature, reaction time and H_2S gas flow rate.

Energy dispersive X-ray analysis (EDX) was used to determine quantitatively the composition of the films. In addition, the films were also characterised by X-ray photoelectron spectroscopy, X-ray diffractometry, Raman microscopy, UV/visible spectroscopy, scanning electron microscopy and electron microprobe Film adherence to the glass was assessed using the Scotch tape test and by scratching the surface with a scalpel. Solubility of one of the films was assessed in various solvents. A flake of the film deposited at 450 °C (during a 3 min reaction of oxovanadium(V) chloride with hydrogen sulfide) was analysed by infrared spectroscopy. These analyses were all performed as described in Chapter 2.

(a.)Deposition temperature / °C	Bubbler temperature / °C	H_2S gas flow / $dm^3 min^{-1}$
300	95	0.5
350	92	0.5
400	90	0.5
450	92	0.5
450	94	0.5
500	91	0.5
500	92	1.0
500	91	0
550	94	0.5
600	91	0.5

(b.)Deposition temperature / °C	Bubbler temperature / °C	H_2S gas flow / $dm^3 min^{-1}$
450	96	0.5

Table 3.2 Reaction conditions used during the APCVD reaction of oxovanadium(V) chloride and hydrogen sulfide. a) for reactions of 0.5 min duration b) for reaction of 3 min duration.

3.4 Results

3.4.1 Film colour and uniformity

Table 3.3 below contains descriptions of the visual appearance of films deposited on the day of manufacture and any changes noticed subsequently on storage. The film colours described below are as they appeared lying flat on a white sheet of paper illuminated from above. Films are described from the gas inlet end of the substrate to the exhaust end as they would be seen when looking into the reactor. In each case below the predominant colour of the film is highlighted in bold script. The films as described had not changed in appearance 2 months after deposition.

(a.)Deposition temperature / °C	H_2S gas flow / $dm^3 min^{-1}$	Visual appearance of film on day of manufacture and any changes noticed subsequently
300	0.5	No film present on substrate.
350	0.5	No film present on substrate.
400	0.5	*c.* 4 cm very thin, reflective black/grey film, thick matt **black** film. A stripe *c.*2-3 cm across, running along the length of the bottom of the coated region turned a **yellow/green** colour after two weeks storage in air.
450	0.5	Due to a partial blockage in the brass block only two stripes of **black** film were deposited, these were along the length of the substrate at the edges. After two weeks two **yellow/green** stripes had formed within black areas at the very edges of the substrate.
450	0.5	Fairly reflective **black** coating. Film visually unchanged after two weeks.
500	0.5	**Black** reflective coating. Film visually unchanged after two weeks.
500	1.0	**Black** reflective coating. Film visually unchanged after two weeks.
500	0	No film present on substrate.
550	0.5	Matt black coating *c.* 3 cm, thick reflective **black** film over the rest of the substrate. Film visually unchanged after two weeks.
600	0.5	The entire substrate has a **black** coating, however it gets thinner from right to left, i.e. it was thicker at the end that was next to the reactor inlet. After two weeks the colour of the film was visually unchanged, however some of the film peeled away from the areas that it had been thickest.

(b.)Deposition temperature / °C	H_2S gas flow / $dm^3 min^{-1}$	Visual appearance of film on day of manufacture and any changes noticed subsequently
450	0.5	A thick matt **black** film was deposited, parts of which later flaked off in the middle of the substrate. After two weeks a 1 cm region at the entry end of the substrate had turned a **green/yellow** colour.

Table 3.3 Descriptions of the visual appearance of films produced by the APCVD reaction of oxovanadium(V) chloride and hydrogen sulfide. a) from reactions of 0.5 min duration b) from a reaction of 3 min duration.

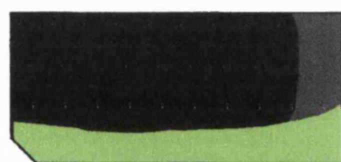

a.)

b.)

c.)

Figure 3.4 Sketches after two weeks of the appearances of films deposited by the APCVD reaction (30 s) of oxovanadium(V) chloride and hydrogen sulfide at a) 400 °C, b) 450 °C and c) 600 °C.

Green areas of the films had a cracked appearance when viewed under a microscope, whereas black areas appeared smooth in comparison. A picture of a green film taken at 180 x magnification is shown below, this film was produced by the APCVD reaction of oxovanadium(V) chloride and hydrogen sulfide at 450 °C.

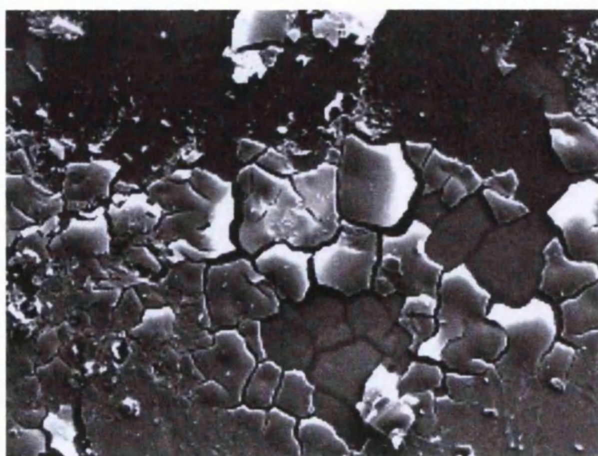

Figure 3.5 Photograph of a green area of a film deposited by the APCVD reaction (30 s) of oxovanadium(V) chloride and hydrogen sulfide at 450 °C. Shown at 180x magnification using an EDX (Jeol) instrument.

3.4.2 Film adhesion

All of the films produced by the reaction of oxovanadium(V) chloride and hydrogen sulfide could be scratched with a scalpel to reveal the plain glass substrate. The black films deposited by the reaction of 0.5 $dm^3\ min^{-1}$ flow of hydrogen sulfide with oxovanadium(V) chloride all passed the Scotch Tape test. The film deposited at 500 °C with a 1.0 $dm^3\ min^{-1}$ flow of hydrogen sulfide was damaged by the Tape test, but some film was left on the substrate probably due to the thickness of the coating. The green regions of the films tested were all damaged by the tape, however some film remained on the substrate after each was tested.

3.4.3 Solubility

Samples of the film deposited at 450 °C were cut into 1 cm^2 sections in order to test the solubility of the deposited film in various solvents, these were compared after 24 hours with a sample left in air. The film was not noticeably decolourised or dissolved by dilute sulfuric acid, water, propan-2-ol, acetone or 40-60 petroleum spirit. The sample left in dilute potassium hydroxide solution had significantly decolourised and after the test appeared a very pale grey, in comparison to the black control sample.

3.4.4 Four-probe resistance measurements

A four-probe meter was used to measure the sheet resistance of the films deposited in this study, the results are shown below in table 3.6. As can be seen below, the resistance of the green areas of film is generally higher than the resistance measured for the black areas.

(a.)Deposition temperature / °C	H_2S gas flow / $dm^3 min^{-1}$	Resistance Ω/ □
400	0.5	Black film 249 Green film 204
450	0.5	Black film 250 Green film 700
500	0.5	Black film 60
500	1.0	Black film 15
550	0.5	Black film 23
600	0.5	Black film 261
(b.)Deposition temperature / °C	**H_2S gas flow / $dm^3 min^{-1}$**	**Resistance Ω/ □**
450	0.5	Black film 16 Green film 1166

Table 3.6 Resistance measurements of the films deposited from the APCVD reaction of oxovanadium(V) chloride and hydrogen sulfide. a) for reactions of 0.5 min duration b) for the reaction of 3 min duration.

3.4.5 Raman microscopy and infrared spectroscopy

Raman spectra were recorded (at room temperature) from all films deposited by the APCVD reaction of oxovanadium(V) chloride and hydrogen sulfide. These spectra are shown below in Figures 3.7a-i It can be seen from the spectra below that none of the films deposited contained any oxovanadium(V) sulfate. These spectra were recorded 1-2 weeks after film deposition.

None of the films deposited initially contained any vanadium pentoxide. However prolonged exposure to laser light at 632.8 nm, as used in the analysis of these films, did cause some of the films to undergo a transformation to V_2O_5 see fig. 3.7i. A visual check by microscope, was made of each point after analysis to see if any change was noticeable.

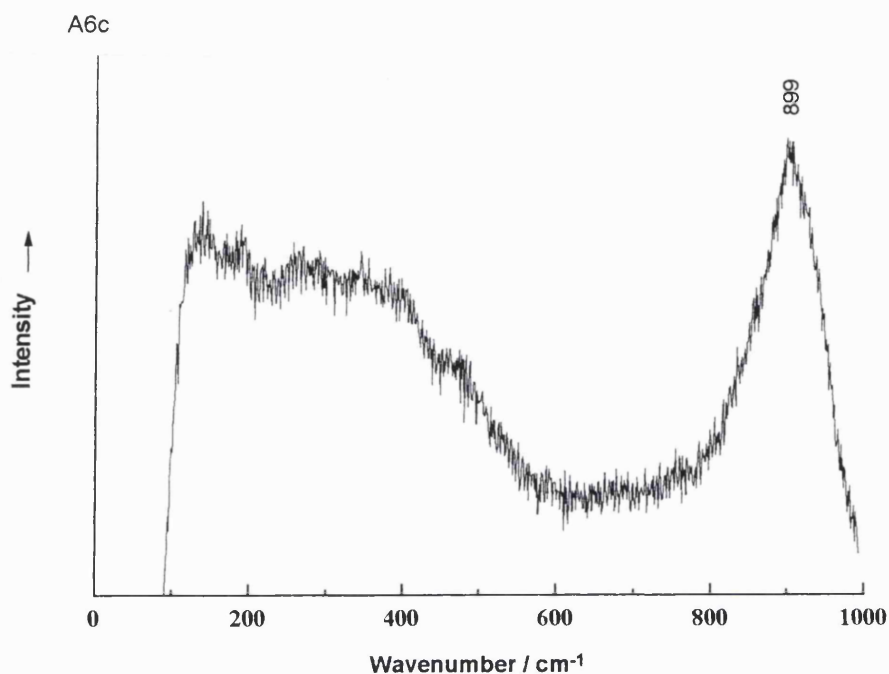

Figure 3.7a Raman spectrum of the film deposited at 400 °C by the APCVD reaction (30 s) of oxovanadium(V) chloride and hydrogen sulfide.

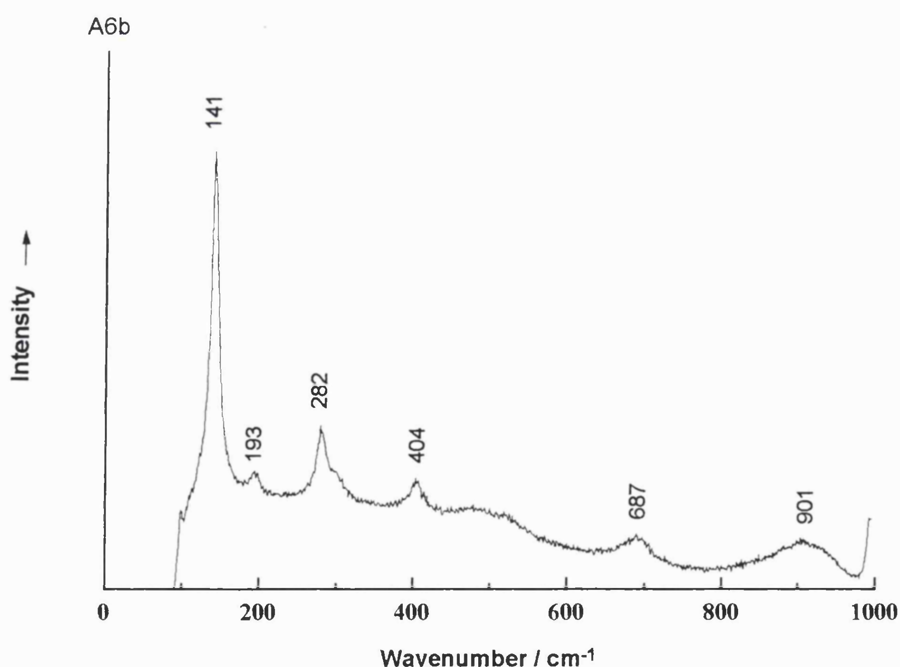

Figure 3.7b Raman spectrum of the film deposited at 400 °C by the APCVD reaction (30 s) of oxovanadium(V) chloride and hydrogen sulfide. Spectrum shows the effect of prolonged laser irradiation (causing the formation of vanadium pentoxide with bands at 141, 193, 282, 404, and 687 cm^{-1}) on a film produced at 400 °C.

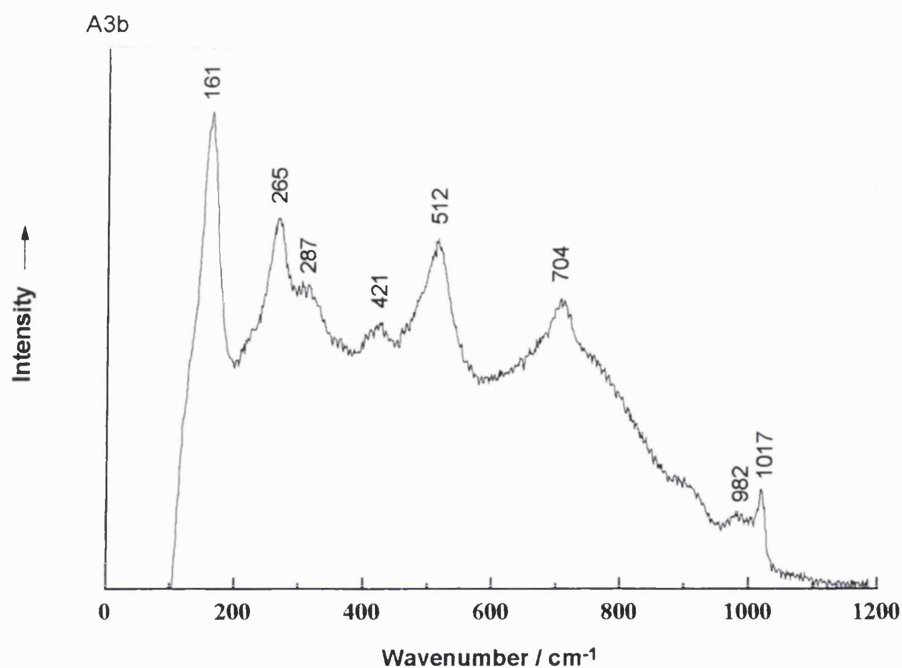

Figure 3.7c Raman spectrum of the film deposited at 450 °C by the APCVD reaction (30 s) of oxovanadium(V) chloride and hydrogen sulfide.

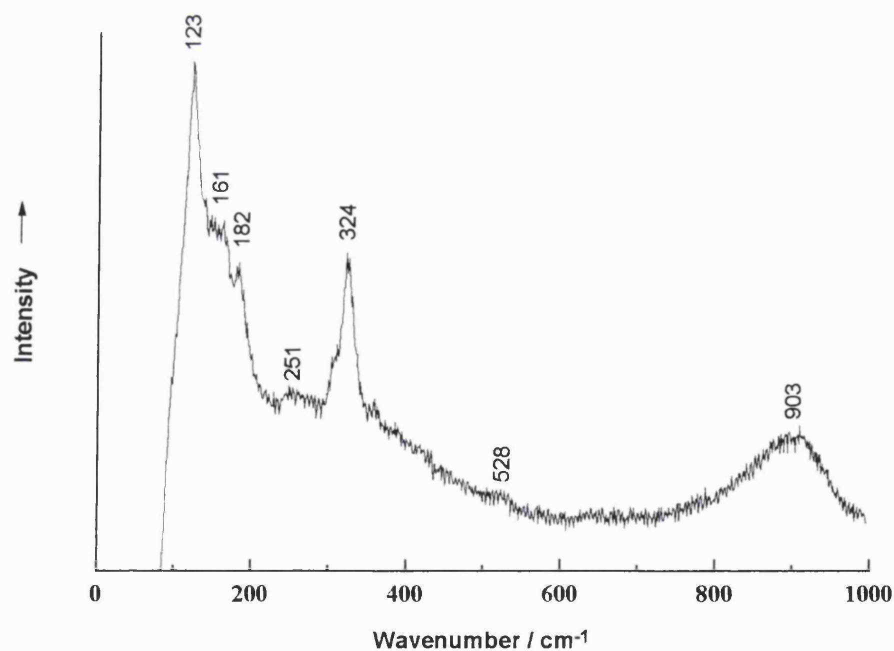

Figure 3.7d Raman spectrum of the film deposited at 450 °C by the APCVD reaction (180 s) of oxovanadium(V) chloride and hydrogen sulfide.

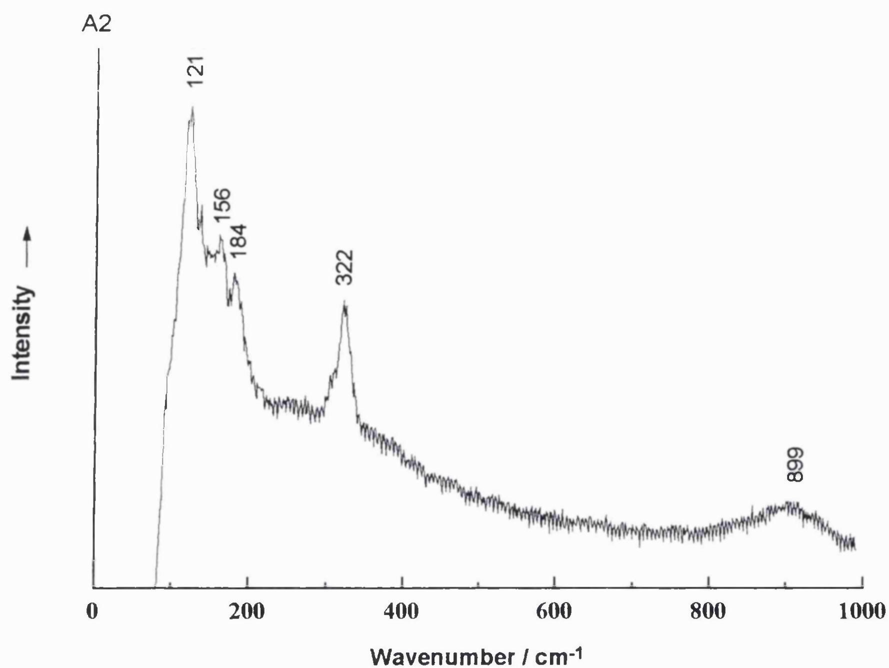

Figure 3.7e Raman spectrum of the film deposited at 500 °C by the APCVD reaction (30 s) of oxovanadium(V) chloride and hydrogen sulfide.

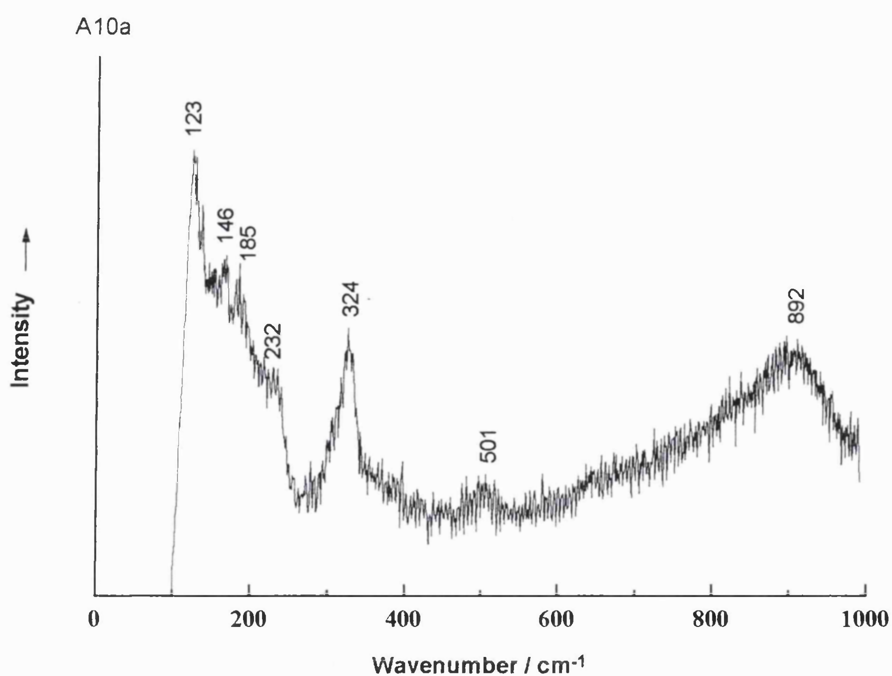

Figure 3.7f Raman spectrum of the film deposited at 550 °C by the APCVD reaction (30 s) of oxovanadium(V) chloride and hydrogen sulfide.

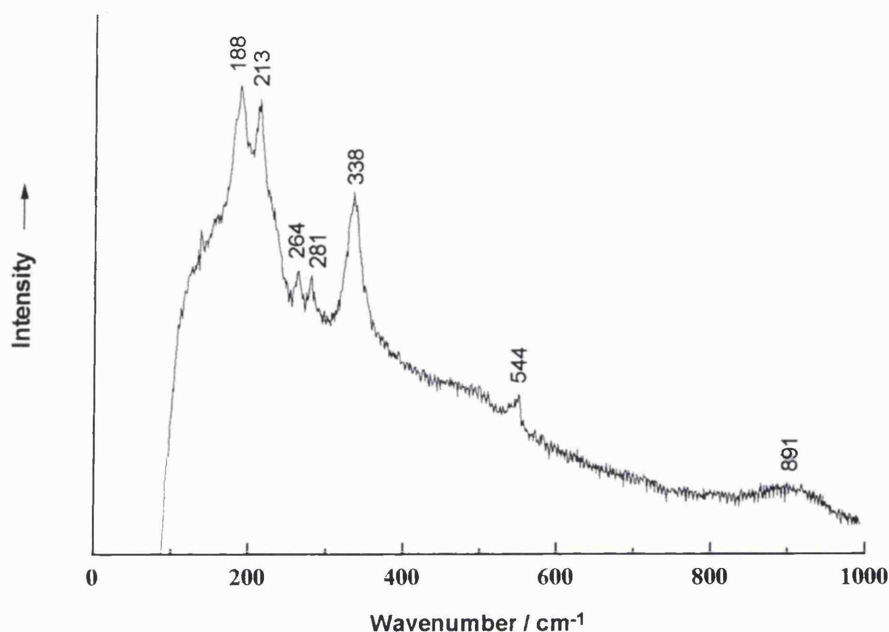

Figure 3.7g Raman spectrum of the film deposited at 600 °C by the APCVD reaction (30 s) of oxovanadium(V) chloride and hydrogen sulfide.

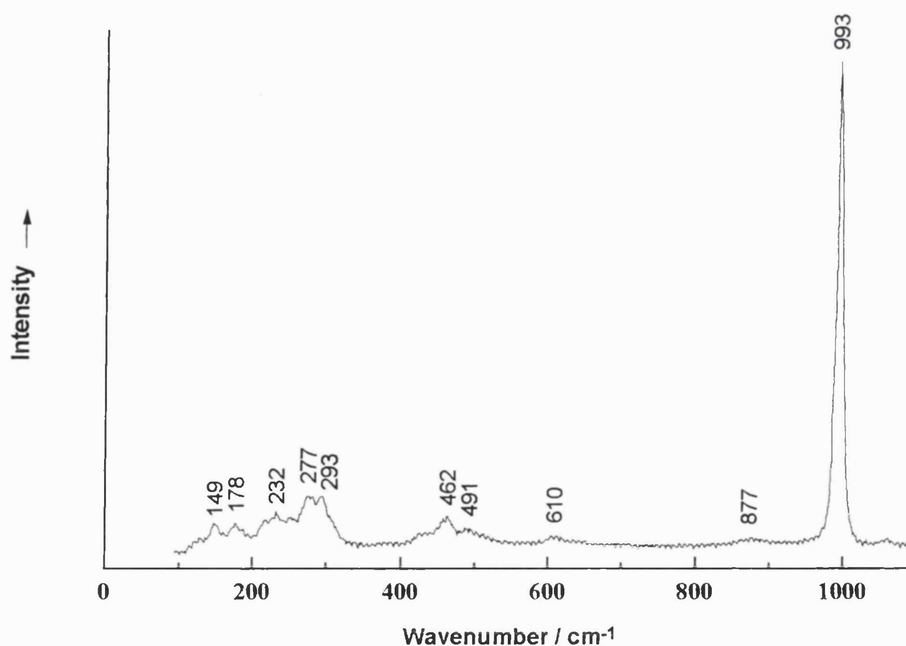

Figure 3.7h Raman spectrum of oxovanadium(V) sulfate. This spectrum was recorded using the same conditions as used in the analysis of the films deposited by the APCVD reaction (30 s) of oxovanadium(V) chloride and hydrogen sulfide.

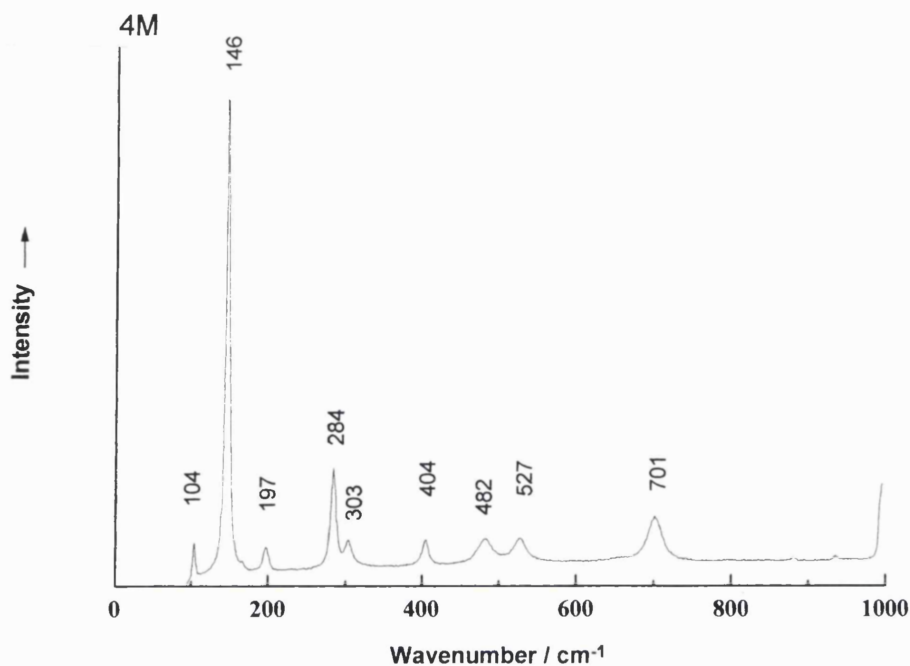

Figure 3.7i A vanadium pentoxide standard spectrum. A Raman spectrum recorded from a film deposited at 500 °C by the APCVD reaction of oxovanadium(V) chloride and water.[30]

A flake of the film deposited at 450 °C during a 3 min reaction of oxovanadium(V) chloride with hydrogen sulfide was analysed by infrared spectroscopy. The spectrum has features at c. 3750 and 1600 cm^{-1} caused by water vapour in the atmosphere around the sample. The band at 3450 cm^{-1} is due to the presence of water in the KBr even after storage in a drying oven. There are also bands at 660, 839, 1092 cm^{-1} due to the vanadium oxysulfide dispersed in the disk.

Compound or deposition temperature / °C		Run time / s	H_2S flow rate /dm^3min^{-1}	Bands / cm^{-1}
450	IR	180	0.5	660 (m), 839 (m), 1092 (m).
450	R	180	0.5	123 (m), 161 (w, sh), 182 (w, sh), 251 (w), 324 (m), 528 (w), 903 (m, br).
$VOSO_4$	R			149 (w), 178 (w), 232 (w), 277 (m), 293 (m, sh), 462 (m), 491 (w), 610 (w), 877 (w), 993 (s).
V_2S_3	R			122 (s), 161 (m, sh), 322 (m), 907 (m, br).
V_2O_5	R			100 (w), 144 (s), 282 (m), 300 (w,sh), 405 (w), 485 (w), 700 (w), 995 (m). [28]
VO_2	R			142 (m), 191 (s), 223 (m), 262 (w), 310 (w), 392 (m), 443 (w), 500 (w), 613 (m, br). stoichiometric.[31] 202 (s), 232 (w), 266 (w), 305 (w), 382 (w), 455 (w), 504 (w), 580 (w), 640 (m, br). oxygen rich.[31]

Table 3.8 Showing the Raman and IR bands recorded from a sample of a film deposited at 450 °C by the 3 min APCVD reaction of oxovanadium(V) chloride and hydrogen sulfide. These are compared with Raman bands from a selection of related compounds. w = weak, m = medium, s = strong, sh = shoulder and br = broad.

The Raman spectrum shown in Figure 3.7a has no bands attributable to oxovanadium(IV) sulfate, bands for vanadium oxides are also absent. The band at 899 cm^{-1} is quite similar in appearance to the band at 907 cm^{-1} due to vanadium(III) sulfide; however the overall appearance of the spectrum suggests that V_2O_5, VO_2 and V_2S_3 are not produced by this reaction. The bands in the spectrum did not lead to a positive identification of the compound produced by the APCVD reaction of oxovanadium(V) chloride and hydrogen sulfide at 400 °C. It was possible to produce vanadium pentoxide in the film deposited at 400 °C by laser irradiation, this is shown in figure 3.7b. Bands at 141, 282, 404 and 995 cm^{-1} compare with bands at 144, 282, 405 and 995 cm^{-1} for V_2O_5.[28] EDX results however indicate that the initial composition of the film was V_2O_4S.

The Raman spectrum of the film deposited at 450 °C (by a 30 s reaction) shown in figure 3.7c did not lead to a positive identification of the compound deposited.

However it does show that no vanadium sulfide, di- or pentoxide was produced. The EDX results indicate the formation of V_2O_4S during the 30 s and 180 s reactions at this temperature. A Raman spectrum recorded from the film deposited by the 180 s reaction has bands at 123, 161, 324 and 903 cm^{-1} these compare to 122, 161, 322 and 907 cm^{-1} for V_2S_3 recorded from a standard. No bands due to vanadium oxides were identified. The identification of vanadium(III) sulfide does not account for the ratio of vanadium to sulfur given by EDX results for this film as this has too little sulfur to account for the formation of V_2S_3. Therefore V_2S_3 must be a minor phase in the composition of this mixed phase film. It was not possible to identify positively the other phases present.

A Raman spectrum of the film deposited at 500 °C is shown in figure 3.7e this indicates the absence of vanadium oxides. The bands at 121, 322 and 899 cm^{-1} compare with 122, 322 and 907 cm^{-1} for V_2S_3. EDX results for this film give a ratio of vanadium to sulfur of 1:1, this again suggests that the film has too little sulfur to be phase pure vanadium(III) sulfide, so the film must consist of more than one compound. The overall stoichiometry suggested by EDX is $V_2O_3S_2$. Raman microscopy did not produce results that could identify other phases present in this film, therefore Raman results can not be used as the principle form of analysis to identify the composition of the films deposited in this study.

The Raman spectrum shown in figure 3.7f from the film deposited at 550 °C has Raman bands at 123, 324 and 892 cm^{-1}; these are similar to the values for V_2S_3. The ratio of vanadium to sulfur according to EDX data is 2:3 for vanadium to sulfur. It is unlikely that the film consists of a single phase however and EDX results imply that a formula of $V_2O_2S_3$ is more likely for the film as a whole.

No Raman bands could be matched to vanadium oxides for the film deposited at 600 °C shown in figure 3.7g. The single band at 891 cm^{-1} might be due to V_2S_3; however this is unlikely as the other bands do not match those of vanadium(III) sulfide. EDX results suggest a formula of V_2O_4S for the film.

No Raman bands were identified as being due to sulfate, these should be easily recognised due to their position and appearance as a narrow intense band in comparison to other bands identified.

3.4.6 Energy dispersive analysis by X-rays

There is a similarity in the vanadium and sulfur content of the films produced at 400, 450 and 600 °C; this may explain why they transformed to a sulfur-depleted lime green coloured compound. The films deposited at 400 and 450 °C took two weeks for a region of the coating to change colour, from black to lime green. The film produced at 600 °C took two months for this transformation. After two months the other films were examined visually and were found to be unchanged. However one year later all of the films produced by this system had turned a yellow-green colour. The data recorded in the table below were produced between 2-4 weeks after film deposition.

Deposition Temp./ time °C / s	**Atomic % V**	**Atomic % S**	**V:S ratio / atomic %**	**Formula**
400 / 30	35.5	20.2	$VS_{0.57}$	V_2O_4S
450 / 30	35.9	16.7	$VS_{0.47}$	V_2O_4S
450 / 180	62.2	37.6	$VS_{0.60}$	V_2O_4S
500 / 30	30.8	30.1	$VS_{0.98}$	$V_2O_3S_2$
550 / 30	26.2	39.4	$VS_{1.50}$	$V_2O_2S_3$
600 / 30	19.0	12.1	$VS_{0.64}$	V_2O_4S

Table 3.9 Table comparing the atomic concentrations of vanadium and sulfur as determined by EDX. Recorded from samples of the black films produced by the APCVD reaction of oxovanadium(V) chloride and hydrogen sulfide with 0.5 dm^3 min^{-1} flow of H_2S.

Varying the flow rate of hydrogen sulfide for reactions at 500 °C does affect the extent of sulfur incorporation into the films deposited. Increasing the flow rate of hydrogen sulfide also causes a decrease in the size of the crystallites deposited during the 30 s reactions studied.

H_2S flow rate / $dm^3 min^{-1}$	Atomic % V	Atomic % S	V:S ratio / atomic %	Formula
0.5	30.8	30.1	$VS_{0.98}$	$V_2O_3S_2$
1.0	26.7	36.5	$VS_{1.37}$	$V_2O_2S_3$

Table 3.10 Table comparing the atomic concentrations of vanadium and sulfur as determined by EDX. Recorded from samples of the films produced by the APCVD reaction of oxovanadium(V) chloride and hydrogen sulfide at 500 °C with either a 0.5 or 1.0 $dm^3 min^{-1}$ flow of H_2S.

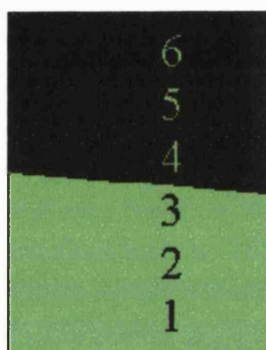

Figure 3.11 A representation of a 1 x 1.2 cm sample of the film deposited at 400 °C by the APCVD reaction (30 s) of oxovanadium(V) chloride and hydrogen sulfide.
The diagram depicts the sample which includes the boundary region between the green and black areas of the film. The numbers shown on the film indicate the spots analysed by EDX, these data being tabulated below.

Analysis number	Atomic % V	Atomic % S	V:S ratio / atomic %
6	38.4	10.3	$VS_{0.27}$
5	38.8	10.5	$VS_{0.27}$
4	41.4	11.8	$VS_{0.29}$
3	41.1	7.9	$VS_{0.19}$
2	41.3	5.9	$VS_{0.14}$
1	44.3	2.1	$VS_{0.05}$

Table 3.12 EDX results from a line crossing the boundary between green and black regions of the film deposited at 400 °C by the APCVD reaction (30 s) of oxovanadium(V) chloride and hydrogen sulfide.

The above table confirms the change of stoichiometry across the boundary between the green and black regions of the film deposited at 400 °C. The data for oxygen concentration is not very reliable from EDX results due to oxygen's low atomic mass

and the thickness of the film analysed (which is thin enough to allow a break-through of excitation volume to the underlying glass) so this was not recorded for this sample. The significance of the above data is that the transformation from the black film to the green film involves the loss of sulfur.

3.4.7 Scanning electron microscopy

Electron microscopy photographs of the films deposited in this study are shown in figures 3.13a-d.

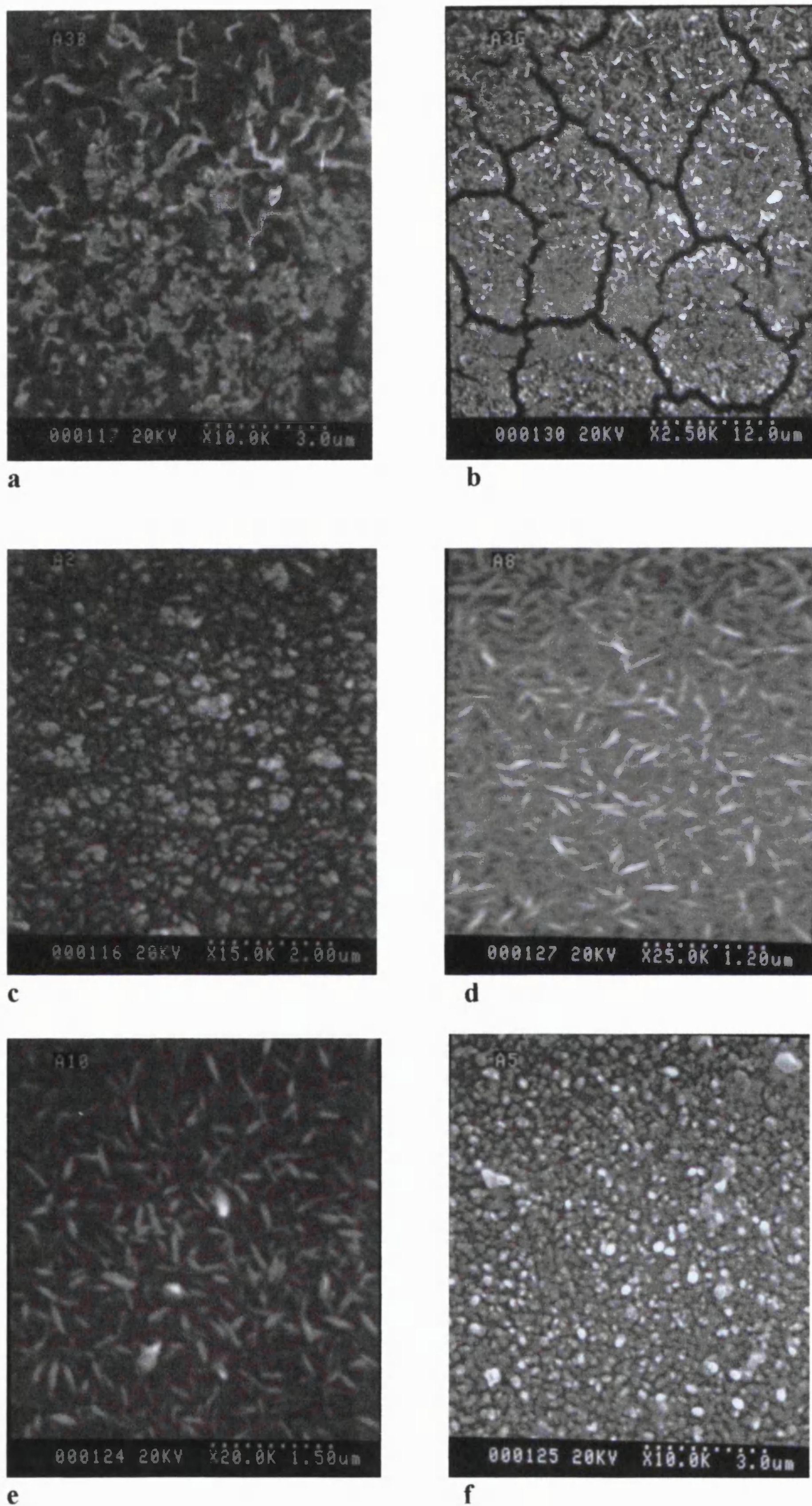

Figure 3.13 Scanning electron micrographs of films deposited at: a) 400 °C, b) 450 °C, c) 500 °C, e) 550 °C and f) 600 °C by the APCVD reaction (30 s) of oxovanadium(V) chloride and hydrogen sulfide; each with 0.5 dm^3 min^{-1} flow of hydrogen sulfide. d) 500 °C with 1.0 dm^3 min^{-1} flow of hydrogen sulfide.

3.4.8 Electron microprobe

Electron probe results indicate that the green areas of the film deposited at 450 °C have transformed to vanadium pentoxide, a result which has been confirmed by Raman microscopy. Figure 3.14 below shows a photograph at 180 x magnification of the film deposited at 400 °C by the APCVD reaction of oxovanadium(V) chloride and hydrogen sulfide. A spot analysis of this film near the boundary area gave a composition of V_6O_7S; this has a lower sulfur content than the 2:1 ratio measured previously, the change is due to the sample losing sulfur during storage in air. The analysis was performed 2 months after the film was manufactured.

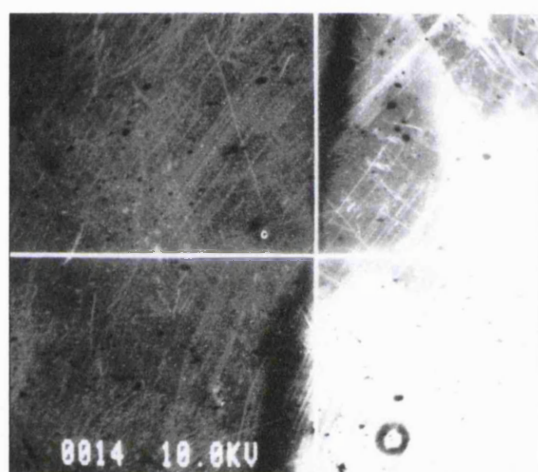

Figure 3.14 A picture of a 2 mm^2 dual coloured sample, with a green (LHS in picture) and black film boundary shown using 180 x magnification. This film was deposited at 400 °C by the APCVD reaction (30 s) of oxovanadium(V) chloride and hydrogen sulfide.

3.4.9 X-ray diffractometry

An XRD pattern of the film deposited at 600 °C by the APCVD reaction (30 s) of oxovanadium(V) chloride and hydrogen sulfide is shown below in fig. 3.15. Using the indexing programmes celref, crysfire and chekcell[32] the following two unit cells were identified as the most likely solutions:

P21/a, $a = 8.871$, $b = 10.274$, $c = 5.737$, $\beta = 99.97$

P21/n, $a = 11.371$, $b = 10.274$, $c = 5.738$, $\beta = 129.79$.[32]

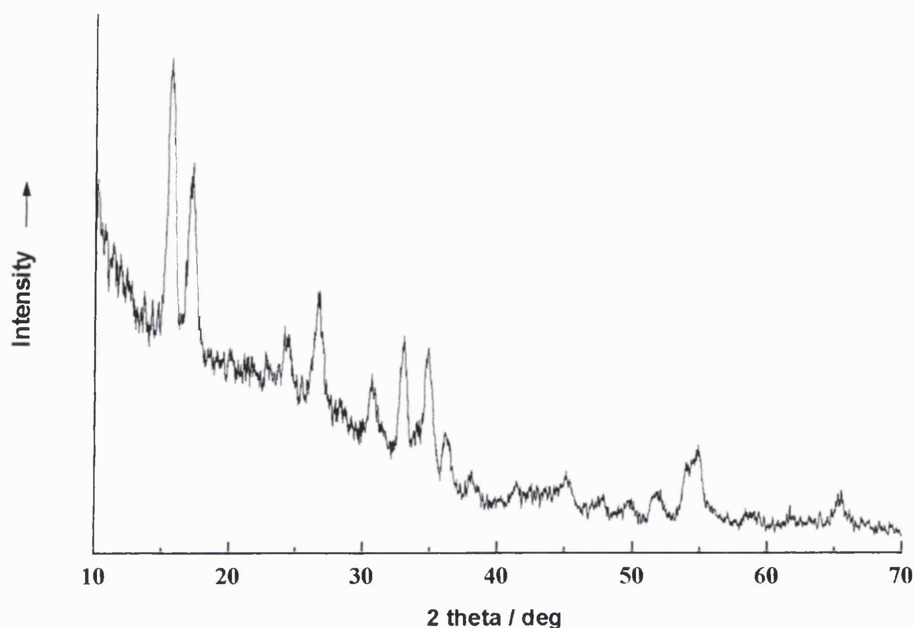

Figure 3.15 An X-ray diffraction pattern recorded from the film deposited at 600 °C by the APCVD reaction (30 s) of oxovanadium(V) chloride and hydrogen sulfide.
The diffraction pattern has been smoothed by adjacent averaging across 5 points to improve the signal-to-noise ratio.

3.4.10 X-ray photoelectron spectroscopy

XPS results (recorded by Mark Field) from a film deposited at 600 °C by the APCVD reaction (30 s) of oxovanadium(V) chloride and hydrogen sulfide are shown below in fig 3.16. This analysis was performed three months after film deposition. These spectra show XPS chemical shifts at 520.8, 515.4 and 513.2 eV due to vanadium; 530.5 eV due to oxygen and 162.1 eV due to sulfur. The value for oxygen compares well with expected values for transition metal oxides at 529.5 – 531.3 eV[33] The value for sulfur is closest to that for a transition metal sulfide such as ZnS at 160.7, rather than a sulfate or sulfite.

The peak areas indicate that the compound has the composition VOS with the following atomic percentages: 41% vanadium, 51% oxygen and 8% sulfur.

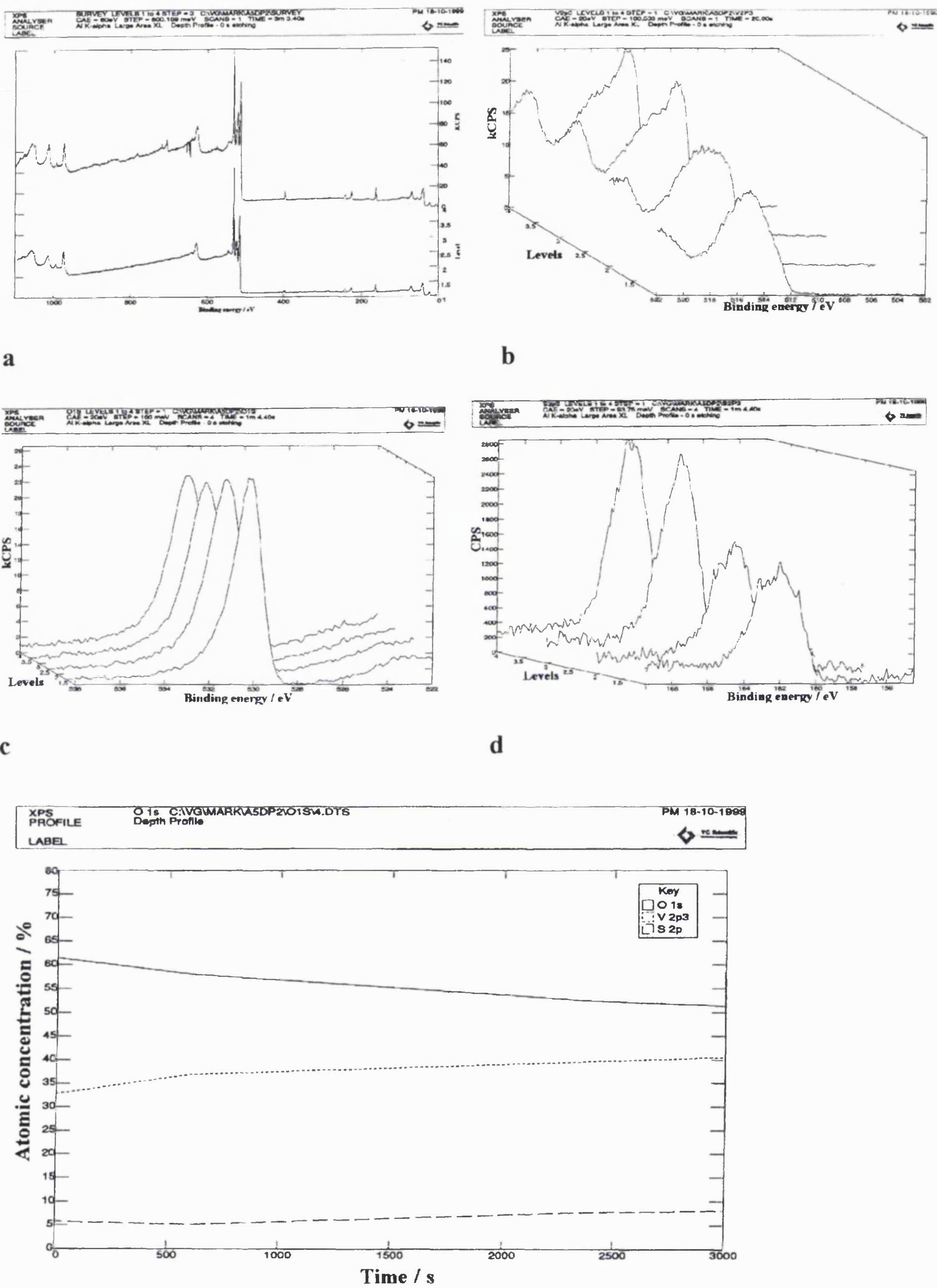

e

Figure 3.16 XPS results from a film deposited at 600 °C by the APCVD reaction (30 s) of oxovanadium(V) chloride and hydrogen sulfide. a) survey spectrum, b) vanadium, c) oxygen, d) sulfur peaks and e) shows the atomic concentrations of these elements at different levels in the film as revealed by argon etching.

3.4.11 UV/visible spectroscopy

A UV/visible spectrum recorded from the film deposited at 500 °C is shown below in figure 3.17. The spectrum shows that the material deposited on the substrate has a band gap of 1.2 eV, this is similar to tin(II) sulfide which has a band gap of 1.3 eV.[34]

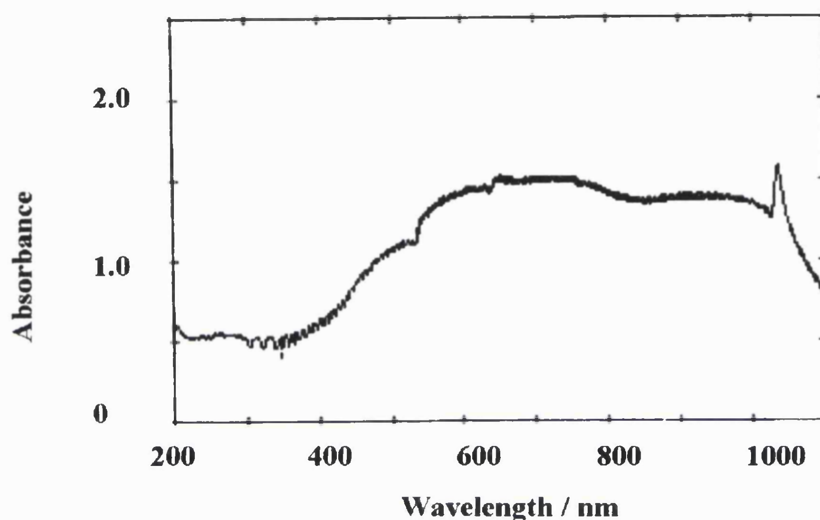

Figure 3.17 An UV/visible spectrum of a thin film of vanadium oxysulfide deposited at 500 °C by the APCVD reaction (30 s) of oxovanadium(V) chloride and hydrogen sulfide.

3.4.12 Transmittance/reflectance spectroscopy

The transmittance and reflectance spectra of films produced by the reaction of oxovanadium(V) chloride and hydrogen sulfide are shown below in figures 3.18a-b. These spectra indicate that the material is unsuitable for use in heat mirrors as they do not transmit enough visible light, or reflect sufficient ultraviolet radiation.

KEY – to the following transmittance/reflectance spectra

—— Reflectance spectra

—— Transmittance spectra

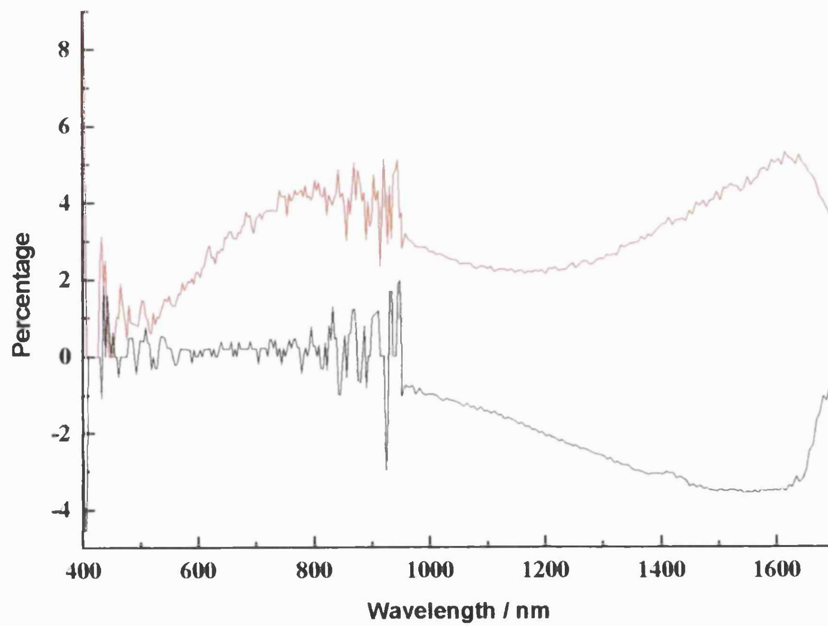

Figure 3.18a Transmittance and reflectance plots for the film deposited at 500 °C by the APCVD reaction (30 s) of oxovanadium(V) chloride and hydrogen sulfide.

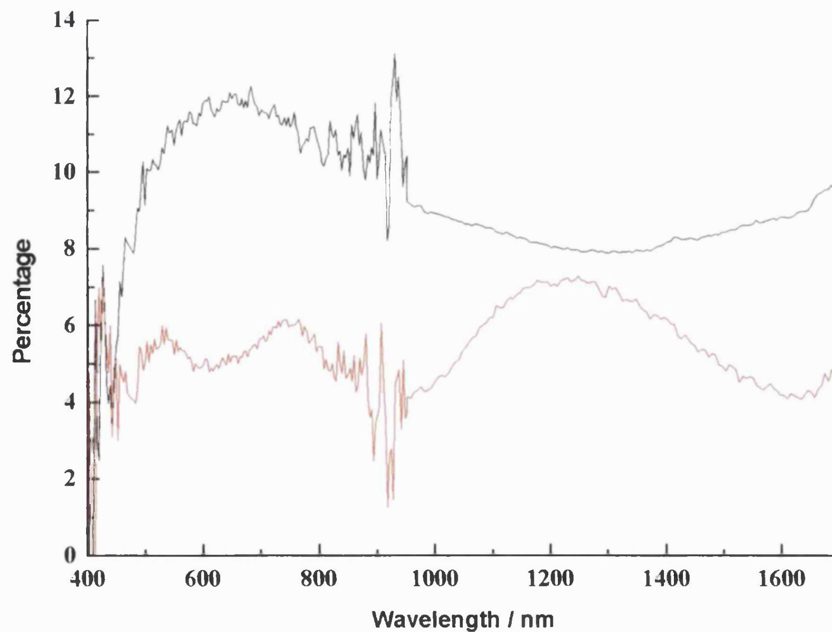

Figure 3.18b Transmittance and reflectance plots for the film deposited at 600 °C by the APCVD reaction (30 s) of oxovanadium(V) chloride and hydrogen sulfide.

The reflectance plot of the films deposited at 500 and 600 °C shown above in figs. 3.18a-b have a sinusoidal appearance caused by interference between radiation reflected

by the top surface of the film, and that reflected by the boundary between the coating and the underlying substrate. The Film Thickness Module from FTG software was used to analyse the interference patterns and determine the thickness of the films produced at 500 and 600 °C.

The film deposited at 500 °C was found to be 0.71 μm thick, the film deposited at 600 °C was found to be 1.24 μm thick assuming a refractive index of 2.3.

The other films deposited from the reaction of oxovanadium(V) chloride and hydrogen sulfide at 400, 450 and 600 °C had transmittance and reflectance properties as follows: 400 °C, both green and black areas of the film reflect between 0 – 5 % incident light and transmit 0 – 18 %; 450 °C both green and black areas of the film reflect between 0 – 3 % incident light and transmit 0 – 17 %; The film deposited at 600 °C reflects between 0 – 18 % incident light and transmits none of the incident light.

3.5 Discussion

Vanadium pentoxide films have been deposited by Mark Field using the APCVD reaction of oxovanadium(V) chloride and water, and from vanadium tetrachloride and water. With a oxovanadium(V) chloride precursor, films of vanadium pentoxide were deposited with substrate temperatures of between 350 – 600 °C. With vanadium tetrachloride and water, films were only produced with a substrate temperature of 450 °C or above.[30]

Some of the films produced at low temperatures in this study, changed colour from black to lime green inside two weeks from deposition. Raman microscopic analysis caused some transformation to V_2O_5 of the film deposited at 400 °C, but this was limited to the *c.* 1 μm diameter spot illuminated by the laser during analysis. The spectrum resulting from this transformation can be seen in figure 3.7b. Raman microscopy did not identify any oxovanadium(V) sulfate in the films produced. Transmittance and reflectance spectra indicate that the films produced by the 30 s APCVD reaction of oxovanadium(V) chloride and hydrogen sulfide are approximately 1 μm thick.

Raman microscopy did lead to the identification of vanadium(III) sulfide on the films deposited at 450 °C (during a 180 s reaction,) 500 and 550 °C. The presence of V_2S_3 on

three of the films implies that the films did not consist of a single pure phase, and that Raman microscopy could not be used to identify all of the compounds present in the coatings produced in this study. This analysis is supported by EDX results, which did not confirm the ratios of vanadium to sulfur required for the presence of pure vanadium(III) sulfide. No V_2S_3 was identified on the films deposited at 400, 450 °C (during 30 s reactions,) and 600 °C. The X-ray diffraction pattern measured from the film deposited at 600 °C did not have peaks corresponding to vanadium(III) sulfide.

EDX showed that the change of colour of the film was accompanied by a loss of sulfur. There was also a slightly sulfurous smell around the films on storage, probably caused by the evolution of H_2S during V_2O_5 formation. SEM photos showed that the areas of the film that had turned green appeared cracked as a result of the transformation.

XPS, EDX and electron microprobe gave conflicting results for film composition; however EDX should give the most accurate ratio of vanadium to sulfur as the other analyses were performed after the films had been exposed to air. In general the tendency to transform to vanadium pentoxide, indicates that the films lose sulfur and gain oxygen over time. Even the small region analysed by EDX around the boundary indicated an 80% loss of sulfur. It also seems that not all the molecules transform at the same rate or at the same time. The change is probably caused by the molecule's environment, by reacting with water vapour or oxygen. The presence of different coloured regions of the film also shows that deposition temperature dictates the initial product stoichiometry and thickness, which in turn will affect the time taken for the film to transform to the green product.

The compounds formed in this study correspond to V_2O_5, with some of the oxygen substituted by sulfur. Increasing the temperature or flow of hydrogen sulfide causes an increase in sulfur substitution between 400 and 550 °C. The films become harder and less porous at higher deposition temperatures, therefore the transformation to V_2O_5 takes longer.

If the transformation of $V_2O_xS_y \rightarrow V_2O_5$ takes place with the loss of H_2S it might be reasonable to assume that the vanadium oxysulfide reacts with water to gain oxygen and lose sulfur. This could be tested by taking a sample of freshly prepared film and

splitting it into three, leaving one piece in dry air, another in dry nitrogen and the third open to the atmosphere. The changes could then be monitored as they occurred.

4.0 Vanadium sulfide

4.1 Introduction

The vanadium sulfide films described in this chapter were produced by the APCVD reaction of vanadium tetrachloride and hydrogen sulfide. The films were characterised by EDX, electron microprobe, XPS, XRD, and Raman microscopy.

4.2 Background

There are many potential uses for vanadium sulfide including: layers in composite hydrogen separation membranes,[35] visible-light generation of hydrogen from hydrogen sulfide in aqueous solutions,[36,37] mercury removal from hydrocarbon fluids,[38] hydrorefining/cracking of heavy hydrocarbon oils,[39,40,41] catalysts for oxidising hydrogen sulfide to sulfur dioxide in environmental applications[42] and high energy-density batteries.[43]

Many different vanadium sulfides are known and have been characterised by X-ray diffractometry.[44] Literature information about the structure of V_2S_3 is conflicting. Hewston et al. produced single crystals of V_2S_3 by direct combination of the elements at 500 °C in a sealed ampoule. After removal of the unreacted elements, crystals were grown by heating the mixture in sulfur for one month at 500 °C. The crystals of V_2S_3 grown by this method were hexagonal or elongated platelets with a hexagonal unit cell.[44] V_3S_4 has a monoclinic unit cell.[44] More recently Bensch and Koy have characterised V_3S_4 reporting that the structure is hexagonal and isotypic with Nb_3Se_4 at temperatures between 100 – 295 K. They report a structure with quasi-one-dimensional metal, zig-zag chains parallel to the crystallographic c-axis with V-V distances of 2.864(1) Å within the chains and 3.120(1) Å between the chains; the presence of these chains confer quasi-one-dimensional metallic properties to the material. Bensch also reports that V_3S_4 is metastable and transforms to a monoclinic structure at elevated temperatures.[45]

Single crystals of V_5S_8, V_2S_3 and V_3S_4 have been grown by Taniguchi *et al.* by chemical transport using iodine as a transport agent.[46] Vanadium sulfide powders were

sealed in a quartz tube with iodine at 10^{-6} torr and was left for five to ten days in a temperature gradient of 150 – 250 °C. The electrical conductivity of the single crystals obtained by this method was measured from liquid nitrogen temperature to 25 °C.[46]

Vanadium sulfide films and powders have been produced by Schleich *et al.* at 250 °C using a plasma to enhance the reactivity of hydrogen sulfide with vanadium tetrachloride. This resulted in the formation of powders at high hydrogen sulfide concentrations (total pressure of 900 mtorr.) If the H_2S to VCl_4 ratio is greater than 5:1, VS_4 is produced. Vanadium tetrasulfide can be identified by its IR band at 520 cm^{-1} due to a S-S absorption. Films were deposited onto silica slides with, or without rf plasma. Vanadium disulfide cannot be produced by direct combination of the elements.[47] Therefore Schleich concluded that films could not be produced by classical chemistry. Combination of vanadium and sulfur at high temperature results in the formation of V_5S_8.[47]

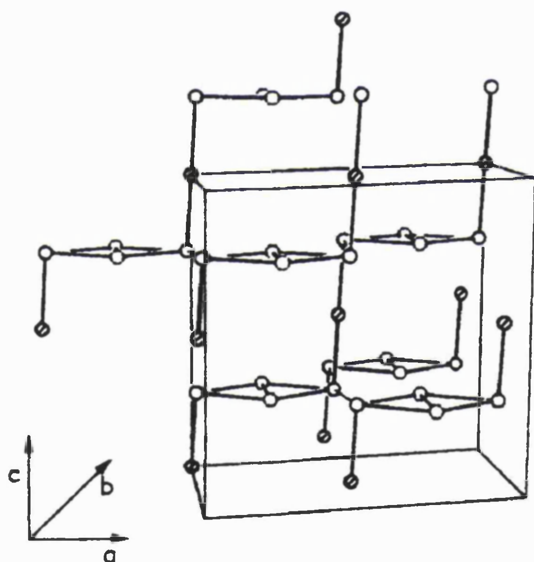

Figure 4.1 A schematic representation of locations of the vanadium atoms inside the unit cell of V_5S_8.[48]

Three different hexagonal $B8_1$ phases have been reported between compositions $V_{0.89}S$, $V_{0.95}S$ and $V_{0.98}S$. Metal-rich vanadium monosulfide structures contain sulfur vacancies; metal deficient vanadium monosulfide samples contain vanadium vacancies in the lattice. At room temperature the B31 phase is stable for compositions in the range $0.85 \leq S/V < 1.06$, and $B8_1$ becomes stable for S/V compositions of 1.06.[49]

4.3 Experimental

Vanadium sulfide thin films were produced from the APCVD of vanadium tetrachloride and hydrogen sulfide. The design of the rig is discussed in Chapter 2. The vanadium tetrachloride was admitted to the reactor via a bubbler, which was heated to 98 – 103 °C during the reaction. A nitrogen gas flow of 0.5 $dm^3\ min^{-1}$ was passed through the bubbler to carry the vanadium tetrachloride into the reactor. The hydrogen sulfide was allowed to flow into the gas stream at the rate of either 0.5 or 1.0 $dm^3\ min^{-1}$ with 1 $dm^3\ min^{-1}$ nitrogen as a diluent gas. The carrier gas passed through a mass flow controller prior to the bubbler. The precursors were separately transported to the reactor with 10 $dm^3\ min^{-1}$ nitrogen carrier gas. The precursor gas flows joined at the inlet of the reactor and were premixed in the brass block prior to being passed over the glass substrate.

Eight depositions were carried out for this system, each deposition being conducted for 1 min at temperatures between 300 - 600 °C inclusive, at 50 °C intervals. All other conditions were unchanged unless otherwise stated. The conditions used for each run are shown below in table 4.2. Energy dispersive X-ray analysis (EDX) was used to determine quantitatively the composition of the films produced. In addition, the films were also characterised by Raman microscopy, UV/visible spectroscopy and scanning electron microscopy. Film adherence to the glass was assessed using the Scotch tape test and by scratching the surface with a scalpel. The solubility of one of the films was assessed in various solvents as described in Chapter 2.

Deposition temperature / °C	**Bubbler temperature / °C**	**H_2S gas flow /$dm^3\ min^{-1}$**
300	102	0.5
350	101	0.5
400	101	0.5
400	98	1.0
450	103	0.5
500	103	0.5
550	101	0.5
600	99	0.5

Table 4.2 Deposition conditions for the APCVD reactions of vanadium tetrachloride and hydrogen sulfide.

4.4 Results

4.4.1 Film colour and uniformity

The APCVD reactions of vanadium(IV) chloride and hydrogen sulfide resulted in good coverage of the glass substrates. In some of the films pinholes were detected due to gas phase nucleation. The thin films deposited were opaque, or a translucent brown/black in colour when viewed with a light source behind the film. Table 4.3 below contains descriptions of the visual appearance of films deposited on day of manufacture and any changes noticed subsequently. The film colours are described below, as they appeared lying flat on a white sheet of paper illuminated from above. Films are described from the gas inlet end of the substrate to the exhaust end. In each case below the predominant colour of the film is highlighted in bold script.

Deposition temperature / °C	**H_2S gas flow /dm^3 min^{-1}**	**Visual appearance of film on day of manufacture and any changes noticed subsequently**
300	0.5	1-4 cm silver reflective, **grey/black film** with a brown region *c.*5 cm long and 4 cm wide at the top left hand side viewed from above along the length in the reactor. After several weeks 2-5 cm of the right hand side of the film had turned a **lime green** colour as had the top 3-5 cm.
350	0.5	The surface was coated with a **thick black film**, which was slightly thinner at the entry and exit ends of the substrate.
400	0.5	The surface had a powdery – amorphous **black** coating that appeared smoother at the edges.
400	1.0	The substrate had an amorphous looking **black** coating that became reflective at the edges.
450	0.5	The entire substrate was coated with **black** material with an extended elliptical area *c.*12 cm long in the centre appearing smoother than the surrounding film.
500	0.5	Two small powdery black areas at the start of a dull **grey/black** unreflective film, with a very reflective opaque black region of coating on the top left hand side.
550	0.5	*c.* 5 cm grey unreflective film, the rest of the film consisted of a **black** reflective material.
600	0.5	The substrate had a thick **black** coating thinning out slightly along the length and at the edges where it appeared brown/black in colour.

Table 4.3 Descriptions of the appearances of films deposited by the APCVD reactions of vanadium tetrachloride and hydrogen sulfide.

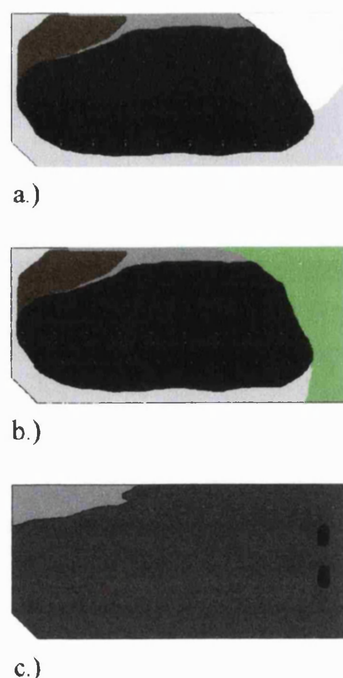

Figure 4.4 A schematic representation of two films deposited by the APCVD reaction of vanadium tetrachloride and hydrogen sulfide. a) at 300 °C, c) 500 °C on the day of deposition and b) the same film as in (a) after 2 months storage in air.

4.4.2 Film adhesion

All of the films produced by the reaction of vanadium(IV) chloride and hydrogen sulfide could be scratched with a scalpel to reveal plain glass. All of the films however passed the Scotch Tape test.

4.4.3 Solubility

The solubility of a sample of the film deposited at 550 °C was tested as described in Chapter 2. This film was not soluble in water, acetone, methanol, dilute sodium hydroxide and petroleum spirit. However ribbons of the film peeled off the substrate when placed in dilute nitric acid.

4.4.4 Raman microscopy

Raman analysis was performed at room temperature (using 632.8 nm excitation) 1 – 2 weeks after manufacture of the films, the spectra are shown below in figure 4.5a-i. Some of the spectra have been slightly smoothed by using a single 5-point adjacent averaging procedure. The films were compared with a standard Raman spectrum of vanadium(III) sulfide shown below in figure 4.5a. In addition Raman spectra reported in Chapter 3 were used as a comparison.

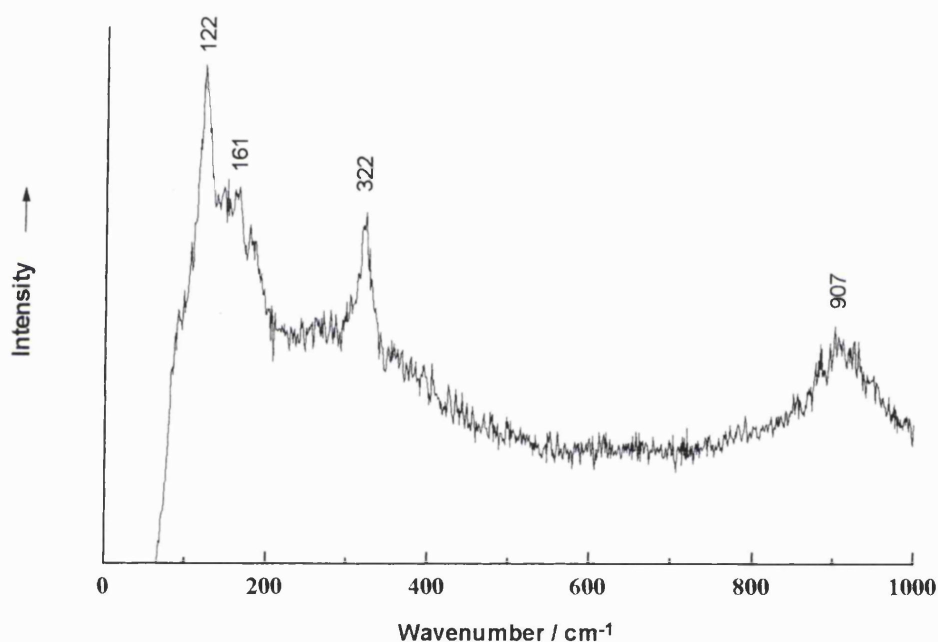

Figure 4.5a Raman spectrum of vanadium(III) sulfide powder used as a standard. Prepared by a liquid mediated metathesis reaction of sodium sulfide and vanadium trichloride in toluene at reflux.

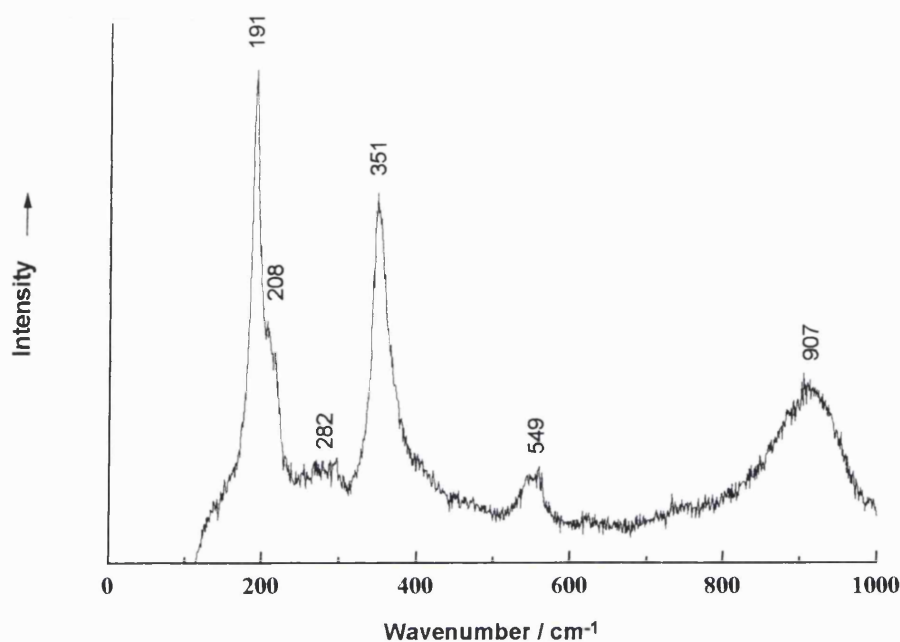

Figure 4.5b Raman spectrum of the film deposited at 300 °C by the APCVD reaction of vanadium tetrachloride and hydrogen sulfide.

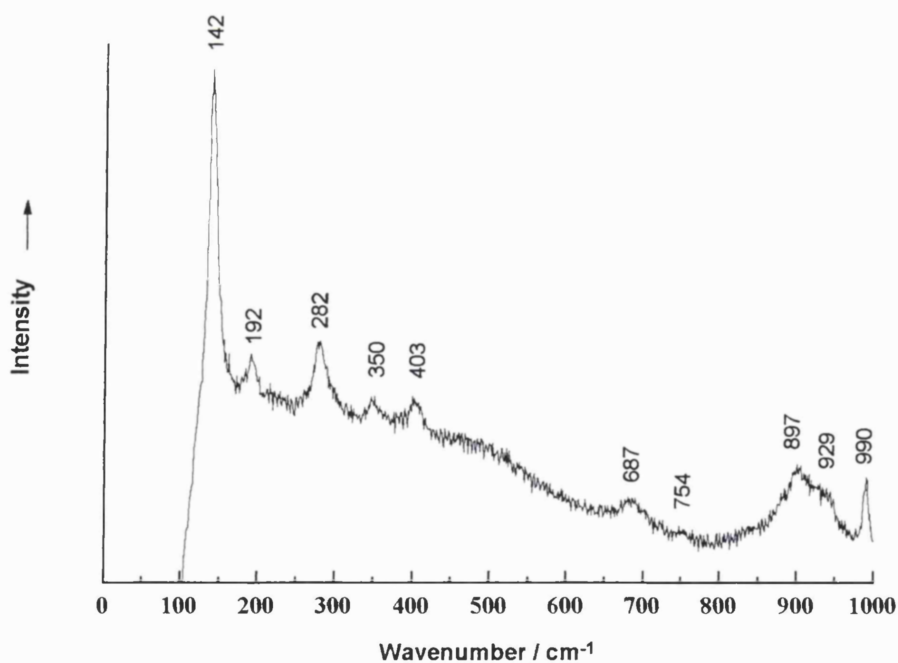

Figure 4.5c Raman spectrum (from a different point to the one analysed for figure 4.5b) from the film deposited at 300 °C by the APCVD reaction of vanadium tetrachloride and hydrogen sulfide.

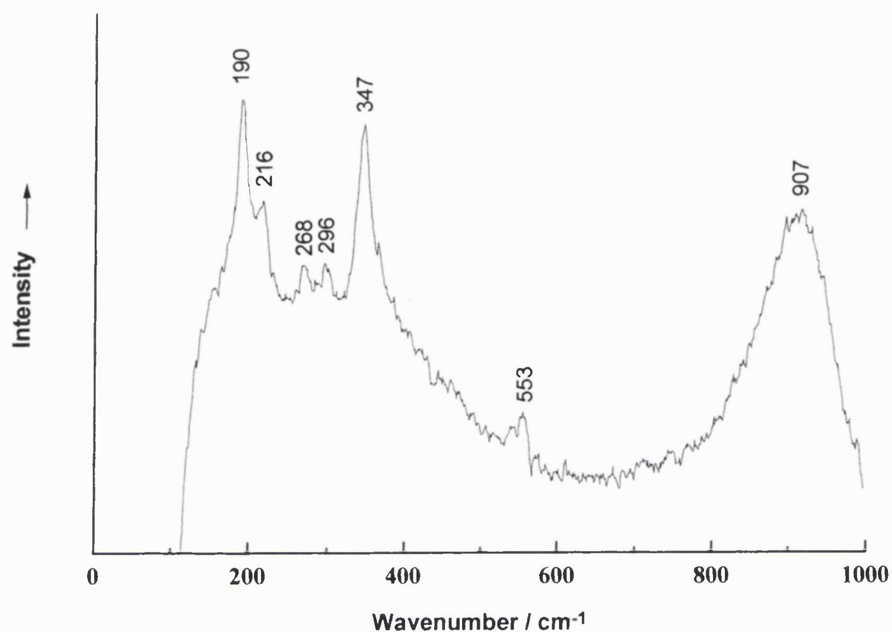

Figure 4.5d Raman spectrum of the film deposited at 350 °C by the APCVD reaction of vanadium tetrachloride and hydrogen sulfide.

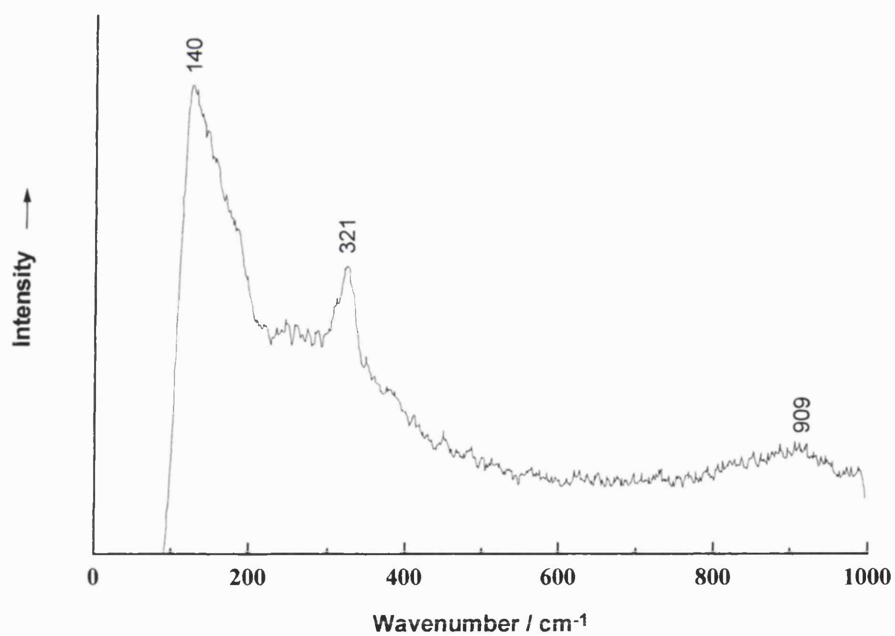

Figure 4.5e Raman spectrum of the film deposited at 400 °C by the APCVD reaction of vanadium tetrachloride and hydrogen sulfide.

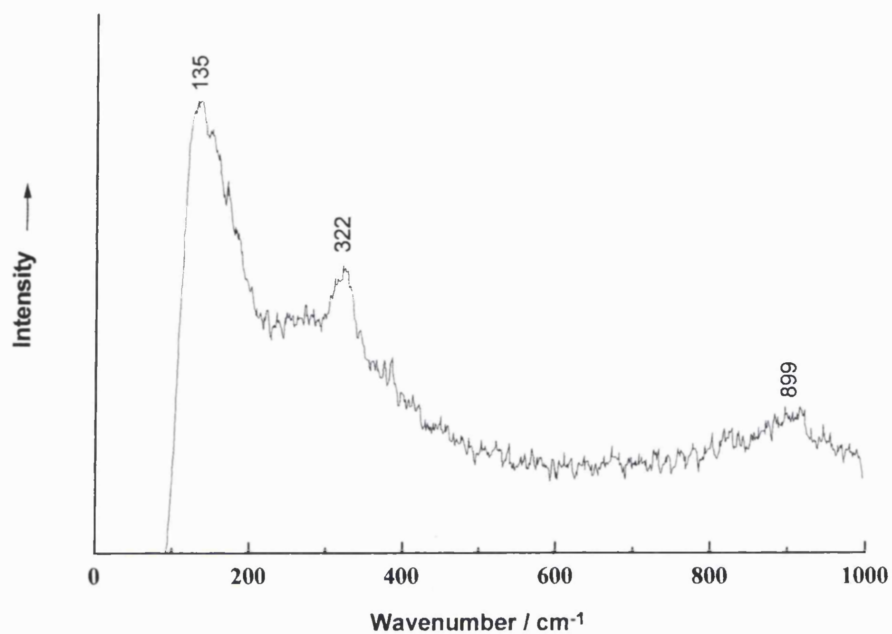

Figure 4.5f Raman spectrum of the film deposited at 450 °C by the APCVD reaction of vanadium tetrachloride and hydrogen sulfide.

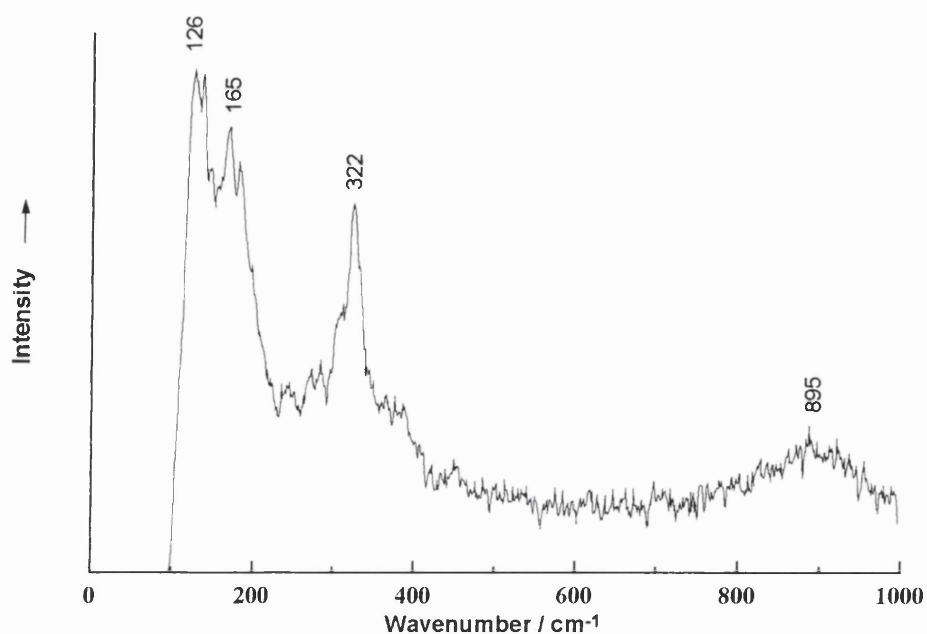

Figure 4.5g Raman spectrum of the film deposited at 500 °C by the APCVD reaction of vanadium tetrachloride and hydrogen sulfide.

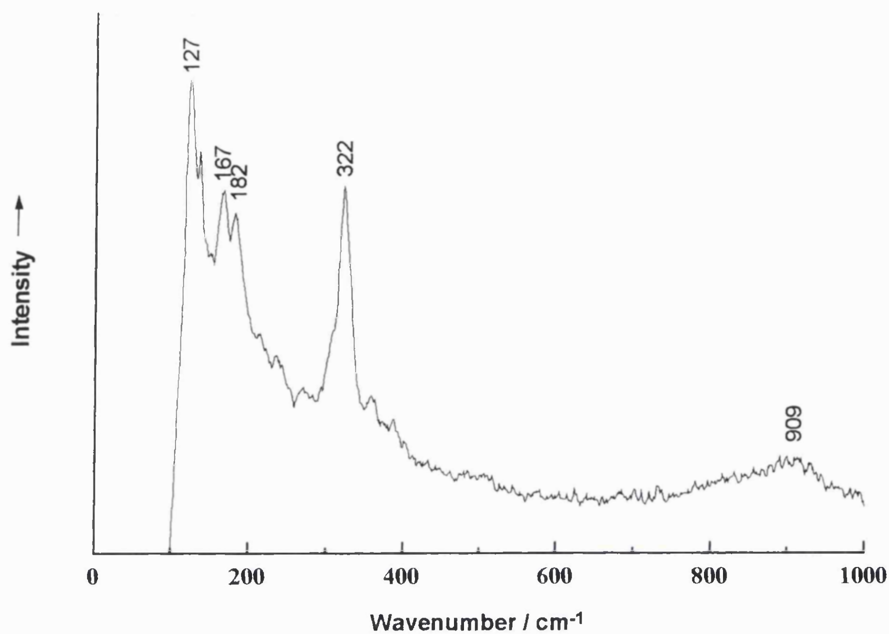

Figure 4.5h Raman spectrum of the film deposited at 550 °C by the APCVD reaction of vanadium tetrachloride and hydrogen sulfide.

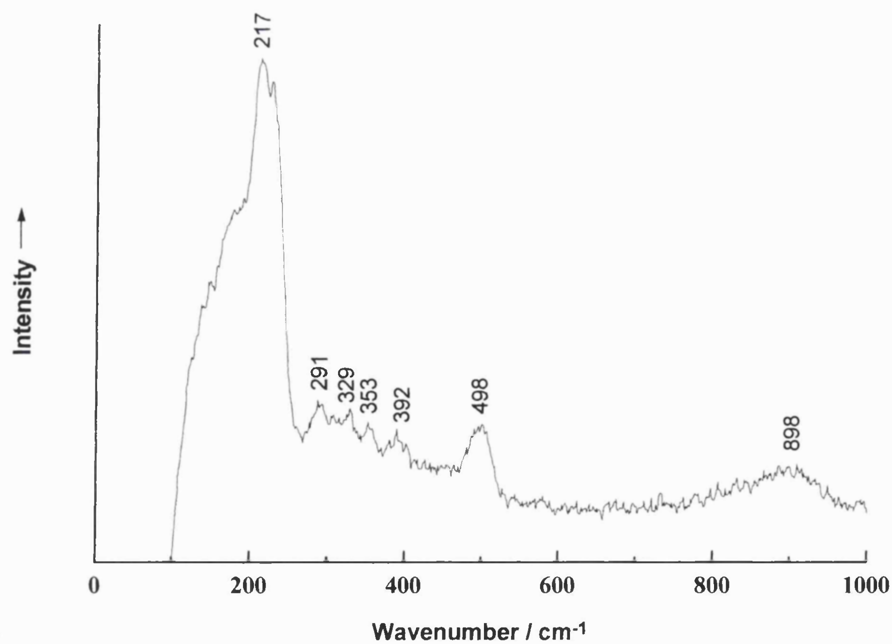

Figure 4.5i Raman spectrum of the film deposited at 600 °C by the APCVD reaction of vanadium tetrachloride and hydrogen sulfide.

The Raman spectrum shown in figure 4.5b was recorded from an area of film found to consist of vanadium(IV) sulfide according to EDX data. The Raman bands at 191, 351, 549 and 907 cm^{-1} must therefore be due to VS_2. A Raman spectrum recorded from a different area of film deposited at 300 °C, near the end of the substrate (figure 4.5c), had bands which corresponded to vanadium pentoxide. Bands at 142, 282, 403 and 990 cm^{-1} compare with bands at 144, 282, 405 and 995 cm^{-1} for V_2O_5. Raman bands at 192, 350, and *c.* 900 cm^{-1} compare with 191, 351 and 907 cm^{-1} for VS_2.

The Raman spectrum shown in figure 4.5d was recorded from a film deposited at 350 °C this had Raman bands at 190, 347, 553 and 907 cm^{-1} in comparison to those recorded from VS_2 previously at 191, 351, 549 and 907 cm^{-1}. At 350 °C there are no bands due to vanadium oxides present in the spectrum.

The film deposited at 400 °C was found to consist of vanadium(III) sulfide by EDX, the Raman spectrum in figure 4.5e supports this analysis with bands at 140, 321 and 909 cm^{-1} in comparison to 122, 161, 322 and 907 cm^{-1} recorded from a standard shown in figure 4.5a. This is a reasonable match although the first two peaks have not been resolved. The films deposited at 450 and 500 °C were also found to consist of vanadium(III) sulfide by EDX. The Raman spectra for these films are shown in figures 4.5f and 4.5g these have bands at 135, 322 and 899 and 126, 165, 322 and 895 cm^{-1} respectively.

The film deposited at 550 °C consists of V_3S_4 according to EDX analysis, however the Raman spectrum is similar to the one recorded from V_2S_3. It is possible that the coating deposited consists of a mixed phase. There are however no bands that indicate the presence of vanadium oxides or oxovanadium(IV) sulfate, so there must be a mixture of vanadium sulfides present.

The film deposited at 600 °C consists of VS according to EDX analysis. The Raman bands do not correspond to vanadium oxides or oxovanadium(IV) sulfate. The band at 898 cm^{-1} is close to that of the 907 cm^{-1} band of vanadium(III) sulfide however the other bands are absent from the spectrum. There are no standards to compare this spectrum against; however the band at 498 cm^{-1} has not appeared in any other spectra of vanadium sulfides recorded in this study so may be characteristic of vanadium(II) sulfide.

4.4.5 Energy dispersive analysis by X-rays

Quantitative EDX analysis (at 20 keV) showed the presence of vanadium and sulfur with some breakthrough of excitation volume to the glass substrate. This analysis was performed two weeks after manufacture of the films. The excitation depth of the EDX set-up used was approximately 1 μm and therefore the thickness of the film was less than this. The presence of *c.* 30% silicon would suggest a film growth rate of 0.7 - 1 $\mu m\ min^{-1}$.

EDX results show that as the deposition temperature is raised reactions occur that lead to increasing vanadium incorporation into the film. These results also show that at 400 °C an increased concentration of hydrogen sulfide does not lead to an increase in the vanadium incorporation.

Deposition Temp. / °C	**Atomic % V**	**Atomic % S**	**V:S ratio / atomic %**	**Formula**
300	10.52	20.86	1 : 1.98	VS_2
350	15.24	30.88	1 : 2.03	VS_2
400	11.59	20.20	1 : 1.74	V_2S_3
400 (1 $dm^3 min^{-1}$) H_2S flow rate	15.59	27.55	1 : 1.77	V_2S_3
450	21.03	35.62	1 : 1.69	V_2S_3
500	18.46	31.62	1 : 1.71	V_2S_3
550	15.45	21.54	1 : 1.39	V_3S_4
600	11.63	12.91	1 : 1.11	VS

Table 4.6 Table of the atomic concentrations by percentage of vanadium and sulfur for films deposited by the APCVD reaction of vanadium tetrachloride and hydrogen sulfide.

The 1 cm^2 region of the films sampled for the above results were chosen in each case from the centre of the film in an area that was representative of the largest domain of

uniform single coloured coating. Each square analysed by EDX had 6-8 individual spot analyses performed with the average compositions used in the above table 4.6.

4.4.6 Electron microprobe

A 2 cm transect of the film deposited at 500 °C was analysed by electron probe with one step every 17 μm to give 117 point analyses in total. The percentages of vanadium to sulfur along this line are shown below in figure 4.7. This analysis was performed 4 months after deposition. This analysis shows that at there is some variation in film composition over the surface of the substrate after storage.

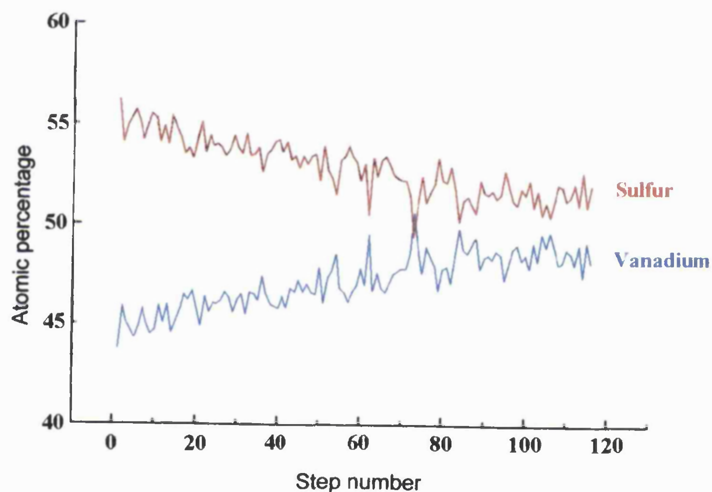

Figure 4.7 A plot of vanadium and sulfur composition by atomic percentage along a 2 cm line. On the film deposited at 500 °C by the APCVD reaction of vanadium tetrachloride and hydrogen sulfide.

4.4.7 Scanning electron microscopy

These micrographs were taken 1 – 2 weeks after film deposition and prior to the changing of colour of the film.

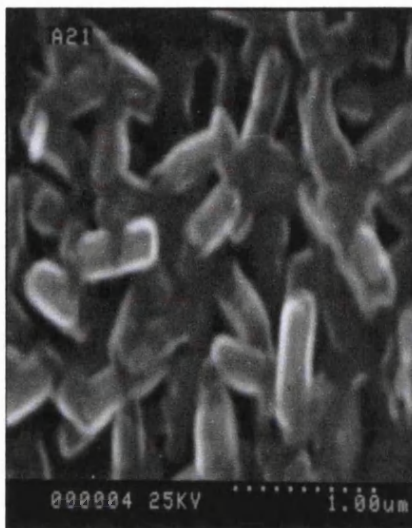

a

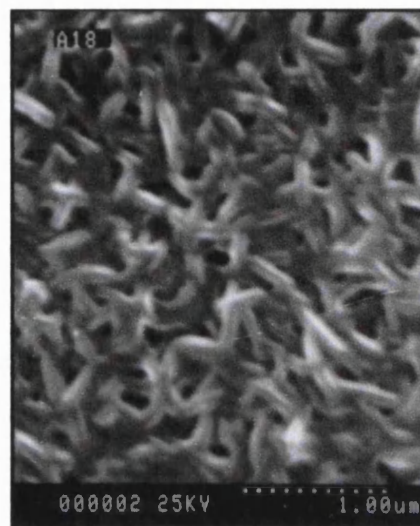

b

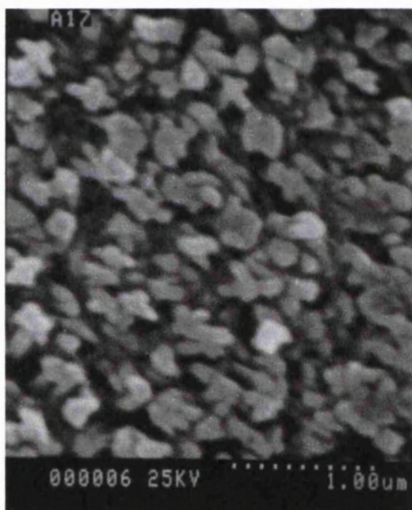

c

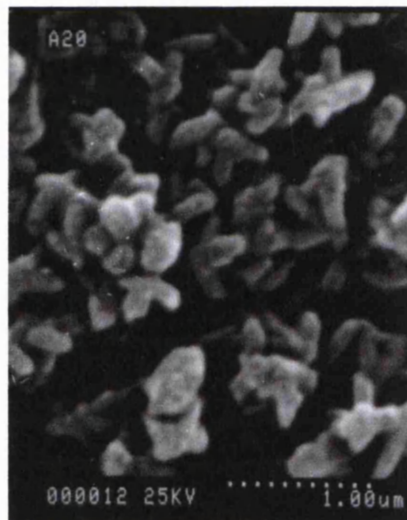

d

Figure 4.8a Scanning electron micrographs of films deposited by the APCVD reaction of vanadium tetrachloride and hydrogen sulfide at: a) 300 °C, b) 350 °C, c) 400 °C with 0.5 dm^3 min^{-1} flow of hydrogen sulfide, and d) 400 °C with 1.0 dm^3 min^{-1} flow of hydrogen sulfide.

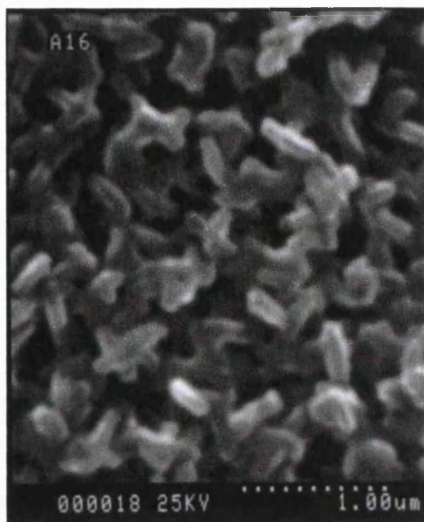

e

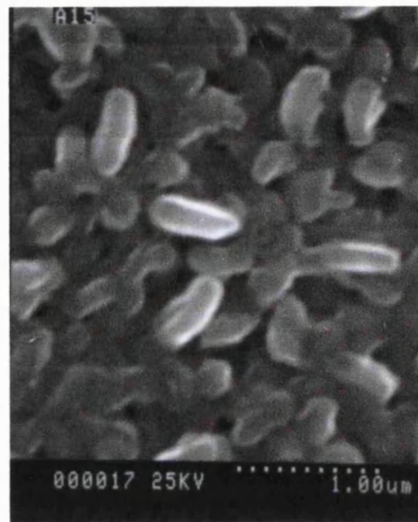

f

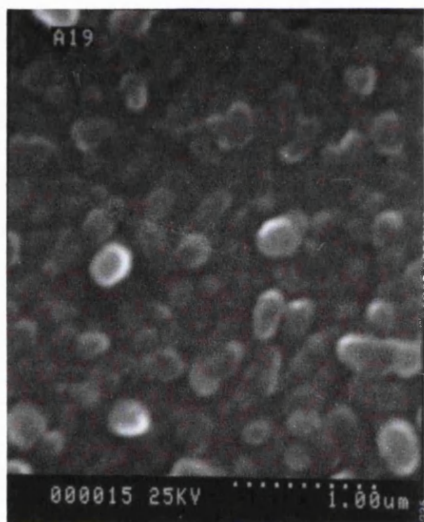

g

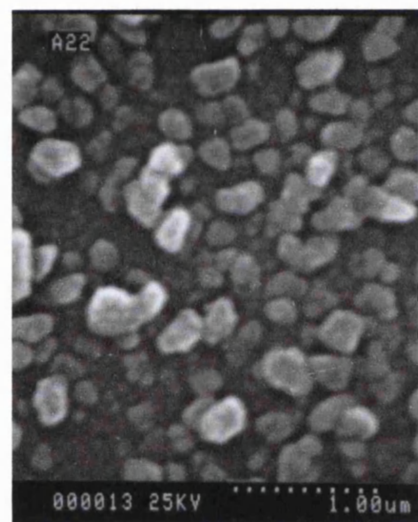

h

Figure 4.8b Scanning electron micrographs of films deposited by the APCVD reaction of vanadium tetrachloride and hydrogen sulfide at: e) 450 °C and f) 500 °C, g) 550 °C and h) 600 °C with 0.5 dm^3 min^{-1} flow of hydrogen sulfide.

Scanning electron micrographs are shown in figures 4.8a-h, these pictures show that 100-900 nm particles were produced.

Figure 4.8a-h above shows that the particle size decreases with increasing deposition temperature.

4.4.8 X-ray diffractometry

An X-ray diffraction pattern of the film deposited at 500 °C shows the presence of vanadium(III) sulfide. The diffraction pattern was indexed using Unit Cell software, see figure 4.9. There are also two additional peaks marked with asterisks, due to the presence of a second unidentified phase. The unit cell parameters of the vanadium(III) sulfide hexagonal lattice were found to be a = 6.88(1) and c = 22.07(30) Å which compares to literature values of a = 6.634(3), b = 22.49(4) Å.[44] The experimental values measured from the film match those of the literature vanadium(III) sulfide within the errors quoted.

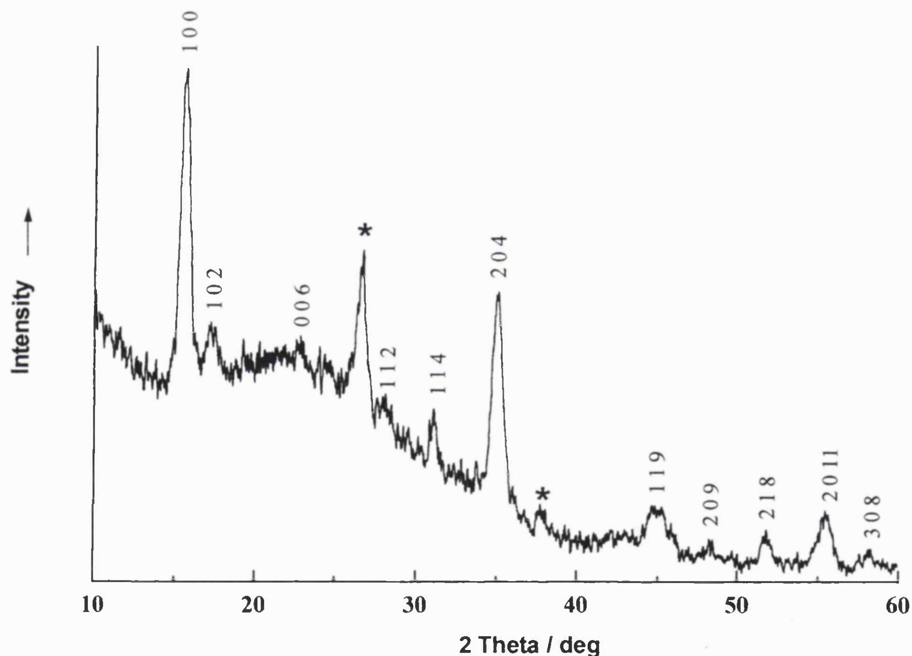

Figure 4.9 An X-ray diffraction pattern recorded from the film deposited at 500 °C by the APCVD reaction of vanadium tetrachloride and hydrogen sulfide. The diffraction pattern has been smoothed by adjacent averaging across 5 points to improve the signal-to-noise ratio.

Figure 4.10 below shows an X-ray diffraction pattern recorded from the film deposited at 600 °C the phase present could not be identified from its diffraction pattern. The

pattern did not match any vanadium sulfide in the literature. The EDX data however indicate that the film is composed of vanadium monosulfide.

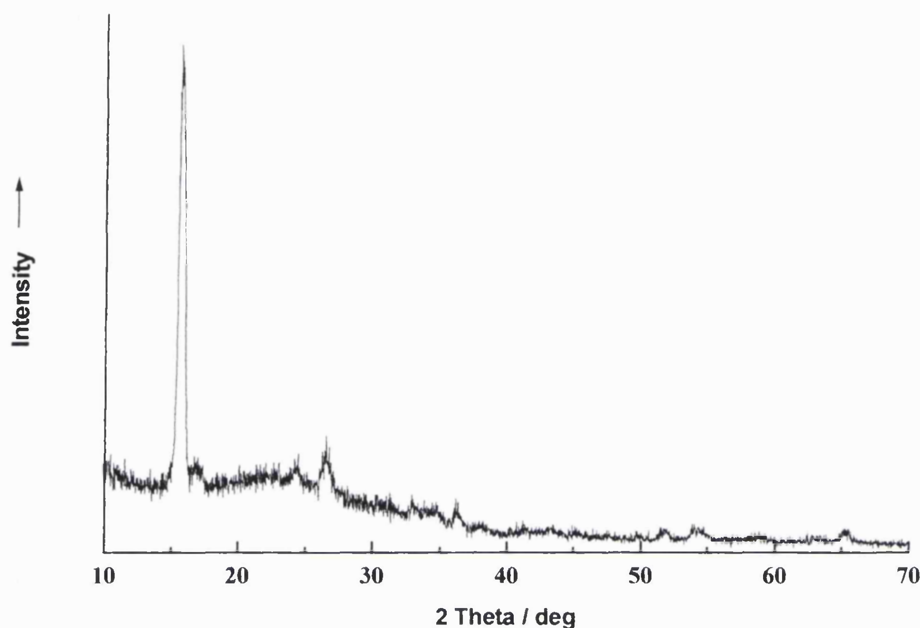

Figure 4.10 An X-ray diffraction pattern recorded from the film deposited at 600 °C by the APCVD reaction of vanadium tetrachloride and hydrogen sulfide.

4.4.9 X-ray photoelectron spectroscopy

The results of XPS measurements on a film deposited at 500 °C by the APCVD reaction of vanadium tetrachloride and hydrogen sulfide are shown in Figures 4.11a-d below. These show the presence of oxygen in addition to vanadium and sulfur in the film deposited at 500 °C, no other elements being present in the film. The presence of oxygen is attributed to the vanadium oxysulfide or vanadium oxide formed in the film on storage in air; XPS analysis of the film was performed approximately four months after deposition.

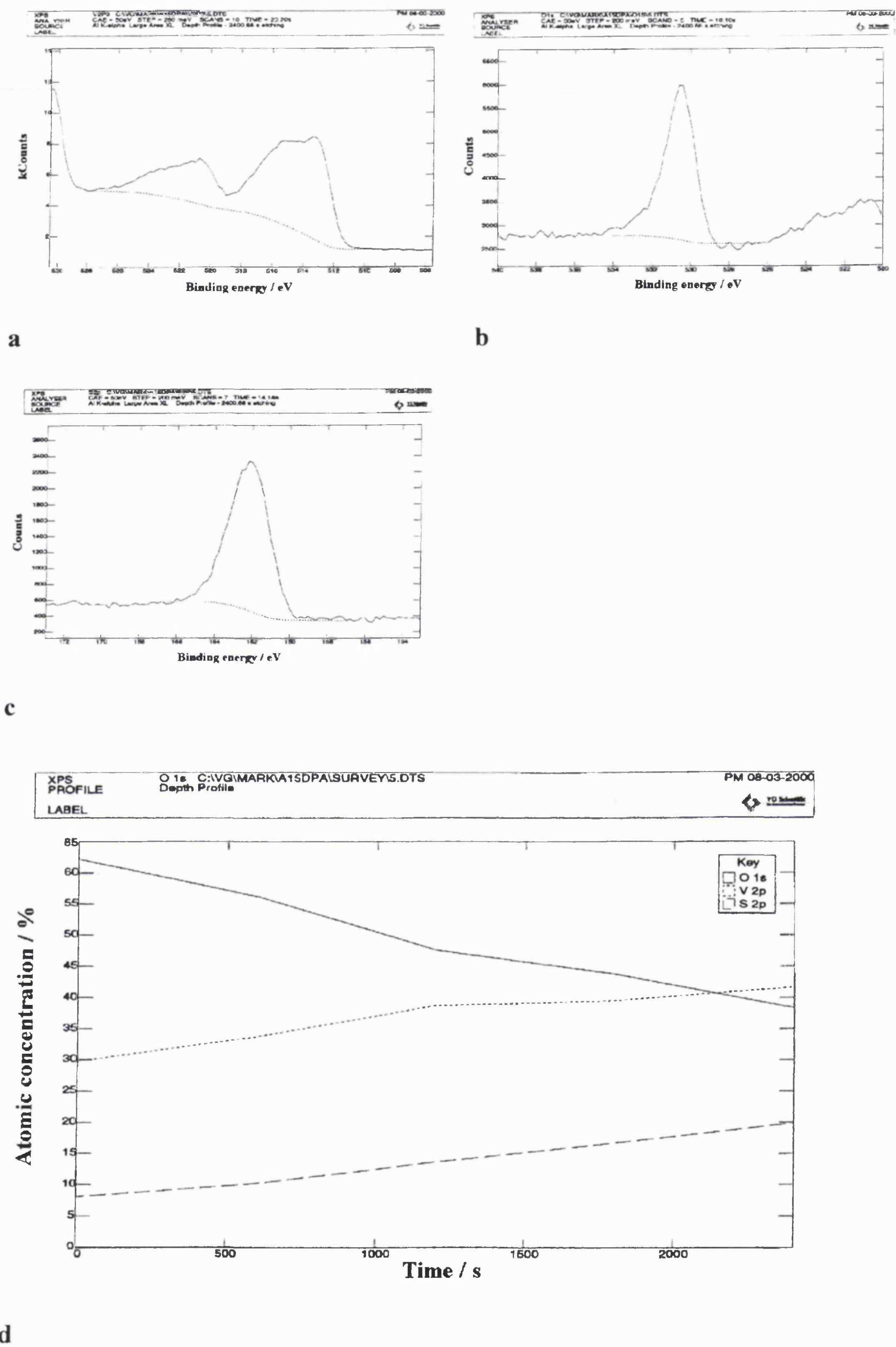

Figure 4.11 XPS results from a film deposited at 500 °C by the APCVD reaction of vanadium tetrachloride and hydrogen sulfide showing peaks for a) vanadium, b) oxygen, and c) sulfur with d) a plot of the atomic concentrations during argon etching of the surface.

XPS results from a film deposited at 500 °C by the APCVD reaction of vanadium tetrachloride and hydrogen sulfide are shown above in fig 4.11a-d. These spectra show XPS chemical shifts at 520.8, 515.1 and 514.2 eV due to vanadium, 530.0 eV due to oxygen and 162.2 eV due to sulfur. The value for oxygen compares well with expected values for transition metal oxides at 529.5 – 531.3 eV[50] The value for sulfur is closest to that for a transition metal sulfide such as ZnS at 160.7, rather than a sulfate or sulfite. The peak areas indicate a compound of VS with the atomic percentages 44% vanadium and 22% sulfur. 34% oxygen was also present due to the interval between deposition and analysis.

4.4.10 UV/visible spectroscopy

UV/visible spectra indicate that the vanadium sulfides produced all have a band gap of *c.* 1.2 eV, which is similar to the band gap of tin(II) sulfide at 1.3 eV [51]. The value of the band gap was calculated from the high wavelength edge of the wide band these films give rise to in their UV/visible spectrum. The films deposited at 300 and 350 °C had a band gap of 1.15 eV, and the films deposited between 400 – 600 °C had band gaps of 1.2 eV. The values for the band gap appear similar due to the units used. These results imply that the films deposited at 300 and 350 °C are slightly better electrical conductors than the other films deposited as the band gap is smaller.

4.4.11 Four-probe resistance measurements

A four-probe meter was used to measure the resistance of the films deposited in this study, the results being shown below in table 4.12.

Deposition temperature / °C	**H_2S gas flow /$dm^3 min^{-1}$**	**Resistance Ω/ □**
300	0.5	146
350	0.5	201 – 297
400	0.5	47
400	1.0	25
450	0.5	32
500	0.5	46
550	0.5	43
600	0.5	166

Table 4.12 Resistance measurements of the films deposited by the APCVD reaction of vanadium tetrachloride and hydrogen sulfide.

The four-probe sheet resistance measurements show different film conductivities for films with different compositions. The films identified by EDX as vanadium(IV) sulfide (300 and 350 °C) and the film composed of vanadium(II) sulfide (600 °C) have higher conductivities than the vanadium(III) sulfide films. The V_2S_3 films have resistance values between 25-47 Ω / □, the other films have resistance values approximately three times higher.

4.4.12 Transmittance / reflectance spectroscopy

KEY – to the following transmittance/reflectance spectra

——— Reflectance spectra

——— Transmittance spectra

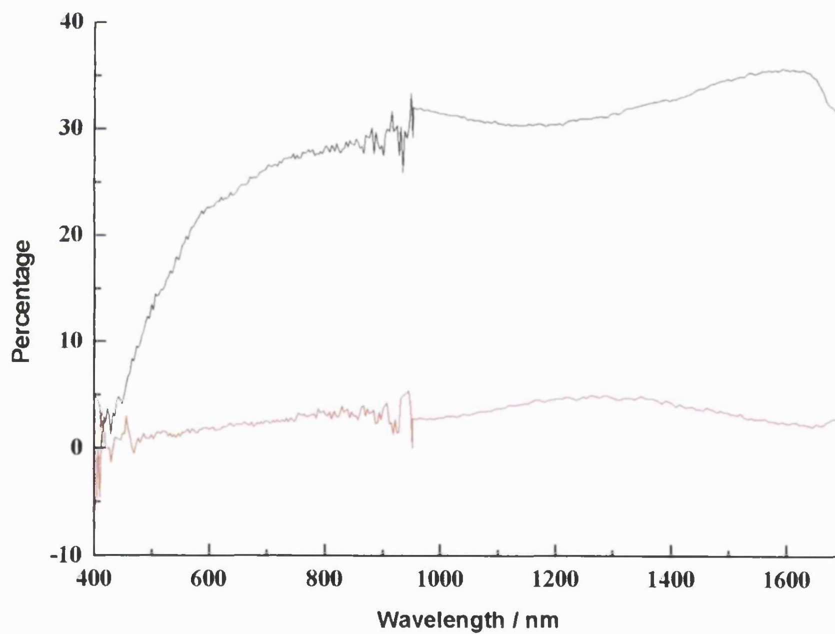

Figure 4.13 Reflectance and transmittance spectra from a green region of the film deposited at 300 °C by the APCVD reaction of vanadium tetrachloride and hydrogen sulfide.

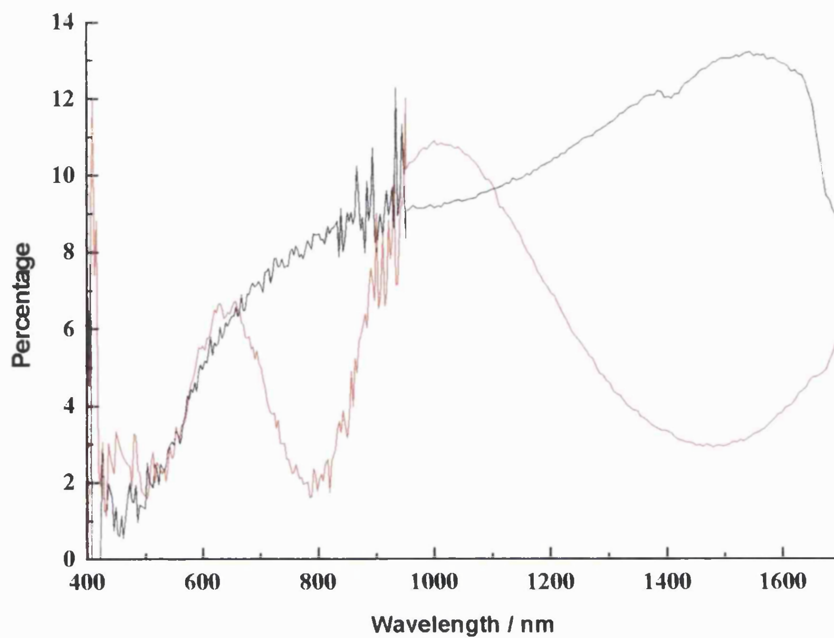

Figure 4.14 Reflectance and transmittance spectra of the film deposited at 350 °C by the APCVD reaction of vanadium tetrachloride and hydrogen sulfide.

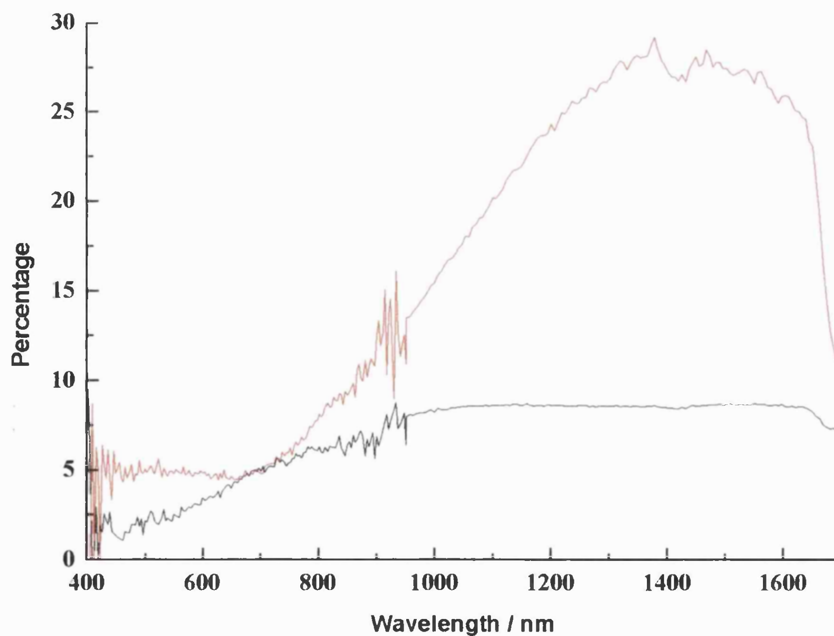

Figure 4.15 Reflectance and transmittance spectra of the film deposited at 600 °C by the APCVD reaction of vanadium tetrachloride and hydrogen sulfide.

The films deposited at 400 – 550 °C had the following transmittance and reflectance properties; at 400 °C the film reflected up to 11 % and transmitted 3 % of the incident radiation, at 450 and 500 °C the films reflected and transmitted less than 5 % of the incident radiation. The film deposited at 550 °C reflected up to 27 % and transmitted less than 3 % of the incident radiation.

The reflectance plot of the film deposited at 350 °C, shown above in fig.4.14, has a sinusoidal appearance caused by interference between radiation reflected by the top surface of the film, and that reflected by the boundary between the coating and the underlying substrate. The period of this wave can be used to determine the thickness of the layer that causes the interference. The Film Thickness Module from FTG software was used to analyse the interference pattern and determine the thickness of the film produced at 350 °C. The film was found to be 0.97 μm thick assuming a refractive index of 2.3.

4.5 Discussion

The APCVD reactions of vanadium(IV) chloride and hydrogen sulfide resulted in good coverage of the glass substrates. The films deposited were opaque, or a translucent brown/black in colour when viewed with a light source behind the substrate. The films would therefore be unsuitable for use as a window glass coating because black compounds are never used for this purpose. The films could all be scratched with a scalpel to reveal plain glass, but were not removed by Scotch tape. These films would be unsuitable for use in any application where abrasion might occur. The film deposited at 550 °C was not soluble in water, acetone, methanol, dilute sodium hydroxide and petroleum spirit. However nitric acid caused the coating to peel away from the substrate. Taking these properties into account the vanadium sulfide films produced may have potential uses in high-energy-density batteries or catalysis.[35-43] Electron microprobe results show that film composition varies across the substrate. It may be possible to make films of constant composition by coating the glass during the manufacturing process, with glass moving under a strip spraying the precursors onto the hot glass surface.

EDX was used to establish the composition of the films deposited in this study by the reaction of vanadium tetrachloride and hydrogen sulfide. Films of the following

compounds were produced: VS_2 at 300 and 350 °C, V_2S_3 at 400, 450 and 500 °C, V_3S_4 at 550 °C and VS at 600 °C.

The reaction of tin tetrachloride and hydrogen sulfide produces SnS_2 up to 500 °C, with Sn_2S_3 produced at 525 °C and a small amount of SnS_2, and at 545 °C SnS films are deposited.[52] The trend in composition of tin and vanadium sulfides is similar, although the M_2S_3 (M = V or Sn) composition is produced at a lower temperature for vanadium.

The growth rate of the vanadium sulfide films was approximately 1 μm min^{-1}. The films formed were of generally uniform appearance over the substrate. The Film Thickness Module from FTG software was used to determine the thickness of the film produced at 350 °C. The film was found to be 0.97 μm thick. SEM pictures show that 100-900 nm particles were produced. The particle size is dependant on deposition temperature. The film thickness determined by this method is based on the assumption that the material has the same refractive index as anatase, this adds inaccuracy to the model as the film in this study appears porous by SEM and probably has a different refractive index. Other methods which could be used to determine film thickness are; XPS etching or SEM of a slice of the film, or a step in the film produced by etching away a section, then imaging the height difference between the substrate and the top of the film. It might be possible to use nitric acid to etch the surface if an area could be successfully masked off and analysed.

Raman microscopy is useful in the analysis of thin films to show general trends linking colour or appearance of films to composition, although care has to be taken when recording spectra. Laser irradiation of some of the vanadium sulfides produced led to a conversion to vanadium(V) oxide. No other oxides of vanadium were identified by Raman microscopy as either being present initially or formed by laser degradation.

The film deposited at 300 °C was found to consist of VS_2 by EDX, it had Raman bands at 191, 351, 549 and 907 cm^{-1}. Part of the film deposited at 300 °C had transformed to V_2O_5 with bands at 142, 282, 403 and 990 cm^{-1}, which compare with bands at 144, 282, 405 and 995 cm^{-1} recorded from a standard. The film deposited at 350 °C was also identified as VS_2 by EDX, with Raman bands at 190, 347, 553 and 907 cm^{-1} which are similar to those listed above.

EDX analysis of the films deposited at 400 – 500 °C inclusive show that vanadium(III) sulfide was formed at these temperatures. These films had Raman bands at 140, 321 and 909; 135, 322 and 899; 126, 165, 322 and 895 cm^{-1} respectively which compare with bands at 122, 161, 322 and 907 cm^{-1} recorded from a vanadium(III) sulfide standard. XRD analysis also confirmed the presence of V_2S_3 at 500 °C, as shown in figure 4.9.

The film deposited at 550 °C was found to consist of V_3S_4 by EDX, however it had Raman bands at 322 and 909 cm^{-1} which indicates the presence of vanadium(III) sulfide, this shows that a mixed phase coating was formed at this temperature. The film deposited at 600 °C had Raman bands at 217, 291, 329, 353, 392, 498 and 898 cm^{-1} and was identified as vanadium(II) sulfide by EDX.

The XPS results from the film deposited at 500 °C indicate that the film had reacted with oxygen. Therefore the result bears little relationship to the composition of the film at the time of deposition.

The films prepared in this study were stored in air, but were found to lose sulfur over time and finally to oxidise to vanadium pentoxide. The films were initially black, but became lime green after a few weeks finally turning yellow after several months.

5.0 Titanium sulfides

5.1 Introduction

In this chapter titanium sulfide films were studied. This complements the chapter on tin sulfides, as titanium and tin disulfides are isostructural; both have a cadmium iodide structure with hexagonal-close-packed layers. Films were grown from the APCVD reactions of titanium tetrachloride and hydrogen sulfide at 400, 500 and 600 °C. The coatings were analysed by EDX, XRD and Raman microscopy. The Raman spectra of TiS_2 films have not been reported previously.

5.2 Background

5.2.1 Titanium monosulfide

Titanium monosulfide was synthesised from a stoichiometric mixture of the elements. The procedure involved pressing the elements into pellets and firing at 800 °C under $1x10^{-5}$ torr argon.[53] The resulting titanium monosulfide is non-stoichiometric, both sulfur- rich and tin-rich sulfides may be produced. TiS_{1-x} where $x \cong 0.05$ has the hexagonal $B8_1$ nickel arsenide structure with a crystallographic $c/a \approx 1.92$ axial ratio.[53] $Ti_{1-x}S$ has the hexagonal 9R polytype structure with metal atom vacancies. The TiS produced in this way has metal-metal bonding with partially filled d-orbitals which affect the properties. The material exhibits metallic properties and is paramagnetic. These properties may lead to electronics applications. $Ti_{1-x}S$ materials are air-sensitive.[53]

5.2.2 Titanium disulfide

Titanium disulfide has a hexagonal cadmium-iodide type layered crystal structure. The titanium cations are in octahedral sites between alternate hcp layers of sulfide anions. Thin films of the disulfide are bronze/gold in colour, [54,55] with thicker films being golden-black .[55]

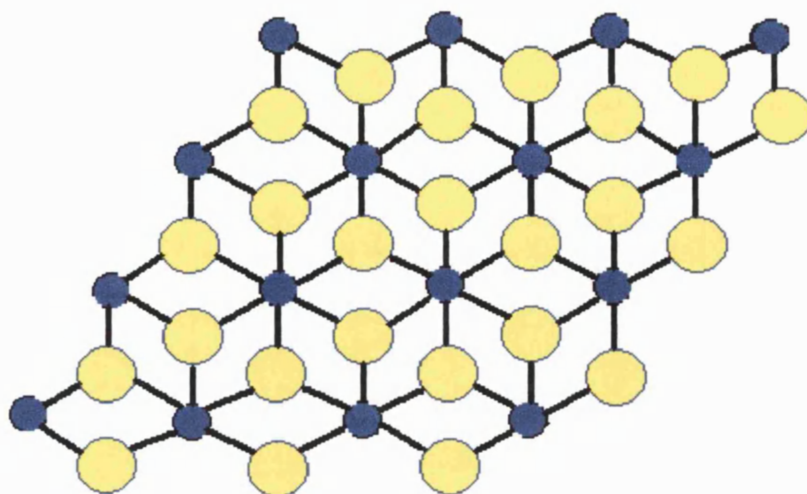

Figure 5.1 Structure of TiS_2. Titanium atoms are represented by dark blue circles and sulfur by yellow circles.

TiS_2 may be used as a solid lubricant due to weak van der Waals interactions between adjacent crystal layers. This enables layers to slide over one another.[54] Another use of titanium disulfide is as a cathode in high energy-density batteries, see fig. 5.2 below.[56] Titanium disulfide is used as a cathode material in high-energy-density secondary, rechargeable cells because lithium can reversibly intercalate in the crystal lattice of the material. Small batteries using this material could be used in low current electronic devices.[57] Battery charging and discharging occurs with lithium intercalation and deintercalation. Both processes may be aided by crystal orientation in the TiS_2 layer, and are favoured when the basal plane is perpendicular to the lithium electrode.[55] This places the crystallographic *c*-axis parallel to the substrate.[57]

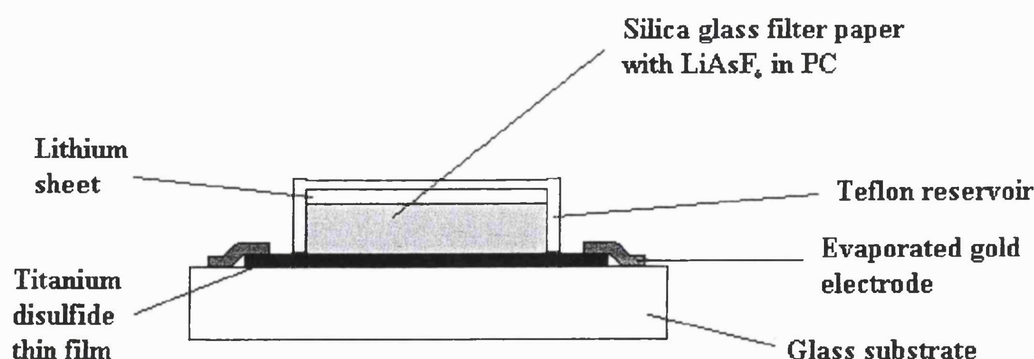

Figure 5.2 A schematic diagram of a thin film lithium/titanium disulfide cell on a glass substrate.

5.2.3 CVD reactions used to deposit titanium disulfide

The fabrication of titanium disulfide thin films has been reported by many groups using either single source or dual precursor systems. Reactions have been performed using LPCVD, APCVD and (plasma enhanced) PECVD these reports are summarised below.

Kikkawa et al. reported the deposition of TiS_2 from the PECVD reaction of $TiCl_4$ and H_2S. Film growth rates of $4x10^{-3}$ g cm^{-2} h^{-1} were obtained. Reaction times were between 2 and 60 min, with a substrate temperature of 450 °C. The coatings were deposited on slide glass, stainless steel and carbon ribbons. The films produced were identified as being single phase hexagonal titanium disulfide, with the preferred crystal orientation having its basal plane parallel to the substrate in thinner films, and perpendicular to the substrate for films greater than 10 μm thick. Crystals with the basal plane perpendicular to the substrate are reported to have a high discharge capacity in lithium secondary cells. Thin films are a gold metallic colour, and thicker films tend to be darker and had a columnar appearance in cross-section.[55]

Kanehori et al.[57] report a study of the kinetics of the reaction between titanium tetrachloride and hydrogen sulfide using a cold-walled LPCVD reactor to coat silicon wafers or borosilicate glass plates. The substrates were heated to 510 °C, and 60 min reaction times were used to deposit thin films of hexagonal TiS_2 with the *c*-axis parallel to the substrate. Kanehori reported that the rate-determining step for the reaction was

the activation of hydrogen sulfide. This was a first-order reaction and deposition rate increased in direct proportion to the hydrogen sulfide partial pressure. The deposition rate was found to increase up to 510 °C, at which point the deposition rate reached its maximum value. It was suggested that the *c*-axis was parallel to the substrate surface when the reaction was controlled by surface reaction alone. However the degree of orientation decreased if the rate of reaction was controlled by diffusion. Reactions occurring in the presence of excess of hydrogen sulfide led to crystallites that grew perpendicular to the substrate. The maximum deposition rate occurred when the reactant ratio was 0.7 = H_2S / (H_2S + $TiCl_4$).[57]

Winter et al.[58] reported APCVD reactions of titanium tetrachloride with organothiols at temperatures between 200 – 600 °C. Glass, silica and stainless steel were coated in a horizontal hot-walled reactor, resulting in reflective gold titanium sulfide thin films, which showed good adhesion to the substrates. Winter found that if thiol was introduced into the reactor 1-2 min prior to the reaction as a 'sulfur pretreatment' the result was a 247-280 Å s^{-1} growth of titanium disulfide. However if no pretreatment was used the resulting film was thin and composed of a mixture of titanium dioxide (anatase) and titanium disulfide. It was reported that films produced using hydrogen sulfide instead of thiol were thinner and less adherent to the glass.

Schleich et al. reported the PECVD reaction of $TiCl_4$ with H_2S. No reaction between these compounds was observed below 400 °C in the absence of a plasma. TiS_2 films were deposited at 250 °C in the presence of a plasma.[59] Winter confirmed that, under APCVD reaction conditions, $TiCl_4$ and H_2S react between 430 – 540 °C.[54]

Chang *et al.* [60] reported the formation of titanium disulfide films from the thermal CVD reaction of titanium tetrachloride with three sulfur sources; hexamethyldisilthiane $(CH_3)_3Si\text{-}S\text{-}Si(CH_3)_3$, *t*-butyl sulfide $(CH_3)_3C\text{-}S\text{-}C(CH_3)_3$ and *t*-butyl disulfide $(CH_3)_3C\text{-}S\text{-}S\text{-}C(CH_3)_3$. These were mixed near the reactor inlet cold zone to prevent reaction prior to entry to the reactor.

Chang produced a gold coloured thin film at 230 °C from the reaction of titanium tetrachloride and hexamethyldisilthiane, the film being characterised as (001) TiS_2 by

X-ray diffractometry.[60] The presence of only one diffraction peak allows the identification of film orientation, which in this case has the crystallographic *c* axis perpendicular to the substrate. It was also reported that it was possible to control film orientation, with different film orientations being found at different temperatures in the range 200 – 260 °C. In fact at temperatures below 250 °C only (001) TiS_2 was reported, at 260 °C two diffraction peaks were identified, one corresponding to (101) and the other (110) TiS_2. These relate to crystal orientation of the *c* axis either parallel or close to parallel to the substrate. The film produced at 260 °C is most suited to use in lithium cells as the van der Waals gaps are perpendicular to the direction of the substrate. This is thought to aid lithium intercalation into the layers of the electrode, i.e. the titanium disulfide. Chang deposited TiS_2 films on glass, aluminium foil, stainless steel foil and titanium foil. The film growth rate was reported to be unaffected by deposition temperature in the range 200 – 260 °C. This indicates that mass transfer controls the rate of reaction.

Chang also reported investigations into two other systems. The reaction of titanium tetrachloride with *t*-butyl disulfide at 260 °C resulted in the formation of a black film. Analysis of the film by XRD allowed the deposited layer to be identified as titanium trisulfide. However, raising the deposition temperature to 300 – 350 °C caused titanium disulfide to be favoured. At 400 °C a gold film of TiS_2 was reported. The reaction of titanium tetrachloride with *t*-butyl sulfide is similar to that of hexamethyldisilthiane as it is possible to deposit a gold film of TiS_2 at 260 °C with a similar X-ray diffraction pattern reported, i.e. two diffraction peaks corresponding to (101) and (110) reflections of titanium disulfide. The film growth rate is temperature dependant, with the rate undergoing a ten-fold increase on increasing the deposition temperature from 250 – 550 °C.[60]

Single source precursors are single compounds, both elements of interest being present, which yield the desired product on thermal decomposition. These precursors have the potential to be of use in the production of titanium disulfide thin films as they reduce the toxic, foul smelling waste produced by the process. They also eliminate problems of premixing reactants prior to entry to the reactor.

Winter reported the use of two precursors of the type $[TiCl_4(HSR)_2]$ to produce TiS_2 thin films, via LPCVD in a hot-walled reactor at temperatures between 200 - 600 °C.[61]

5.2.4 Titanium trisulfide

Chang *et al.* [60] reported the formation of titanium trisulfide from the reaction of titanium tetrachloride with *t*-butyl disulfide at 260 °C. It was postulated that titanium trisulfide could be produced from other systems if the sulfur vapour pressure in the reactor was sufficient to stabilise the trisulfide with respect to the disulfide as shown in the following reaction: $2TiS_3 \leftrightarrows 2TiS_2 + S_2$.

Titanium trisulfide has a quasi-one-dimensional structure with chains of TiS_6 trigonal prisms sharing bases; the structure has a monoclinic unit cell. The titanium-to-sulfur bond lengths between chains in the unit cell are similar to those within chains, see figure 5.3. The overall molecular appearance of TiS_3 is of a layered structure similar to that for tin sulfides. Interlayer van der Waals bonds between sulfur atoms hold the titanium sulfide layers together. The band gap of titanium trisulfide is *c.* 1 eV, which is similar to that of tin monosulfide, which has a band gap of 1.2 eV. Raman bands recorded from a single crystal of TiS_3 are reported with their symmetry assignments at, 152 B_g, 175 A_g, 264 B_g, 278 A_g, 300 A_g, 366 B_g, 370 A_g, 394 B_g, 434, 472, 557 A_g and 645 cm^{-1}.[62] The structure of ZrS_3 shown below in figure 5.3 is reported to be isostructural with TiS_3.[62]

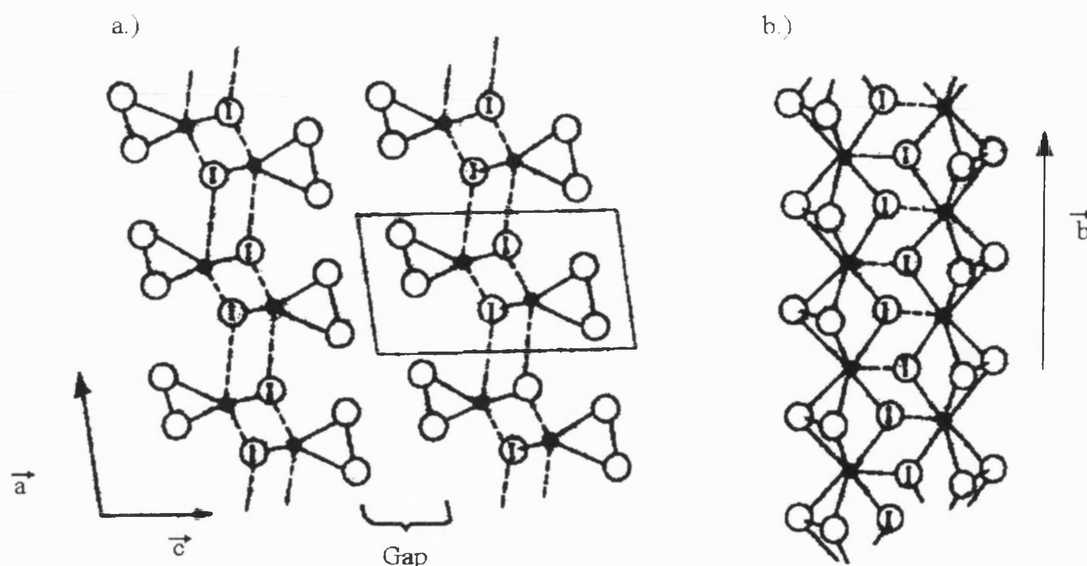

Figure 5.3 Crystal structure of the iso-structural ZrS_3 showing the projection along (010) (a) and a representation of two chains along the *b*-axis (b); broken lines indicate inter-chain bonds.

5.2.5 Non-stoichiometric titanium sulfides

Both metal- and sulfur-rich TiS have been reported. The metal rich TiS_{1-x} ($x \approx 0.05$) phase has the $B8_1$ structure with a *c/a* axial ratio of 1.92. The sulfur rich $Ti_{1-x}S$ phase has the 9R-polytype structure with metal atom vacancies.[53]

There are also various phases between TiS and TiS_2 including $Ti_{1.16}S_2$ and $Ti_{1.54}S_2$; the structures of these titanium sulfides are based on close-packed sulfur layers. In the composition range between TiS_2 and $Ti_{1.4}S_2$ the titanium sites are fully and partially occupied in alternating titanium layers.[63]

5.3 Experimental

Titanium disulfide thin films were formed from the APCVD reaction of titanium tetrachloride and hydrogen sulfide. The titanium tetrachloride was admitted to the reactor using a bubbler, which was heated to 80 – 83 °C. A nitrogen gas flow of 0.5 $dm^3\ min^{-1}$ was passed through the bubbler to carry the titanium tetrachloride towards the reactor. The hydrogen sulfide was allowed to flow into the gas stream at a rate of either

0.5 or 1.0 $dm^3 min^{-1}$ with 1 $dm^3 min^{-1}$ nitrogen as a diluent gas. The precursors were separately transported to the reactor with the addition of 10 $dm^3 min^{-1}$ of nitrogen carrier gas. The precursor gas flows joined at the inlet of the reactor and were premixed in the brass block prior to being passed over the glass substrate.

Four reactions were carried out for this system; each reaction lasted 1 min, which was timed between the opening and closing of the three-way valve. Four substrates were coated in this investigation, with a reaction at 400 °C, two at 500 °C, one at 600 °C, and with all other conditions unchanged unless otherwise stated. The conditions used for each run are shown below in table 5.4.

Energy dispersive X-ray analysis (EDX) was used to determine quantitatively the film composition. The films were also analysed by use of UV/visible spectroscopy and scanning electron microscopy. Film adherence to the glass was assessed using the Scotch tape test and by scratching the surface with a scalpel. Solubility of one of the films was assessed in various solvents as described in Chapter 2. Raman microscopy was used to record spectra of 1-2 μm spots visually selected with the microscope as being representative of the different areas of film on the coated glass. Depending on the appearance of the film up to seventeen Raman spectra were recorded from different areas of each substrate. This allowed data from other analyses to be crosschecked so as to provide better evidence for the identification of the composition of the film.

Deposition temperature / °C	**Bubbler temperature / °C**	**H_2S gas flow rate / $dm^3 min^{-1}$**
400	83	0.5
500	83	0.5
600	82	0.5
500	80	1.0

Table 5.4 Deposition and bubbler temperatures used during the APCVD reaction of titanium tetrachloride and hydrogen sulfide.

5.4 Results

5.4.1 Film colour and uniformity

The films produced by the APCVD reaction of titanium tetrachloride and hydrogen sulfide covered the whole of the substrate, but the coatings were of non-uniform colour and thickness over the glass. The appearance of the films are tabulated below in table 5.5 The film produced at 400 °C appeared the most uniform, with the film produced at 600 °C having the most non-uniform appearance. Sketches of two of the films are shown in figure 5.6.

Deposition temperature / °C	H_2S flow rate / $dm^3\ min^{-1}$	Description of appearance and uniformity of coating on the substrate
400	0.5	Silver/grey at end of the substrate nearest the entrance of the reactor. Brown/black film covers the rest of the substrate.
500	0.5	Black section at the centre along the entire length of the substrate, forming a third of the coating. White/grey towards the edges of the film along the length of the substrate.
600	0.5	Matt black section at the centre along the entire length of the substrate, forming a third of the coating. White/grey towards the edges of the film along the length of the substrate.
500	1.0	The substrate had a black coating deposited, which was slightly thinner towards the exit end of the reactor.

Table 5.5 Descriptions of the visual appearance of films produced by the APCVD reaction of titanium tetrachloride and hydrogen sulfide.

The variation in film colour and composition reported here is probably due to a combination of incomplete mixing of the precursors prior to flowing over the substrate and the substrate temperature.

a.)

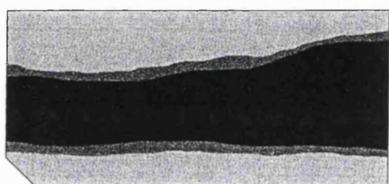

b.)

Figure 5.6 Schematic representation of two of the films deposited by the APCVD reaction of titanium tetrachloride and hydrogen sulfide. These were deposited at a) 400 °C and b) 500 °C.

5.4.2 Four-probe resistance measurements

A four-probe meter was used to measure the sheet resistance of the films deposited in this study, the results being shown below in table 5.7.

Deposition temperature / °C	**H_2S gas flow / $dm^3 min^{-1}$**	**Resistance (colour of film tested) Ω/ □**
400	0.5	1174 (black) 1384 (silver)
500	0.5	1 (grey/black) 29 (grey/brown)
600	0.5	471 (black) 5 (grey/white)
500	1.0	216 (black)

Table 5.7 Resistance measurements of the films deposited from the APCVD reaction of titanium tetrachloride and hydrogen sulfide.

5.4.3 Raman microscopy

The films deposited in this study were visually inhomogeneous, both in terms of the apparent thickness of the films and the colour of the coatings. This was probably due to

variations in the concentration of reactants in the gas stream as it passed over the substrate. All films were analysed at room temperature, using 632.8 nm excitation.

Figure 5.8a below shows a Raman spectrum recorded from a dark black region, near the middle of the substrate, of the film deposited at 500 °C, with a 0.5 dm^3 min^{-1} flow of hydrogen sulfide. This is a spectrum of titanium disulfide with bands at 334 and 382 cm^{-1} which compare to bands of TiS_2 reported in the literature at 335 cm^{-1} with a shoulder at 380 cm^{-1}.[64]

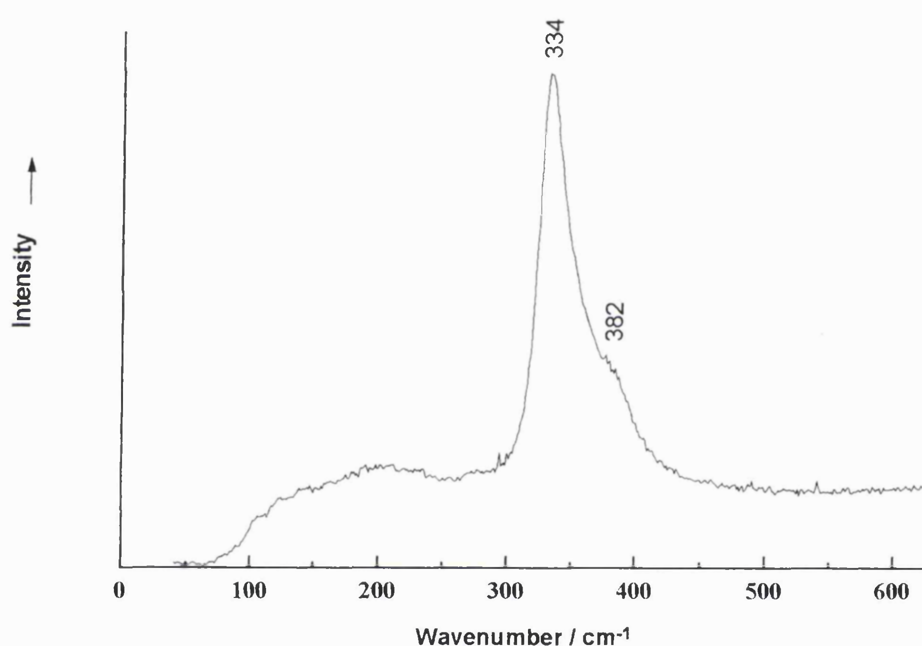

Figure 5.8a Raman spectrum recorded from the film deposited at 500 °C, 0.5 dm^3 min^{-1} hydrogen sulfide by the APCVD reaction of titanium tetrachloride and hydrogen sulfide.

Figure 5.8b shows a Raman spectrum recorded from the film deposited at 600 °C, 0.5 dm^3 min^{-1} hydrogen sulfide. The spectrum is from a grey/black area on the boundary between the middle of the coating, which is matt black and the edge of the coating which is a grey white colour. The spectrum has Raman bands due to titanium disulfide at 335 and 386 cm^{-1}. It also has bands at 146 and 520 cm^{-1}, which compare favourably with Raman bands recorded from the anatase phase of titanium dioxide, at 147 and 515 cm^{-1}.[65]

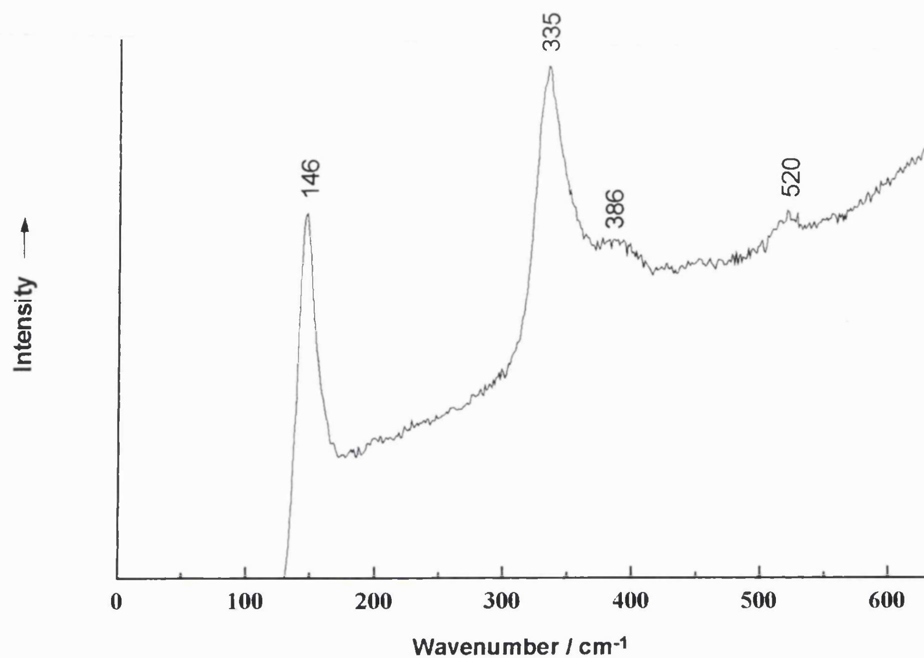

Figure 5.8b Raman spectrum recorded from the film deposited at 600 °C by the APCVD reaction of titanium tetrachloride and hydrogen sulfide.

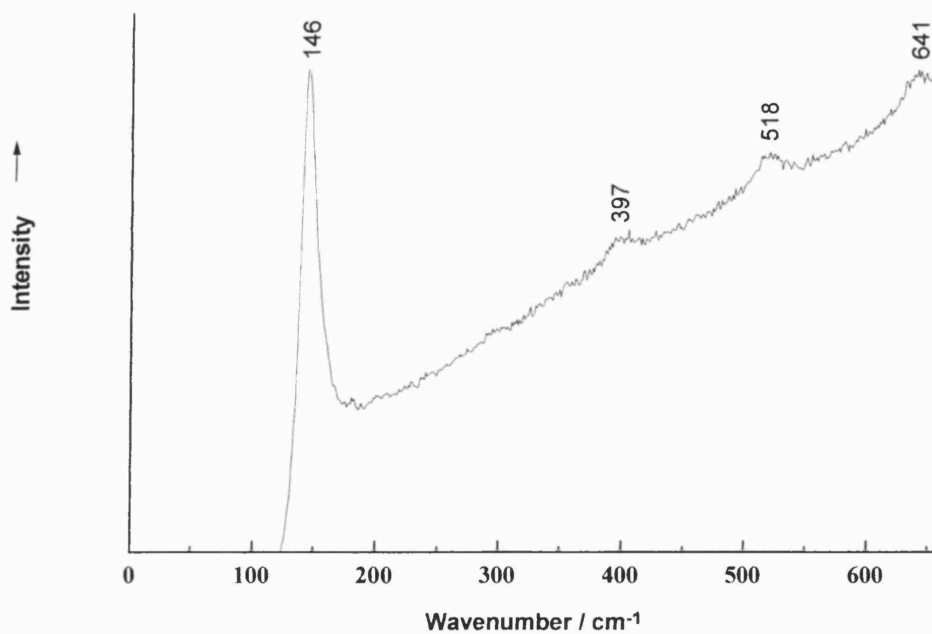

Figure 5.8c Raman spectrum recorded from the film deposited at 600 °C by the APCVD reaction of titanium tetrachloride and hydrogen sulfide.

Figure 5.8c above shows a Raman spectrum of phase pure anatase, which was recorded from a yellow/grey area of film deposited at 600 °C at the edge of the substrate near the entry end of the reactor. This spectrum has Raman bands at 146, 397, 518 and 641 cm^{-1}, these compare to literature values of 147, 398, 515, 640 cm^{-1} for the anatase phase of titanium dioxide.[65]

A summary of Raman spectra results for all of the films in this study appears in table 5.9 to allow comparison of Raman and EDX data in the next section of this Chapter. Raman microscopy data indicates that no free sulfur was deposited on the films studied. Raman band wavenumbers listed below indicate that some titanium dioxide in the form of anatase was deposited on films produced at 500 and 600 °C with a 0.5 dm^3 min^{-1} flow of H_2S, and at 500 °C with a 1.0 dm^3 min^{-1} flow of H_2S. The coating produced at 400 °C, however, did not contain any detectable titanium dioxide. Titanium trisulfide was not detected by Raman microscopy on any of the films deposited.

Deposition temperature / °C	**H_2S flow rate / dm^3 min^{-1}**	**Raman bands / cm^{-1}**
400	0.5	336, 382. TiS_2 only
500	0.5	334, 382. TiS_2 only 146, 203, 396, 521, 640. TiO_2 (anatase) only
600	0.5	146*, 335^+, 386^+. * = TiO_2 (anatase), $^+$ = TiS_2 146*, 397*, 518*, 641*.
500	1.0	336, 382. TiS_2 only 147*, 338^+, 382^+.
TiS_2[64]		234, 335.
TiO_2 (anatase)[65]		147, 398, 515, 640.
TiS_3[62]		152, 175, 264, 278, 300, 366, 370, 394, 434, 472, 557, 645.

Table 5.9 Table of Raman bands recorded from films deposited by the APCVD reaction of titanium tetrachloride and hydrogen sulfide.

5.4.4 Energy dispersive analysis by X-rays

The black titanium disulfide coatings were analysed by EDX to establish quantitative elemental composition, the results are summarised below in table 5.10. The amount of silicon present from the underlying glass was used to estimate film thickness. The films are between 0.6 – 0.9 μm thick.[66]

Deposition temperature / °C	**H_2S flow rate / $dm^3\ mol^{-1}$**	**Film composition**
400	0.5	$TiS_{2.05}$
500	0.5	$TiS_{0.92}$
600	0.5	$TiS_{0.83}$
500	1.0	$TiS_{1.78}$

Table 5.10 A summary of elemental analysis by EDX of titanium sulfide films produced by the APCVD reaction of titanium tetrachloride and hydrogen sulfide.

The region of the sample selected for analysis by EDX was chosen from the centre of the substrate surface as the area that appeared, visually, to be the most representative of the coating.

Both Raman and EDX results confirm that (within experimental error for EDX) stoichiometric titanium disulfide was produced at 400 °C. These results also show that anatase was not deposited at this temperature as Raman microscopy would be expected to detect even low concentrations of anatase on the surface.

EDX results are ambiguous for the other films deposited because the data produced does not take into account the concentration of oxide on the surface. When considered with the Raman data presented above, the combined results show that films produced at 500 and 600 °C contain both titanium disulfide and titanium dioxide (anatase). It is possible to estimate the amount of oxide present in the coatings using EDX data, based on the above data. At 500 °C the ratio of Ti : S is 1 : 0.92, which implies a ratio of titanium disulfide to titanium dioxide of 46 : 54, as there must be two parts of sulfur to one of titanium in TiS_2. This falls to 41.5 (TiS_2) : 58.5 (TiO_2) at 600 °C. This shows

that at higher temperatures titanium dioxide increases in stability in comparison to titanium disulfide.

At 500 °C an increase in the flow rate of hydrogen sulfide caused a reduction in the amount of titanium dioxide deposited relative to titanium disulfide. With an approximate ratio of 89:11 of TiS_2:TiO_2 in the film deposited at this temperature. This means that the reaction products are controlled by thermodynamics and equilibrium position.

The above estimations are made on the assumption that no free sulfur or titanium trisulfide was deposited, Raman results indicate that neither was deposited.

5.4.5 Scanning electron microscopy

Scanning electron micrographs are shown in figures 5.11a-d. Figures 5.11a-c show that crystal size increases from 600 – 1500 nm between 400 – 600 °C with a 0.5 dm^3 min^{-1} flow of hydrogen sulfide. Increasing the flow rate of H_2S at 500 °C to 1.0 dm^3 min^{-1} causes a slight decrease in crystal length and a slight increase in packing density.

a

b

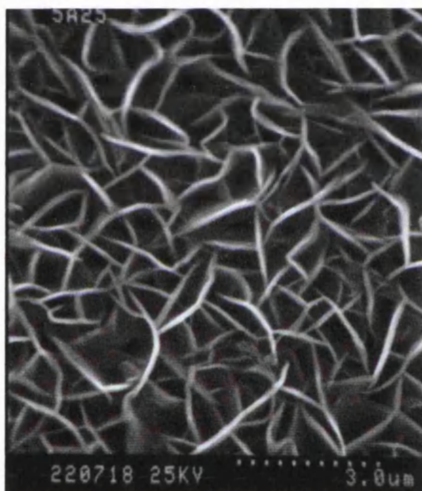

c

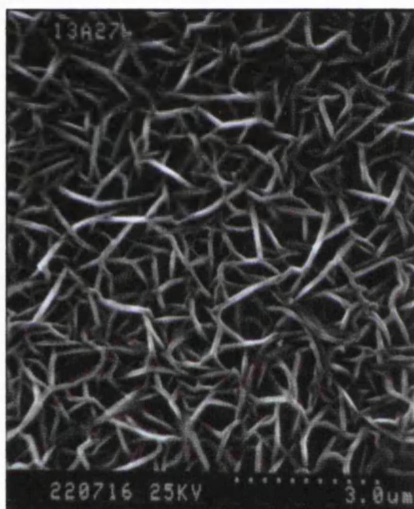

d

Figure 5.11 Scanning electron micrographs of films deposited at: a) 400 °C, b) 500 °C c) 600 °C with 0.5 dm^3 min^{-1} flow of hydrogen sulfide. d) 500 °C with 1.0 dm^3 min^{-1} flow of hydrogen sulfide. These photographs were taken of the films deposited by the APCVD reaction of titanium tetrachloride and hydrogen sulfide.

5.4.6 X-ray diffractometry

An X-ray diffraction pattern was recorded for the film deposited at 600 °C for 2θ values between 10 and 70 °. The pattern was recorded from a black region of the film deposited and can be seen below in figure 5.12. The diffraction peaks of the (001), (101) and (110) TiS_2 are labelled on the plot below. The other peaks labelled with asterisks are from an unidentified phase.

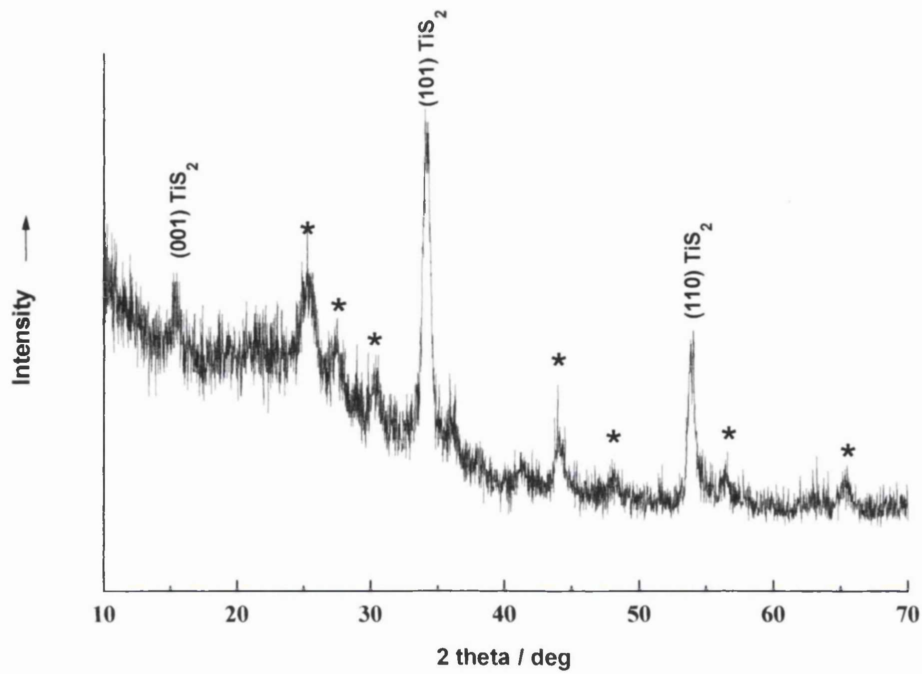

Figure 5.12 An XRD pattern recorded from the film deposited by the APCVD reaction of titanium tetrachloride and hydrogen sulfide at 600 °C.

5.4.7 Transmittance/reflectance spectroscopy

The transmittance/reflectance spectra of films produced in this study are shown below in figures 5.13a-c.

KEY – to the following transmittance/reflectance spectra

—— Reflectance spectra

—— Transmittance spectra

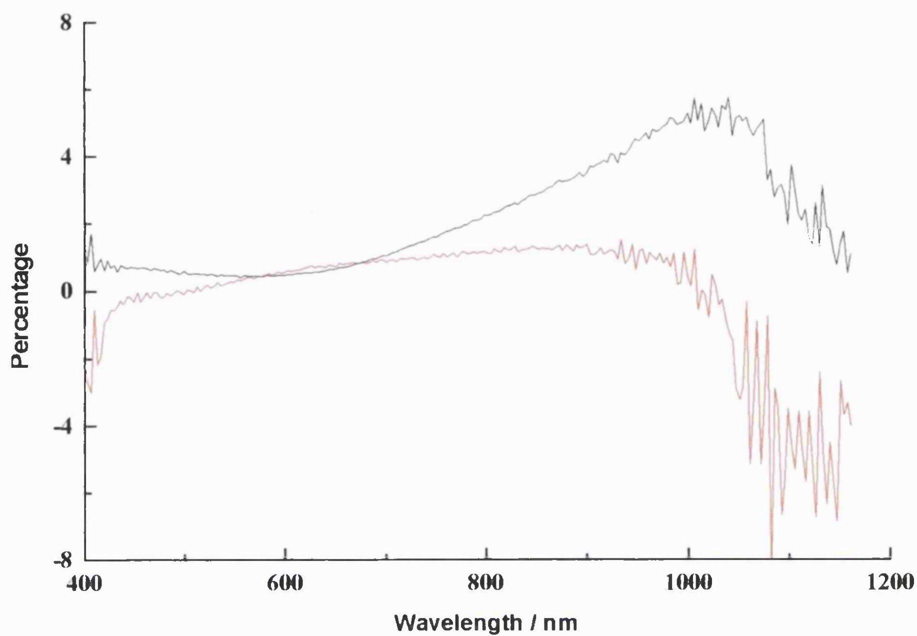

Figure 5.13a Reflectance and transmittance spectra of the black film deposited at 400 °C by the APCVD reaction of titanium tetrachloride and hydrogen sulfide.

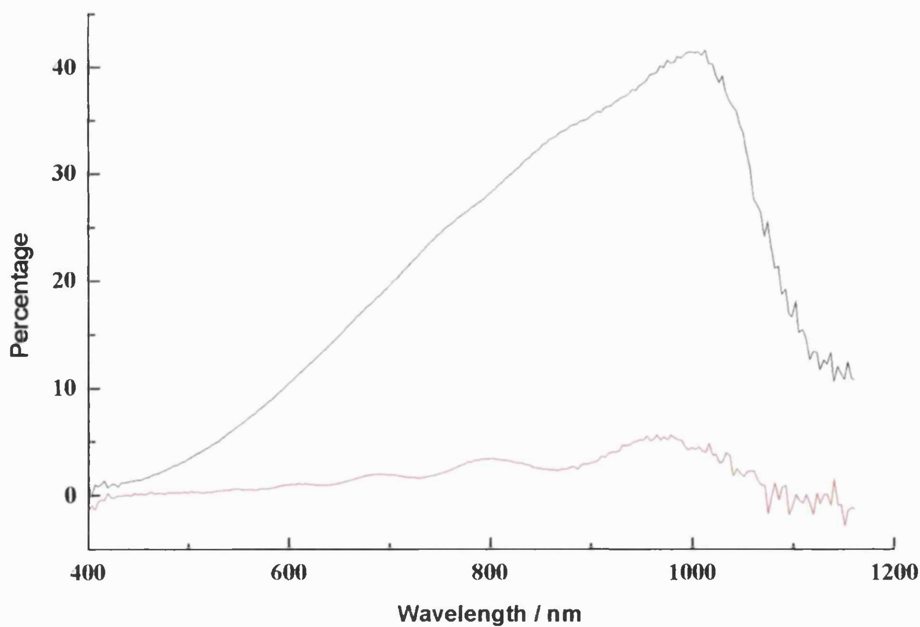

Figure 5.13b Reflectance and transmittance spectra of the black film deposited at 500 °C by the APCVD reaction of titanium tetrachloride and hydrogen sulfide.

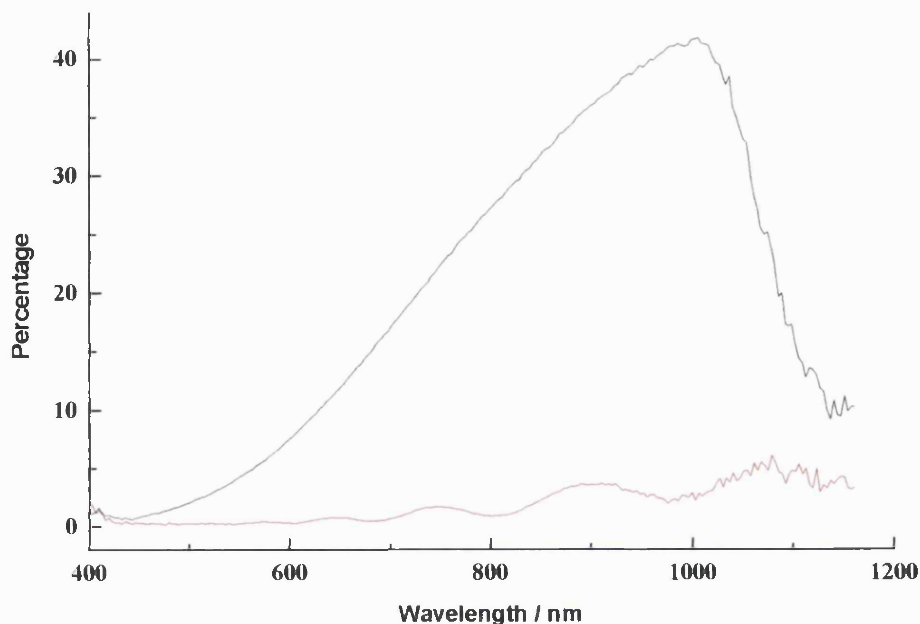

Figure 5.13c Reflectance and transmittance spectra of the grey region of the film deposited at 600 °C by the APCVD reaction of titanium tetrachloride and hydrogen sulfide.

The transmittance and reflectance spectra characteristics of the films deposited were as follows: At 500 °C and 1 dm^3 min^{-1} hydrogen sulfide the coated substrate reflects and transmits less than 7 % incident light. The spectrum of the film deposited at 600 °C indicates that black areas of the film are opaque and non-reflective in the region of the spectrum examined.

The reflectance plots of the films deposited at 500 and 600 °C shown above in figures 5.13b and 5.13c have a sinusoidal appearance caused by interference between radiation reflected by the top surface of the film, and that reflected by the boundary between the coating and the underlying substrate. The Film Thickness Module from FTG software was used to analyse the interference patterns and to determine the thickness of the films produced at 500 and 600 °C.

The film deposited at 500 °C was found to be 0.96 μm thick and the film deposited at 600 °C was found to be 1.19 μm thick assuming a refractive index of 2.3.

5.4.8 Film adhesion

Film adhesion was tested by using the Scotch tape test and by scratching the surface of coated substrates with a scalpel blade, as described in Chapter 2. The results are tabulated below in table 5.14. The titanium disulfide films deposited in this study are not suitable for use where films might undergo abrasion, but would be usable for battery terminals.

Deposition temperature / °C	**H_2S gas flow rate / $dm^3\ min^{-1}$**	**Film appearance**	**Scotch tape test Pass?**	**Scalpel test Pass?**
400	0.5	thick black	yes	no
		silver/grey	yes	no
		thin golden brown	yes	no
500	0.5	thin grey/brown	yes	no
		grey/black	yes	no
		white	yes	no
600	0.5	matt black	yes	no
		grey/white	yes	no
500	1.0	matt black	Some film removed	no
				no
		silver/black (reflective)	yes	

Table 5.14 Table of film adhesion data for coatings produced by the APCVD reaction of titanium tetrachloride and hydrogen sulfide.

5.4.9 Solubility

The solubility of one of the films produced in this system was measured as described in Chapter 2 using the solvents listed below in table 5.15. The black film chosen was deposited at 600 °C; this was representative in both appearance and its Raman spectrum, of the black regions of films deposited at other temperatures. Only methanol seemed to affect the film tested.

Solvent	Visual appearance after 24 hours of solvent and coating on glass
control – no solvent used	grey/black coating
acid – $HNO_{3\,(aq)}$ (dilute)	grey/black coating unchanged, solution colourless
alkali – $NaOH_{(aq)}$ (dilute)	grey/black coating unchanged, solution colourless
water	grey/black coating unchanged, solution colourless
acetone	grey/black coating unchanged, solution colourless
Methanol	grey/black coating paler, due to dissolution of some of the film
Petroleum spirit (60 – 80 °C)	grey/black coating unchanged, solution colourless

Table 5.15 Table of solubility data for coatings produced by the APCVD reaction of titanium tetrachloride and hydrogen sulfide.

5.5 Discussion

The APCVD reactions of titanium tetrachloride and hydrogen sulfide produced good surface coverage of the substrates. The films were not totally uniform over the surface, but did have large domains of homogeneity at the centre of each substrate. The film deposited at 400 °C was found to consist of pure TiS_2; films produced at higher temperatures all showed the presence of both TiS_2 and TiO_2 in the form of anatase. None of the coatings contained TiS_3 or free sulfur.

EDX results confirm that stoichiometric titanium disulfide was produced at 400 °C. The results are ambiguous for the other films deposited, because the EDX data produced does not take into account the concentration of oxide on the surface. When considered with the Raman data presented above, the combined results show that films produced at 500, and 600 °C contain both titanium disulfide and titanium dioxide (anatase) with

more titanium dioxide deposited at the higher temperature (with a 0.5 dm^3 min^{-1} flow rate of H_2S). These results also show that anatase was not deposited at 400 °C. Both Raman and EDX results indicate that titanium trisulfide was not produced during the reactions studied. EDX results also show that an increase of hydrogen sulfide concentration in the reactor at 500 °C did cause an increase in titanium disulfide deposition, favouring this over the oxide. The presence of titanium dioxide in this study was caused by the use of nitrogen with some oxygen present as an impurity. It may also have been due to the use of undried carrier gas. The films did not change on storage therefore if 100 % dry nitrogen had been used as a diluent gas during the reaction, the oxide phase would most probably have been eliminated.

This study has shown the use of Raman microscopy for surface mapping of CVD films. In this study the surface was visually assessed and analysed manually; however it shows the potential to automate fully the step-analysis in order to map a film. This would give composition data for the entire coating with a resolution of about 2 μm.

Transmittance and reflectance spectra indicate that the coatings produced are not suitable for use in heat mirrors as they do not have the ideal spectra for this purpose. Using reflectance spectra the film deposited at 500 °C was found to be 0.96 μm thick, and the film deposited at 600 °C was found to be 1.19 μm thick. It was shown by SEM that 600-1500 nm particles were formed by the reactions studied. As discussed in the previous chapter film thickness measurements contain a consistent inaccuracy due to the assumption that all films studied have the same refractive index as TiO_2 in the form of anatase. This was assumed as there were no available data for the compounds produced in this study. The quoted values for film thickness could be calibrated by SEM measurements of cross sections of these films.

The films could all be scratched off the substrate by use of a sharp object. These coatings would be of no use in applications where abrasion might occur as the surface would be lost rapidly leaving bare glass. The film did however generally pass the Scotch tape test so could be used in some applications such as in solid state, high energy density secondary cells, see the design pictured above in figure 5.2.

Chang *et al.* identified titanium di- and trisulfides in the films reported from the reaction of titanium tetrachloride and *t*-butyl disulfide, at temperatures between 260 – 400 °C.

The only phase of titanium sulfide identified from the APCVD reaction of titanium tetrachloride and hydrogen sulfide at 600 °C studied above was TiS_2. This was identified using XRD by comparison with Chang's paper.[60] Under APCVD reaction conditions it is reported that $TiCl_4$ and H_2S react between 430 – 540 °C.[54] The study reported in this chapter uses slightly different conditions, with films grown from 400 – 600 °C.

Winter *et al.*[58] reported APCVD reactions of titanium tetrachloride with organothiols at temperatures between 200 – 600 °C. It was reported that if thiol was introduced into the reactor 1-2 min prior to the reaction, as a 'sulfur pretreatment' the resulting film produced consisted of titanium disulfide. If no pretreatment was used the resulting film was thin and composed of a mixture of titanium dioxide (anatase) and titanium disulfide. In this study even though the experimental procedure used allowed a 1-2 min hydrogen sulfide pre-treatment, some of the resulting films still contained anatase.

6.0 Chromium oxysulfide

6.1 Introduction

The APCVD reaction of chromyl chloride and hydrogen sulfide was studied at deposition temperatures between 400 – 600 °C. This reaction has not been reported previously. Various analytical techniques including Raman microscopy were used to identify the composition of the films deposited in this study.

6.2 Chromium oxysulfide

There are no reports of chromium oxysulfide in the literature. Several compositions of chromium oxide have been reported. The most thermodynamically stable phase at 500 °C and above is Cr_2O_3. Chromium(III) oxide, Cr_2O_3, has a corundum structure with a hexagonal closed packed layer of oxygen ions. Chromium ions occupy two-thirds of the octahedral sites.[67] Chromium(III) oxide is a semiconductor[68] which could be used as the absorbing layer in a solar thermal-energy collector.[69] Many chromium sulfides have been reported, these range in stoichiometry from $CrS_{1.13-1.5}$. These compounds may be monoclinic, trigonal or rhombohedral.[70] Chromium sufides may have uses as battery cathodes or catalysts.[71]

6.3 Experimental

A preliminary study of chromium oxysulfide thin films was performed using chromyl chloride and hydrogen sulfide precursors. The chromyl chloride was admitted to the reactor using a bubbler, which was heated to 79 – 82 °C. During the reaction a nitrogen gas flow of 0.5 $dm^3 min^{-1}$ was passed through the bubbler to carry the chromyl chloride towards the reactor. The hydrogen sulfide was allowed to flow into the gas stream at the rate of 0.5 $dm^3 min^{-1}$with 1 $dm^3 min^{-1}$ nitrogen as a diluent gas. The substrates were then coated as described in Chapter 2.

Five reactions were carried out for this system. Each deposition lasted 1 min, which was timed between the opening and closing of the three-way valve. Glass substrates were coated by the APCVD reaction of chromyl chloride and hydrogen sulfide at temperatures of 400, 450, 500, 550 and 600 °C with all other conditions unchanged. The conditions used for each run are shown below in table 6.1. Energy dispersive X-ray analysis (EDX) was used to determine quantitatively the composition of the films

produced. In addition, the films were also characterised by Raman microscopy, UV/visible spectroscopy and scanning electron microscopy. Film adherence to the glass was assessed using the Scotch tape test and by scratching the surface with a scalpel. Solubility of one of the films was assessed in various solvents as described in Chapter 2.

Deposition temperature / °C	**Bubbler temperature / °C**
400	80
450	82
500	81
550	79
600	79

Table 6.1. Deposition and bubbler temperatures used during the APCVD reaction of chromyl chloride and hydrogen sulfide.

6.4 Results

6.4.1 Film colour and uniformity

The APCVD reaction of chromyl chloride and hydrogen sulfide resulted in very thin brown, golden brown or grey/brown films, which covered one-third to two-thirds of the substrate. The film was thickest at the entrance to the reactor. The colour of the films all followed the same pattern, with only the relative areas covered changing. Moving away from the entry end of the reactor the colour of the film produced was golden brown, brown, with a very thin grey coating over the rest of the film. Some of the films had a striped appearance in the brown region, which was due to the film thickness causing interference patterns when viewed in visible light.

On standing in air up to 1.5 cm of the golden brown region of film (from the entry end of the reactor) turned dark green in colour with a damp appearance, as if it had gained water from the atmosphere. The change occurred within two hours of removal from the reactor, after which the green discolouration did not spread for over three weeks. A sample of the same (golden brown) region (shown on the far right hand side of the films depicted below) stored under dry nitrogen did not change colour, even when left for

three weeks. This area of the film, formed on the first centimetre or so of the substrate was deposited on a strip of the glass that was not heated directly by the heater block, so would have been 10-20 °C below the temperature of the rest of the substrate. With the exception of the unheated area, the film was thickest at the point the gas stream entered the reactor as the concentration of reactants was highest at this point, being depleted further along the substrate as the film was deposited.

a.)

b.)

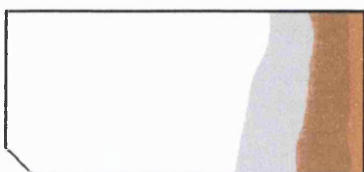

Figure 6.2 Schematic representations of films deposited at a.) 400 °C and b.) 500 °C by the APCVD reaction of chromyl chloride and hydrogen sulfide.

6.4.2 Four-probe resistance measurements

A four-probe meter was used to measure the resistance of the films deposited in this study. All of the films were found to be electrical insulators.

6.4.3 Energy dispersive analysis by X-rays

It was only possible to establish elemental composition of the films produced for this chapter by EDX. This is because the films were too thin to get a result from X-ray diffraction, and no other relevant analytical techniques were available at the time of producing these films. These results were collected using a Jeol EDX instrument with an accelerating voltage of 20 keV. The elemental compositions recorded are given below in table 6.3.

Deposition temperature / °C	Elemental composition, elements quantified by atomic %				Product stoichiometry
	Cr	O	Cl	S	
400	41.3	2.7	27.0	29.0	$CrS_{0.70}Cl_{0.65}O_{0.07}$
450	27.1	37.4	16.1	19.4	$CrS_{0.72}Cl_{0.59}O_{1.38}$
500	45.8	0.3	28.3	25.6	$CrS_{0.56}Cl_{0.62}O_{0.01}$
550	40.6	10.6	16.0	32.8	$CrS_{0.81}Cl_{0.39}O_{0.26}$
600	23.9	52.8	8.2	15.2	$CrS_{0.64}Cl_{0.34}O_{2.21}$

Table 6.3 EDX results for the films deposited by the APCVD reaction of chromyl chloride and hydrogen sulfide.

The above results show significant amounts of chlorine incorporation, with varying oxygen incorporation. This is the reverse of the composition for other films analysed, (in Chapters 3,4 and 5) which had no chlorine incorporation into the layer of film/glass interrogated by the electron beam. The ratio of chromium to sulfur is relatively consistent in the products analysed. It is possible that the reaction produces chromium thiochlorides in addition to some oxysulfides, assuming this to be the case the resulting products are given above in Table 6.3. The ratio of sulfur to chlorine incorporation is approximately 1:1 at 400 – 500 °C inclusive and 2:1 at 550 and 600 °C.

6.4.4 Raman microscopy

All samples were analysed by Raman microscopy at room temperature using 632.8 nm excitation. Additionally Raman spectra were recorded from areas of different appearance on the same sample. The brown films analysed from this system were very thin which means less sample being present in the laser beam. The laser beam can ordinarily pass through up to 1 μm of sample, which is dependent on the sample itself. This is advantageous to analysis as it means that the effective area, (volume) giving rise to scattering is greater than if it was a purely surface based technique. There is no advantage in this for these films however, as the films are thin enough that their entire cross section will scatter light, as will a layer of glass underneath. Therefore the Raman signal scattered is weaker than if a thicker film had been produced. It was also noted that the compound produced did not scatter Raman signal as well as other films such as

titanium dioxide of similar thickness. Representative Raman spectra are shown below in figures 6.4 –6.6.

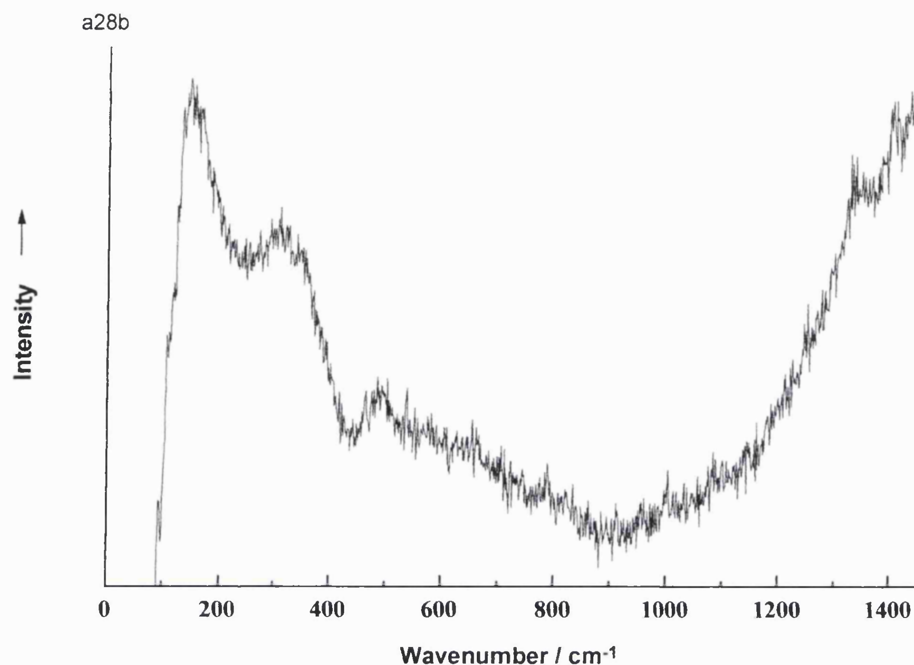

Figure 6.4 Raman spectrum recorded from the film deposited at 600 °C by the APCVD reaction of chromyl chloride and hydrogen sulfide.

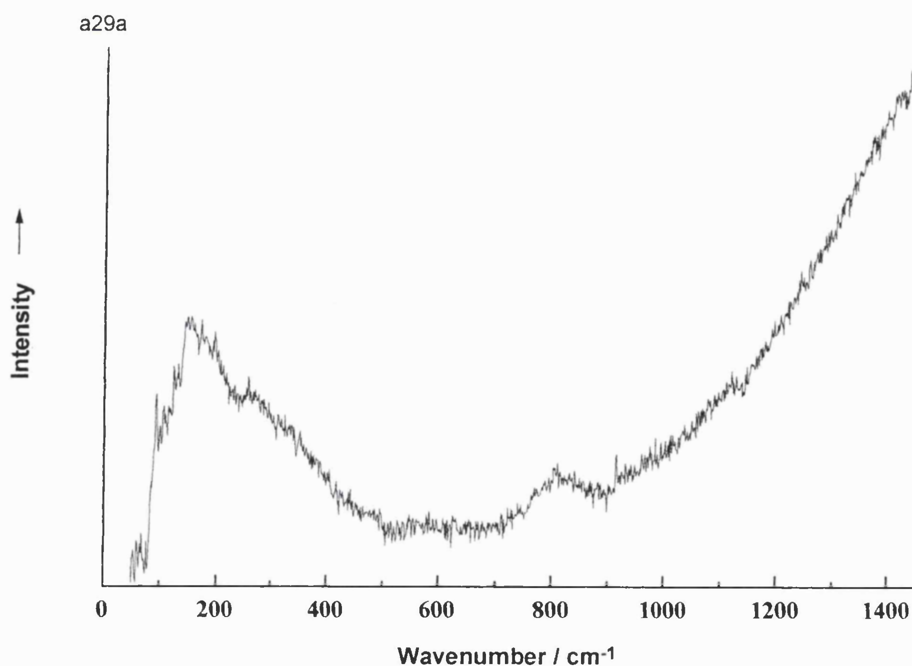

Figure 6.5 Raman spectrum recorded from the film deposited at 550 °C by the APCVD reaction of chromyl chloride and hydrogen sulfide.

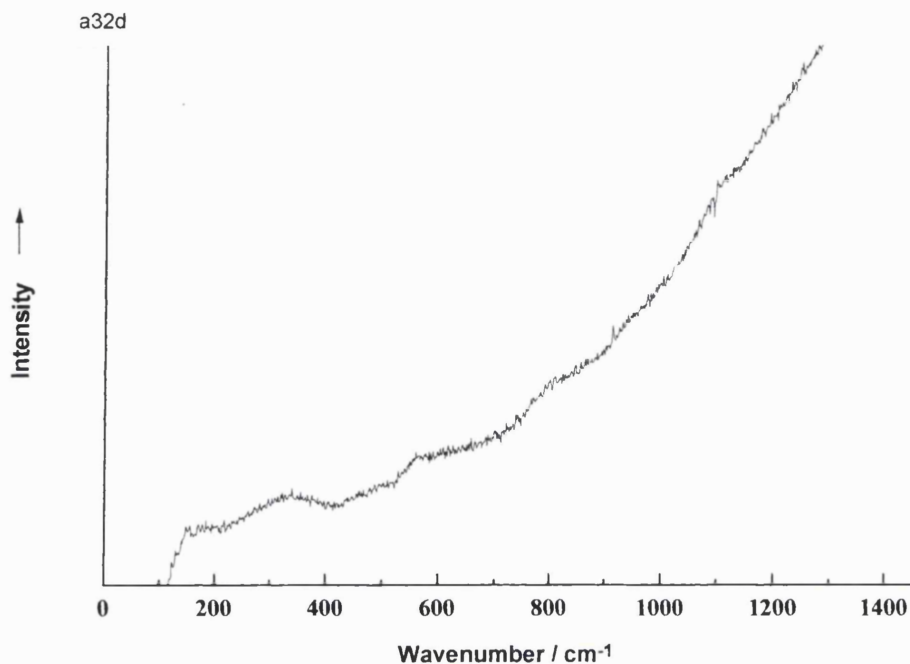

Figure 6.6 Raman spectrum recorded from the film deposited at 400 °C by the APCVD reaction of chromyl chloride and hydrogen sulfide.

The Raman spectra above in figures 6.4 – 6.6 inclusive indicate that free sulfur is not deposited in these films. The films do not give rise to much Stokes Raman scattered light from the surface. None of the Raman spectra produced in the study of these films indicates the presence of chromium(III) oxides which should be thermodynamically stable at the temperatures used for film depositions. The films are unlikely to contain oxide or sulfate materials as these compounds give intense Raman bands. The percentages of oxygen quoted from EDX data probably indicate excitation breakthrough to analyse the surface of the underlying glass substrate in addition to the coating in some cases, as in general as the films deposited were very thin. The Raman spectra above are therefore probably of a mixture of chromium thiochlorides and oxysulfides as indicated by EDX data.

6.4.5 Scanning electron microscopy

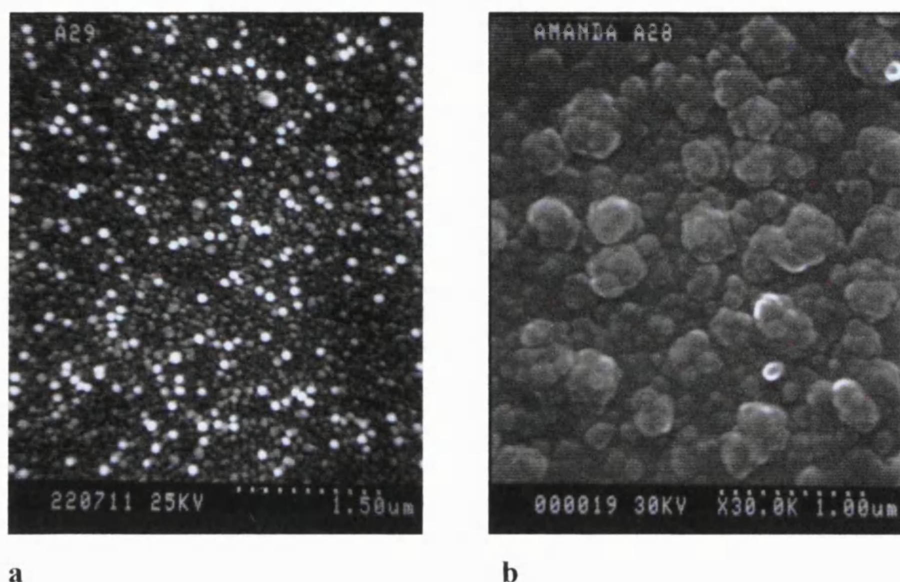

Figure 6.7 Scanning electron micrographs of the films produced by the APCVD reaction of chromyl chloride and hydrogen sulfide. At a.) 550 °C and b.) 600 °C with 0.5 dm^3 min^{-1} hydrogen sulfide flow.

Films produced by this system at 400 – 550 °C inclusive looked like figure 6.7a. This shows a sample taken from the brown area of the coating, in the middle of the coated region. The particle size in the films deposited between 400 – 550 °C was approximately 100 nm. The film deposited at 600 °C had similar sized particles, but these were present as clusters, as seen in figure 6.7b.

6.4.6 Transmittance/reflectance spectroscopy

Reflectance and transmittance spectra of all samples were recorded in the visible and near infrared region, from 386 – 1160 nm.

KEY – to the following transmittance /reflectance spectra

—— Reflectance spectra

—— Transmittance spectra

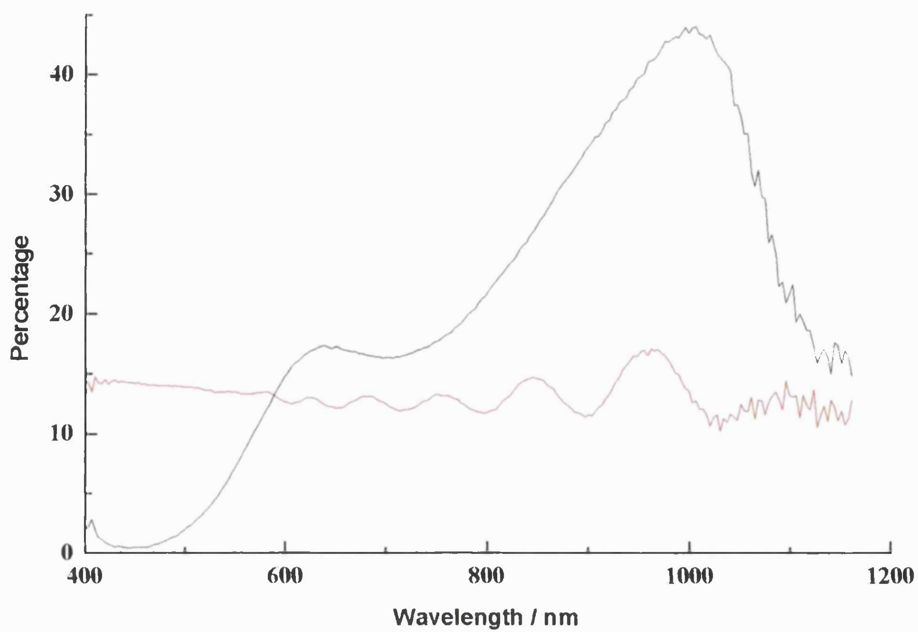

Figure 6.8 Reflectance and transmittance spectra of the film deposited at 400 °C by the APCVD reaction of chromyl chloride and hydrogen sulfide.

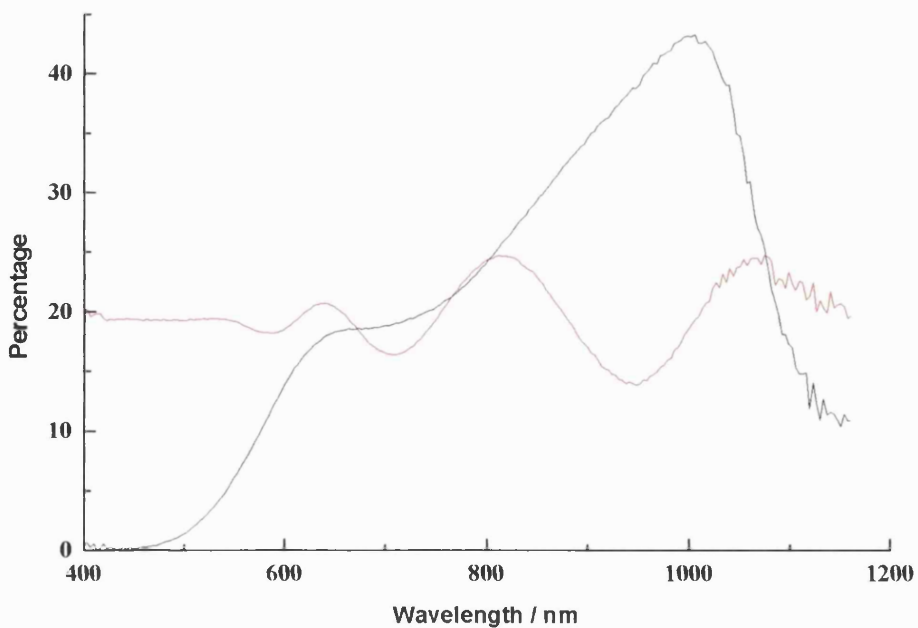

Figure 6.9 Reflectance and transmittance spectra of the film deposited at 450 °C by the APCVD reaction of chromyl chloride and hydrogen sulfide.

The films deposited at 500, 550 and 600 °C all displayed 40-50 % transmittance and reflectance at 400 nm changing to 58 – 63 % transmittance and 22-28 % reflectance at 1050 nm. The Film Thickness Module from FTG software was used to analyse the interference pattern and determine the thickness of the films produced at 400 and 450 °C. The film deposited at 400 °C was found to be 1.15 μm thick, the film deposited at 450 °C was found to be 0.68 μm thick assuming a refractive index of 2.3.

The transmittance and reflectance spectra all indicate that the films produced are unsuitable for use as heat mirrors, as the optical characteristics do not meet the criteria for this purpose, as described in Chapter 1.

6.4.7 Solubility

The solubility of the films was tested by taking a 1 cm^2 piece of glass, placing it in *c.* 1 cm depth of solvent in a sample tube and leaving for 24 hours. After this time the appearance of the sample was compared with that of a control sample, which had not been exposed to any solvent.

The film deposited at 400 °C was not soluble in water, acetone, methanol, dilute sodium hydroxide or petroleum spirit. The film placed in dilute nitric acid was not apparently changed, on examination however, bubbles had formed on the glass on the coated side, so the film had obviously reacted with the acid. If the material deposited in this study was used commercially it would be unsuitable for applications that might expose the film to acidic solutions.

6.4.8 Film adhesion

Film adhesion was tested by scratching the surface of the film with a scalpel, and by using the Scotch tape test as described in the Chapter 2. All of the films could be scratched off the glass by use of a scalpel. Grey and brown regions of all films deposited in this study were undamaged by Scotch tape. Areas of film that had transformed to the green compound were damaged where the film appeared wet, whereas areas that had dried remained unchanged. This means that part of the film could not be used in air, and would require a protective atmosphere. The bulk of the

film however was relatively air stable, but would be unsuitable in applications where abrasion might occur.

6.5 Discussion

The films produced by the reaction of chromyl chloride and hydrogen sulfide were of non-uniform appearance. The films deposited were thin and did not cover the entire surface of the substrate. Part of the film changed colour when exposed to air. However if the film was protected, by placing in a dry nitrogen atmosphere, no further reaction was detected.

The composition of the films was determined by EDX. At 400 °C the film consisted of $CrS_{0.70}Cl_{0.65}O_{0.07}$. This material has not been reported in the literature previously. The sulfur to chlorine ratio of films deposited between 400 – 500 °C inclusive was approximately 1:1. The ratio for films deposited at 550 and 600 °C was 2:1.

Raman spectra recorded from the films deposited did not show any Raman bands attributable to chromium oxides, sulfur or sulfates, all of which should give strong Raman bands if they were present. The area of the film, which had turned green, did not show any Raman bands due to chromium oxide either, even though the films deposited at 450 and 600 °C had significant amounts of oxygen incorporation. This suggests that a small amount of a weakly Raman scattering chromium oxysulfide was deposited at 450 and 600 °C, in addition to a chlorine-containing compound perhaps a chromium thiochloride.

The film deposited at 400 °C was found to be 1.15 μm thick, the film deposited at 450 °C was found to be 0.68 μm thick assuming a refractive index of 2.3. This explains the suggested oxygen incorporation as given by EDX data. EDX interrogates the top micrometre of the sample. The film deposited at 400 °C is thicker than the depth EDX analyses, therefore the analysis is of the film, rather than both the film and the substrate. The film deposited at 400 °C consists of $CrS_{0.70}Cl_{0.65}O_{0.07}$, which should be an accurate analysis. The film deposited at 450 °C is thinner, so the analysis as $CrS_{0.72}Cl_{0.59}O_{1.38}$ is probably inaccurate, and the true composition is likely to be $CrS_{0.72}Cl_{0.59}O_{0.07}$. It is not possible to assign a thickness to the other films deposited (and hence a more accurate understanding of EDX data) as they did not show interference effects in their optical

spectra. It can be seen that the films deposited at 400 and 450 °C have almost identical composition. Both of these films gave poor Raman spectra, so Raman microscopy is unlikely to be a suitable tool in the analysis of these films, however it can certainly be used to rule out the presence of oxides, sulfur or sulfates in this study. The films deposited at 400 and 450 °C consisted of $CrS_{0.7}Cl_{0.6}O_{0.1}$.

The films produced in this study are new, however further work is required to fully characterise the coatings deposited.

7.0 Tin Sulfides

7.1 Introduction

Three APCVD reactions were used to produce tin sulfide. The resulting thin films were characterised by Raman microscopy. The APCVD reactions studied were as follows: tin tetrachloride and hydrogen sulfide with deposition temperatures between 300 – 545 °C; tin tetrabromide and hydrogen sulfide with deposition temperatures between 250 – 600 °C and tri-n-butyltin trifluoroacetate and hydrogen sulfide with deposition temperatures between 300 – 600 °C. The AACVD reaction of tetra(phenylthiolato) stannane and hydrogen sulfide was also studied between 300 – 600 °C.

7.2 Tin Sulfides

X-ray diffraction and energy dispersive X-ray data included in this chapter were recorded from tin sulfide thin films produced and analysed by Louise S. Price.[72] The purpose of this chapter is to show how useful Raman microscopy is in the analysis of tin sulfide films. A large selection of tin sulfide films were analysed for this chapter. The films were deposited using both aerosol assisted-, and atmospheric pressure chemical vapour deposition, the same CVD rig was used for all of the systems studied for this thesis.

Both tin and sulfur have at least two oxidation states available for forming compounds, in addition to different modes of coordination. Sulfur also has the ability to undergo catenation, forming chains of S_n, with n = 2 to 200 000, for polymeric chains of sulfur. Interatomic distances in sulfur range from 188.9 – 218.1 pm and S-S-S bond angles vary between 101.5 – 107.8°.[73] The properties of tin and sulfur both influence those of tin sulfides leading to a rich and varied chemistry; both in terms of oxidation states, structure, colour and electronic properties. Tin sulfides with chains, sheets or 3-D lattice structures may be produced by a variety of means including solid state reactions, flux methods[74] and chemical vapour deposition.[75]

Three types of tin sulfide have been produced by APCVD, tin monosulfide, tin disulfide and tin sesquisulfide. The composition of the tin sulfide deposited may be controlled by temperature and by choice of precursor. Tin monosulfide, SnS, has an orthorhombic, GeS structure[76] with each tin atom coordinated by six sulfurs in a distorted octahedral geometry. Each having three short Sn-S bonds of c. 2.7 Å and three long Sn-S bonds of

almost 3.4 Å. There are two SnS layers in each unit cell with one of the long distance sulfurs residing on a neighbouring SnS layer. Chandrasekhar et al. recorded polarised Raman spectra of freshly cleaved, and mechanically polished and etched single crystals of SnS. The use of an incident laser beam parallel to each of the *a*, *b* and *c*-axes in turn allowed Chandrasekhar to assign bands' symmetry. These were A_g bands at 40, 95, 192 and 218 cm^{-1}; B_{3g} bands at 49 and 164 cm^{-1}; B_{1g} 70 and 208 cm^{-1}; and B_{2g} bands at 70, 85, 160 and 290 cm^{-1}.[76]

Tin disulfide was the first of the tin sulfides to be identified; its laboratory synthesis has been possible for about two hundred years. Tin disulfide has been used as the pigment 'mosaic gold,' due to its gold colour. It has been used to illuminate manuscripts instead of using gold leaf, or gold paint.[77] Tin disulfide has a hexagonal unit cell; it adopts a PbI_2 layered structure with tin atoms in octahedral sites between two hexagonally close-packed sulfur slabs. The SnS_2 is composed of edge sharing octahedral SnS_6 units, with sulfur atoms being coordinated to three tin atoms and having trigonal pyramidal geometry. SnS_2 layers are stacked up along the crystallographic *c*-axis, with weak van der Waals interlayer forces holding the lattice together. There are more than seventy polytypes of tin disulfide known due to the many ways of stacking the layers of its lattice, but all have the same *a* unit cell parameter. It is the *c* unit cell parameter, which varies between polytypes; hence, the size of the unit cell also varies with one polytype having 258 tin sulfide sheets in its unit cell.[74] It is difficult to identify individual polytypes in a crystallite, as usually more than one domain or phase is present.[74] Katahama et al. recorded unpolarised Raman spectra from single crystals of three polytypes of SnS_2 these were grown by chemical transport using iodine as the transport agent; the polytypes produced were then identified by X-ray crystallography. The polytypes produced were 2H-, 4H-, and 18R-SnS_2. Raman spectra were then measured at liquid nitrogen temperature. The most intense band in each spectrum was at around 317 cm^{-1} this was caused by A symmetry, intra-layer modes. The three bands at around 200 cm^{-1} were caused by E symmetry intra-layer modes. The band at 209 cm^{-1} in the 2H-SnS_2 polytype is of E_g symmetry.[78]

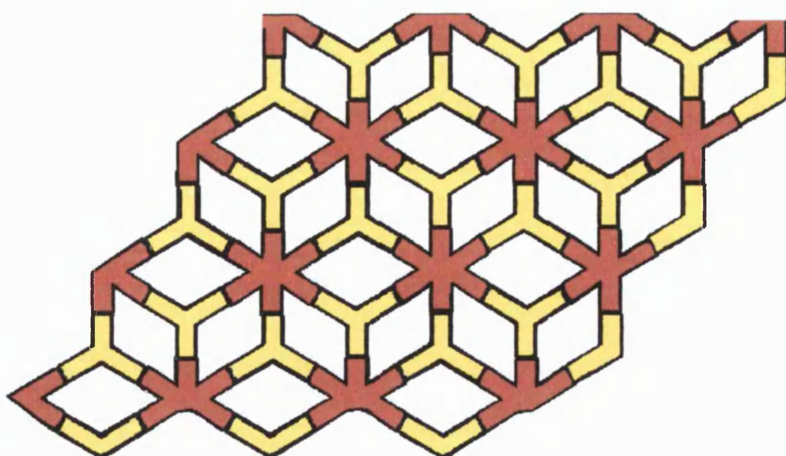

Figure 7.1 A schematic representation of SnS_2 with sulfur shown in yellow and tin in red.[74]

Tin sesquisulfide, Sn_2S_3, can be found in nature as the mineral ottemannite, it may also be produced on heating the elements together. It has a ribbon structure with tin(IV) sites having octahedral coordination, the tin(II) sites have trigonal pyramidal geometry.[74] Tin sesquisulfide is orthorhombic with unit cell parameters of a = 8.878(2), b = 3.751(1), c = 14.020(3) Å. It forms needle crystals when produced from the elements.[79] Chandrasekhar and Mead observed a total of ten Raman active modes from single crystals of Sn_2S_3. These were denoted as being XX or XY; with XX denoting polarisation vectors of the incident and scattered light being parallel, and XY denoting them being crossed. The crossed polarisation spectra were almost identical to each other, as were the crossed polarisation spectra although band intensities varied. Raman bands were observed at 63, 73, 90, 154, 236 and 308 cm^{-1} for XX spectra and 54, 192, 209 and 252 cm^{-1} for XY spectra.[80]

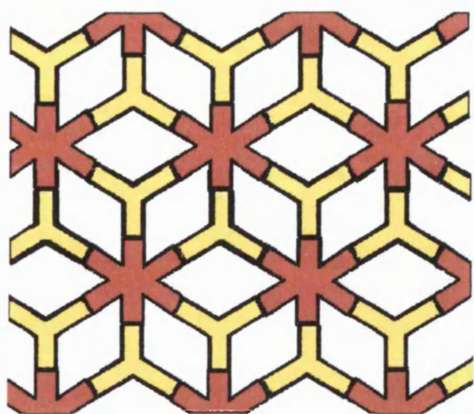

Figure 7.2 A schematic representation of the ribbon structure of Sn_2S_3 with sulfur shown in yellow and tin in red. The structure has trigonal-pyramidal tin(II) located at the edges of the ribbon and octahedral tin(IV) at the centre.[74]

Prior to the CVD studies of tin sulfides reported here, there were only two references to tin monosulfide CVD deposited thin films in the literature.[75] This is surprising as SnS, SnS_2 and Sn_2S_3 are semiconductors with band gaps of 1.3, 2.18 and 0.35 eV respectively.[80,81,82]

There are many possible uses for tin sulfide films produced by APCVD these include the following; photovoltaic materials[83] due to high-energy conversion and use in holographic recording media.[84] It was also initially thought that the coatings might be used on window glass as heat mirrors in a solar control coating.[83]

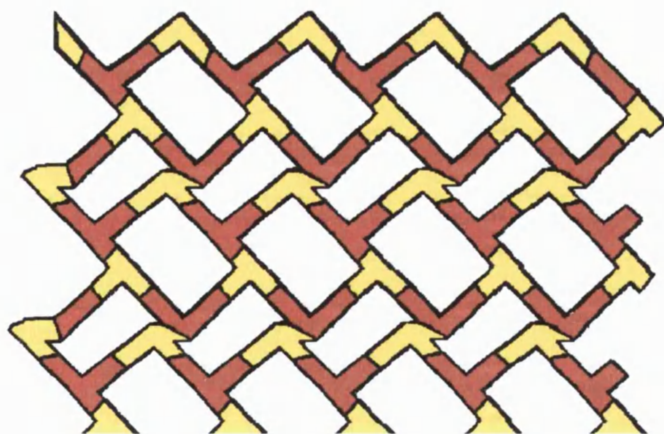

Figure 7.3 A schematic representation of the structure of a layer of SnS with sulfur shown in yellow and tin in red.[74]

7.3 Experimental, results and discussion

Since films produced using several systems will be discussed in this chapter, the experimental, results and discussion section for each will be grouped together, with each system having a separate subheading. All the systems will then be discussed in one section to allow comparisons to be made.

7.3.1 APCVD reactions of Tin tetrachloride and hydrogen sulfide

Nitrogen (99.99 %, BOC) and H_2S (99.9 %, BOC), were used as supplied as carrier gas and precursor respectively in these reactions. The second precursor, $SnCl_4$ (99.9 % Aldrich Chemical Co.) was also used as supplied and introduced into the gas stream via a stainless steel bubbler using a 1.5 dm^3 min^{-1} nitrogen flow rate. The glass substrates were supplied with a SiCO precoating onto which thin films were deposited as described in Chapter 2. The bubbler was heated to temperatures between 60 and 90 °C for different reactions. The APCVD reactions were of 30 or 180 s duration at 300 – 545 °C.[72]

7.3.2 Results

Films deposited at substrate temperatures between 300 – 500 °C consisted of single phase SnS_2. The film deposited at 525 °C was Sn_2S_3, and at 545 °C SnS was produced. These compositions were initially determined by EDX, XPS and electron probe measurements.[72] These did not detect the presence of chlorine or other elements. The films deposited between 300 – 500 °C during 30 s reactions were all yellow. However at 300 °C if a reaction was allowed to run for 180 s the film deposited appeared black. The film deposited at 525 °C was brown with a yellow edge. The film deposited at 545 °C was grey.[72]

7.3.3 Raman spectroscopy

Raman spectra are shown below for three films that were chosen as being representative of the films sharing the same composition. The Raman spectrum shown below in figure 7.4 corresponds to that of SnS_2. Bands at 215 and 312 cm^{-1} compare favourably with reported literature values of 317 cm^{-1} caused by A symmetry, intra-layer modes, and a band at 209 cm^{-1} in the 2H-SnS_2 polytype with E_g symmetry.[78] All Raman spectra were

recorded at room temperature. The spectra in figures 7.4 and 7.5 were recorded using 647.1 nm excitation with 632.8 nm used for spectra in figures 7.6 and 7.7.

The Raman spectrum shown below in figure 7.5 corresponds to that of Sn_2S_3. Bands at 36, 52, 60, 71, 93, 155, 183, 226 and 307 cm^{-1} compare with reported literature values of 63, 73, 90, 154, 236 and 308 cm^{-1} for XX spectra[80] and 54, 192, 209 and 252 cm^{-1} for XY spectra.[80] The overall appearance of the spectrum, however, matches the band positions and intensities reported for the YY polarised Sn_2S_3.[80] This implies a preferred orientation for Sn_2S_3 crystals when deposited by this APCVD reaction.

The Raman spectrum shown below in figure 7.6 corresponds to that of SnS. Bands at 96, 163, 189, 220 and 288 cm^{-1} compare with crystals with random orientations with respect to the substrate. The reported literature values for SnS have A_g bands are at 95, 192 and 218 cm^{-1}; B_{3g} bands at 164 cm^{-1}; and B_{2g} bands at 160 and 290 cm^{-1}.[76]

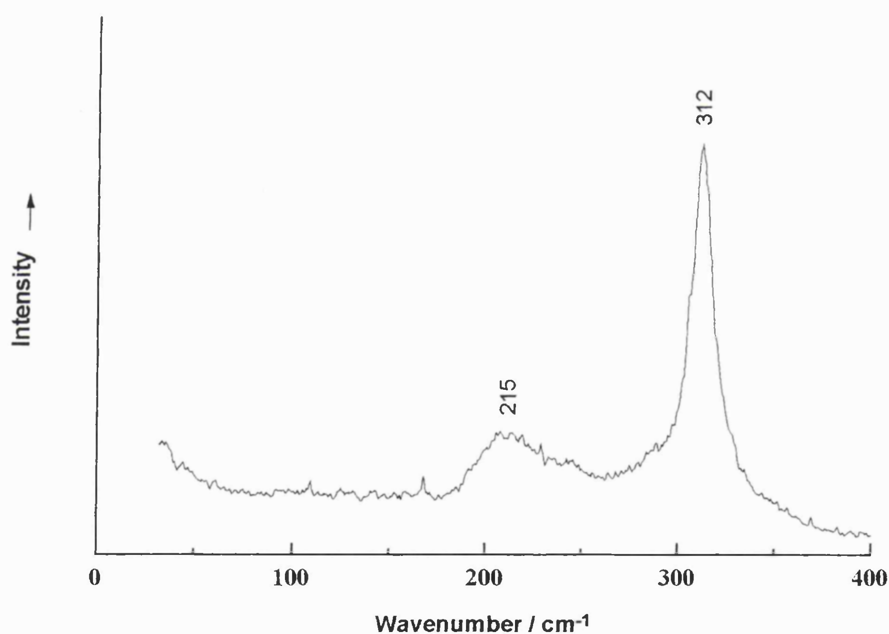

Figure 7.4 Raman spectrum of a film deposited at 300 °C by the APCVD reaction of tin tetrachloride and hydrogen sulfide.

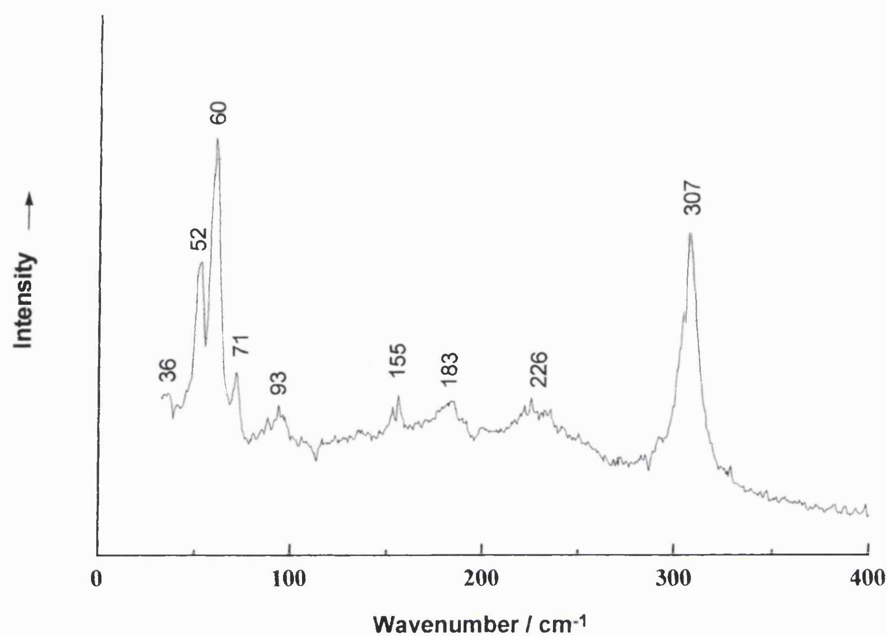

Figure 7.5 Raman spectrum of a film deposited at 525 °C by the APCVD reaction of tin tetrachloride and hydrogen sulfide.

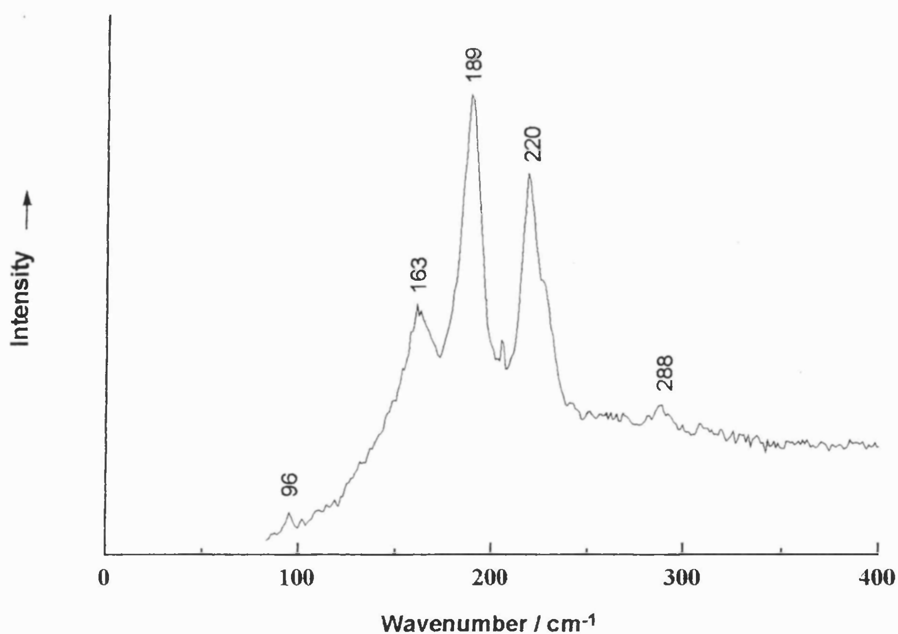

Figure 7.6 Raman spectrum recorded from the centre of the film deposited at 545 °C by the APCVD reaction of tin tetrachloride and hydrogen sulfide.

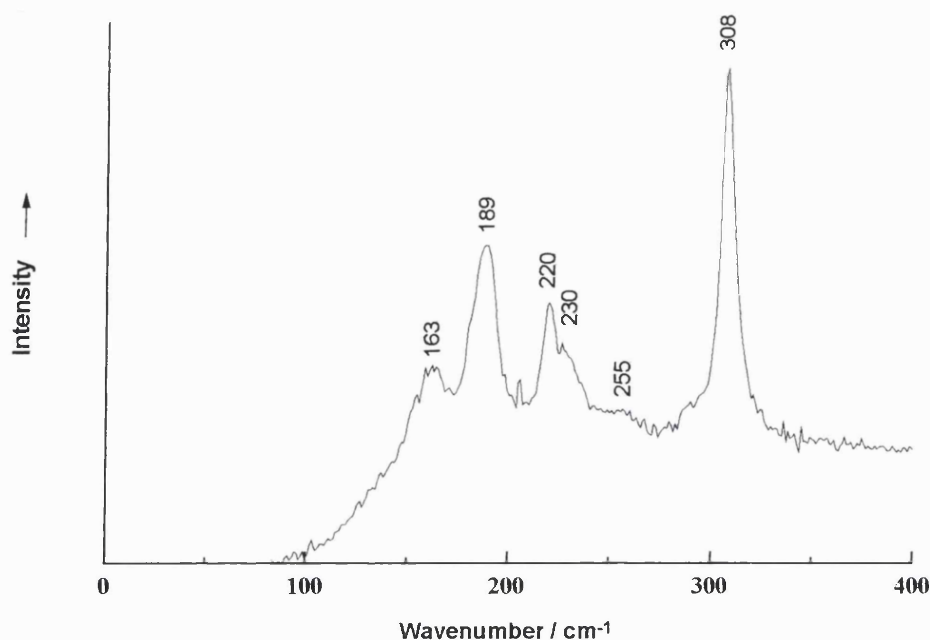

Figure 7.7 Raman spectrum recorded from the edge of the film deposited at 545 °C by the APCVD reaction of tin tetrachloride and hydrogen sulfide.

The Raman spectrum shown above in figure 7.7, was recorded from a brown region at the edge of the film deposited at 545 °C. A spectrum recorded from the centre of the film deposited at this temperature showed the presence of phase pure tin monosulfide, however as can be seen from figure 7.7, the edges of the substrate were coated with a mixture of SnS and Sn_2S_3. With bands at 163, 189 and 220 due to SnS and bands at 230, 255 and 308 due to the presence of Sn_2S_3.[76,80]

This was possible because the edges of the substrates were up to 20 °C cooler than the centre of the substrates during the deposition reactions. At temperatures below 500 °C, SnS_2 is deposited by the reaction studied and at 525 °C Sn_2S_3 is produced. Therefore the film deposited at 545 °C had brown film at the cooler edges, whereas films deposited at 525 °C had yellow stripes of SnS_2 at the edge of the substrates.

7.3.4 Scanning electron microscopy

Photographs of SEM images of the films deposited from the reaction of tin tetrachloride and hydrogen sulfide are shown below in figures 7.8a-d.

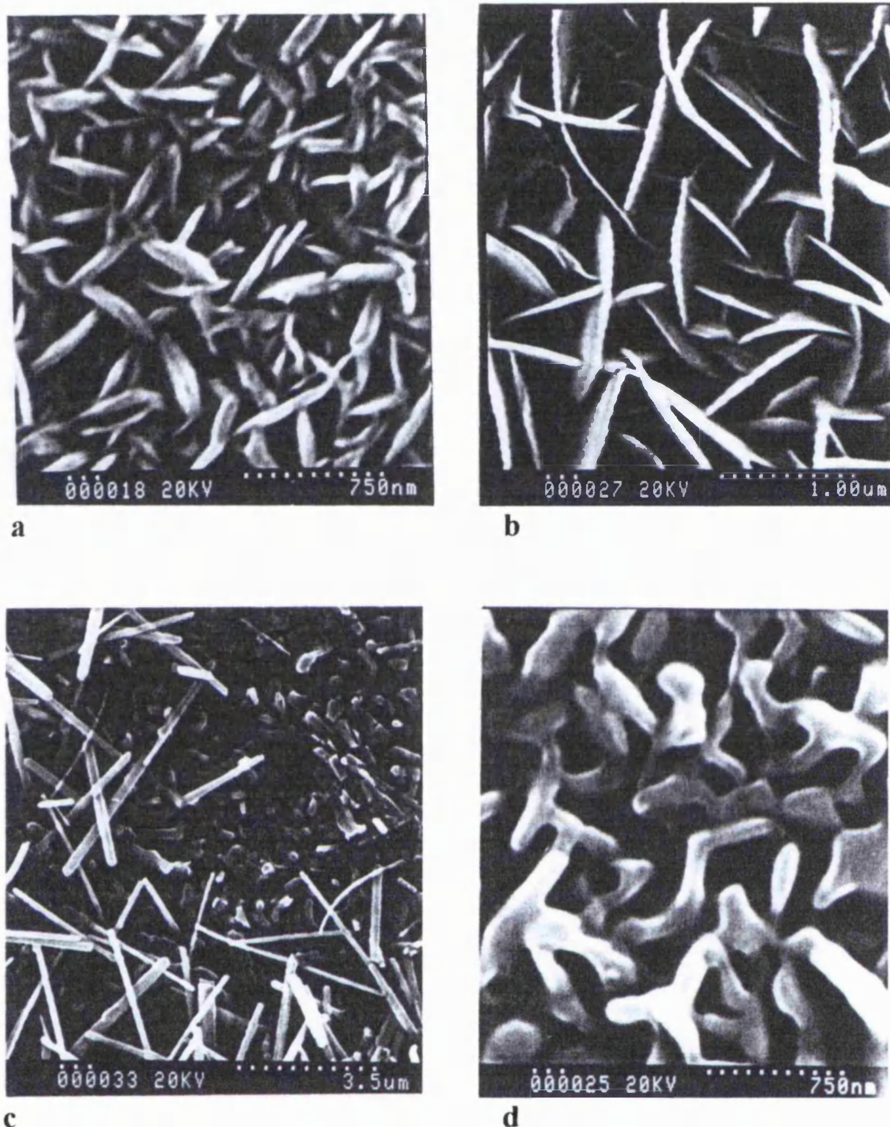

Figure 7.8 Scanning electron micrographs of films deposited from the APCVD reaction of tin tetrachloride and hydrogen sulfide at a.) 300°C, b.) 450 °C, c.) 525 °C and d.) 545 °C.[72]

7.4 APCVD reactions of Tin tetrabromide and hydrogen sulfide

Nitrogen and H_2S were used as described above in section 6.2i, the second precursor used in this system was $SnBr_4$ (99 %, Aldrich Chemical Co.). These products were used as supplied and introduced into the gas stream via a stainless steel bubbler using a 1.5 dm^3 min^{-1} nitrogen flow rate through it. The glass substrates were supplied with a SiCO precoating onto which thin films were deposited as described in Chapter 2. The bubbler was heated to temperatures between 130 – 150 °C for each reaction. Substrates were coated at reaction temperatures between 250 – 600 °C, with reactions being performed in 50 °C increments. In addition some reactions were carried out at 525 °C because there was a phase transition in the temperature range 500 – 550 °C. Reactions

were performed using H_2S flow rates of 0.6, 1.2 or 1.8 $dm^3 min^{-1}$, the total gas flow through the reactor was kept constant at 12 $dm^3 min^{-1}$ and the reactions lasted either 30 or 180 s.[72]

7.4.1 Results

The films produced passed the Scotch tape test but could be scratched off using a scalpel.[72] The films deposited at substrate temperatures of 450 °C or below were yellow in colour. The composition of these films was shown to be SnS_2 by X-ray diffractometry[72] and Raman microscopy. A Raman spectrum of the film deposited at 450 °C is shown in figure 7.9, this has a Raman band at 315 cm^{-1}. Films deposited at 500 and 525 °C had brown and grey regions. X-ray diffraction[72] identified the film deposited at 500 °C with 1.2 $dm^3 min^{-1}$ flow of H_2S as being Sn_2S_3; with the film produced at 600 °C being SnS. At 550 °C and above the films were grey, with yellow edges.

7.4.2 Raman spectroscopy

At substrate temperatures between 250 – 450 °C SnS_2 was deposited as a single phase yellow film. At 500 – 525 °C films consist of Sn_2S_3 with small amounts of SnS_2 present as thin yellow strips at the edges of the substrate. These films were mostly brown i.e. Sn_2S_3. The films deposited at 550 and 600 °C were grey in colour due to the presence of SnS. It was also possible to deposit tin monosulfide at 525 °C if a 1.8 rather than 1.2 $dm^3 min^{-1}$ flow of H_2S was used during the reaction.

The Raman spectrum shown below in figure 7.9 has a single Raman band at 315 cm^{-1} this corresponds to the literature value of 317 cm^{-1} caused by A symmetry, intra-layer modes of SnS_2. The expected E symmetry band is absent, this is because its intensity relates to crystal orientation and the signal-to-noise ratio was not high enough to allow this band to be distinguished from the background noise.[78] All Raman spectra reported in section 7.4 of this thesis were recorded using 647.1 nm excitation.

The Raman spectrum shown below in figure 7.10 has bands at 51, 59, 70, 86, 95, 153, 181, 233 and 307 cm^{-1} which correspond literature values of 63, 73, 90, 154, 236 and 308 cm^{-1} for XX spectra and 54 and 192 cm^{-1} for XY spectra of Sn_2S_3. The band intensities and positions are an exact match with those of YY polarised Sn_2S_3 crystals.[80] This implies that Sn_2S_3 deposited by APCVD has a preferred crystal orientation with respect to the substrate.

The Raman spectrum shown below in figure 7.11 has bands at 39, 48, 66, 94, 160, 189 and 218 which correspond to the following literature values for SnS; A_g bands at 40, 95, 192 and 218 cm^{-1}; B_{3g} bands at 49 and 164 cm^{-1}; and B_{2g} bands at 70, 85, 160 and 290 cm^{-1}.[76]

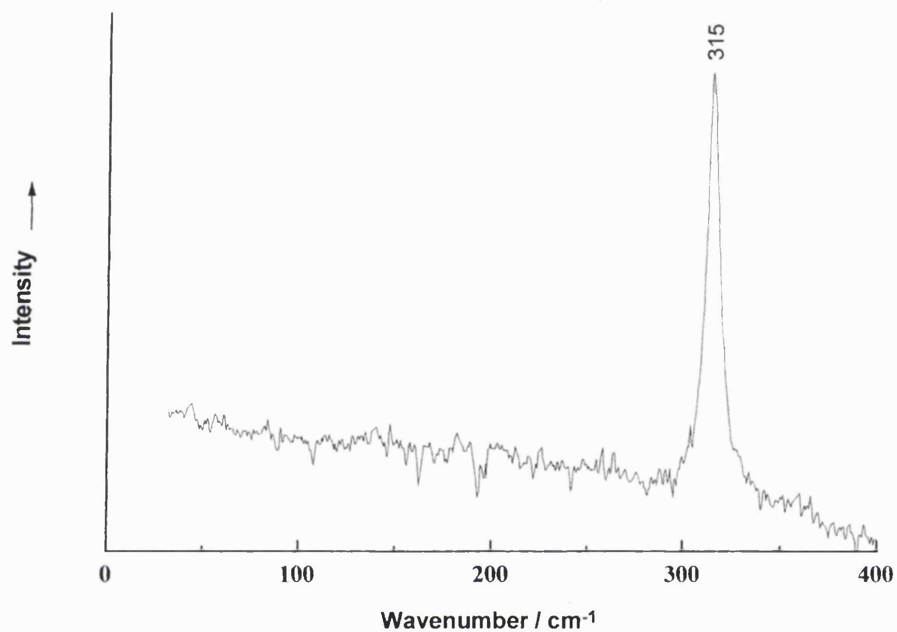

Figure 7.9 Raman spectrum of a film deposited at 450 °C by the APCVD reaction of tin tetrabromide and hydrogen sulfide.

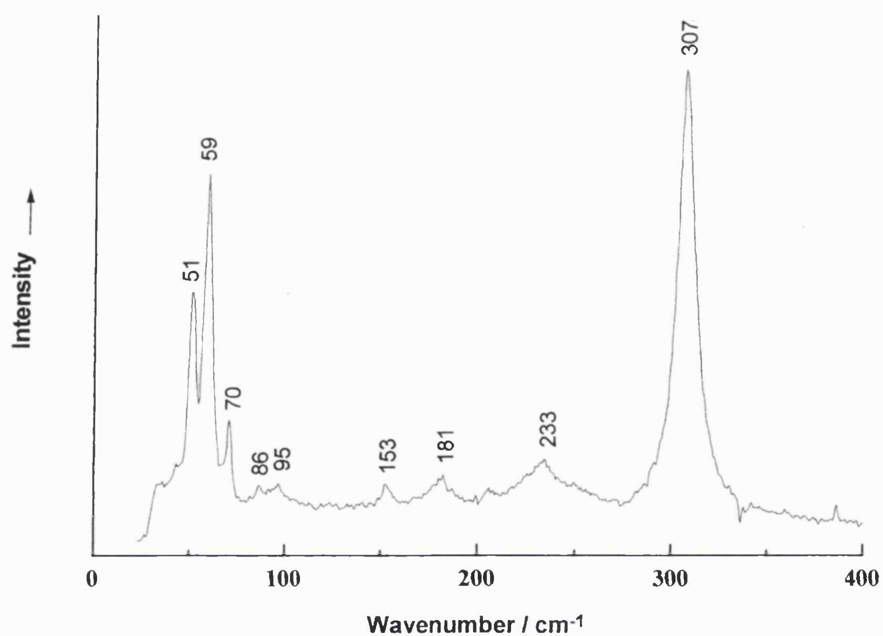

Figure 7.10 Raman spectrum of a film deposited at 525 °C by the APCVD reaction of tin tetrabromide and hydrogen sulfide.

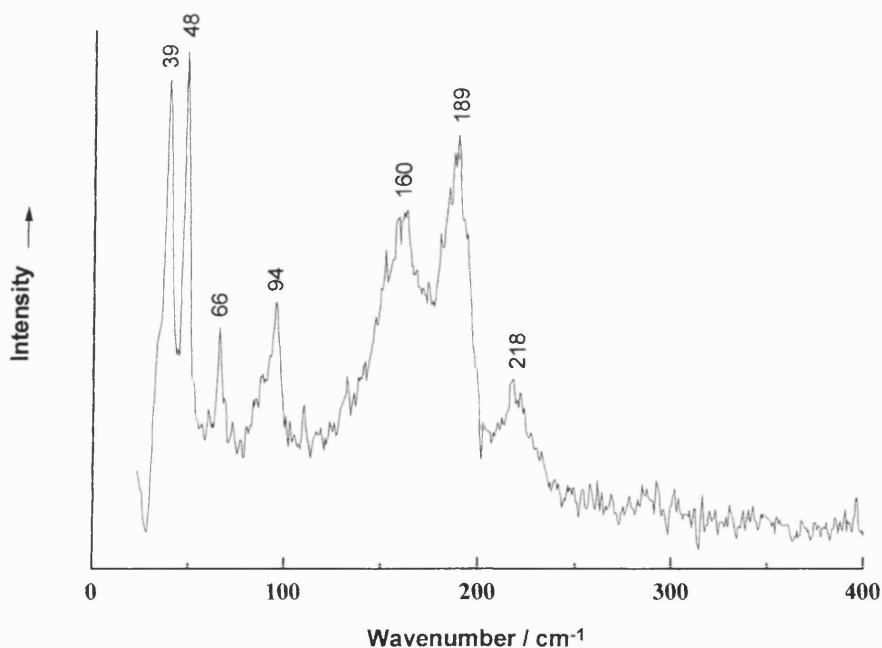

Figure 7.11 Raman spectrum of a film deposited at 600 °C by the APCVD reaction of tin tetrabromide and hydrogen sulfide.

7.5 APCVD reactions of n-$Bu_3SnO_2CCF_3$ and hydrogen sulfide

Nitrogen and H_2S were used as described above in section 6.2i, the second precursor used in this system was tri-n-butyltin trifluoroacetate[85] which was synthesised by Tom Hibbert as described in Chapter 2. SiCO coated glass supplied by Pilkington Glass plc was used as the substrate for these reactions. The tri-n-butyltin trifluoroacetate was admitted to the gas stream through the rig using a bubbler, which was heated to c. 130 °C, with a 0.4 $dm^3 min^{-1}$ flow of nitrogen through the bubbler once it was opened. A 0.6 $dm^3 min^{-1}$ flow rate of H_2S was used for these reactions. The reactions were each allowed to run for 15 minutes. Reactions were carried out with substrate temperatures between 300 – 600 °C at 50 °C intervals, giving seven reactions in total.[72]

7.5.1 Results

The reaction at 300 °C did not result in a coating being deposited; the film deposited at 350 °C appeared to be very thin. All films deposited by this reaction were grey and passed the Scotch tape test, but could be removed by scraping with a scalpel. EDX showed the ratios of Sn:S in deposited films were all approximately 1:1 regardless of deposition temperature. X-ray photoelectron spectroscopy did not detect fluorine in the films. X-ray diffraction measurements result in diffraction patterns that match tin monosulfide data as reported by Boudjouk et al.[86,87,88] The unit cell parameters were found to be a = 11.27(4), b = 3.972(6), c = 4.24(1) Å in comparison to unit cell parameters reported by Boudjouk et al. of a = 11.18-11.21, b = 3.98-4.02 and c = 4.30-4.33 Å. X-ray diffraction results did not show contamination with other phases of tin sulfide, tin or sulfur.[72]

7.5.2 Raman spectroscopy

Raman microscopy showed that the films produced in these studies were single phase tin monosulfide with randomly oriented crystallites; by comparison with single crystal, rather than thin film studies by Chandrasekhar et al.[89] There was no sulfur contamination detected in the films deposited, which would be obvious in the Raman spectrum as sulfur has two intense bands at 153 and 218 cm^{-1}, which can be seen even at low concentration in a sample. One of the Raman spectra recorded is shown below in figure 7.12, this has bands at 94, 159, 185 and 217 cm^{-1}, which correspond to literature values of 95 (A_g), 164 (B_{3g}), 192 (A_g) and 218 (A_g) cm^{-1}.

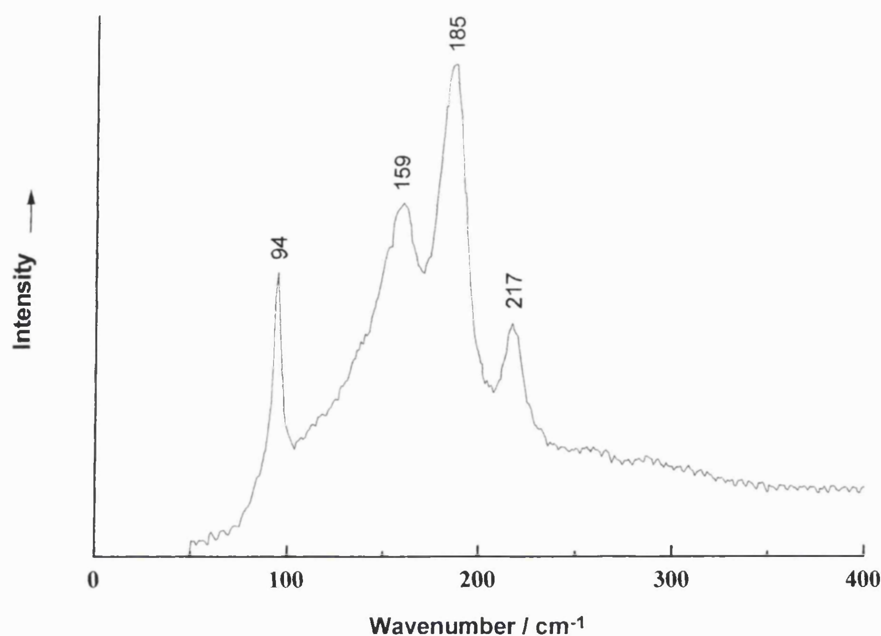

Figure 7.12 Raman spectrum of a film deposited at 450 °C by the APCVD reaction of tri-n-butyltin trifluoroacetate and hydrogen sulfide.

7.6 AACVD reactions of tetra(phenylthiolato) stannane and hydrogen sulfide

Nitrogen and H_2S as described above in section 6.2i were used in a modified APCVD rig. The rig used a humidifier to replace the bubbler as a means of introducing the precursor. This allowed the introduction of an aerosol of solvent and precursor into the reactor, without the need for heating the precursor. The substrates coated in this study were supplied with a 100 nm thick precoating of SiO_2. The humidifier used was a Pifco Health ultrasonic humidifier which was used to nebulise a solution of the precursor. The resulting aerosol was carried into the reactor with a 2 dm^3 min^{-1} flow of nitrogen. Other experimental details are the same as for the APCVD reactions studied with the exception of the start and end of reactions being marked by the switching on and off of the humidifier. The flow of H_2S used for the reactions presented was 0.4 dm^3 min^{-1}, with reactor temperature set between 300 – 600 °C. The reactions were allowed to run for about 20 min.[72]

7.6.1 Results

When the reactions were carried out in the absence of hydrogen sulfide, tin oxide films were produced, these were identified by their XRD pattern as Sn_3O_4, with no SnO_2 or

SnO. The source of oxygen was assumed to be the nitrogen gas used to carry the precursor through the rig. Even though this contained only 0.01% oxygen, it also contained some water as it was not dried prior to entering the gas stream through the reactor, no sulfide was identified in the film produced. It is therefore assumed that the reactions in the presence of hydrogen sulfide use the sulfur present in the H_2S to form tin sulfide, rather than sulfur from the ligands. No oxide phase was identified in films deposited in the presence of H_2S. At 450 °C films produced were found to be SnS_2 by use of XRD and EDX. Films deposited at or above 500 °C were identified as SnS.[72]

7.6.2 Raman spectroscopy

As can be seen below in figure 7.13 a Raman spectrum of the film produced at 450 °C has both SnS_2 present as a major phase, and SnS as a minor component of the coating. The SnS_2 deposited has a Raman band at 313 cm^{-1} which compares to the literature value of 317 cm^{-1} caused by A symmetry intra-layer modes, as discussed above the expected E symmetry band is absent due to crystal orientation.[78] The SnS component of the coating has Raman bands at 96, 155, 184 and 218 cm^{-1}, which compare with 95 (A_g), 160 (B_{2g}), 192 (A_g), and 218 (A_g) cm^{-1}.[76] This is also true of the film deposited at 500 °C, however the ratio is reversed with the film being predominately SnS as can be seen in figure 7.14.

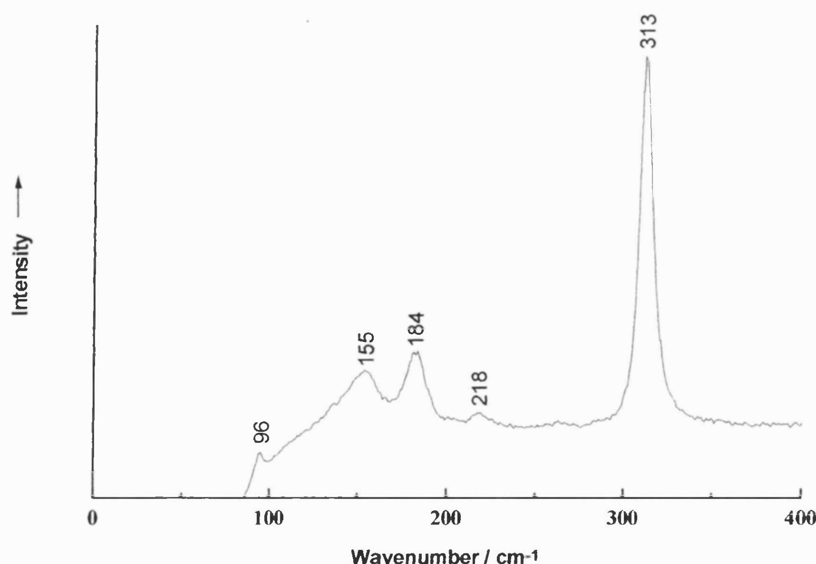

Figure 7.13 Raman spectrum of a film deposited at 450 °C by the AACVD reaction of tetra(phenylthiolato) stannane and hydrogen sulfide.

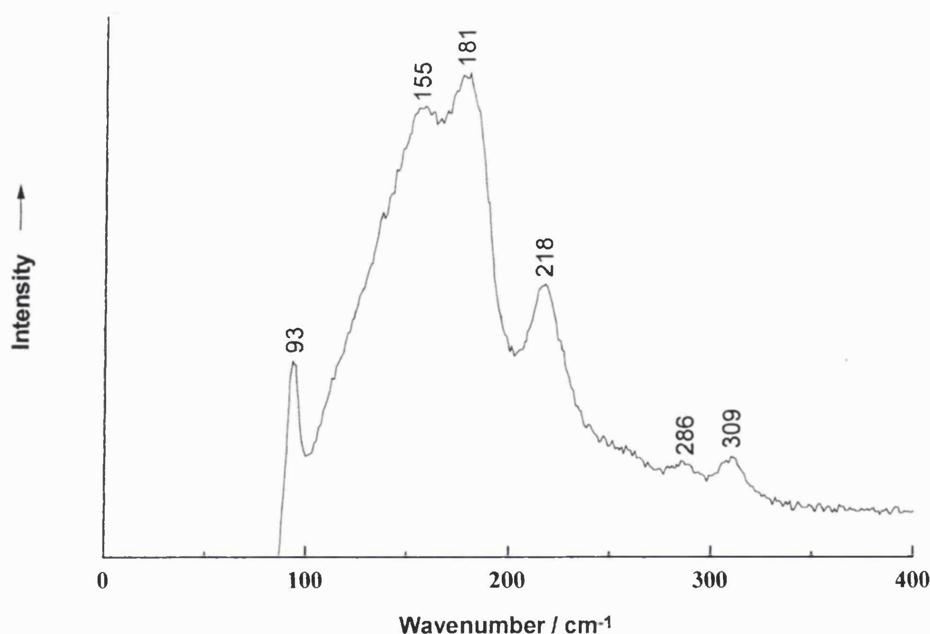

Figure 7.14 Raman spectrum of a film deposited at 500 °C by the AACVD reaction of tetra(phenylthiolato) stannane and hydrogen sulfide.

All Raman spectra in this section were recorded using 632.8 nm radiation to analyse the sample.

7.7 Discussion

The reaction of tin tetrachloride with hydrogen sulfide on a glass substrate produces the same products as the reaction between tin tetrabromide and hydrogen sulfide. The difference in experimental conditions arises from the higher bubbler temperature required for tin tetrabromide due to its higher boiling point; $SnCl_4$ boils at 114 °C, whereas $SnBr_4$ boils at 202 °C. It was noted that film composition could be controlled either by substrate temperature or by an equilibrium shift in the CVD reaction caused by altering the flow rate of hydrogen sulfide. Hence, the most convenient method for industrial control of film composition could be selected.

The films deposited by the reaction of tri-n-butyltin trifluoroacetate and hydrogen sulfide were all tin monosulfide. Raman microscopy can easily identify other phases of tin sulfide in thin films, therefore these films were assumed to be phase pure with no evidence of sulfur contamination.

The films deposited by the reaction of tetra(phenylthiolato) stannane and hydrogen sulfide resulted in films which were found not to be phase pure when studied by Raman microscopy. This also indicated that the individual crystallites present in the film were smaller than 1 μm in diameter.

As can be seen clearly illustrated by the films deposited from the APCVD reactions of tin tetrachloride and hydrogen sulfide, the colour of the tin sulfide film can be correlated with its composition. Raman microscopy clearly show that this is the case as the use of a microscope during the analysis allows individual coloured crystals to be analysed. SnS_2 films are yellow for thin films and black for thicker films, Sn_2S_3 is brown and SnS is grey when deposited as a thin film.

The presence of a yellow strip of tin disulfide at the very edges of some of the high temperature coatings is due to the temperature gradient at the very edge of the substrate during the reaction. If the temperature at the edge of the substrate is low enough i.e. 500 °C or less, SnS_2 can be deposited during the reaction. This multiple phase analysis was possible due to the capability of Raman microscopy to allow Raman analysis to be performed on very small regions of a sample. These can be selected either for the position on the sample or due to their visual appearance.

Raman microscopy can be used is some instances to assign crystal orientation of a film. If a film consists of an anisotropic compound its Raman spectra may vary with respect to laser orientation on individual, or multiple aligned crystal faces. It is also possible to map the composition of a film over the entire surface of a substrate. This can produce a composition map with a resolution of *c.* 2 μm. This would show the changes in film composition due to deposition temperature variation over the substrate, and the effect of deviation from homogeneous linear gas flow over the substrate during the reaction.

As can be seen from the above reactions the lower temperature phase of tin sulfide is SnS_2, with SnS usually produced at or above 500 °C. However because the reactions studied only lasted 0.5 – 20 mins (for AACVD), APCVD can also be used to produce the kinetic reaction product, rather than that favoured by thermodynamics alone. The reactions of tri-n-butyltin trifluoroacetate and hydrogen sulfide produced films consisting of SnS only, between 350 – 600 °C. Normally in the above studies, only SnS_2 is produced at substrate temperatures below 450 °C.

Prior to the above reported studies, there were only two reports of tin sulfide formation by CVD in the literature. These both produced SnS.[79,90] Therefore this is the first study to include Raman spectra from tin sulfides deposited by APCVD. Band symmetry assignments given in brackets after wavenumber values come from literature reports based on single crystal studies, which list space/point groups for Sn_2S_3 and SnS as *Pnma*[80] and D_{2h}.[76]

7.8 Conclusion

Raman microscopy was able to confirm or complement other analysis performed on the films studied in this chapter. The films deposited were as follows:

The APCVD reaction of tin tetrachloride and hydrogen sulfide deposited films of SnS_2 at temperatures between 300 – 500 °C, Sn_2S_3 at 525 °C and SnS at 545 – 600 °C.

The APCVD reaction of tin tetrabromide and hydrogen sulfide deposited films of SnS_2 at temperatures between 250 – 450 °C, Sn_2S_3 at 500 and 525 °C and SnS at 550 – 600 °C.

The APCVD reaction of tri-n-butyltin trifluoroacetate and hydrogen sulfide deposited films of SnS only, with films deposited between 350 – 600 °C.

The AACVD reaction of tetra(phenylthiolato) stannane and hydrogen sulfide deposited films of SnS_2 at 450 °C and SnS at 500 and 550 °C.

Raman microscopic analysis showed that elemental sulfur was absent from the films deposited in this study.

8.0 Mixed metal coatings

8.1 Introduction

In this chapter Raman spectra are presented from two APCVD systems. These were oxovanadium(V) chloride ($VOCl_3$) / tin tetrachloride ($SnCl_4$) and hydrogen sulfide and vanadium tetrachloride (VCl_4) / tin tetrachloride ($SnCl_4$) and hydrogen sulfide. These were used to attempt an APCVD preparation of tin vanadium oxysulfide and tin vanadium sulfide.

8.2 Background

Mixed tin/vanadium oxide/sulfide coatings are of interest as they may be useful compounds for chemical sensors. Tin/vanadium oxide compounds have already been reported for use as hydrocarbon sensors.[91] The Raman data presented in this chapter is a key part of this thesis. The material in this chapter has been included in this thesis as it relevant to the CVD reactions covered in Chapters 3 and 4. Two APCVD systems are presented in this chapter; both include two precursors; one of which contains tin and the other vanadium. The tin source precursor used in both cases was tin tetrachloride as it had been studied previously and was found to have suitable properties to produce moderately thick, largely uniform films in a relatively short period of time. It was also known from the previous study what reactor conditions are required to produce the three principle forms of tin sulfide, ie. SnS, Sn_2S_3 and SnS_2 (see Chapter 7).

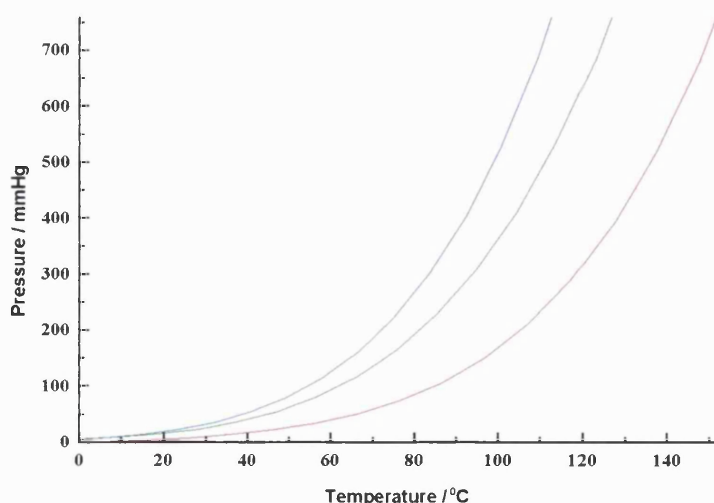

Figure 8.1 Vapour pressure plots of the precursors used in this chapter. The blue line represents tin tetrachloride, the green line vanadium oxychloride and the red one vanadium tetrachloride.

8.3 Tin vanadium oxysulfide

8.3.1 Experimental

Three precursors were used to try and make tin vanadium oxysulfide, these were oxovanadium(V) chloride ($VOCl_3$), tin tetrachloride ($SnCl_4$) (which were admitted to the reactor via gas flow through two bubblers), and hydrogen sulfide gas (which was taken from a gas cylinder and admitted to the reactor via a nitrogen diluent gas stream). The bubbler containing oxovanadium(V) chloride was heated to *c.* 100 °C and the second bubbler, which contained tin tetrachloride was heated to a temperature between and 68 - 100 °C. The exact temperature chosen in each case being governed by the requirement to have enough material in the gas stream flowing through the reactor to form a film; and the temperature required for each bubbler to allow the ratio of vanadium to tin compound in the gas to be predicted and controlled. The flow rates used for this mixed system were 0.5 $dm^3\ min^{-1}$ of nitrogen through each of the bubblers, and a flow of 0.6 $dm^3\ min^{-1}$ of H_2S combined with a 1.2 $dm^3\ min^{-1}$ flow of nitrogen. Each deposition was for 30 s; the start and finish of each run was marked by the turning of a four-way valve. The substrate used in each case was a sheet of precoated glass with a silicon dioxide surface. The precoating was used as a diffusion barrier to protect the experimental coating from contamination by constituent ions from the glass.

In total nine reactions were completed for this system, three at each of the temperatures chosen to represent the formation temperatures of the three tin sulfides. At each temperature a reaction was set up where the ratio of vanadium to tin gave a precursor mixture, which was in turn vanadium rich, tin rich or an equal concentration of each metal. A table of the conditions used is shown below in table 8.2.[92]

Precursors	Deposition temperature / °C	Tin : vanadium vapour pressure	Bubbler 1 ($VOCl_3$) temperature / °C	Bubbler 2 ($SnCl_4$) temperature / °C
$SnCl_4$ + $VOCl_3$	350	5:3	96	100
$SnCl_4$ + $VOCl_3$	350	1:1	96	91
$SnCl_4$ + $VOCl_3$	350	1:2	102	75
$SnCl_4$ + $VOCl_3$	480	5:3	98	100
$SnCl_4$ + $VOCl_3$	480	1:1	96	91
$SnCl_4$ + $VOCl_3$	470	1:2	107	68
$SnCl_4$ + $VOCl_3$	575	5:3	98	100
$SnCl_4$ + $VOCl_3$	575	1:1	94	88
$SnCl_4$ + $VOCl_3$	570	1:2	101	74

Table 8.2 Table of conditions used for the APCVD reactions of oxovanadium(V) chloride, tin tetrachloride and hydrogen sulfide.

The reactor temperature was set to one of three values, each known to produce predominantly one of the tin sulfides rather than a mixture. One set of reactions was carried out at 350 °C because a reaction mixture of tin tetrachloride and hydrogen sulfide was found to deposit tin(IV) sulfide at temperatures below 400 °C (see Chapter 6). A second set of reactions was carried out at *c.* 475 °C, as tin(II) tin(IV) trisulfide could be deposited at this temperature. The final set of reactions was carried out at *c.* 575 °C, as tin tetrachloride and hydrogen sulfide deposit only tin(II) sulfide at this temperature. The second variable was the relative concentrations of the metal containing precursors in the reactor.

8.4 Results

8.4.1 Film colour and uniformity

The film colour and uniformity are described below in table 8.3.[92]

Precursor ratio → Temperature	Rich in tin (a)	Equal tin and vanadium (b)	Rich in vanadium (c)
350	Brown	Brown	Brown
470	Dark grey, purple, dark yellow, grey yellow, yellow	Black, purple, dark yellow, grey, yellow	Black, blue black, grey, silver, purple, brown
570	Black, yellow brown, brown, grey, half glass uncoated	Grey brown, grey, half glass uncoated	Black, grey brown, grey, half glass uncoated

Table 8.3 Colours of films deposited from the APCVD reaction of tin tetrachloride, oxovanadium(V) chloride and hydrogen sulfide. (Lists of colours are in order from inlet end to the exhaust end of the glass plate.)

8.4.2 Raman microscopy

All of the films produced from the reaction of oxovanadium(V) chloride, tin tetrachloride and hydrogen sulfide were analysed by Raman microscopy. This was done because, unlike EDX results which give elemental composition, Raman spectra (using 632.8 nm excitation) allow the identification of specific phases present. This is particularly important in a mixed metal system as free elements, such as sulfur may be distinguished from their oxides, also it is in principle possible to distinguish between metal oxides, sulfides and oxysulfides. In films with several phases, or regions of different thickness and/or colour a Raman spectrum was recorded from representative spots of each area. Some of these spectra are shown below in figures 8.4 –8.8.

The Raman spectrum shown below in figure 8.4 was recorded from a film deposited at 350 °C with a precursor ratio of $SnCl_4$: $VOCl_3$ of 5:3. This spectrum matches the material identified as VS_2 in Chapter 4 figure 4.5b which has bands at 191, 351, 549 and 907 cm^{-1}, in comparison to the spectrum shown below which has bands at 192, 346, 549 and 902 cm^{-1}. These Raman results seem to show that even with the presence of tin in the system, either it does not get incorporated, or, the difference between the Raman spectrum of VS_2 and Sn_xVS_2 (where x has not been identified) is minimal.

The Raman spectrum shown in figure 8.5 below has band at 153 (due to V_2S_3), 266 and 314 (due to SnS_2, which compares to a reported literature value of 317).[93] Figure 8.6 indicates that at 470 °C with a ratio of $SnCl_4$ to $VOCl_3$ of 1:2, VS_2 is deposited, having bands at 193, 350, 543 and 909 cm^{-1} in comparison to the values reported in Chapter 4, in figure 4.5b, at 191, 351, 549 and 907 cm^{-1}

The spectrum in figure 8.7 has bands due to V_2O_5 at 141, 192, 282, 301, 403, 473, 521, 686 and 991 cm^{-1}, these compare with reported values of 144, 282, 300, 405, 485, 700 and 995 cm^{-1}.[94] Figure 8.8 shows a Raman spectrum of SnS with bands at 95, 160, 218 and 300 cm^{-1}. These compare to the bands reported for SnS at 95 (A_g), 164 (B_{3g}), 218 (A_g) and 290 (B_{2g}).[95]

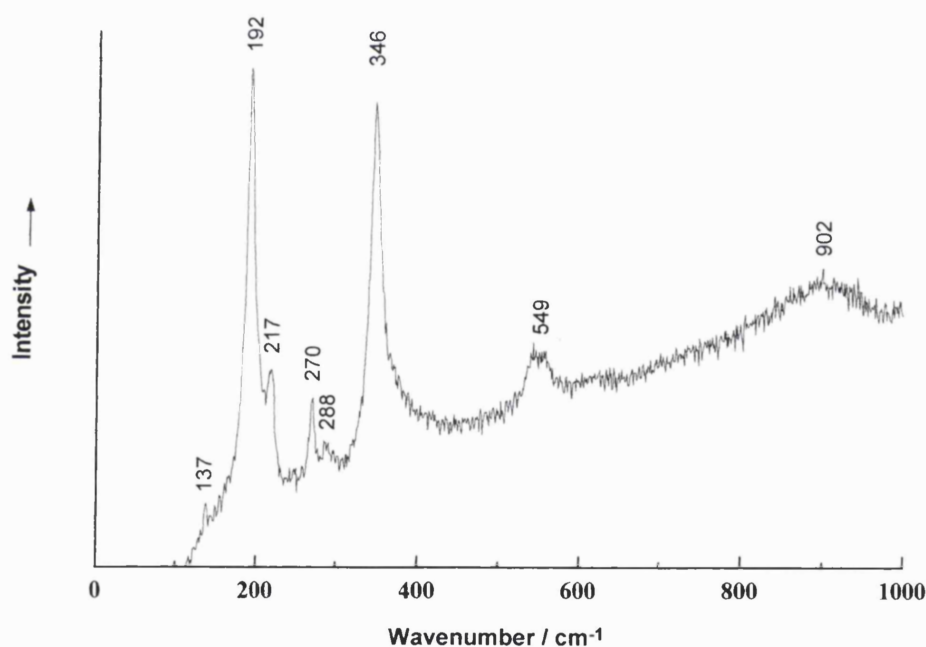

Figure 8.4 Raman spectrum of a film deposited by the APCVD reaction of $SnCl_4$ + $VOCl_3$ + H_2S at 350 °C. The ratio of $SnCl_4$ to $VOCl_3$ was 5:3.

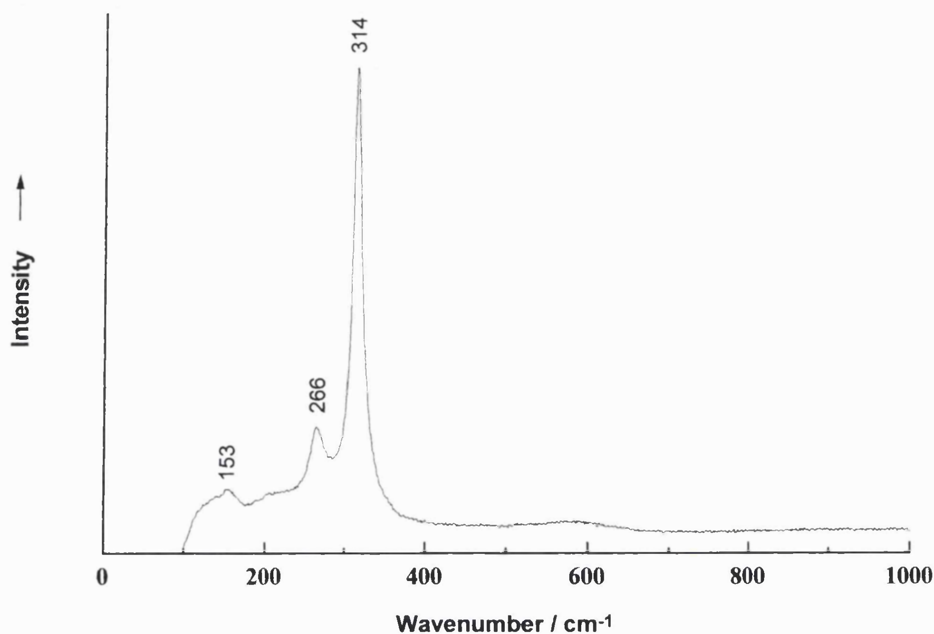

Figure 8.5 Raman spectrum of a film deposited by the APCVD reaction of $SnCl_4$ + $VOCl_3$ + H_2S at 480 °C. The ratio of $SnCl_4$ to $VOCl_3$ was 1:1.

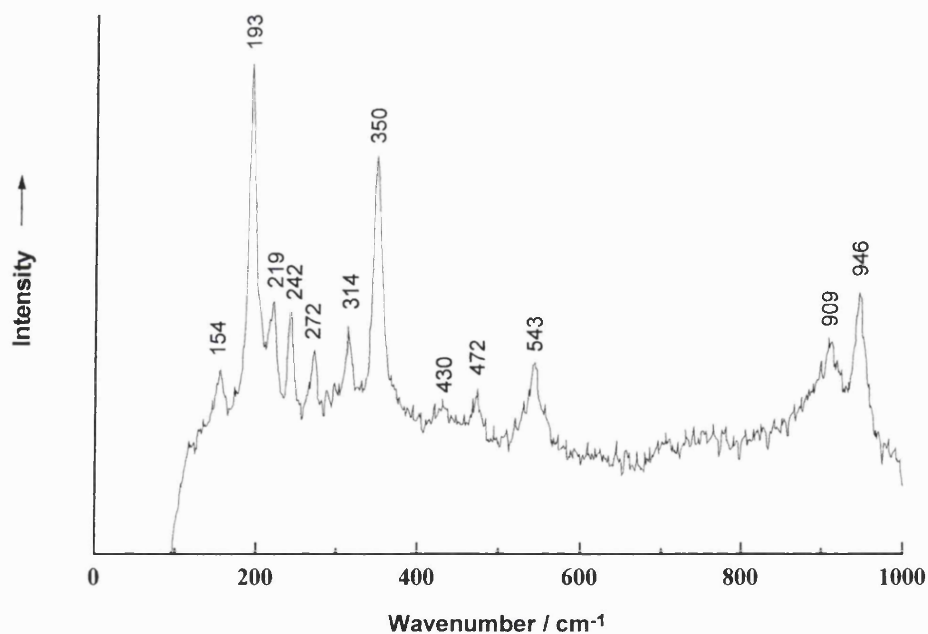

Figure 8.6 Raman spectrum of a film deposited by the APCVD reaction of $SnCl_4$ + $VOCl_3$ + H_2S at 470 °C. The spectrum was smoothed by averaging five adjacent points around each data point plotted. The ratio of $SnCl_4$ to $VOCl_3$ was 1:2.

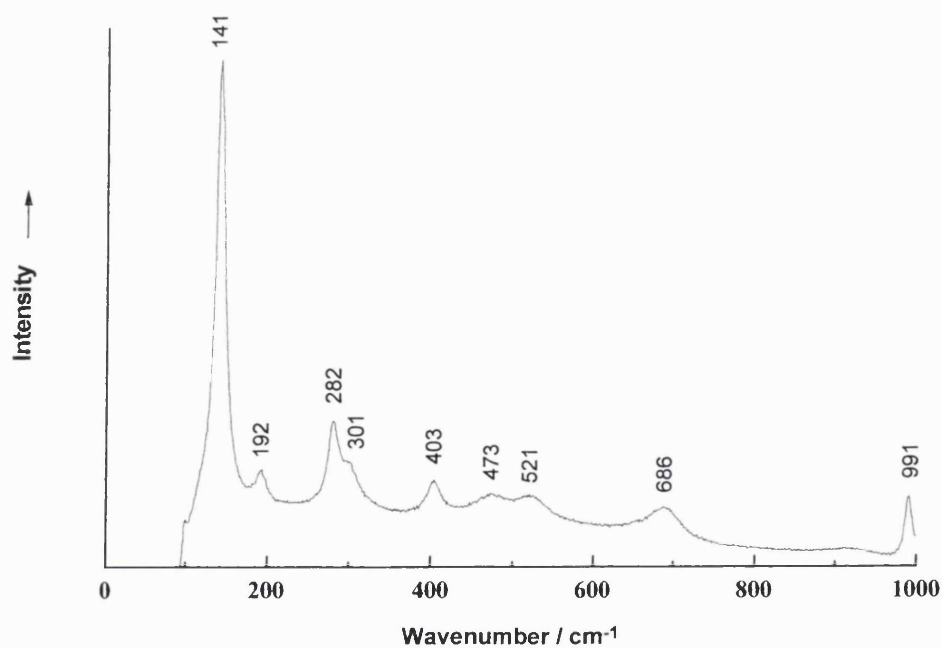

Figure 8.7 Raman spectrum of a film deposited by the APCVD reaction of $SnCl_4$ + $VOCl_3$ + H_2S at 470 °C. The ratio of $SnCl_4$ to $VOCl_3$ was 1:2.

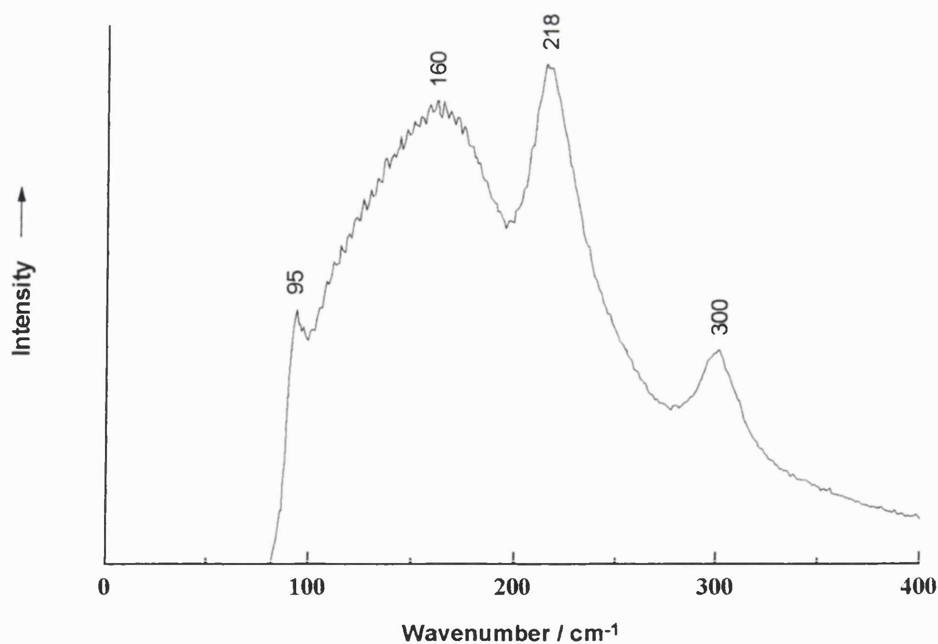

Figure 8.8 Raman spectrum of a film deposited by the APCVD reaction of $SnCl_4$ + $VOCl_3$ + H_2S at 575 °C. The ratio of $SnCl_4$ to $VOCl_3$ was 5:3.

Deposition temperature / °C	tin:vanadium vapour pressure ratios	Raman band positions / cm^{-1}	Compounds present
350	5:3	137w*^{v}, 192vs$^{\sim}$, 217m*, 270m*, 288w^{V}, 346vs$^{\sim}$, 549m$^{\sim}$, 902m,br$^{\sim}$.	* = VO_2, ^{v} = V_2O_5, $^{\sim}$ = VS_2
350	1:1	138w, 192s, 352s, 556m, 917m,br.	V_2S_3
350	1:2	136w, 181s, 558w, 898m,br.	V_2S_3
480	5:3	151w, 226m, 260m,310v.s.	Sn_2S_3
480	1:1	153w$^{\square}$, 266m$^{?}$, 314v.s$^{¥}$.	V_xS_y, $^{¥}$ = SnS_2.
470a	1:2	154m$^{\square}$, 193s$^{\sim}$, 219m*, 242m$^{?}$, 272m*, 314m$^{¥}$, 350s$^{\sim}$, 430m*, 472m$^{?}$, 543m$^{\sim}$, 909m,br$^{\sim}$, 946s^{v}.	$^{\square}$ = V_2S_3, VS_2, VO_2, SnS_2,V_2O_5.
470b	1:2	141v.s^{v}, 192w ^{v}, 282m ^{v}, 301w ^{v}, 403w ^{v}, 473w ^{v}, 521w^{v}, 686 ^{wv}, 991m^{v}.	V_2O_5.
575a	5:3	96w, 139w, 154m, 182m, 220m, 259m, 311s.	Sn_2S_3, SnS
575b	5:3	96w, 152m, 179m, 224w, 306w.	SnS, Sn_2S_3
575c	5:3	95w, 160m,br, 218m, 300w.	SnS
575a	1:1	95w, 152m, 179m, 222m, 306s.	SnS, Sn_2S_3
575b	1:1	95w, 155m, 217m, 260m, 311s.	SnS, SnS_2
570a	1:2	95w, 137m, 159m, 184m, 218m, 261w, 288w, 312s.	SnS, SnS_2
570b	1:2	95w, 152m, 182m, 220m, 233m, 252m, 306v.s.	Sn_2S_3

Table 8.9 Raman band positions for compounds identified on films deposited by the APCVD reaction of $SnCl_4$ + $VOCl_3$ + H_2S.[93,94,96] The notation a, b or c after the temperature refer to different spot analyses on the same sample.
Key: * = VO_2, ^{v} = V_2O_5, $^{\sim}$ = VS_2, $^{¥}$ = SnS_2, $^{\square}$ = V_2S_3. w = weak, m = medium, s = strong, v.s = very strong, br = broad.

At 350 °C a tin rich precursor mixture results in vanadium oxides and vanadium disulfide. Equal or vanadium rich mixtures result in the formation of vanadium(III) sulfide, with no vanadium disulfide or oxides found during the analysis of these films.

At 470 - 480 °C a tin rich precursor mixture results in the formation of Sn_2S_3. An equal mixture of precursors results in SnS_2 with additional bands similar in appearance to V_2S_3. A vanadium rich precursor mixture results in the formation of V_2S_3, VO_2, SnS_2 and V_2O_5.

At 570 - 575 °C all precursor mixtures result in the formation of tin sulfides only. Precursor mixtures that were rich in tin gave Raman bands for Sn_2S_3 and SnS with no

SnS_2 identified. When a precursor mixture of equal tin and vanadium concentration was used all three tin sulfides were identified in the film produced. The film produced from a vanadium rich precursor mixture resulted in the formation of Sn_2S_3 only.

8.5 Tin vanadium sulfide

8.5.1 Experimental

Three precursors were also used for these experiments; tin tetrachloride, vanadium tetrachloride and hydrogen sulfide.

Precursors	Deposition temperature / °C	tin:vanadium vapour pressure	Bubbler 1 (VCl_4) temperature / °C	Bubbler 2 ($SnCl_4$) temperature / °C
$SnCl_4$+VCl_4	400	2:1	79	71
$SnCl_4$+VCl_4	400	1:1	108	80
$SnCl_4$+VCl_4	400	1:2	126	71
$SnCl_4$+VCl_4	500	2:1	81	76
$SnCl_4$+VCl_4	500	1:1	106	92
$SnCl_4$+VCl_4	500	1:2	127	73
$SnCl_4$+VCl_4	600	2:1	86	81
$SnCl_4$+VCl_4	600	1:1	106	77
$SnCl_4$+VCl_4	600	1:2	132	71

Table 8.10 A table of conditions used for the APCVD reactions of vanadium tetrachloride, tin tetrachloride and hydrogen sulfide.

8.6 Results

8.6.1 Raman microscopy

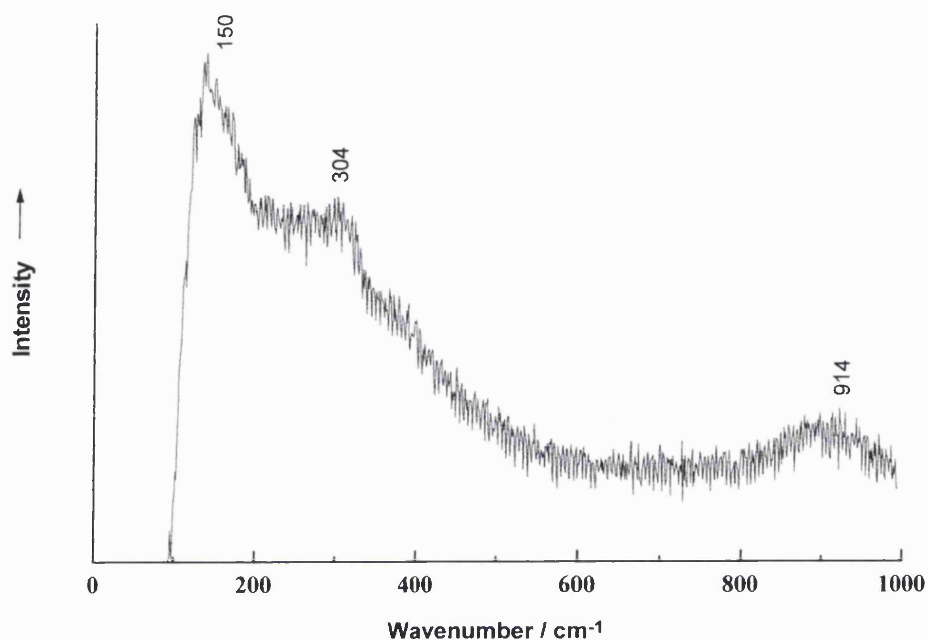

Figure 8.11 Raman spectrum of a film deposited by the APCVD reaction of $SnCl_4$ + VCl_4 + H_2S at 400 °C. The ratio of $SnCl_4$ to VCl_4 was 1:2.

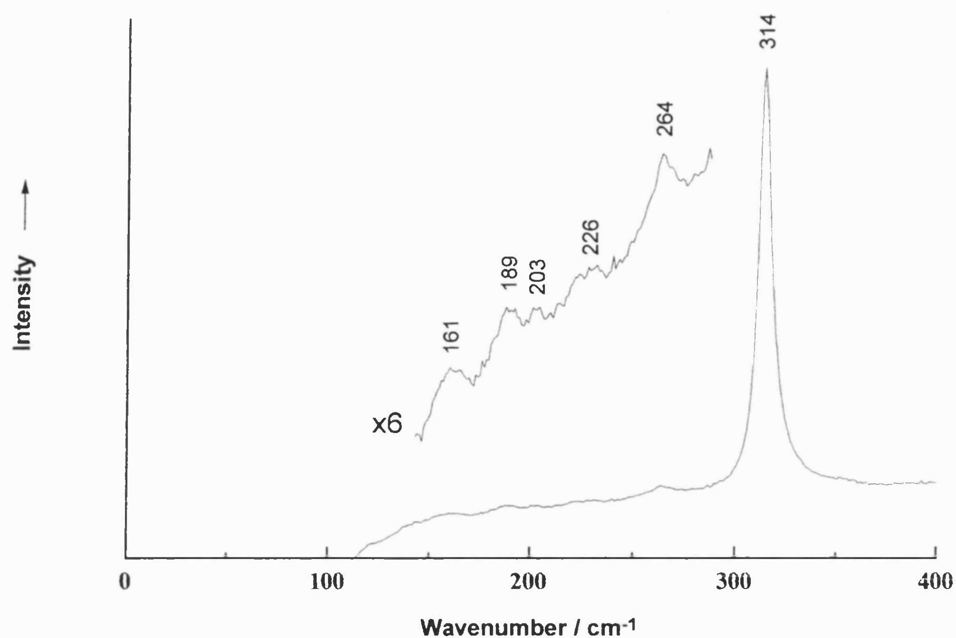

Figure 8.12 Raman spectrum of a film deposited by the APCVD reaction of $SnCl_4$ + VCl_4 + H_2S at 500 °C. The ratio of $SnCl_4$ to VCl_4 was 1:1.

The film deposited from the APCVD reaction of $SnCl_4$, VCl_4 and H_2S at 400 °C, with a ratio of $SnCl_4$ and VCl_4 of 1:2, shown in figure 8.11, gave Raman bands at 150, 304 and 914 cm^{-1} due to vanadium(III) sulfide. This compared with a standard spectrum of V_2S_3 which has Raman bands at 121, 161(shoulder), 322 and 907 cm^{-1}.

The film deposited from the reaction of $SnCl_4$, VCl_4 and H_2S at 500 °C, with a ratio of $SnCl_4$ and VCl_4 of 1:1, shown in figure 8.12, has Raman bands at 161, 189, 203, 226, 264 and 314 cm^{-1}. These bands compare with 164 and 192 cm^{-1} for SnS[95] and 317 cm^{-1} for the A symmetry intralayer mode of SnS_2.[93]

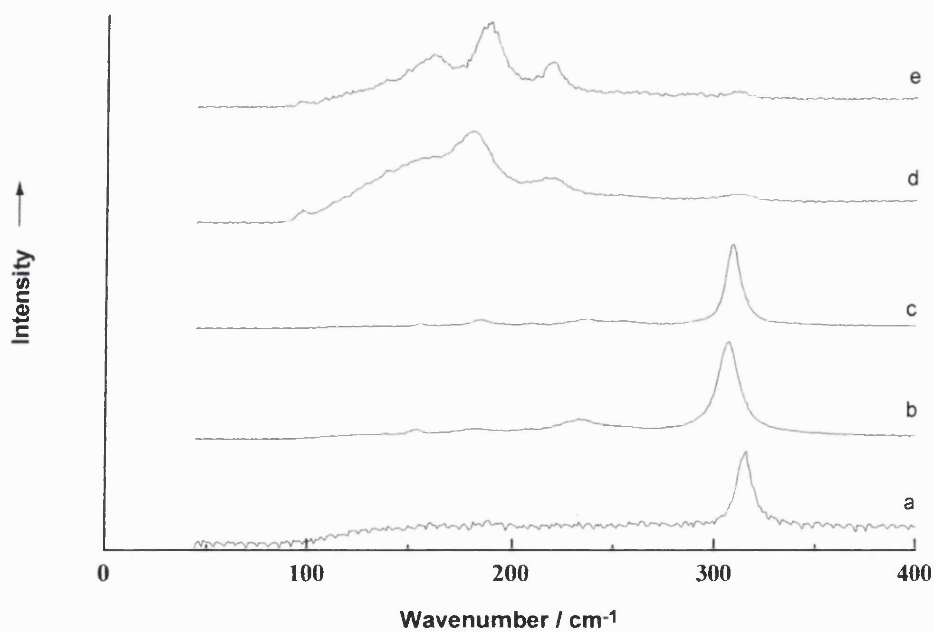

Figure 8.13 Raman spectra recorded from a film deposited by the APCVD reaction of $SnCl_4$ + VCl_4 + H_2S at 600 °C. The spectrum labelled 'a' was at the edge of the substrate nearest the entrance to the reactor, with 'e' near the centre of the substrate. Raman spectra were recorded at different points along a line on the film from the entry end towards the exhaust end of the reactor. The ratio of $SnCl_4$ to VCl_4 was 2:1.

The Raman spectra recorded from the film deposited by the reaction of $SnCl_4$, VCl_4 and H_2S at 600 °C, with a ratio of $SnCl_4$ to VCl_4 of 2:1 shown in figure 8.13 has the following compounds, as identified by Raman microscopy. From the point where the precursor gases enter the reactor SnS_2 with a band at 315 cm^{-1}, in comparison to a reported value of 317 cm^{-1}, for the A symmetry intralayer mode of SnS_2.[93] Further into the reactor Sn_2S_3 was deposited with bands at 154, 182, 234, 307 cm^{-1}, which compare with literature values.[97] Finally in the centre of the film there is a mixture of SnS and Sn_2S_3. The Raman bands corresponding to SnS are at 97, 160, 188 and 218 cm^{-1} which compare with literature values of 95 (A_g), 164 (B_{3g}), 192 (A_g) and 218 (A_g).[95]

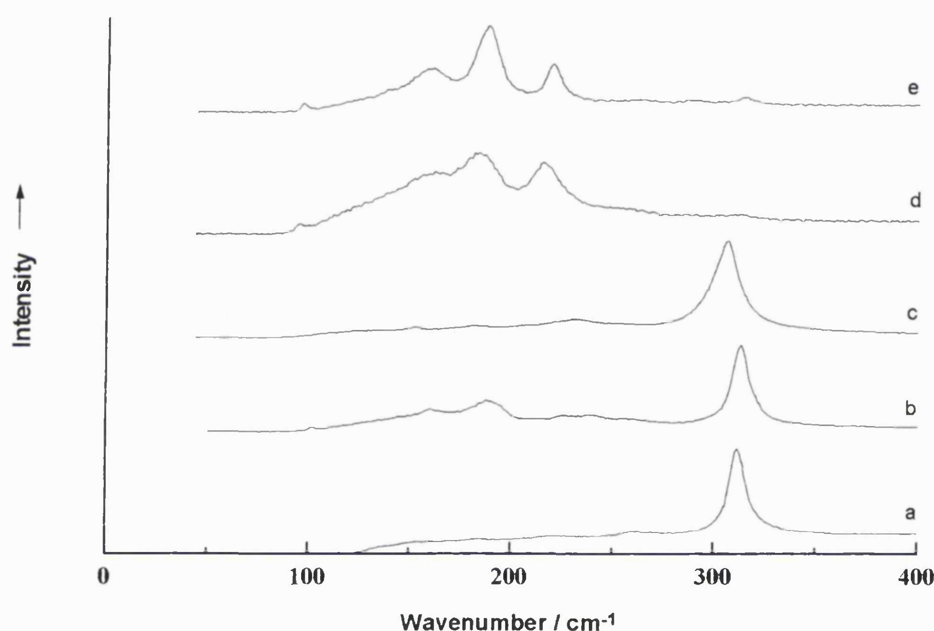

Figure 8.14 Raman spectra recorded from a film deposited by the APCVD reaction of $SnCl_4$ + VCl_4 + H_2S at 600 °C. Raman spectra were recorded at different points along a line on the film from the entry end towards the exhaust end of the reactor. The spectrum labelled 'a' was at the edge of the substrate nearest the entrance to the reactor, with 'e' near the centre of the substrate. The ratio of $SnCl_4$ to VCl_4 was 1:2.

The edges of the films deposited at 600 °C, (the Raman spectra of which are shown above in figures 8.13 and 8.14) had yellow edges due to the presence of tin disulfide. The rest of these films were grey/brown due to the presence of tin monosulfide and tin sesqisulfide. The film deposited at 600 °C with a ratio of $SnCl_4$ to VCl_4 of 1:2, shown in figure 8.14 had a similar pattern to that shown in figure 8.13. Figure 8.14 shows that

SnS_2 is deposited where the gases enter the reactor. This has a Raman band at 312 cm^{-1}, in comparison to the Raman band at 317 cm^{-1} reported for the A symmetry intralayer mode of SnS_2.[93] Further into the reactor both SnS_2 and SnS is deposited. The tin(II) sulfide has Raman bands at 102, 160, 188 and 226 cm^{-1}, these compare with reported values of 95 (A_g), 164 (B_{3g}), 192 (A_g) and 218 (A_g).[95] Further still into the reactor a mixture of patches of Sn_2S_3 or SnS or SnS and SnS_2 are deposited.

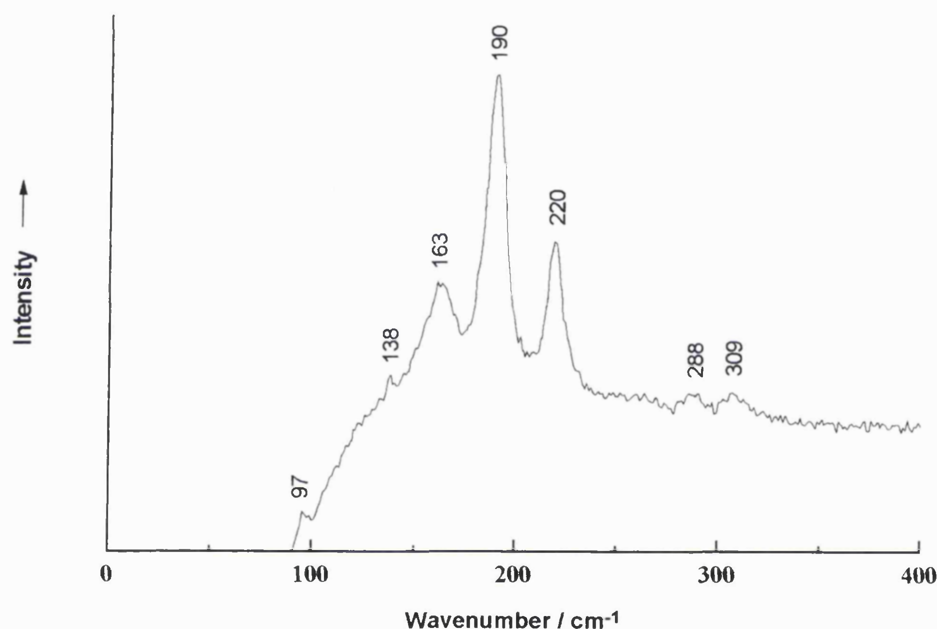

Figure 8.15 Raman spectra recorded from a film deposited by the APCVD reaction of $SnCl_4 + VCl_4 + H_2S$ at 600 °C. The ratio of $SnCl_4$ to VCl_4 was 1:1.

The Raman spectrum shown above in figure 8.15 shows Raman bands due to SnS and Sn_2S_3 with bands at 97, 163, 190, 220 and 288 cm^{-1} due to SnS[95], and 309 cm^{-1} due to Sn_2S_3.[97]

Deposition temperature / °C	tin:vanadium vapour pressure	Raman band positions / cm^{-1}	Compounds present
400	1:2	150m,br$^{\square}$, 304m,br$^{\square}$, 914m,br$^{\square}$.	$^{\square}$ = V_2S_3
400	1:1	153m,br$^{\square}$, 263m$^{?}$, 314s$^{¥}$.	$^{¥}$ = SnS_2, V_2S_3
400	2:1	154m,br$^{\square}$, 304m,br$^{\square}$.	V_2S_3
400	2:1	153m,br$^{\square}$, 263m$^{?}$, 315s$^{¥}$.	V_2S_3, SnS_2
500	1:2	262m$^{?}$, 315s$^{¥}$.	SnS_2
500	1:2	149m$^{\square}$, 263m$^{?}$, 315s$^{¥}$.	SnS_2, V_2S_3
500	1:1	161w$^{¤}$, 189w$^{¤}$, 203w$^{?}$, 226w$^{¤}$, 264w$^{?}$, 314s$^{¥}$.	$^{¤}$ = SnS, $^{¥}$ = SnS_2.
500	1:1	142m$^{?}$, 206m$^{?}$, 263m$^{?}$, 315s$^{¥}$.	SnS_2
500	1:1	155m$^{\square}$, 264m$^{?}$, 314s$^{¥}$.	SnS_2, V_2S_3
500	2:1	153m$^{\square}$, 264m$^{?}$, 315s$^{¥}$.	SnS_2, V_2S_3
500	2:1	262m$^{?}$, 315s$^{¥}$.	SnS_2
600a	1:2	184w$^{?}$, 222w$^{?}$, 261w$^{?}$, 312s$^{¥}$.	SnS_2.
600b	1:2	102w$^{¤}$, 160m$^{¤}$, 188w$^{¤}$, 226m$^{¤}$, 239m$^{?}$, 313s$^{¥}$.	SnS, SnS_2.
600c	1:2	153w§, 183m§, 231w§, 306s§.	Sn_2S_3.
600d	1:2	95w$^{¤}$, 162m,br$^{¤}$, 182s,br$^{¤}$, 216m$^{¤}$, 256w$^{?}$, 310w§.	SnS, Sn_2S_3.
600e	1:2	97w$^{¤}$, 138m,br$^{?}$, 160m,br$^{¤}$, 186m$^{¤}$, 220w$^{¤}$, 261w$^{?}$, 289w$^{¤}$, 314w$^{¥}$.	SnS, SnS_2.
600	1:1	96w$^{¤}$, 154m$^{\square}$, 177m$^{¤}$, 222m$^{¤}$, 261w$^{?}$, 285m$^{¤}$, 314m$^{¥}$.	SnS, SnS_2, V_2S_3
600	1:1	97w$^{¤}$, 138w$^{?}$, 163m$^{¤}$, 190s$^{¤}$, 220m$^{¤}$, 288w$^{¤}$, 309w§.	SnS, Sn_2S_3
600	1:1	160m$^{¤}$, 188s$^{¤}$, 223m$^{¤}$, 264w$^{?}$, 315m$^{¥}$.	SnS, SnS_2
600a	2:1	315s$^{¥}$.	SnS_2.
600b	2:1	154m§, 182m§, 234w§, 307s§.	§ = Sn_2S_3.
600c	2:1	155w§, 185w§, 210w§, 236w§, 254w§, 309s§.	Sn_2S_3.
600d	2:1	97w$^{¤}$, 153m$^{¤}$, 179m$^{¤}$, 218m$^{¤}$, 254w§, 310w§.	SnS, Sn_2S_3.
600e	2:1	97w$^{¤}$, 160m$^{¤}$, 188m$^{¤}$, 218m$^{¤}$, 310w§.	SnS, Sn_2S_3.

Table 8.16 Raman band positions for compounds identified on films deposited by the APCVD reaction of $SnCl_4$ + VCl_4 + H_2S.[93,95,97]

Key: $^{\square}$ = V_2S_3, $^{¥}$ = SnS_2, $^{¤}$ = SnS, § = Sn_2S_3, $^{?}$ = unknown.

w = weak, m = medium, s = strong, v.s = very strong, br = broad

As the above table shows, at 400 °C with a 1:2 ratio of tin tetrachloride to vanadium tetrachloride precursors, only vanadium(III) sulfide was identified by Raman microscopy of the film deposited. With a ratio of 1:1 or 2:1, SnS_2 and V_2S_3 were identified from their Raman spectra.

At 500 °C with a 1:2 ratio of tin tetrachloride to vanadium tetrachloride precursors SnS_2 and V_2S_3 were identified from their Raman spectra. However the use of a 1:1 ratio of precursors led to the deposition of a film with SnS, SnS_2 and V_2S_3. A 2:1 ratio of precursors led to the production of a film with SnS_2 and V_2S_3.

At 600 °C all ratios of tin tetrachloride to vanadium tetrachloride precursors gave films with all three tin sulfides deposited with no vanadium sulfide detected by Raman microscopy, with the exception of the 1:1 ratio in which some V_2S_3 was detected.

No Vanadium(IV) sulfide was detected by Raman microscopy in the films produced by the APCVD reactions of tin tetrachloride, vanadium tetrachloride and hydrogen sulfide.

8.7 Discussion

Raman microscopy was able to identify a selection of tin sulfides, vanadium sulfides and oxides. However Raman microscopy did not provide definitive evidence for the formation of either tin vanadium oxysulfide or tin vanadium sulfide. Raman microscopy was however useful in the composition mapping of the surface.

The APCVD reaction of oxovanadium(V) chloride, tin tetrachloride and hydrogen sulfide produced vanadium sulfides, vanadium dioxide or vanadium pentoxide at deposition temperatures below 500 °C depending on the ratio of tin to vanadium in the reactant gas flow. At 570 and 575 °C SnS_2, Sn_2S_3 and SnS were detected by Raman microscopy in preference to vanadium compounds. Raman microscopy however, may be more sensitive to tin sulfides that vanadium sulfides, and hence not detect low concentrations of vanadium sulfide in this study.

The APCVD reaction of vanadium tetrachloride, tin tetrachloride and hydrogen sulfide produced either vanadium sulfide, V_2S_3, or the three previously identified tin sulfides ie SnS_2, Sn_2S_3 or SnS. At a high vanadium partial pressure in the precursor mixture at 400 °C V_2S_3 was detected by Raman analysis, rather than tin sulfides. An increase in tin partial pressure relative to vanadium caused tin rather than vanadium sulfide deposition. At 500 and 600 °C tin sulfides were detected by Raman microscopy rather than vanadium sulfide in most of the data recorded.

The Raman spectrum recorded from the film deposited (by the APCVD reaction of $SnCl_4$, $VOCl_3$ and H_2S) at 575 °C, with a ratio of $SnCl_4$ to $VOCl_3$ of 5:3 was different to the spectrum shown in figure 8.15, also of SnS (from the reaction of $SnCl_4$, VCl_4 and H_2S at 600 °C, with a ratio of $SnCl_4$ to VCl_4 of 1:1). In figure 8.8 the expected bands at 164 (B_{3g}) and 192 (A_g) cm^{-1},[95] were merged to form a single broad feature at 160 cm^{-1}. This was not expected as the spectrum of tin(II) sulfide recorded from a film deposited by the reaction of $SnCl_4$ and H_2S only, had distinct bands at 163 and 189 cm^{-1}. It is possible that the merging of these bands indicates intercalation of vanadium into the tin(II) sulfide structure, revealed by an apparent increase in the intensity of the B_{3g} band of SnS. This is not observed in figure 8.15 when VCl_4, rather than $VOCl_3$ was used as the second precursor. It is therefore assumed that there are no vanadium inclusions in the structure of the tin(II) sulfide deposited at 600 °C by the APCVD reaction of $SnCl_4$, VCl_4 and H_2S.

The APCVD reactions of tin tetrachloride and hydrogen sulfide deposited films of SnS_2 at temperatures between 300 – 500 °C, Sn_2S_3 at 525 °C and SnS at 545 – 600 °C. In comparison, the films deposited using oxovanadium(V) chloride in addition to the above precursors deposited: no tin sulfides at 350 °C, SnS_2 and Sn_2S_3 at 470 – 480 °C and all three tin sulfides at 570 – 575 °C. These results are based on Raman microscopic data, it would therefore be expected that if tin(IV) sulfide was present on films deposited at 350 °C it would detected. However it was absent in the above study with vanadium oxides and sulfides being deposited in preference to tin sulfides. At deposition temperatures of 470 – 480 °C and 545 – 600 °C the expected tin sulfides were produced.

The films deposited using vanadium tetrachloride in addition to the above precursors deposited: SnS_2 in addition to V_2S_3 at 400 °C, this was expected based on the above

results for $SnCl_4$ and H_2S. At 500 °C SnS_2 and SnS were deposited, no Sn_2S_3 was identified by Raman microscopy, even though this was the expected phase at this temperature. At 600 °C, however all three tin sulfides were identified, this was not unexpected due to the temperature gradient across the substrate, however SnS was expected to be the favoured phase at this temperature.

It would be interesting to do a further study of these systems to try and get both tin and vanadium incorporation into a thin film of metal sulfide. It should be possible to do this by carrying out a two-stage reaction once the reactor has reached the desired temperature, first with one precursor then the other, without removing the substrate between reactions. It may also be possible to achieve a mixed metal film by reducing the pressure in the rig during the deposition process and by slowing down the carrier gas flow to increase precursor residence time in the reactor.

9.0 Conclusions

As described, a selection of sulfides, oxysulfides and oxides have been analysed for this thesis. The tin sulfides, titanium sulfides, vanadium pentoxide and titanium dioxide films were unaffected by storage in air. However the vanadium sulfides and oxysulfides including those that incorporated tin into the films were not stable in air in the long term. The chromium oxysulfide films produced were not entirely stable in air either, as part of the films changed colour.

The films deposited in this study were found to be free of chlorine contamination, with the exception of the chromium oxysulfide films deposited, which all contained fairly large percentages of chlorine, for example the film deposited at 400 °C had a formula of $CrS_{0.70}Cl_{0.65}O_{0.07}$ according to EDX data.

The tin sulfide thin films studied were of particular interest as the films were found to be stable in air, they did not oxidise during storage. The colour of these films could be used to identify the phases present, as the different phases had noticeably different colours. The identity of the different coloured phases was confirmed by use of Raman microscopy. Raman microscopy could be used in an automated process to map the composition of films deposited. The three tin sulfides identified in this study each had Raman bands that gave comparable intensities to that of silicon (which is used as a standard to check signal throughput when setting up the spectrometer).

The studies reported in this thesis show that it is possible to deposit coatings with metal sulfides in a different oxidation state from that present in the precursor. This was noted for vanadium sulfides in various oxidation states which could be deposited from a vanadium(IV) chloride precursor and tin(II) sulfide or ditin(II,IV) trisulfide when deposited from precursors of tin(IV) halides and tin(IV) thiolate. It is assumed that the difference in oxidation state between the precursor and the product is due to the deposition of the kinetic rather than the thermodynamic product due to the relatively short duration of reactions. The APCVD reactions of vanadium(IV) chloride and hydrogen sulfide deposited vanadium(IV) sulfide at temperatures between 300 – 350 °C inclusive, vanadium(III) sulfide at 400 – 500 °C, the mixed valent vanadium(III,II) sulfide at 550 °C and vanadium(II) sulfide at 600 °C. There is a trend for decreasing oxidation state with increasing deposition temperature. This trend is mirrored by the tin

sulfides deposited in this study. In general tin(IV) sulfide is deposited at low temperatures, i.e. below 500 °C, tin(II) sulfide is produced at 550 °C and above and the mixed valent tin(II, IV) sulfide is produced at intermediate temperatures.

9.1 Future work

A future study of the air sensitive films produced for this thesis should make extensive use of a glove box, for both storage of, and handling these coatings. A more complete study of vanadium oxysulfide and chromium oxysulfide systems would be interesting as neither has been extensively covered in the literature. In addition it would be interesting to attempt to produce mixed metal tin/vanadium sulfide thin films as described in the discussion section of Chapter 8. The films produced for this thesis consisted of domains of tin sulfides and vanadium sulfides with little evidence of intercalation to give a new compound.

Appendix 1

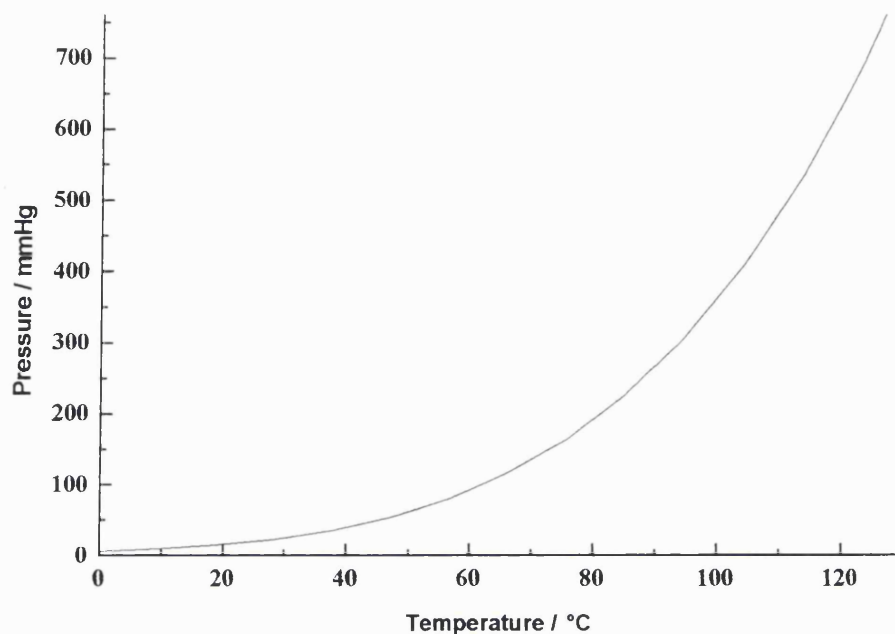

Figure 9.1 Plot showing the vapour pressure of vanadyl chloride against temperature.

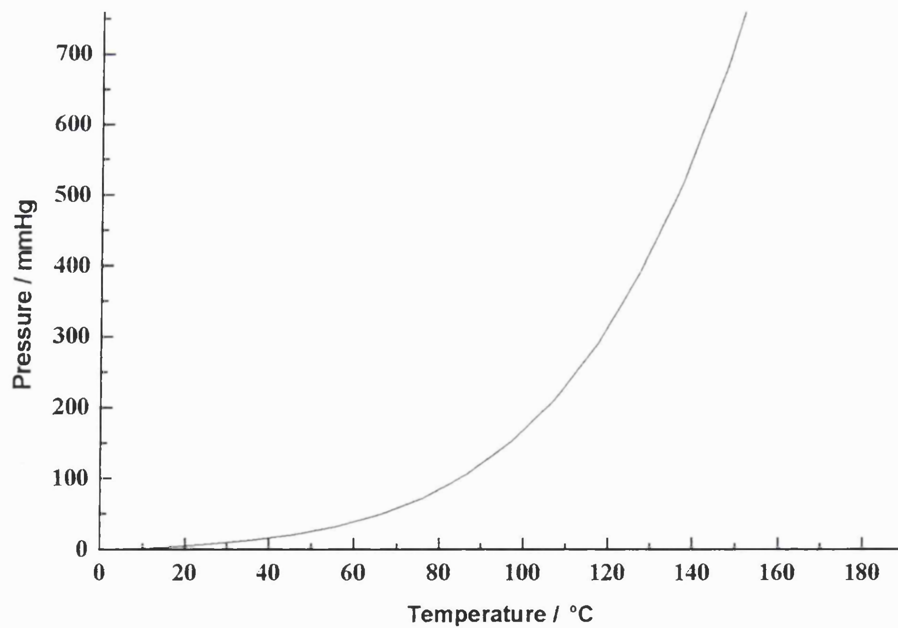

Figure 9.2 Plot of vapour pressure of vanadium tetrachloride against temperature.

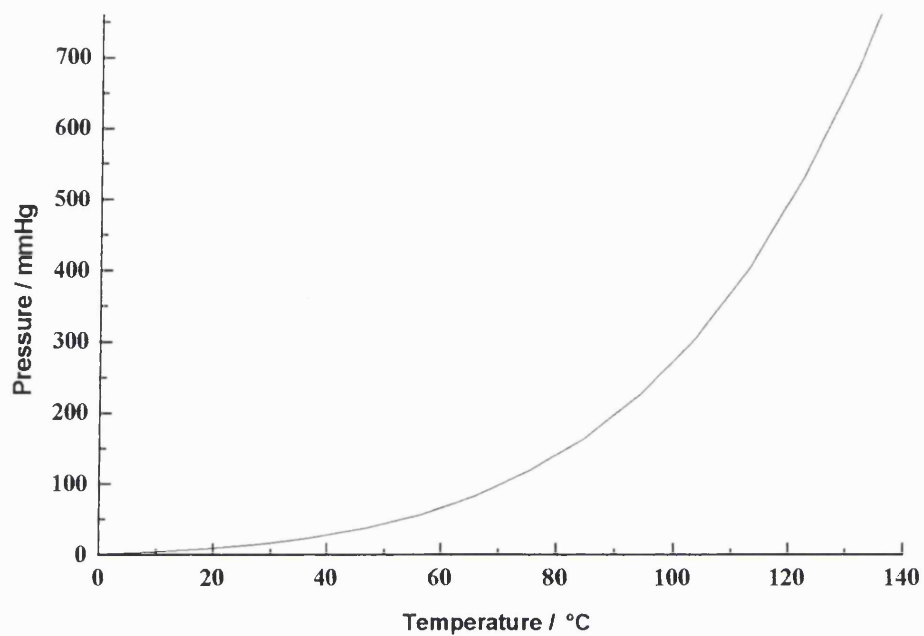

Figure 9.3 Plot of vapour pressure of titanium tetrachloride against temperature.

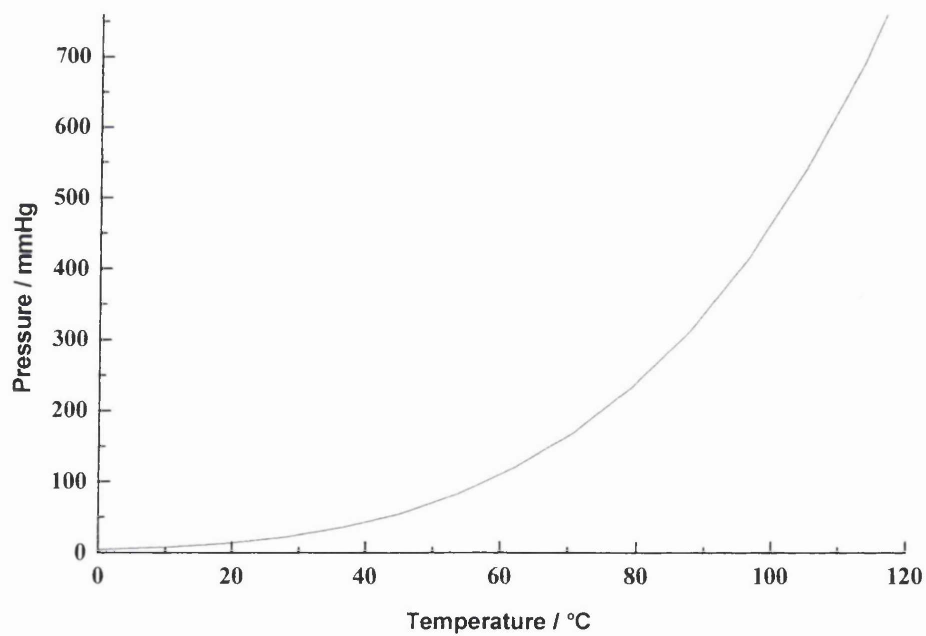

Figure 9.4 Plot of vapour pressure of chromyl chloride against temperature.

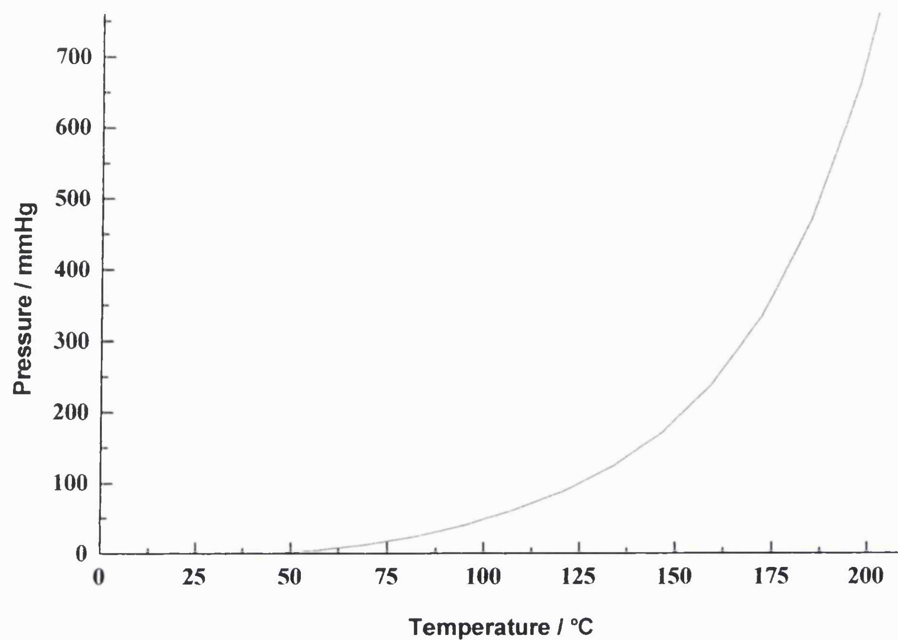

Figure 9.5 A vapour pressure plot of tin tetrabromide against temperature.

Due to the absence of published literature values the above plot was produced by extrapolating from the melting point and boiling point data using tin tetrachloride as a comparison. These values were taken from the Aldrich catalogue.

Appendix 2 Other films analysed by Raman microscopy

Vanadium dioxide

Experimental

The two precursors used to produce a vanadium dioxide film were vanadium tetrachloride (Aldrich), which was used as supplied in addition to the second precursor, which was distilled water. Only one reaction was attempted to check the rig was working prior to manufacture of vanadium sulfide thin films, described in Chapter 4. The bubbler containing VCl_4 was heated to 100 °C, with a 0.5 dm^3 min^{-1} flow of nitrogen passing through it. A 0.5 dm^3 min^{-1} flow of H_2S was used. A film was deposited at 500 °C, this was analysed by Raman microscopy as shown below in figure 10.1.

Results and discussion

A Raman spectrum recorded from the film deposited by the APCVD reaction of VCl_4 and H_2O has Raman bands at 136, 145, 193, 222, 266, 306, 338, 388, 430, 448, 497, 576 and 615 cm^{-1}.

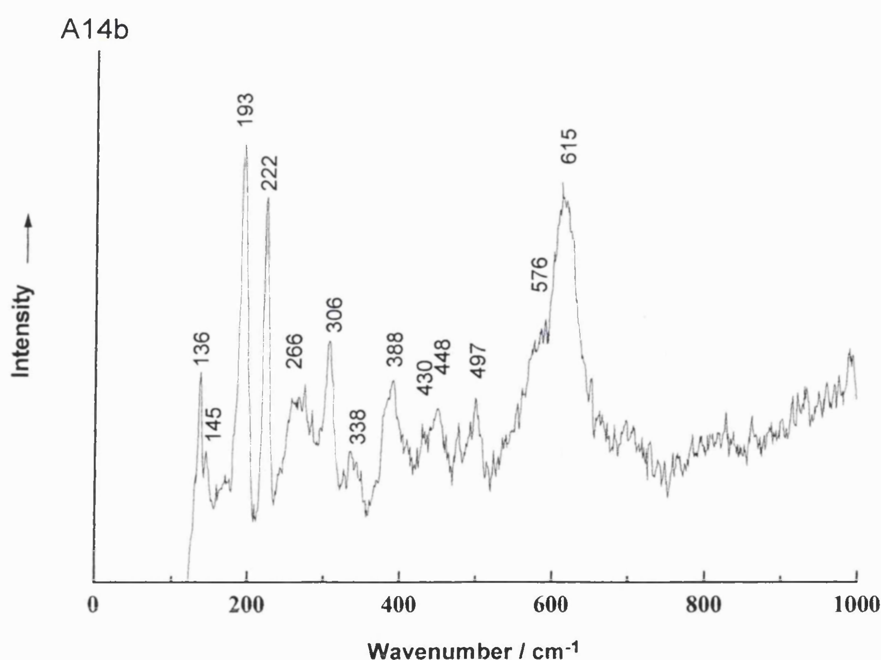

Figure 10.1 Raman spectrum recorded from the film deposited by the APCVD reaction of vanadium tetrachloride and water at a deposition temperature of 500 °C.

The above figure shows a spectrum of the vanadium oxide film produced by APCVD. This is only partially oxidised; it has not transformed to vanadium pentoxide, which as can be seen below in figure 10.2, has a very intense band at 145 cm^{-1}. There is a band at 145 cm^{-1} present in the spectrum of VO_2 shown, but it is only a minor contribution to the Raman spectrum. The Raman bands present in the spectrum shown in figure 10.1 may be attributed to stoichiometric vanadium dioxide with bands at 145, 193, 222, 388, 497 and 615 cm^{-1}, cf. 142, 191, 223, 392, 500 and 613 cm^{-1},[98] with some additional bands attributed to oxygen-rich vanadium dioxide at 266, 306 and 576 cm^{-1}, cf. literature values of 266, 305 and 580 cm^{-1}.[98]

Vanadium pentoxide

The vanadium pentoxide films studied were deposited by Mark Field.

Experimental

The APCVD reaction of oxovanadium(V) chloride and water was used to produce vanadium pentoxide thin films during 90 s reactions. The bubbler containing the oxovanadium(V) chloride was heated to *c.* 92 °C. The reactor was heated to 500 °C for the reaction.

Results and discussion

A Raman spectrum of vanadium pentoxide is shown below in figure 10.2.

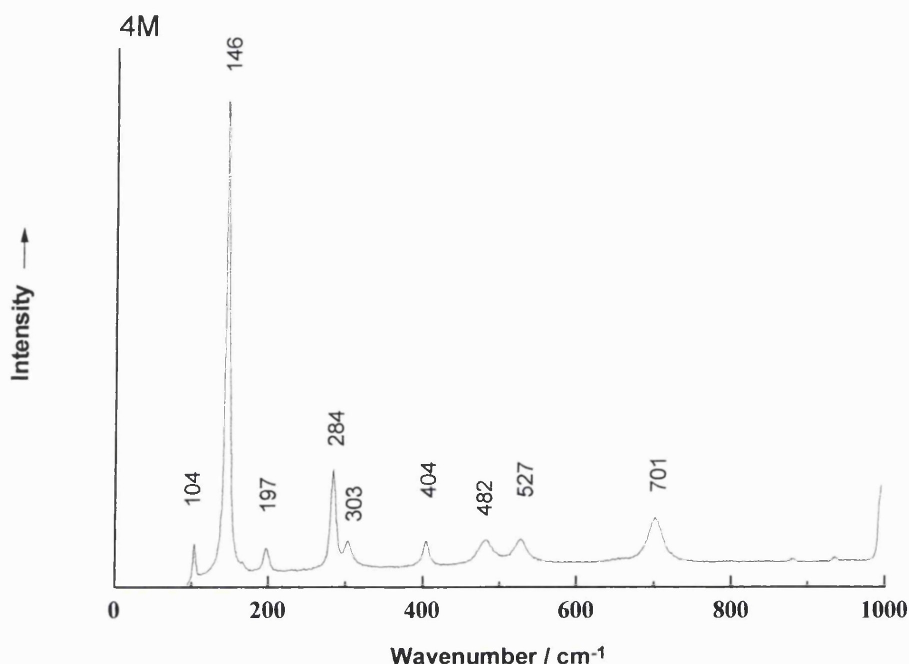

Figure 10.2 A Raman spectrum recorded from a film deposited at 500 °C by the APCVD reaction of oxovanadium(V) chloride and water.

The Raman spectrum above has bands at 104, 146, 197, 284, 303, 404, 482, 527 and 701 cm^{-1}, these compare favourably with literature values of 100, 144, 282, 300, 405, 485 and 700 cm^{-1} for V_2O_5.[99]

Chromium oxide

The chromium oxide film studied was deposited by Mark Field.

Experimental

The APCVD reaction of chromyl chloride and water was used to produce a chromium oxide thin film during a 180 s reaction. The bubbler containing the chromyl chloride was heated to 105 °C. The reactor was heated to 600 °C for the reaction.

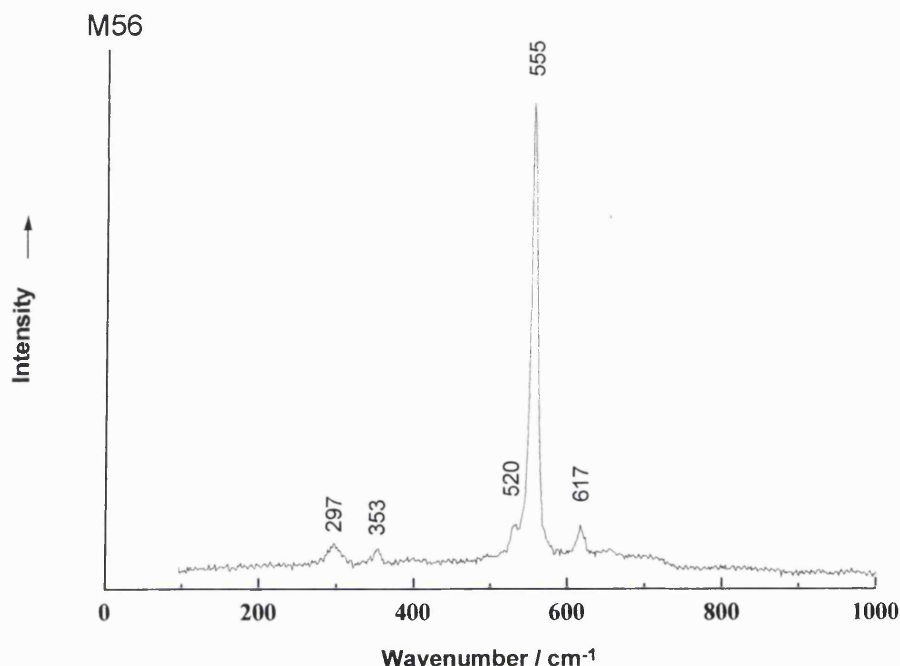

Figure 10.3 A Raman spectrum recorded from a film deposited at 600 °C by the APCVD reaction of chromyl chloride and water.

Results and discussion

The Raman spectrum above has bands at 297, 353, 520, 555 and 617 cm^{-1}, these compare favourably with literature values of 352, 531, 557 and 619 cm^{-1} for Cr_2O_3.[100]

Titanium dioxide

The titanium dioxide films studied were deposited by Shane O'Neil.

Experimental

The APCVD reaction of titanium tetrachloride and propan-2-ol, or methanol, were used to produce titanium oxide thin films during 30 - 180 s reactions. The bubbler containing titanium tetrachloride was heated to *c.* 68 °C. The reactor was heated to 500 or 600 °C for the reactions studied below.

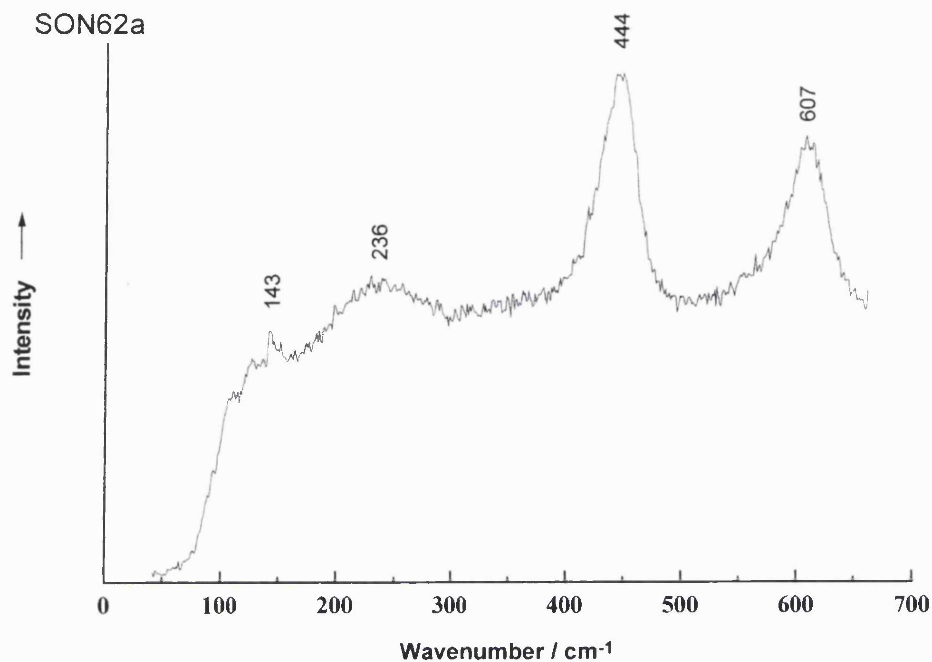

Figure 10.4 A Raman spectrum recorded from a film deposited at 600 °C by the 180 s APCVD reaction of titanium tetrachloride and methanol.

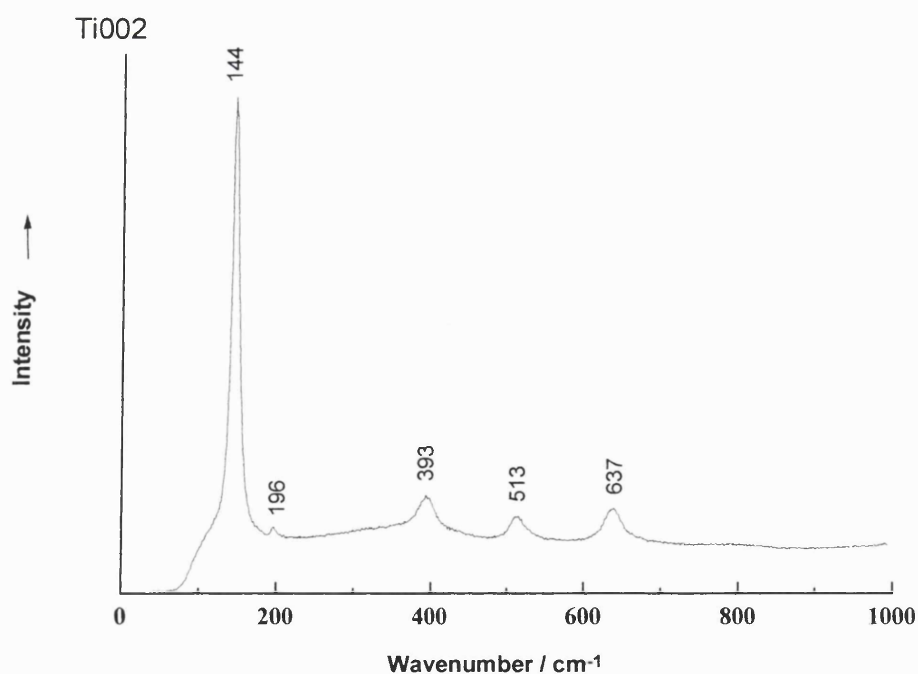

Figure 10.5 A Raman spectrum recorded from a film deposited at 500 °C by the 30 s APCVD reaction of titanium tetrachloride and propan-2-ol.

Results and discussion

The Raman spectrum above has bands at 143, 236, 444 and 607 cm^{-1}, these compare favourably with literature values of 144, 235, 448 and 612 cm^{-1} for the rutile form of TiO_2. The spectrum shown in figure 10.5 has bands at 144, 196, 393, 513 and 637 cm^{-1}, these compare to literature values of 147, 198, 398, 515, and 640 cm^{-1} for the anatase form of TiO_2.[101]

Appendix 3 A list of abbreviations used in this thesis

AACVD	Aerosol assisted chemical vapour deposition.
APCVD	Atmospheric pressure chemical vapour deposition.
CVD	Chemical vapour deposition.
EDX	Energy dispersive analysis by X-rays.
hcp	Hexagonal close packed.
JCPDS	Joint committee on power diffraction standards
LECVD	Laser enhanced chemical vapour deposition.
LPCVD	Low pressure chemical vapour deposition.
PECVD	Plasma enhanced chemical vapour deposition.
SEM	Scanning electron microscopy.
XPS	X-ray photoelectron spectroscopy.
XRD	X-ray diffraction.
XRF	X-ray fluorescence.

References

1 V.H. Pitt, *Dictionary of physics*, 1987, Penguin Books Ltd, Middlesex.

2 D.W.A. Sharp, *Dictionary of chemistry*, 1987, Penguin Books Ltd, Middlesex.

3 P.W. Atkins, *Physical chemistry*, 5th edn, 1994, Oxford University Press, Oxford.

4 D.F. Shriver, P.W. Atkins and C.H. Langford, 2nd edn, 1994, Oxford University Press, Oxford.

5 C.V. Raman and K.S. Krishnan, *Nature*, 1928, **121**, 501.

6 G. Landsberg and L. Mandelstam, *Naturwissenschaften*, 1928, **16**, 557.

7 P.J. Hendra, C. Jones and G. Warnes, *Fourier Transform Raman Spectroscopy – Instrumentation and Chemical Applications*, 1st Edn., Ellis Horwood, London, 1991.

8 T. Nagahara, H. Kakigi, Y. Okayasu, K. Kumagai, Jpn. Kokai Tokkyo Koho 1991, 5.

9 W. F. A. Besling and A. Goossens, *Schoonman, Proc. - Electrochem. Soc.*, 1997, **25** (Chemical Vapor Deposition), 676.

10 S.A. Stuart, S. Prawer and P.A. Weiser, *Diamond Relat. Mater.*, 1993, **2**, 753.

11 P. Alers, H.E. Hintermann, and I. Hayward, *Thin Solid Films*, 1995, **259**, 14.

12 Q.H. Fan, A. Fernandes, E. Pereira, and J. Gracio, *J. Appl. Phys.*, 1998, **6**, 84.

13 P.S. Dobal, M.S. Navati, H.D. Bist, T. Som and V.N. Kulkarni, *J. Raman Spectrosc.*, 1998, **29**, 567.

14 I.P. Hayward, K.J. Baldwin, D.M. Hunter, D.N. Batchelder and G.D. Pitt, *Diamond and Related Materials*, 1995, **4**, 617.

15 T. Okuhara, K. Inumaru, M. Misono, and N. Matsubayashi, *Stud. Surf. Sci. Catal.*, 1993, **75** (New Frontiers in Catalysis, Pt. B), 1767.

16 J.M. McGraw, J.D. Perkins, J.-G. Zhang, P. Liu, P.A. Parilla, J. Turner, D. L. Schulz, C.J. Curtis and D.S. Ginley, *Solid State Ionics*, 1998, **113-115**, 407.

17 R.J.H. Clark, *Science and Technology for Cultural Heritage,* 1998, **7**, 663.

18 M.L. Hitchman and K.F. Jensen, (Eds), *Chemical Vapour Deposition, Principles and Applications*, 1993, Academic Press, London.

19 O.Auciello and J. Engemann, *Multicomponent and Multilayered Thin Films for Advanced Microtechnologies: Techniques, Fundamentals and Devices*, Kluwer Academic Publishers, London, 1993.

20 P.W. Atkins, *Physical Chemistry*, 1994, 5th Edn, Oxford University Press, Oxford.

21 V.D. Scott, G. Love and S.J.B. Reed, *Quantitative Electron Probe Microanalysis*, 2nd Edn., Ellis Horwood, London, 1995.

22 G.S. Elwin, *PhD thesis*, 1999.

23 L.S. Price, I.P. Parkin, M.N.Field, A.M.E. Hardy, R.J.H. Clark, T.G. Hibbert and K.C. Molloy, *J. Mater. Chem.*, 2000, **10**, 527.

24 K.L. Brown, *Personal communication*, 2000.

25 G. Tchangbédji, D.A. Odink and G. Ouvrard, *J. Power Sources,* 1993, **43/44**, 577.

26 G. Tchangbédji, E. Prouzet and G. Ouvrard, *Mater. Sci. Forum*, 1994, **152/153**, 319.

27 G. Ouvrard, G. Tchangbédji, P. Deniard and E. Prouzet, *J. Power Sources,* 1995, **54**, 246.

28 M. Benmoussa, E. Ibnouelghazi, A. Bennouna and E.L. Ameziane, *Thin Solid Films*, 1995, **265**, 22.

29 K. Stocks, G. Eulenberger and H. Hahn, *Z. Anorg. Allg. Chem.,* 1980, **463**, 105.

30 M.N. Field, and I.P. Parkin, *J. Mater. Chem.*, 2000, **10**, 1863.

31 J.C. Parker, *Phys. Rev. B*, 1990, **42**, 3164.

32 K. Jewell, *by personal communication*, Sept., 2001.

33 G.S. Elwin, *PhD thesis*, London, 1999, 82.

34 A. Ortiz, J.C. Alonso, M. Garcia and J. Toriz, *J. Semicond. Sci. Technol.*, 1996, **11**, 243.

35 D.J. Edlund, 1995, *Patent Application*: US 93-148999 19931108.

36 S.A. Naman, S.M. Aliwi, K. Al-Emara, *Int. J. Hydrogen Energy.* 1986, **11**, 33-8.

37 S.A. Naman, M. Graetzel, *J. Photochem. Photobiol.*, A, 1994, **77**, 249-53.

38 A. Furuta, K. Sato, K. Sato, T. Matsuzawa, R. Ogata, 1990, *Patent Application* JP 88-197986 19880810.

39 Chiyoda Chemical Engineering and Construction Co., Ltd., Japan, Jpn. Kokai Tokkyo Koho, 1984, *Patent Application*, JP 82-216361 19821210.

40 W.K.T. Gleim, J.G. Gatsis, 1974, *Patent Application,* CA 91-102966 19910118.

41 Universal Oil Products Co., 1972, *Patent Application*, FR 71-06432.

42 R.H. Hass, R.C. Hansford, 1981, *Patent Application*,US 74-528845 19741202.

43 A. Belanger, F. Morin, M. Gauthier, W.A. Adams, A.R. Dubois, *NATO Conf. Ser.*, [Ser.] 6,1980, 2 (Mater. Adv. Batteries), 211-22.

44 T.A. Hewston and B.L. Chamberland, *Mat. Res. Bull.,* 1984, **19**, 423-428.

45 W. Bensch and J. Koy, *Acta Cryst.*, 1993, **C49**, 1133-1135.

46 M. Taniguchi, M. Wakihara, Y. Shirai, *Z. Anorg. Allg. Chem.*, 1980, **461**, 234-240.

47 D.M. Schleich, R. Gieger, R. McManus, J.N. Carter, *Proc. SPIE-Int. Soc. Opt. Eng.* 1989, **1037**, 125-129.

48 W. Bensch and J. Koy, *Inorg. Chim. Acta*, 1993, **206**, 221-223.

49 L. Henderson Lewis and J.B. Goodenough, *J. Solid State Chem.*, 1995, **114**, 346 – 358.

50 G.S. Elwin, *PhD thesis*, London, 1999, 82-3.

51 A. Ortiz, J.C. Alonso, M. Garcia and J. Toriz, *J. Semicond. Sci. Technol.*, 1996, **11**, 243-247.

52 L.S. Price, I.P. Parkin, A.M.E. Hardy, R.J.H. Clark, T.G. Hibbert and K.C. Molloy, *Chem. Mater.,* 1999, **11**, 1792.

53 L. Henderson Lewis and J.B. Goodenough, *J. Solid State Chem.*, **114**, 1995, 346.

54 T.S. Lewkebandara and C.H. Winter, *Adv. Mater.*, **6**, 1994, 237.

55 S. Kikkawa, M. Miyazaki and M. Koizumi, *J. Mater. Res.*, **5**, 1990, 2894.

56 D. Zehnder, C. Deshpandey, B. Dunn and R.F. Bunshah, *Solid State Ionics*, **18-19**, 1986, 813.

57 K. Kanehori, F. Kirino, Y. Ito, K. Miyauchi and T. Kudo, *J. Electrochem. Soc.*, **136**, 1989, 1265.

58 C.H. Winter, T.S. Lewkebandara and J.W. Proscia, *Chem. Mater.*, **4**, 1992, 1144.

59 D.M. Schleich, R. Gieger, R. McManus and J.N. Carter, *SPIE*, **1037**, 1988, 125.

60 H.S.W Chang and D.M. Schleich, *J. Solid State Chem.*, **100**, 1992, 62.

61 C.H. Winter, T.S. Lewkebandara, J.W. Proscia and A.L. Rheingold, *Inorg. Chem.*, **32**, 1993, 3807.

62 P. Gard, F. Cruege, C. Sourisseau and O. Gorochov, *J. Raman Spectrosc.*, **17**, 1986, 283.

63 M. Ishii, M. Saeki and I. Kawada, *Physica Status Solidi B*, **124**, 1984, K109.

64 S. Jimẽnez Sandoval, X.K. Chen and J.C. Irwin, *Phys. Rev. B*, **45**, 1992, 14 347.

65 U. Balachandran and N.G. Eror, *J. Solid State Chem.*, **42**, 1982, 276.

66 V.D. Scott, G. Love and S.J.B. Reed, *Quantitative Electron Probe Microanalysis*, 2nd Edn., Ellis Horwood, London, 1995.

67 K.P. Lillerud and P. Kofstad, *J. Electrochem. Soc.*, 1980, **127**, 2397.

68 T. Maruyama and H. Akagi, *J. Electrochem. Soc.*,1996, **143**, 1955.

69 J.C.C. Fan, *Thin Solid Films*, 1978, **54**, 139.

70 D.J. Young, W.W. Smeltzer and J.S. Kirkaldy, *J. Electrochem. Soc.*, 1973, **120**, 1221.

71 D.A. Rice, S.J. Hibble, M.J. Almond, K.A.H. Mohammad and S.P. Pearse, *J. Mater. Chem.*, 1992, **2**, 895.

72 L.S. Price, *PhD thesis*, 2001.

73 N.N. Greenwood and A. Earnshaw, *The Chemistry of the Elements*, Pergamon Press, New York, 1984, Edn 1.

74 T. Jiang and G.A.Ozin, *J. Mater. Chem.*, 1998, **8**, 1099.

75 L.S. Price, I.P. Parkin, T.G. Hibbert and K.C. Molloy, *Chem. Vap. Deposition*, 1998, **4**, 222.

76 H.R. Chandrasekhar, R.G. Humphreys, U. Zwick and M. Cardona, *Phys. Rev. B*, 1977, **15**, 2177.

77 L. Burgio, D.A. Ciomartan and R.J.H. Clark, *J. Raman Spectrosc.*, 1997, **28**, 79.

78 H. Katahama, S. Nakashima, A. Mitsuishi, M. Ishigame and H. Arashi, *J. Phys. Chem. Solids.*, 1983, **44**, 1081.

79 R. Kniep, D. Mootz, U. Severin and H. Wunderlich, *Acta Cryst.*, 1982, **B38**, 2022.

80 H.R. Chandrasekhar and D.G. Mead, *Phys. Rev. B*, 1979, **19**, 932.

81 S. Lopez and A.Ortiz, *Semicond. Sci. Technol.*, 1994, **9**, 2130.

82 S. Mandalis, J.A. Kalomiros, K. Kambas, A.N. Anagnostopoulos, *J. Mater. Sci.*, 1996, **31**, 5975.

83 J.P. Singh and R.K. Bedi, *Thin Solid Films*, 1991, **199**, 9.

84 M. Radot, *Rev. Phys. Appl.*, 1977, **18**, 345.

85 E.R.T. Tiekink, *Appl. Organomet. Chem.*, 1991, **5**, 1.

86 P. Boudjouk, D.J. Seidler, D. Grier and G.J. McCarthy, *Chem. Mater.*, 1996, **8**, 1189

87 P. Boudjouk, D.J. Seidler, S.R. Bahr and G.J. McCarthy, *Chem. Mater.*, 1994, **6**, 2108.

88 S.R. Bahr, P. Boudjouk and G.J. McCarthy, *Chem. Mater.*, 1992, **4**, 383.

89 H.R. Chandrasekhar, R.G. Humphreys, U. Zwick and M. Cardona, *Phys. Rev. B*, 1977, **15**, 2177.

90 P.K. Nair, M.T.S. Nair, A. Fernandez, M. Ocampo, *J.Phys.D Appl. Phys.*, 1989, **22**, 829.

91 A. Lavacchi, B. Cortigiani, G. Rovida, U. Bardi, A. Atrei, R. Angelucci, L. Dori, S. Nicoletti and A. Poggi, *Sensors and Actuators B*, 2000, **71**, 123.

92 L.S. Price, *PhD thesis*, 2001.

93 H. Katahama, S. Nakashima, A. Mitsuishi, M. Ishigame and H. Arashi, *J. Phys. Chem. Solids.*, 1983, **44**, 1081.

94 M. Benmoussa, E. Ibnouelghazi, A. Bennouna and E.L. Ameziane, *Thin Solid Films*, 1995, **265**, 22.

95 H.R. Chandrasekhar, R.G. Humphreys, U. Zwick and M. Cardona, *Phys. Rev. B*, 1977, **15**, 2177.

96 J.C. Parker, *Phys. Rev. B*, 1990, **42**, 3164.

97 H.R. Chandrasekhar and D.G. Mead, *Phys. Rev. B*, 1979, **19**, 932.

98 J.C. Parker, *Phys. Rev. B*, 1990, **42**, 3164 – 3166.

99 M. Benmoussa, E. Ibnouelghazi, A. Bennouna and E.L. Ameziane, *Thin Solid Films*, 1995, **265**, 22.

100 W.A. England, S.N. Jenny and D.A. Greenhalgh, *J. Raman Spectrosc.*, 1984, **15**, 156.

101 U. Balachandran and N.G. Eror, *J. Solid State Chem.*, 1982, **42**, 276.